Neural Control Strategies of the Human Focusing Mechanism

by

Shrikant Rajangam Bharadwaj

B S (Birla Institute of Technology and Science, Pilani) 2001

A dissertation submitted in partial satisfaction of the

requirements for the degree of

Doctor of Philosophy

in

Vision Science

in the

GRADUATE DIVISION

of the

UNIVERSITY OF CALIFORNIA, BERKELEY

Committee in charge:

Professor Clifton M. Schor, Chair

Professor Martin S. Banks

Professor Edward L. Keller

Fall 2005

The dissertation of Shrikant Rajangam Bharadwaj is approved:

Clifton M. Schor 12/08/05

Chair Date

12/12/05

Date

Edward L. Keller 12/08/05

Date

University of California, Berkeley

Fall 2005

Neural Control Strategies of the Human Focusing Mechanism

by

Shrikant Rajangam Bharadwaj

Abstract

Neural Control Strategies of the Human Focusing Mechanism

by

Shrikant Rajangam Bharadwaj

Doctor of Philosophy in Vision Science

University of California, Berkeley

Professor Clifton M. Schor, Chair

Ocular accommodation, the ability of human eye to change its optical power, operates by changing the curvature of the crystalline lens in response to constriction of the ciliary muscle. The past century has seen important advances concerning the biomechanical properties of the structures involved in accommodation and the changes in these structures that contribute to presbyopia (an age-related diminution in the ability to accommodate). However, there have been limited advances in our knowledge of the neural control of accommodation. For example, we lack information on how neural signals generated in the cortex and mid-brain control the dynamics of accommodation or how these neural signals respond to age-related changes in biomechanics of the accommodative structures. Hence, the present studies investigated the neural control of accommodation (far-to-near focusing) and disaccommodation (near-to-far focusing) step responses and how the neural control altered with the progression of presbyopia. These experiments employed behavioral changes in the first (velocity)- and second-order (acceleration) dynamics as tools to study the neural control of accommodation and disaccommodation. The results showed distinctive differences in the dynamics of

accommodation and disaccommodation. For accommodation, irrespective of the response starting position, peak velocity increased with response magnitude while peak acceleration remained invariant with response magnitude. When analyzed as a function of age, the peak velocity did not change with age while the peak acceleration decreased with age. For disaccommodation, irrespective of the response magnitude, both peak velocity and peak acceleration increased with the proximity of starting position. These results illustrate that accommodation and disaccommodation step responses utilize different neural control strategies. Accommodation responses are initiated towards their desired final destination with the dynamics determined by magnitude of defocus-step stimuli whereas disaccommodation responses are initiated towards an initial (default) destination with the dynamics determined by dioptric separation between the starting position and initial destination. These neural control strategies could be modeled using independent acceleration-pulse and velocity-step innervations that control the dynamics and magnitude of the step response respectively. Overall, these studies demonstrate that accommodation and disaccommodation step responses do not operate with machine-like properties, but rather they utilize different neural control strategies to optimize the response characteristics.

Table of Contents

List of Figures

Chapter III

Chapter IV

Chapter V

Chapter VI

List of Tables

Chapter I

Chapter II

Chapter III

Chapter IV

Chapter V

Chapter VI

Acknowledgements

First and foremost, I would like to thank Amma, Appa and Chibu for their constant love, care and encouragement during my PhD. I would also like thank my wonderful fiancé, Charanya for putting up with all my eccentricities and insanities. Without them, I would not have made this far.

I am grateful to all those who have been responsible for my professional growth. Mike Webster, for introducing me to psychophysics research and for persuading me to apply to the Vision Science graduate program in UC Berkeley. Cliff Schor, for being instrumental in my growth as a graduate student and as a vision scientist. Jim Maxwell, for painstakingly going through all my manuscripts. My lab mates, Chris Cantor, Tere Hernandez, Kai Schreiber, and Zhi-lei Zhang for helping me cope with my programming disabilities. Marty Banks and the entire Banks-lab folks for being good friends and for creating a conducive learning atmosphere. Dr. Pia Hoenig, for allowing me to work for the Binocular Vision clinic that helped me keep up with my clinical skills.

A special thanks to Karthikeyan, Young Kim, Sivaramakrishnan, and Yu Su for allowing me to guide their research projects. Mentoring their research projects gave me a chance to experience what it takes to be a research advisor, atleast on a smaller scale.

Finally, a big thanks to all my other buddies, especially, Raiju Babu, Manikandan Narayanan, and Sridhar Seralathan for helping me succeed despite my own attempts to do otherwise.

Dissertation Introduction

Ocular accommodation can be defined as the ability of the eye to change the conjugate focus of the retina from one object distance to another. The primary purpose of the focusing mechanism is to make the retinal image optically conjugate to the object of interest thus maximizing the spatial information of the retinal image. Focusing is a two-way process, involving an increase in the optical power of the eye when changing from a distant to a near viewing distance (accommodation) and a decrease in optical power of the eye when changing from a near to a distant viewing distance (disaccommodation). Humans accommodate and disaccommodate primarily by changing the anterior surface curvature of the crystalline lens with the aid of the ciliary muscle, choroid and suspensory zonules. Together these structures form the accommodative apparatus (accommodative plant) in human. Important advances have been made in the past two centuries regarding the biomechanical properties of the accommodative plant and their age-related changes (reviewed by Glasser & Kaufman, 2003). These advances have vastly improved our understanding of the mechanics of accommodation and the role played by the accommodative plant in the progression of presbyopia. Our current view of the mechanism of accommodation stems primarily from the works of Helmholtz (1866), Gullstrand (1924) and Fincham (1937). According to Helmholtz's 'Dual Indirect Active' mechanism of accommodation, forces applied to the lens are changed by agonist-antagonist interactions between the ciliary muscle and choroid. These forces are transferred via the suspensory zonules to change the shape of the lens and its capsule (Figure 1). Gullstrand (1924) elaborated on the model by proposing that the choroid as an

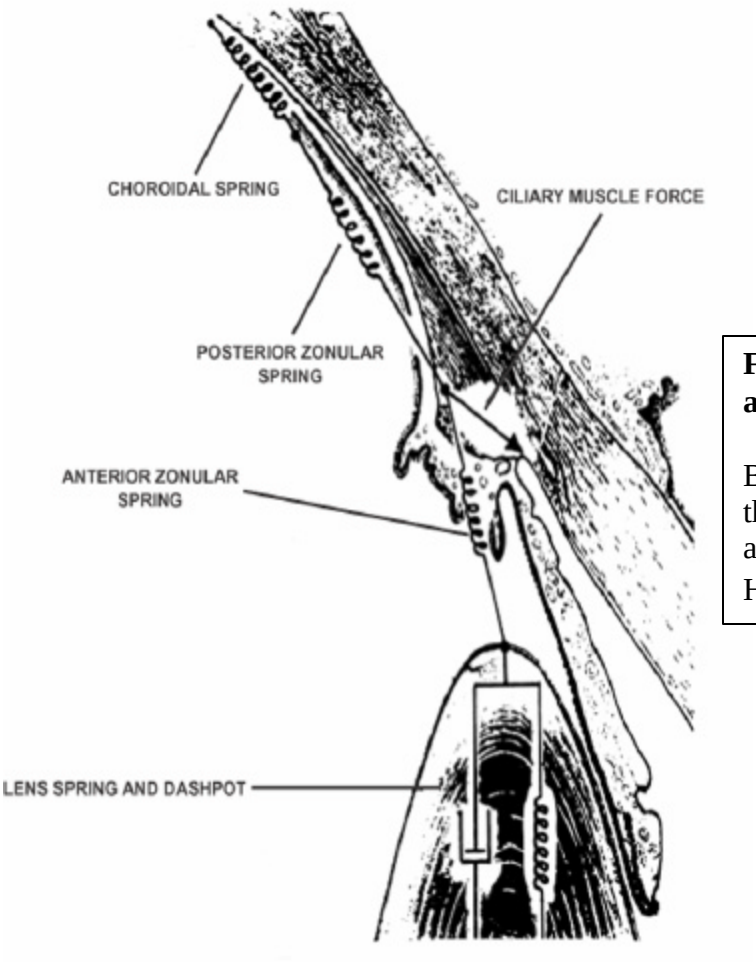

Figure 1. The human accommodative apparatus

Biomechanical correlates for the accommodative apparatus adapted from Beers & van der Heijde, 1994.

antagonist spring to the ciliary muscle. In recent times, Fincham elaborated on the role of the elastic lens capsule in shaping the plastic lens matrix during accommodation. Specifically, during far-to-near accommodation, the ciliary muscle acts as the agonist while the choroid acts as the antagonist. Constriction of the ciliary muscle during accommodation stretches the choroid, releases the zonular tension on the lens, thus increasing the anterior lens curvature. The roles of the ciliary muscle and choroid are reversed during near-to-far disaccommodation: the choroid acts as the agonist while the ciliary muscle acts as the antagonist. During disaccommodation, the elasticity of the choroid pulls the ciliary muscle, increasing the zonular tension on the lens thus flattening the anterior lens curvature.

Advances in our knowledge of the neural control of accommodation and disaccommodation form an integral component in our understanding of the focusing mechanism. Neurophysiological investigations have been our primary source of information about the neural control of accommodation. It is well known that the ciliary muscle is controlled primarily by parasympathetic innervation from the neurons in the Edinger-Westphal (EW) nucleus (Warwick, 1954). Input to the EW nucleus could be derived from a number of areas in the cortex, midbrain and cerebellum that have been identified to control both accommodation and vergence eye movements (reviewed by Gamlin, 2002). Characteristic features of the neurons in these regions could be summarized as follows: one, neurons in the periarcuate region of the frontal eye fields (FEF) exhibit activity related to the sensory-motor transform required to produce accommodation motor responses (Gamlin & Yoon, 2000), two, neurons in the FEF and in the near-response cells of the supra-oculomotor area (SOA) show a transient (phasic) and/or a sustained (tonic) increase in the firing rate that are correlated with the velocity and amplitude of accommodation (Mays *et al*., 1986; Zhang *et al*., 1992; Gamlin & Yoon, 2000), and three, neurons in the nucleus reticularis tegmenti pontis (NRTP) and in the posterior interposed nucleus (IP) modulate their firing rates in response to either changes in accommodation or disaccommodation. Although these studies provide valuable information on the neural circuitry, the functional role of these innervations in controlling accommodation and disaccommodation is still speculative. Questions regarding the patterns of innervation and the control strategies employed by accommodation and disaccommodation step responses and how do the innervational

patterns and control strategies change with age-related changes in the biomechanical properties of the accommodative plant are still unanswered.

The static and dynamic characteristics of a motor response are behavioral manifestations of the neural control strategies employed by the motor system. For example, the extremely fast, yet accurate nature of saccadic eye movements are suggestive that the damping effect of the viscous oculomotor plant is overcome by an initial surge of neural activity (pulse innervation) to produce high response velocities (Robinson, 1973; 1975). The pulse innervation is followed by tonic neural activity (step innervation) that holds the eye in a desired position (Robinson, 1973; 1975). Similarly, constant eye acceleration during the first 20 ms of pursuit eye movement, irrespective of starting position of the stimulus, is suggestive of an initial feedback-independent control in the pursuit motor system (Lisberger & Westbrook, 1985).

The first systematic investigation on the dynamics of accommodation was performed by Campbell & Westheimer (1960). They recorded accommodative responses to a 2 D step change in optical defocus and computed the time taken to complete the step response and the maximum velocity attained during the step response. Since then, a variety of experiments have been conducted to explore the dynamic properties of accommodation under physiological (Schaeffel *et al*., 1993) and pathological conditions (Schnider *et al*., 1984). These studies have characterized accommodation step responses as a first-order system and have described the dynamics in terms of their response duration (Tucker & Charman, 1979; Heron & Winn, 1989; Heron *et al*., 1999; 2001) and peak velocity

(Shirachi *et al*., 1978; Schnider *et al*., 1984; Ciuffreda & Kruger, 1988; Schor *et al*., 1999; Kasthurirangan *et al*., 2003; Mordi & Ciuffreda, 2004). Response duration usually refers to the time constant of the exponential function fit to the accommodative response while the peak velocity refers to the highest value in the velocity profile. In most studies, both the response duration and the peak velocity have been shown to increase with response magnitude (e.g. Tucker & Charman, 1979; Ciuffreda & Kruger, 1988).

Inherent in the description of accommodation as a first-order system is the assumption that accommodation step responses are controlled by a single step change in innervation to the ciliary muscle: the magnitude of the step input increases with the magnitude of the defocus stimulus. This is evident from studies in monkeys that use a step electrical input to stimulate the EW nucleus (Crawford *et al*., 1989; Croft *et al*., 1998; Vilupuru & Glasser, 2002) and from various biomechanical models that use a step signal as input for their accommodation model (Krishnan & Stark, 1975; Beers & van der Heijde, 1994, 1996). However, the assumption of a single step innervation to the ciliary muscle is questioned by two behavioral observations. First, contrary to the prediction that a step increase in innervation proportionally increases the response magnitude, peak velocity and peak acceleration, behavioral data show that only the response magnitude (Morgan, 1944) and peak velocity (Ciuffreda & Kruger, 1988) of accommodation increase with stimulus magnitude while the peak acceleration remains invariant with stimulus magnitude (Bharadwaj & Schor, 2005a). Second, the age-related increases in modulus of elasticity (Fisher, 1971; Krag *et al*., 1997), viscosity (Glasser & Campbell, 1999) and mass (Weale, 1982) of the lens predict that for a given accommodative

stimulus, both the velocity and the acceleration of accommodation should decrease with age. Interestingly however, for defocus stimuli that are within the maximum amplitude of accommodation, only the peak acceleration declines with age (Bharadwaj & Schor, 2005a) while the peak velocity of accommodation does is invariant with age (Heron *et al*., 2001; Mordi & Ciuffreda, 2004; Bharadwaj & Schor, 2005a). Both these observations suggest that the neural input to the ciliary muscle is more sophisticated that a simple step change in innervation.

While discussing accommodation in 1879, Fick wrote, "There is no need to discuss sundry theories of accommodation now that the problem has been solved in its entirety [by Helmholtz]" (quoted by Weale, 1963). The repertoire of behavioral and neurophysiological observations presented so far opens Fick's statement to debate and brings to light how much of the problem is still unresolved. There is a clear need for experiments and analyses that will interpret behavioral data in light of the neurophysiological observations that are documented in literature. The studies presented in this dissertation attempt to achieve this goal by systematically investigating the static and dynamic characteristics of accommodation and disaccommodation and modeling how the neural signals might be organized to control these response characteristics. The first two chapters describe and model (the pulse-step dynamic model of accommodation) the neural control strategies of accommodation step responses and how these strategies might be modified to compensate for the age-related changes in the biomechanics of the accommodative plant. Chapters III and IV describe the neural control strategies of disaccommodation step responses. Chapter V compares and contrasts the neural control

strategies of accommodation and disaccommodation step responses. Finally, Chapter VI employs the pulse-step dynamic model of accommodation that was developed in Chapter II to assess the static and dynamic performance of Accommodating-Intraocular lenses (A-IOL's).

Taken together, the experiments described in this thesis make tow important contributions: first, they illustrate that accommodation and disaccommodation step responses do not operate with machine-like properties but employ interesting neural control strategies to optimize the response characteristics. Second, the pulse-step model of accommodation developed in this thesis can be employed as a useful tool to assess the static and dynamic performance of accommodation under various physiological and experimental conditions.

Chapter I. Dynamic control of ocular accommodation: First- and second-order dynamics

1. Abstract

The static and dynamic characteristics provide valuable information about dynamic control of accommodation. Here, we systematically investigated two first-order properties: peak velocity and time-to-peak velocity (TPV) and two second-order properties: peak acceleration and time-to-peak acceleration (TPA) to step changes in optical defocus. Peak velocity and TPV increased with response magnitude while peak acceleration and TPA remained independent of response magnitude. Independent first-order and second-order dynamic components of accommodation demonstrate that neural control of accommodation has an initial open-loop component that is independent of response magnitude and a closed-loop component that increases with response magnitude.

2. Introduction

Traditionally, accommodation responses to step changes in optical defocus has been described as a first-order control system. Behavioral studies in humans and monkeys describe the dynamics of accommodation step responses using two first-order characteristics: the response duration and the peak velocity. These studies have found both the response duration and the peak velocity to increase linearly with the accommodative response magnitude (Campbell & Westheimer, 1960; Shirachi *et al*., 1978; Tucker & Charman, 1979; Schnider *et al*., 1984; Ciuffreda & Kruger, 1988; Heron & Winn, 1989; Heron *et al*., 1999; 2001; Schor *et al*., 1999; Mordi & Ciuffreda, 2004; *see however,* Kasthurirangan *et al* (2003) for saturation of peak velocity at larger response magnitudes). Similarly, systems engineering and biomechanical models of accommodation describe accommodation step responses with a first-order accommodative plant that is controlled by a first-order neural controller (Toates, 1972; Krishnan & Stark, 1975). However, as indicated by Alvarez *et al*. (1999), the first-order dynamics do not characterize the system in its entirety. Further, the first-order plant, when combined with a first-order neural controller in a negative feedback control system, will have second-order properties (Ogata, 2002). Answers to a number of important questions require a second-order description of the system. For example, a first-order description does not address how the peak velocity of a step response is achieved. The peak velocity could be reached by increasing the peak acceleration in proportion to response magnitude, or by holding fixed peak acceleration for various durations. We can distinguish between these two possibilities by examining the second- order dynamics of the step response.

Another important reason to investigate the second-order properties of the accommodation step response is to gain insight into the neural pattern of innervation to the ciliary muscle. As noted earlier, several studies have assumed that the accommodative step response is controlled by a step change in innervation to the ciliary muscle. Studies on monkeys, in which accommodation was elicited by electrically stimulating the EW nucleus, have used a step input (Crawford *et al*., 1989; Croft *et al*., 1998; Vilupuru & Glasser, 2002). Biomechanical models of accommodation have also assumed a step input to the accommodative system (Krishnan & Stark, 1975; Beers & van der Heijde, 1994, 1996). These studies imply that the amplitude of the step innervation increases proportionally with the size of the accommodative stimulus. This predicts a proportional increase in the peak velocity and peak acceleration with the magnitude of the accommodative response. Both the response magnitude (Morgan, 1944; Toates, 1972) and peak velocity of accommodation (Campbell & Westheimer, 1960; Ciuffreda & Kruger, 1988) are known to increase with the stimulus magnitude; however there is no information concerning the acceleration properties of the system. Information on the acceleration characteristics would provide a test for the step innervation hypothesis.

The main aim of this study was to systematically describe the dynamics of the accommodative step response using two first-order parameters: the peak velocity and time-to-peak velocity (TPV) and two second-order parameters: the peak acceleration and the time-to-peak acceleration (TPA). The variation of each parameter with the response magnitude was analyzed to illustrate how the accommodative step response reaches its peak velocity.

3. Methods

3.1. Subjects

Six subjects (age range: 23 to 35yrs; mean age: 29 yrs) with normal visual and oculomotor functions took part in the experiment. One of the subjects (SRB) was one of the authors. He was aware of the aims of the experiment while the others were naïve observers. Three subjects were ametropic (KB: +1.00 D; RM: -1.00 D; SRB: -1.75 D) and were fully corrected during the experiment. All the subjects took part in the experiment after signing an informed consent form approved by the Center for Protection of Human Subjects (CPHS), University of California at Berkeley.

3.2. Accommodative Stimulus-Response function

Non-linearities in accommodative dynamics are known to occur at the limits of the peak amplitude of accommodation (Shirachi *et al*., 1978). Hence we measured the accommodative stimulus-response function to choose a range of accommodative stimuli that would produce a linear change in accommodative response during measures of the dynamics. A static Badal optometer, which changes the dioptric light vergence subtended by the target while maintaining its angular size (Badal, 1876), was used to measure the stimulus-response function. The apparatus consisted of a point-light-source whose image was collimated when it was positioned 12.5 cm from the Badal lens (+8 D). Subjects' left eye was dilated using 2 to 3 drops of 2.5% Phenylephrine Hydrochloride (PHCL) in order to minimize the effect of depth-of-focus on the amplitude measurements (Ogle & Schwartz, 1959; Tucker & Charman, 1975). Subjects' were instructed to maintain clarity of a row of reduced Snellen targets while bracketing the position of the point light source

until best focus was achieved (Hamasaki *et al.*, 1956). Accommodation was stimulated by introducing negative lenses of powers ranging from 0 D to 11 D in 1 D steps. The amplitude of the accommodative response was calculated from the distance of the point-light-source to the Badal lens, after correcting the subjects' refractive error with lenses. This procedure was repeated three times for each negative lens stimulus.

3.3. Measures of dynamics of accommodation

3.3.1. Recording apparatus

A Generation-V SRI Dynamic Infrared Optometer (Crane & Steele, 1978a, b) was used to stimulate and measure accommodative responses. Optical vergence stimuli were generated using the 'visual stimulus deflector' of the SRI optometer (Crane & Steele, 1978b). The stimulator consists of a positive lens that images a remote target at a point in front of a Badal optometer lens by translating the positive lens along the optic axis of the stimulus optometer. The stimulus to accommodation was determined by the distance of this image point from the anterior focal point of a Badal optometer lens. A Pentium computer, equipped with an A/D and D/A board, drove a motor that controlled the position of this positive lens to produce step changes in defocus over a 6 D range. Accommodative responses were sampled at 200 Hz by the SRI recording optometer, which utilizes the Scheiner principle to monitor the conjugate focus of the eye. The accommodative target was a black and white Maltese cross (Figure 2) centered in a 20? circular aperture of the SRI visual stimulator.

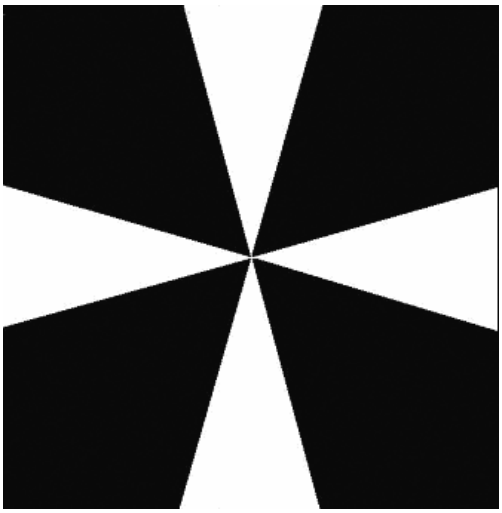

Figure 2. Maltese cross

The black and white Maltese cross was used as an accommodative stimulus for all experiments.

3.3.2. Procedure

The left pupil of each subject was dilated using 2.5% PHCL eye drops until the pupil size was greater than 5 mm to ensure artifact-free recordings of accommodation. Full dilation was achieved 50 to 70 min after drug instillation and was maintained throughout the experimental session, which lasted less than 1 hour. Information on the family history of glaucoma and a measure of the anterior chamber depth using penlight examination was collected prior to dilation. PHCL has been shown to reduce the maximum amplitude of accommodation (Mordi *et al*., 1986a), to reduce the near point of accommodation (Biggs *et al*., 1959) and to slow the accommodative response times (Mordi *et al*., 1986b). However, the drug is expected to influence the static and dynamic response to all stimulus magnitudes equally, thus minimally influencing our results.

All the measurements of accommodation were taken from the left eye while the right eye was occluded. The subjects' refractive correction was placed in the optical path of the

left eye at a point conjugate with the eye's entrance pupil. The subjects' head was positioned in the instrument using a bite bar and a forehead rest.

3.3.3. Calibration trials

Accommodative responses were calibrated using the SRI stimulus optometer. Step changes in dioptric vergence ranged from 0 D to 4 D in 1 D steps and each step stimulus was presented for 4-second duration. The output voltages from the SRI recording optometer were fit with a linear regression calibration equation that was subsequently used to convert optometer output into units of diopters. The calibration was performed on each subject, and it was used on an individual basis for analyzing the data from the test trials.

3.3.4. Test trials

Each experimental session consisted of twenty trials. Every trial contained a single accommodative stimulus and lasted for a period of 4 seconds. Accommodative demands were always within the linear range of accommodation, which was 75% of the stimulus-response function. Table 1 gives the individual accommodative amplitudes of the six subjects who took part in the experiment. Accommodation was stimulated in 0.5 D pseudorandomized steps from 0 D to 4 D in the 4 'young' subjects and 0 D to 3 D in the 2 'older' subjects. Subjects' initiated each trial with a button press following which a defocus stimulus was presented after a randomized delay (0 to 200 ms) to eliminate effects of prediction on the accommodative response. Frequent breaks were provided during the experimental session to prevent the accommodative system from fatiguing.

Lubricating eye drops were administered during the breaks to minimize any corneal irritation caused by refrained blinking during the test trials. Two sessions were conducted on separate days and the data were pooled together for statistical analysis for all subjects except one (SW), for whom only one test session was conducted.

4. Data analysis

4.1. Accommodative stimulus-response function

The static accommodative response to each negative lens power was computed as the average of the three point-source settings. The averaged responses were plotted as a function of the negative lens power (accommodative stimulus) to obtain the accommodative stimulus-response function. The peak region of the stimulus-response function, where the response saturated, defined the amplitude of accommodation.

4.2. Measurement of the dynamics of accommodation

Dynamic accommodative responses (D) to step stimuli were plotted as a function of time. Velocity (D/s) and acceleration (D/s^2) profiles were computed by differentiating the response traces using a 2-point-difference algorithm and subsequently smoothing the data using a 100 ms window. The start and end of the accommodative response were identified using a velocity-criterion algorithm modified after Schor *et al* (1999). The first sample point where the velocity exceeded 0.5 D/s and continued to do so for the next 100 ms was considered the start of the response. Similarly, the sample point where the velocity fell below 90% of the peak velocity and continued to do so for the next 100 ms was considered the end of the response. The start and end of the response computed by

this algorithm was confirmed by visually inspecting the data for each response trace. The difference in dioptric value between the start and end of the response determined the accommodative response magnitude.

Two parameters in the velocity traces were analyzed: peak velocity (D/s) and time-to-peak velocity (ms) of the accommodative response. The peak velocity was obtained from the highest value of the velocity profile. The 'main sequence' relationship was computed by plotting peak velocity as a function of response magnitude. The time-to-peak velocity was the time taken to increase velocity from 0 D/s^2 to the point of peak velocity. Two parameters in the acceleration traces were analyzed: peak acceleration (D/s^2) and time-to-peak acceleration (ms). Peak acceleration was obtained from the highest value of the acceleration profile. Time-to-peak acceleration was the time taken to accelerate from 0 D/s^2 to the point of peak acceleration.

4.3. Measurement of the noise of dynamic accommodation

Noise amplitude in an accommodative response is exaggerated when derivatives are computed. Since our acceleration computation involved differentiating the response profile twice, it was necessary to determine the contribution of the noise amplitude in the acceleration traces. The signal-to-noise (SNR) ratio of the acceleration response was computed and compared for two accommodative states: one in the presence of a non-zero accommodative stimulus (2.5D) and another in the absence of an accommodative stimulus (0D). Twenty accommodative responses, each to a 2.5D and 0D step stimuli, were measured in one subject (SRB) using the same procedure as described in Section

2.3 and averaged to give a single accommodative response. The beginning and end of the response were calculated using the velocity-criterion defined above. To compare the 2.5D & 0D SNR's, the responses were time-locked at the start of the response. The velocity and acceleration profiles were then computed from this averaged response using the same technique described above. The root-mean-square (RMS) noise was calculated from the acceleration data for a 300ms time frame following the end of the response. Every averaged data point in the acceleration trace was subsequently divided by this RMS noise to get a dynamic time-varying acceleration SNR. The SNR's between the 2.5D & 0D response were then compared at the time when the peak acceleration occurred in the 2.5D response.

5. Results

5.1. Accommodative stimulus-response function

The accommodative stimulus-response curve (*not shown*) had the characteristic sigmoid-shape for all our subjects (Morgan, 1944). The amplitudes of accommodation ranged from 8.9 D to 4.1 D across our subjects (Table I) and we selected the range that produced a linear increase in response size to investigate the dynamics of accommodation. Since our primary interest in measuring the accommodative amplitude was only to determine the linear portion of the stimulus-response function, no further statistical analysis was performed on this set of data.

5.2. Measurement of the dynamics of accommodation

Examples of a typical position, velocity and acceleration traces of accommodation for 2.5 D and 0 D step changes in optical vergence are shown in Figure 3a-c. The position traces (Figure 3a) showed a characteristic latency period (approximately 300 ms) followed by a smooth and steady increase until the steady state was achieved. The accommodative response magnitudes increased with the step-stimulus magnitudes. First-order and second-order dynamic characteristics of accommodation were plotted as a function of these response magnitudes in figures 4, 5, 7, 8 & 10.

Figure 3b showed a smooth increase in the velocity during the beginning of the response until the peak velocity was reached. This was followed by a gradual reduction in the velocity to a steady state position. An asymmetry in the rising and the falling portions of the velocity curve was observed in most of the responses. The rising portion of the curve was much steeper than the falling portion. This reflects the presence of an abrupt acceleration phase that was followed by a very gradual deceleration phase in the accommodative response. Since the slopes of the rising and the falling portions of the velocity curve are well represented by the acceleration and deceleration components respectively, no quantitative analysis of the velocity slopes was performed. The peak velocity showed a strongly correlated and statistically significant increase with the response magnitude in each subject (Student's T-test; p-value: <0.001). Five of our six subjects had a main sequence slope ranging from 0.72 s^{-1} – 1.23 s^{-1} while the slope for the one remaining subject (SW) was 1.76 s^{-1} (Table I). Since the main sequence relationship for subject SW contained fewer data points and was more variable than the rest of the

subjects, a combined linear regression equation was fit through the data of the remaining five subjects (y = 1.58x + 3.52) (Figure 4).

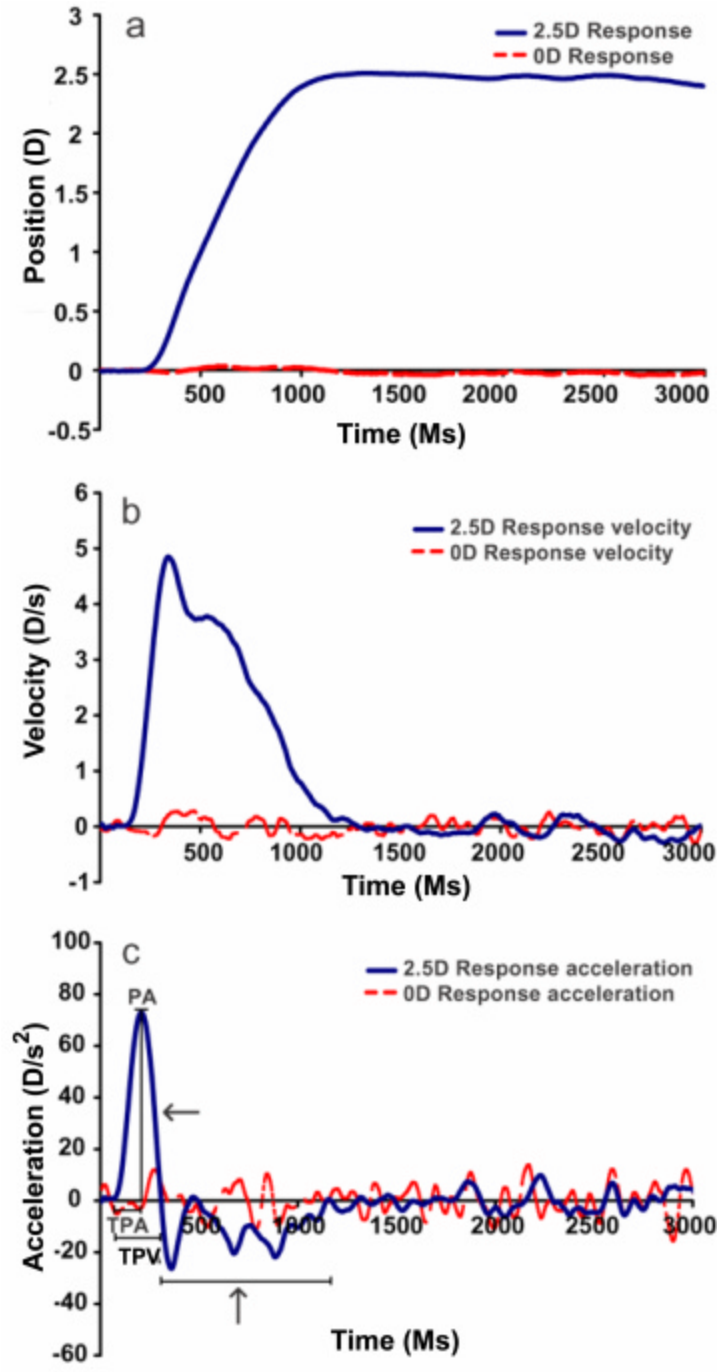

Figure 3. Typical accommodative position (a), velocity (b) and acceleration (c) traces plotted as a function of time

Each trace is an average of 20 recordings. In figure 2a, the step-stimulus was presented at time 0 ms and the response started after a latency period of approximately 300 ms. Leftward-pointing arrow: acceleration phase; upward-pointing arrow: deceleration phase; PV: peak velocity (D/s); PA: peak acceleration (D/s^2); TPA: time-to-peak acceleration (ms); TPV: time-to-peak velocity (ms).

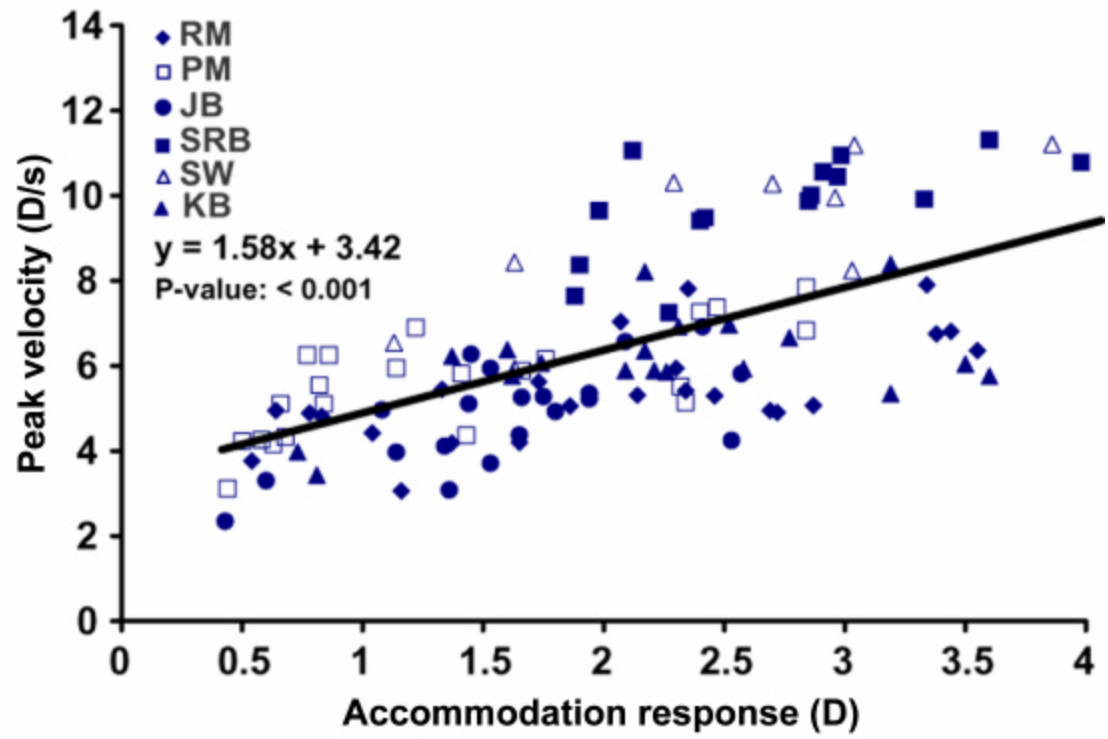

Figure 4. 'Main sequence' relationship (peak velocity as a function of response magnitude)

The peak velocity of accommodation showed a statistically significant increase with the response magnitude for all subjects. The solid line plotted through the data points represents the combined linear regression fit (y = 1.58x + 3.42) for all the data points of five subjects (except SW). The data of subject SW is superimposed along with the other data points for comparison purposes.

The time-to-peak velocity was the time taken to increase velocity from 0 D/s^2 to the point of peak velocity. The time-to-peak velocity correlated very well with the end of the acceleration phase of the response (Figure 5) (r^2: 0.99). The slope and y-intercept of the linear regression equation describing the relationship between the two parameters were o.98 and 0.90 respectively. These observations suggest that the terms time-to-peak velocity and total duration of acceleration could be used interchangeably. A moderately correlated (r^2: 0.45 to 0.55) increase of the time-to-peak velocity with the response

magnitude was seen for all our subjects (Figure 6a-f, Table I). The slopes of the linear regression fits ranged from 24.03 ms/D to 41.8 ms/D across our subjects and they were statistically significant from zero (Student's T-test; p-value: <0.01) (Figure 6a-f).

The acceleration traces showed a very prominent acceleration phase and a less conspicuous deceleration phase (Figure 3c). Figure 7a-f shows the peak acceleration plotted as a function of the response magnitude for each subject. Linear regression equations fit separately to each data set showed a small non-zero but statistically insignificant difference from zero slope (Student's T-test; p-value: >0.7). The mean peak accelerations ranged from 44.5 D/s^2 to 89.9 D/s^2 with standard deviations varying from

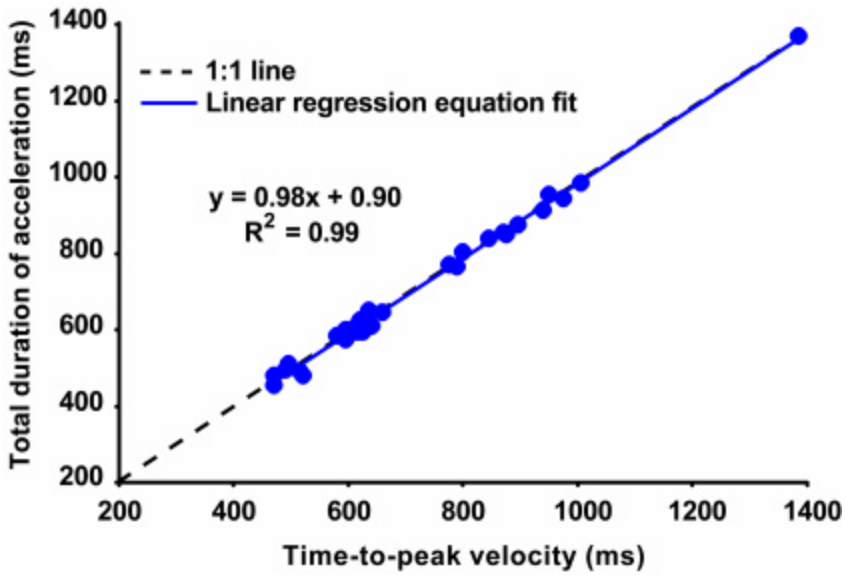

Figure 5. Total duration of acceleration plotted as a function time-to-peak velocity

The total duration of acceleration was correlated very well with the time-to-peak velocity (r^2: 0.99). The slope and y-intercept of the linear regression equation were 0.98 and 0.90 respectively indicating near-perfect correspondence of the two parameters. The data illustrated is from one subject (SRB). All the subjects showed the same trend as SRB.

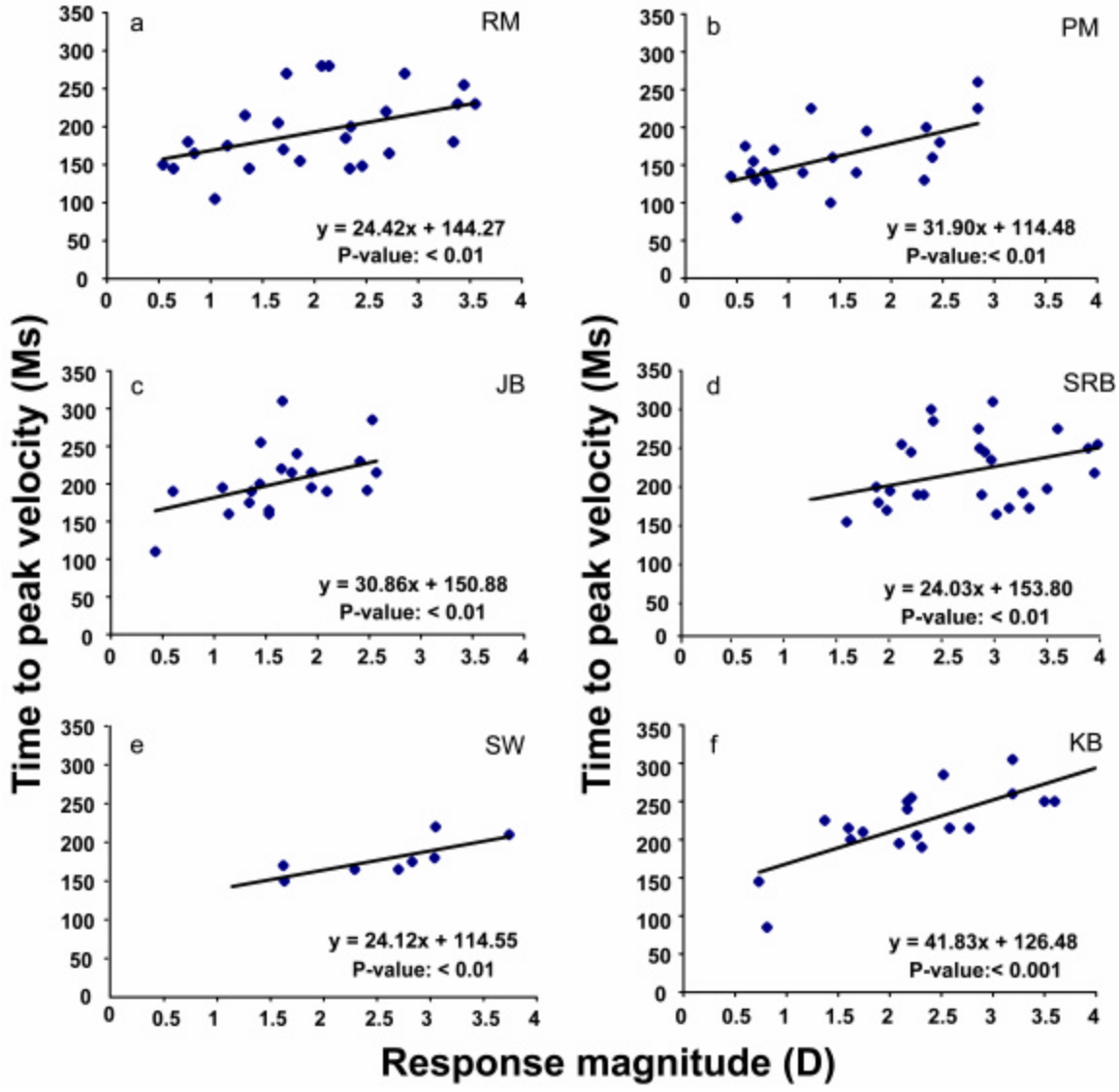

Figure 6. Time-to-peak velocity plotted as a function of response magnitude

Time-to-peak velocity increased proportionally with the response magnitude. The solid line fit through the data points represents the linear regression fit.

10% to 20% of the mean across all the subjects (Figure 8). Similar to the peak acceleration, the time-to-peak acceleration also did not change with the response magnitude. Slopes of the linear regression equation fit separately to each subject's data did not reveal any statistically significant change of the time-to-peak acceleration with the response magnitude (Student's T-test; p-value: >0.7) (Figure 9a-f). The mean time-to-

peak acceleration ranged from 83 ms to 120 ms with a standard deviation ranging from 15% to 25% of the mean for all the subjects (Figure 8). Table II presents the individual mean and standard deviations of the peak acceleration and time-to-peak acceleration as a function of the response magnitude for all the subjects.

	Accommodative Amplitude (D)	**Main Sequence Equation**	**TPV Eq.**
KB	4.08	y = 0.72 x + 4.51	y = 41.83 x + 126.48
JB	4.32	y = 1.23 x + 2.79	y = 30.86 x + 150.88
PM	6.47	y = 1.07 x + 4.51	y = 31.90 x + 114.48
SW	6.73	y = 1.76 x + 4.75	y = 24.12 x + 114.55
RM	7.49	y = 0.83 x + 3.74	y = 24.42 x + 144.27
SRB	8.94	y = 1.07 x + 6.81	y = 24.03 x + 153.80
RM (Defocus + Size)	7.49	y = 0.86 x + 5.26	y = 14.48 x + 154.07

Table I. Maximum amplitude of accommodation, main sequence linear regression equation and time-to-peak velocity (TPV) linear regression equation for all subjects who took part in the defocus-only condition and for one representative subject in the combined defocus + size condition. Variables ‘y’ and ‘x’ in the main sequence relationship denote peak velocity and response magnitude respectively. The slopes of the main sequence and TPV linear regression equations were statistically significantly different from zero at the 99% confidence level.

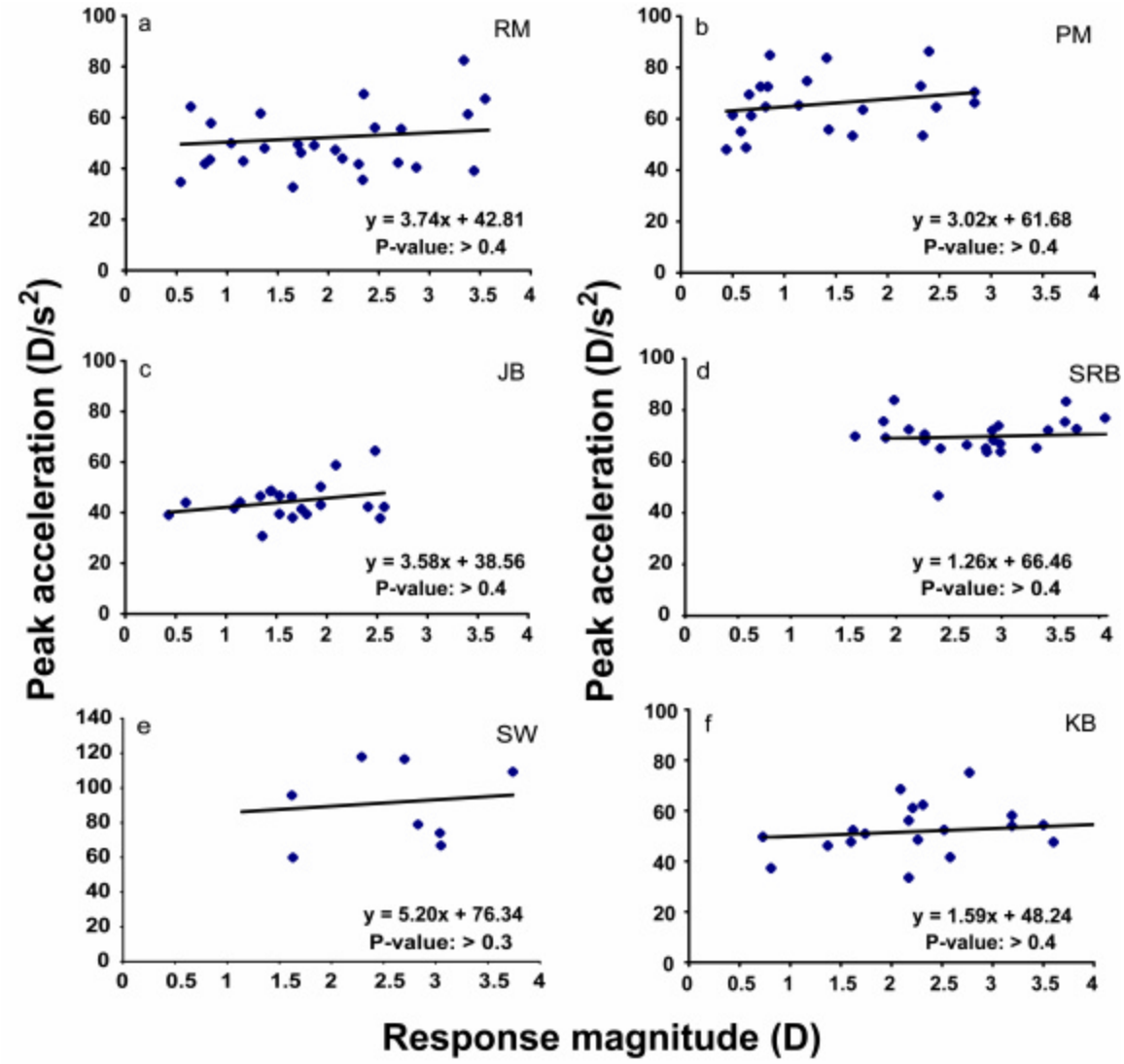

Figure 7. Peak acceleration as a function of response magnitude

The solid line fit through the data points represents the linear regression fit. The slopes of the linear regression equation did not vary significantly from zero indicating that the peak acceleration remained independent of the response magnitude.

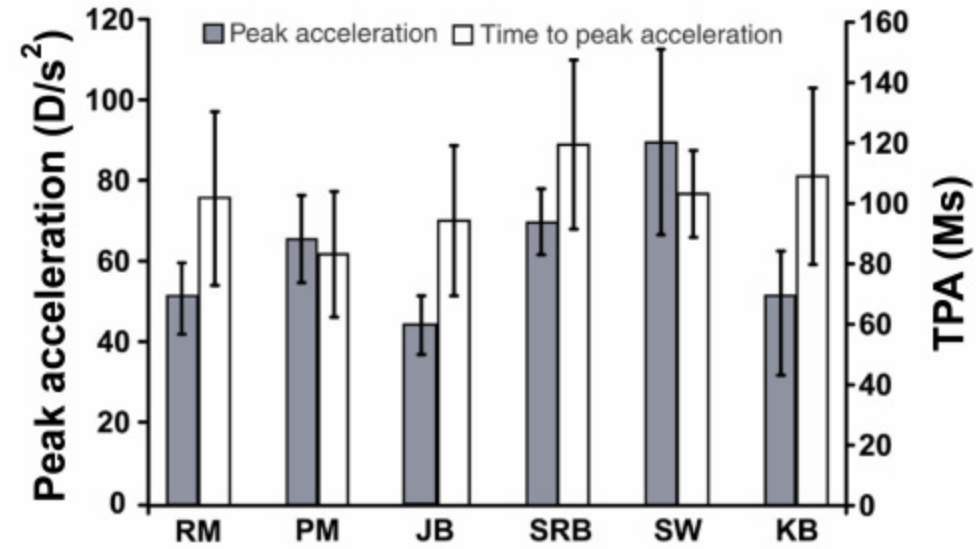

Figure 8. Mean peak acceleration and time-to-peak acceleration for each subject

The solid symbols and the left y-axis represent peak acceleration and the open symbols and the right y-axis represent time-to-peak acceleration (TPA). Error bars in each symbol show +/- 1 standard deviation.

	PA (D/s^2)	TPA (ms)
KB	51.94 +/- 10.91	109.00 +/- 39.19
JB	44.47 +/- 07.30	94.29 +/- 34.90
PM	65.88 +/- 10.85	83.18 +/- 30.80
SW	89.93 +/- 23.03	103.13 +/- 14.38
RM	50.17 +/- 12.04	101.9 +/- 36.28
SRB	70.13 +/- 08.19	119.47 +/- 27.98
RM (Defocus + Size)	69.06 +/- 13.87	111.20 +/- 33.77

Table II. Peak acceleration (PA) and Time-to-peak acceleration (TPA) for all subjects who took part in the defocus-only condition and for one representative subject in the combined defocus + size condition.

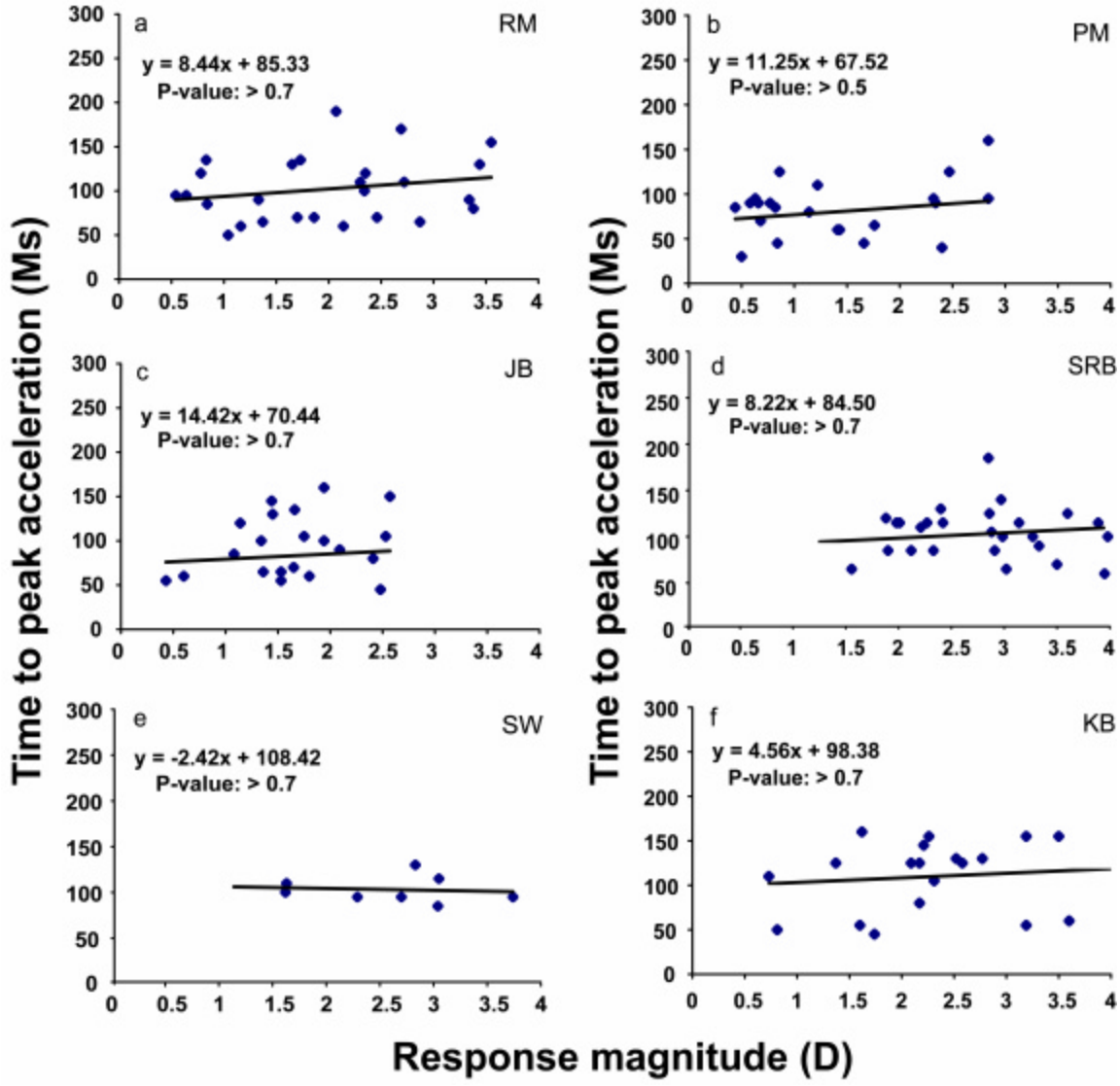

Figure 9. Time-to-peak acceleration plotted as a function of response magnitude

The solid line fit through the data points represents the linear regression fit. The slopes of the linear regression equation did not vary significantly from zero indicating that the time-to-peak acceleration remained independent of the response magnitude.

5.3. Signal to noise ratio for dynamic accommodation

Figure 9 shows the dynamic time-varying acceleration SNR for the 2.5 D & 0 D conditions. For the averaged 2.5 D response, we observed a RMS value of 1.83 D/s^2 and a high SNR (19.9:1) at the time when the peak acceleration occurred. For the averaged 0

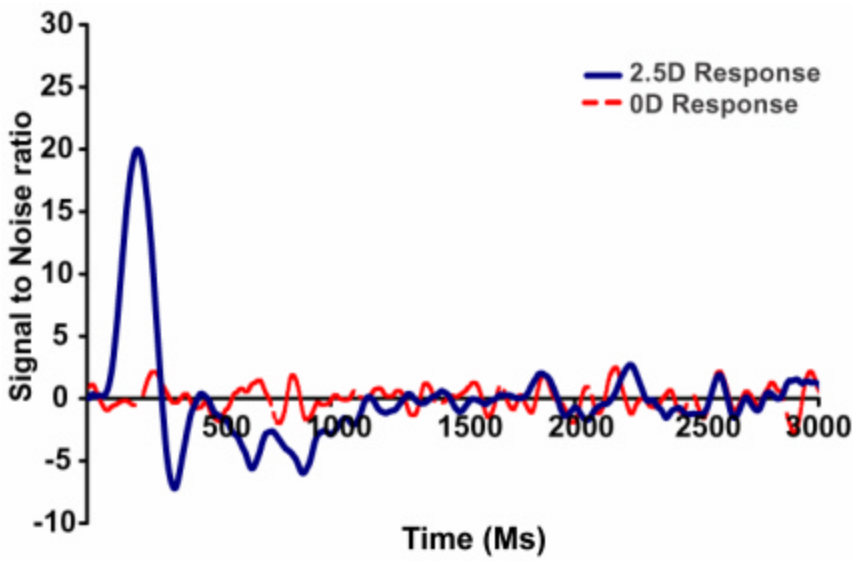

Figure 10. Signal-to-noise ratio (SNR) for acceleration plotted as a function of time

The data shows the presence of a high SNR (19.9:1) at the time when peak acceleration occurs for the 2.5D response and an insignificant SNR (1.5:1) for the 0D response at the same point in time.

D response, the RMS value was similar (2.78 D/s^2) but the SNR (1.5:1) was lower than the 2.5 D response at the same point in time when the peak acceleration occurred.

6. Measures of the dynamics of accommodation to combined defocus and size changes

In the previous experiment, accommodation responded solely to step changes in retinal image defocus. Distance cues of retinal-image disparity and size were eliminated by monocularly viewing the Maltese cross through the SRI Badal optometer. Defocus *per se* has been deemed an insufficient cue for estimating both the magnitude and direction (far vs. near) of accommodation (Fincham, 1951; Campbell & Westheimer, 1959), especially when the defocus magnitude is greater than 2D (Crane, 1966). Hence, it is

possible that, in our earlier experiment, constant peak acceleration resulted from a constant distance estimate by the accommodative system due to the non-availability of reliable magnitude-estimation cues. Thus, the main aim of this experiment was to determine if the accommodative responses showed similar constant second-order dynamics, independent of the response magnitude, when the magnitude-estimation of distance was made more salient by coupling a step change in defocus with a proportional step change in target size.

Five of the six subjects (except subject SW) took part in this experiment. Accommodation defocus stimuli ranged from 1 D – 5 D in 0.5 D pseudo-randomized steps. The defocus change was electronically coupled with the angular size-change of a black and white Maltese cross generated on a CRT screen using the Visual Stimulus Generator graphics board (Cambridge Research Systems Limited). The angular size that the Maltese cross subtended at the entrance pupil of the eye was 1.25° at an optical distance of 100 cm (1 D) and the target was magnified at the rate of 1.25°/D. All other data acquisition and data analysis procedures were similar to the first experiment.

The results for the defocus + size condition showed similar trends as observed in the defocus-only condition. Figure 10a-d and the bottom row of Table I & II show the data obtained from one typical subject (RM). The peak velocity of accommodation increased with the response magnitude ($y = 0.86x + 5.26$) by a statistically significant amount (Student's T-test; P-value: <0.001) (Figure 10a). The peak acceleration remained constant with the response magnitude (mean +/- SD: 69.06 +/- 13.07 D/s^2). The slope of the linear

regression equation of the peak acceleration as a function of the response magnitude did not vary significantly from zero (Student's T-test; P-value: >0.7) (Figure 10b). The time-to-peak acceleration also remained constant with the response magnitude (mean +/- SD: 111.2 +/- 33.77 ms) (Figure 10c). The slope of the linear regression equation of the time-to-peak acceleration as a function of the response magnitude did not vary significantly from zero (Student's T-test; P-value: >0.7). The time-to-peak velocity showed a significant increase with the response magnitude (Figure 10d). The slope of the linear

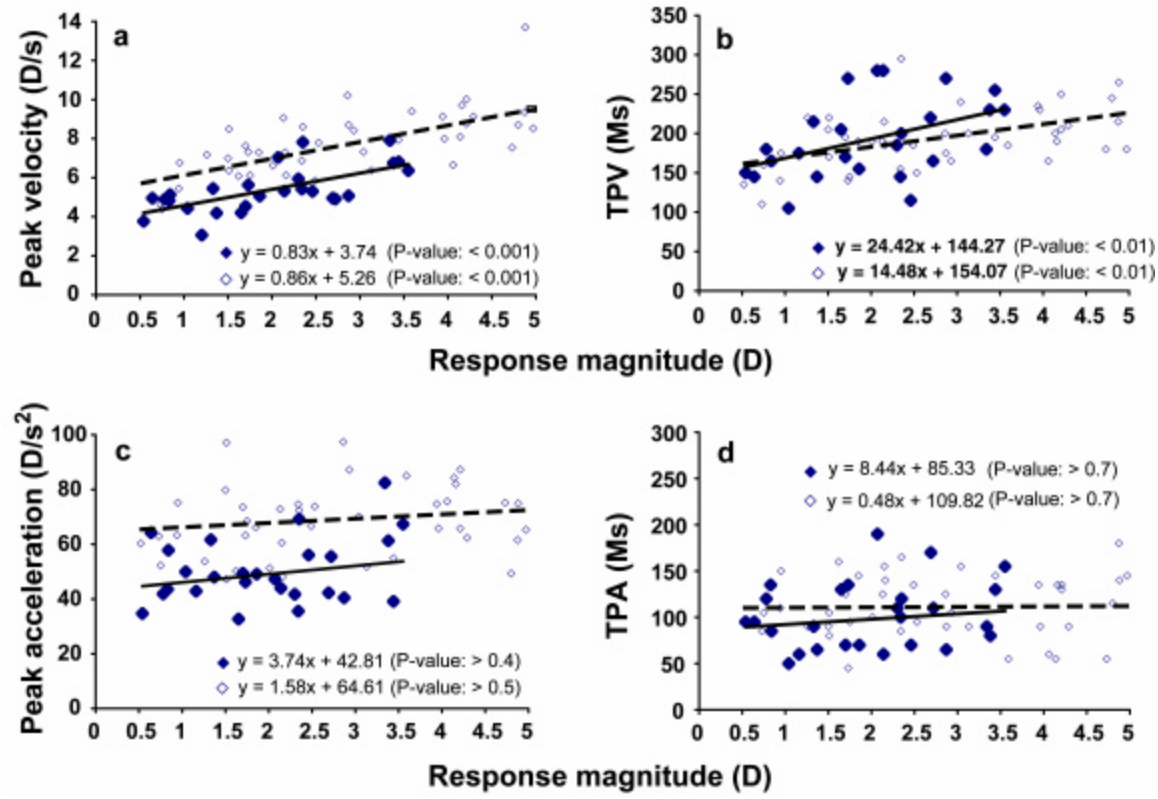

Figure 11. First-order and second-order dynamics for a representative subject (RM) in the combined defocus + size condition and defocus-only condition

a) Peak velocity as a function response magnitude. b) Time-to-peak velocity (TPV) as a function of response magnitude. c) Peak acceleration as a function of response magnitude. d) Time-to-peak acceleration (TPA) as a function of response magnitude. The open symbols and dashed linear regression line represent the combined defocus + size data. The closed symbols and solid linear regression line represents the defocus-only data.

regression equation for the time-to-peak velocity as a function of response magnitude (14.48 ms/D) was statistically different from zero (Student's T-test; P-value: <0.01).

The coefficients (slopes and intercepts) of the linear regression equation to the 'main sequence' relationship for the defocus + size condition were compared to the coefficients of the linear regression equation obtained from of the defocus-only condition using a T-test measure that compares the slopes and intercepts of two straight lines (Kleinbaum *et al*., 1998). The slopes of the 'main sequence' relationship for the defocus + size condition (0.86 s^{-1}) and the defocus-only condition (0.83s^{-1}) did not differ significantly from each other (P-value: >0.7). However, the intercepts differed significantly (P-value: <0.01) in the two conditions (defocus + size condition; 5.26 D/s; defocus-only condition: 3.74 D/s) revealing a higher velocity of the step response when size and defocus were combined than in the defocus-alone condition (Figure 10a).

The mean peak acceleration was higher in the defocus + size condition (69.06 +/- 13.07 D/s^2) than in the defocus-only condition (50.17 +/- 12.04 D/s^2). The slopes of the linear regression equations for the peak acceleration as a function of response magnitude in the defocus + size condition and defocus-only condition did not differ significantly from each other (P-value: >0.7). However, the intercepts differed significantly (P-value: <0.01) in the two conditions (defocus + size condition: 64.61 D/s^2; defocus-only condition: 42.81 D/s^2) revealing a higher peak acceleration of the step response when size and defocus were combined than in the defocus-alone condition (Figure 10b).

No statistically significant difference in the mean time-to-peak acceleration was noted in the two conditions (defocus + size condition: 111.2 +/- 33.77 ms; defocus-only condition: 101.9 +/- 36.26 ms). The slopes and intercepts of the linear regression equation for the time-to-peak acceleration as a function of response magnitude did not differ significantly in the two conditions (P-value: >0.5) (Figure 10c). The slope of the linear regression equation for the time-to-peak velocity as a function of response magnitude was shallower in the defocus + size condition (14.48 ms/D) than in the defocus-only condition (24.42 ms/D) and the slopes were significantly different from each other (P-value: <0.05). However, the intercepts did not differ significantly from each other (P-value: >0.3) (Figure 10d). The longer duration of acceleration in the defocus-alone condition is associated with a lower peak acceleration to yield a lower peak velocity and peak acceleration than in the combined defocus + size condition. In summary, this analysis illustrates an enhancement of the first-order and second-order dynamics of accommodation in the defocus + size condition and that peak acceleration and time-to-peak acceleration are independent of the response magnitude of accommodation, even when size-distance cues are presented in the stimulus.

7. Discussion

Prior studies of the dynamics of accommodation have been restricted to the first-order properties of the system. As indicated by Alvarez *et al*. (1999), the response time constant and peak velocity do not provide a complete representation of the dynamics of the system. The present study has characterized the acceleration properties of the

accommodative step response. Our results can be summarized by the following three points:

1. The peak acceleration remains constant as the peak velocity increases with the response magnitude over the measured range of response magnitudes.
2. The time-to-peak acceleration remains constant as response magnitude increases
3. The time-to-peak velocity increases with the response magnitude

These results answer a question that is not addressed by the 'main sequence' relationship: how does the accommodative system increase its peak velocity with response magnitude? We observed that the peak velocity is achieved by increasing the time-to-peak velocity with the response magnitude, as opposed to changing the amplitude of peak acceleration.

7.1. Influence of noise on the acceleration traces

Noise present in the accommodation position traces can originate from a number of different sources: noise from the accommodative plant, neural noise and noise from the measurement apparatus. Since the magnitude of noise is known to increase with the process of differentiation, it can be difficult to distinguish noise from acceleration signals. The RMS value was calculated for a time period of 300 ms following the end of the response and it was used as an indicator of the total noise from all sources. A high signal-to-noise ratio of 19.9:1 obtained for the 2.5 D response indicates that the peak acceleration was 19.9 times greater than the average noise fluctuations. The RMS value for the 0 D response (2.78 D/s^2) was only marginally higher than that for the 2.5 D

response (1.83 D/s^2) indicating that the acceleration noise fluctuations did not change significantly during the accommodative step response. If we assume that the noise level remained constant across all response magnitudes, then the noise fluctuations only contributed between 4.12% and 2.04% to the peak acceleration that ranged between 44.5 D/s^2 and 89.9 D/s^2 respectively across our subjects. Thus, it is safe to conclude that random noise fluctuations have minimal influence on the peak acceleration data that were obtained in our experiment.

7.2. Effect of size and defocus change on dynamics of accommodation

We tested the possibility that the constant amplitude of the early open-loop phase of acceleration seen in the defocus-only experiment was due to a lack of sufficient distance cues to form a reliable estimate of defocus magnitude. Target-size change was coupled with the defocus to provide a robust cue to estimate the distance cue for accommodation. We observed higher values for peak velocity and peak acceleration with the added size cue even though the response amplitude in either condition did not increase with stimulus magnitude. This result demonstrates that first-order and second-order properties of the step response increase with the salience of the distance cue to accommodation. However, as with the defocus-only condition, combined size and defocus produced a peak acceleration and time-to-peak acceleration that remained constant as step response magnitude increased. This indicated that the non-availability of reliable defocus-magnitude estimation cues was not responsible for the constant of the peak acceleration and time-to-peak acceleration in the first experiment.

7.3. Innervation to the accommodative system

The innervation to the accommodative system has been modeled as a single step-input to the ciliary muscle and the size of the step is increased proportionally with the accommodative stimulus magnitude (Toates, 1972; Krishnan & Stark, 1975; Beers & van der Heijde, 1994, 1996). Such a step-increase in innervation predicts a proportional increase in both the peak velocity and peak acceleration with the accommodative response magnitude. However, we observed that only peak velocity increased proportionally with the response magnitude while the peak acceleration was invariant as response magnitude increased. This relationship was observed even when the saliency of the distance cue was enhanced. The independent control of the first-order and second-order dynamics suggests there is a dual-innervation input to the accommodative step response. The constant peak acceleration and time-to-peak acceleration demonstrates that there is an initial open-loop innervation component that is invariant with the response magnitude and that it is combined with a closed-loop innervation component that changes proportionally with the response magnitude.

The dual-innervation input for the accommodative step response is also suggested by interactions between saccades and accommodation (Schor *et al*., 1999). The peak velocity of accommodation is enhanced when it is accompanied by a saccade even though the response magnitude remains unchanged. This observation is contrary to the single step-position input, which would predict an enhancement of both the position and velocity of the accommodative response in the presence of a saccade.

7.4. 'Main Sequence' relationship: agreement with previous experiments

The peak velocity of accommodation increased linearly with the response magnitude over the range of stimulus magnitudes tested. The combined linear regression slope for the five subjects (except subject SW) was 1.58 s^{-1}, while the individual slopes ranged from 0.72 s^{-1} to 1.76 s^{-1}. The linear increase in the peak velocity with response magnitude is in agreement with the behavioral observations of voluntary and reflex accommodation to step changes in optical vergence by Ciuffreda & Kruger (1988) and EW nucleus stimulated accommodation by Vilupuru & Glasser (2002).

Our results differ from those of Kasthurirangan *et al* (2003) in that we did not observe a saturation of the peak velocity at higher response magnitudes. Kasthurirangan *et al* (2003) observed that the peak velocity of accommodation saturated at response amplitudes larger than approximately 3 D – 3.5 D. In contrast, we found that peak velocity of accommodation increased linearly over the same response range. Differences in the range of accommodative stimuli used in the two studies could explain the difference in results. In our study, the accommodative stimulus range (0 D – 4 D) was designed to lie within the linear range of the accommodative stimulus-response function. However, the accommodative stimulus range (1 D – 7 D) used by Kasthurirangan *et al* (2003) included the soft-saturation limits of the accommodative stimulus-response function in five of their eight subjects (see figure 5 in Kasthurirangan *et al*., 2003). As pointed out by the authors, accommodative dynamics are known to exhibit non-linearities at the limits of the maximum amplitude of accommodation (Shirachi *et al*., 1978). Hence

it is likely that non-linear saturation effects could have caused the peak velocities measured by Kasthurirangan *et al*. to saturate at larger response magnitudes.

7.5. Are the acceleration dynamics unique to the accommodative system?

Accommodation is not the only oculomotor sub-system that exhibits independent control of peak velocity and peak acceleration. The saccadic and the pursuit eye-movement systems have acceleration characteristics similar to those of the accommodative system. Collewijn *et al* (1988) systematically studied the first-order and second-order dynamics of human saccadic eye movements. The authors analyzed the acceleration dynamics using two parameters: the time taken to reach the peak velocity and the initial slope of the velocity profiles. These parameters are equivalent respectively to the time-to-peak velocity and the peak acceleration analyzed in our study. They observed that the time to reach peak velocity increased proportionally with the response magnitude while the initial velocity slope (acceleration) remained constant with the response magnitude. These results are consistent with our observations of the accommodative system. Lisberger & Westbrook (1985) studied first-order and second-order dynamics of pursuit eye movement initiation to step-ramp stimuli in rhesus monkeys. They observed that in the first 20 ms following pursuit initiation, the eye acceleration was independent of the initial position and velocity of the moving stimuli. This suggested there was an early open-loop component of pursuit initiation. It thus appears that the constant peak acceleration property of the accommodative step response is a general characteristic of many oculomotor sub-systems and it is not unique to the accommodative system.

8. Conclusion

This study demonstrates that step changes in optical defocus result in accommodative responses whose magnitude and peak velocity increase with the stimulus magnitude while the peak acceleration remains constant. The peak velocity of accommodation is controlled by the duration of acceleration and not by the amplitude of acceleration. The independent control of first-order and second-order dynamics of accommodation are contrary to the predictions of a simple step-position input and suggest that there is a dual-innervation input to the accommodative step response: an open-loop component that is independent of the response magnitude and a closed-loop component that increases proportionally with the response magnitude.

Chapter II. The pulse-step model of accommodation dynamics

1. Abstract

We have developed a dynamic model of accommodation that combines independent phasic-velocity and tonic-position neural signals to control position, velocity and acceleration properties of accommodative step responses. Phasic and tonic signals were obtained from neural integration of a fixed-height acceleration-pulse and variable-height velocity-step respectively to control independent acceleration and velocity properties of the step response. Duration and amplitude of the acceleration-pulse are increased with age to compensate for age-related increases of visco-elastic properties of the lens to maintain youthful velocity. The model illustrates a neural control strategy that is similar to the classical neural control model of step changes by the saccadic and vergence systems.

2. Introduction

Ocular accommodation, the focusing mechanism of the human eye, operates by changing the shape of the crystalline lens in response to constriction of the ciliary muscle. Forces applied to the lens are changed during accommodation by agonist-antagonist interactions between the ciliary muscle and choroid respectively (Helmholtz, 1866). These forces are transferred via the suspensory zonules (zonular springs) to the lens and its capsule (Figure 11a, b, adapted from Beers & van der Heijde, 1994). This general scheme of the accommodative plant has been elaborated upon in static (Stark, 1987; Wyatt, 1988) and dynamic (Beers & van der Heijde, 1994, 1996) biomechanical models of accommodation. These models have been used to describe how age-related changes in biomechanics of the plant contribute to the reduction in the amplitude of accommodation (presbyopia).

Age-related changes in the biomechanics of the accommodative plant include an increase in the modulus of elasticity of the lens capsule in the operating range near the full amplitude of the accommodative response (Krag *et al*., 1997) and an increase in the viscosity of the lens (Glasser & Campbell, 1999). Interestingly, the velocity of accommodative responses to step changes in optical vergence remains the same within a linear range for young and old eyes that have the capacity to accommodate (Heron *et al*., 2001; Heron, Charman & Gray, 2002; Mordi & Ciuffreda, 2004). How does the velocity of the accommodative-step response remain unaffected by the age-related changes in the biomechanics of the accommodative plant? We developed a model that uses independent acceleration-pulse and velocity-step signals that are neurally integrated to phasic-velocity

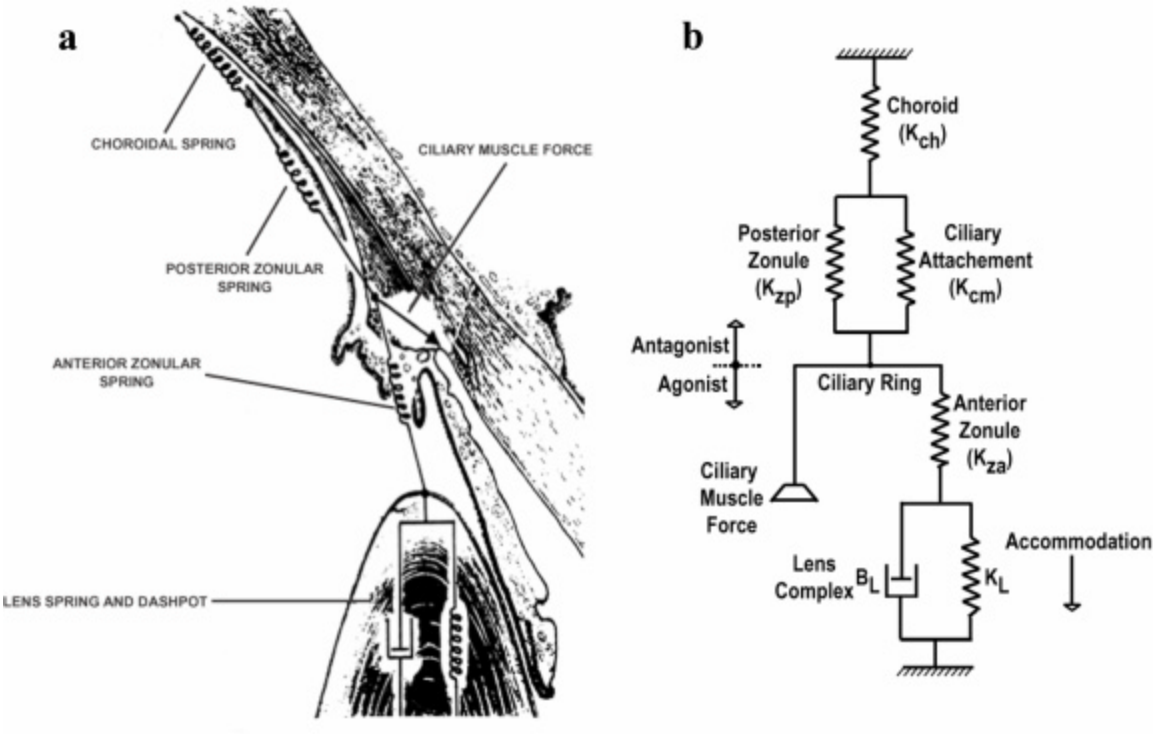

Figure 12. The accommodative apparatus in humans (a) and the lumped biomechanical model of the accommodation plant (b).

(a). Anatomical correlates for the Helmholtz-Gullstrand static model of accommodation. A viscous element is included in the lens to illustrate the plant for the dynamic model of accommodation. (b). Agonist components in the lumped biomechanical model include the anterior zonules, lens-capsule complex. Antagonist components include the choroid spring, ciliary muscle attachment to the choroid, and posterior zonules.

and tonic-position signals. Phasic activity is related to acceleration and velocity components of the response and it refers to neural activity that only occurs during the movement. Tonic activity holds the final position of the response and refers to neural activity that occurs during and after the completion of the movement. This model illustrate how the neural pattern of innervation to the ciliary muscle could be adjusted to compensate for age-related changes in the biomechanics of the plant in order to maintain high velocity step responses of accommodation in the incipient stages of presbyopia.

2.1. Independent control of velocity and acceleration of the accommodative-step response

Three observations suggest that there is independent control of position, velocity and acceleration properties of the accommodative-step response. First, within a given age group, the first-order (velocity) and second-order (acceleration) dynamics of the accommodative-step response change differently with response magnitude. The peak velocity of accommodation increases with response magnitude (Campbell & Westheimer, 1960; Ciuffreda & Kruger, 1988; Kasthurirangan *et al*., 2003), ['main sequence' relationship (Bahill *et al*., 1975)], while the peak acceleration and the time-to-peak acceleration of accommodation remain constant (invariant) of response magnitude (Bharadwaj & Schor, 2005a). Second, only the peak acceleration of accommodation declines with age (Bharadwaj & Schor, 2005a) while the peak velocity remains constant within the linear range of accommodation (Heron *et al*., 2001; Heron *et al*., 2002; Mordi & Ciuffreda, 2004; Bharadwaj & Schor, 2005a). This is surprising given that there is an age-related increase in the visco-elastic properties of the accommodative system (Wyatt, 1993; Beers & van der Heijde, 1996) that could cause a reduction in both the velocity and acceleration of the accommodative-step response. Third, the peak velocity and acceleration of a fixed amplitude accommodative-step response are greater during a saccade than when the eye is stationary (Schor *et al*., 1999) illustrating that the relationship between peak velocity and response magnitude is not invariant.

A simple feedback control system model of accommodation would predict that if there were a single tonic-step innervation to accommodation, then both the peak velocity and the peak acceleration would increase with response amplitude and they would be

affected similarly by age-related changes of the biomechanics of accommodation. The constant peak acceleration and the time-to-peak acceleration properties observed for the accommodative-step response (Bharadwaj & Schor, 2005a) argue against this and suggest the existence of independent phasic and tonic control signals for step changes of accommodation. In our model of dynamic accommodation, a feedback independent (open-loop) phasic-velocity signal is combined with a closed-loop tonic-position signal that holds the final response after it is completed. The independent phasic and tonic components allow peak acceleration to be independent of response amplitude. The model proposes that the open-loop phasic velocity signal is adjusted to compensate for age-related changes in the visco-elastic properties of the accommodative system.

2.2. Motor commands for accommodation

Oculomotor systems, such as saccades, guide step changes in eye position with phasic-velocity signals that are integrated to tonic-position signals in the brainstem (Robinson, 1975; Fukushima *et al*., 1992). These velocity and position signals are combined in the final common pathway to produce high-velocity motor step responses. Is there an analogous organization of control signals for the accommodative step response? Cortical and subcortical pathways are involved in the control of accommodation and vergence. The periarcuate region of the cortical frontal-eye fields (FEF) show neuronal activities that are related to both vergence and accommodation, and the sensory-motor transform required for these movements (Gamlin & Yoon, 2000). Some FEF neurons display phasic and/or tonic activity correlated with velocity and amplitude of the near-step response. The phasic and tonic cells could represent velocity and position signals for

controlling accommodation. It has been hypothesized that the FEF projects either directly or indirectly via the cerebellum to the superior oculomotor area (SOA), a pre-motor site containing near-response cells in the brainstem (Gamlin, 2002). Near-response cells in the SOA have phasic (burst), tonic and combined (burst-tonic) activity (Mays *et al*., 1986; Zhang *et al*., 1992) that code velocity and position signals associated with the near-responses of vergence and accommodation. The tonic near-response cells that code amplitude are thought to be derived from the neural integration of velocity signals (Mays, 1983).

The activity of most near-response cells in SOA is associated with both accommodation and convergence. Interestingly, combined phasic and tonic activity of some near-response cells (burst-tonic cells) that control the velocity and amplitude of the vergence response, are found in the oculomotor nucleus (Judge & Cumming, 1986; Gamlin & Mays, 1992). Because the velocity component of the accommodative-step response is low, it is difficult to illustrate combined velocity and position signals for the step response in the Edinger-Westphal (EW) nucleus. However, cells in the EW nucleus do have clear velocity signals for closed-loop smooth sinusoidal tracking, (Gamlin *et al*., 1994). We have constructed a model to test the plausibility of combined independent phasic-velocity and tonic-position signals in the EW nucleus that would produce a peak acceleration of the step response that was independent of response amplitude and peak velocity that was independent of age.

Our dynamic model of accommodation is based on an adaptation of the biomechanical model of the plant described by Beers & van der Heijde (1994), neurophysiological correlates of the accommodative response described by Gamlin (2002), the behavioral measures of the first-order and second-order properties of the accommodative-step response (Bharadwaj & Schor, 2005a) and their age-related changes (Heron *et al*., 2001). The model explores how neural signals might be organized to control dynamic accommodation, and how they might be adjusted to compensate for the age-related changes in biomechanics of the accommodative system.

3. Model structure

Two basic modules make up the pulse-step dynamic model of accommodation. *The biomechanical module,* developed by Beers & van der Heijde (1994), describes the mechanical linkage between the crystalline lens, ciliary muscle, anterior and posterior suspensory zonules and choroid (Figure 11a, b). The anterior and posterior suspensory zonules link the lens to both the ciliary muscle and elastic choroid respectively. Figure1b is a diagram adapted from a lumped biomechanics model proposed by Beers & van der Heijde (1994) that illustrates opposition between the choroid spring (K_{CH}) and the lens spring (K_L), and the modulation by the ciliary muscle of the force exerted by the choroid on the lens system via zonular suspensory ligaments. This biomechanical module is based on Gullstrand's static model of accommodation (Gullstrand, 1924) with the inclusion of a viscous property of the combined lens and capsule. We have included an elastic property of the ciliary muscle attachment to the choroid (Tamm & Lutjen-Drecoll, 1996) that is in parallel with choroid attachment to the posterior zonule.

The neural module is modeled after behavioral observations that suggest independent control of first-order and second-order dynamic properties of accommodation (Bharadwaj & Schor, 2005a). Several studies have assumed that a single tonic-step innervation to the ciliary muscle drives the accommodative-step response in a simple feedback control system. Studies on monkeys in which accommodation was elicited by electrically stimulating the EW nucleus used a step input (Crawford *et al.*, 1989; Croft *et al.*, 1998; Vilupuru & Glasser, 2002). Control systems engineering models (Krishnan & Stark, 1975) and biomechanical models (Beers & van der Heijde, 1994, 1996) have assumed that EW neurons provide a single tonic-step innervation pattern for the accommodative-step response. An outcome of this assumption is that increasing the amplitude of a single tonic-step in innervation would result in a proportional increase in the position, velocity and acceleration of accommodation. However the independent first-order and second-order properties of the accommodative-step response suggests that several independent signals control the first-order and second-order dynamic properties and the final position of the accommodative-step response (Bharadwaj & Schor, 2005a).

The flow chart for processing of the velocity and position signals by the neural module is illustrated in Figure 12a. The neural module of the model for the step response of accommodation describes an innervation by the EW nucleus of the ciliary muscle composed of combined phasic-velocity and tonic-position signals (Figure 12a). These signals are obtained through neural integration of a fixed-height and adjustable width acceleration-pulse to form the phasic-velocity signal, and a variable-height velocity-step to form the tonic-position signal whose amplitude increases with stimulus magnitude.

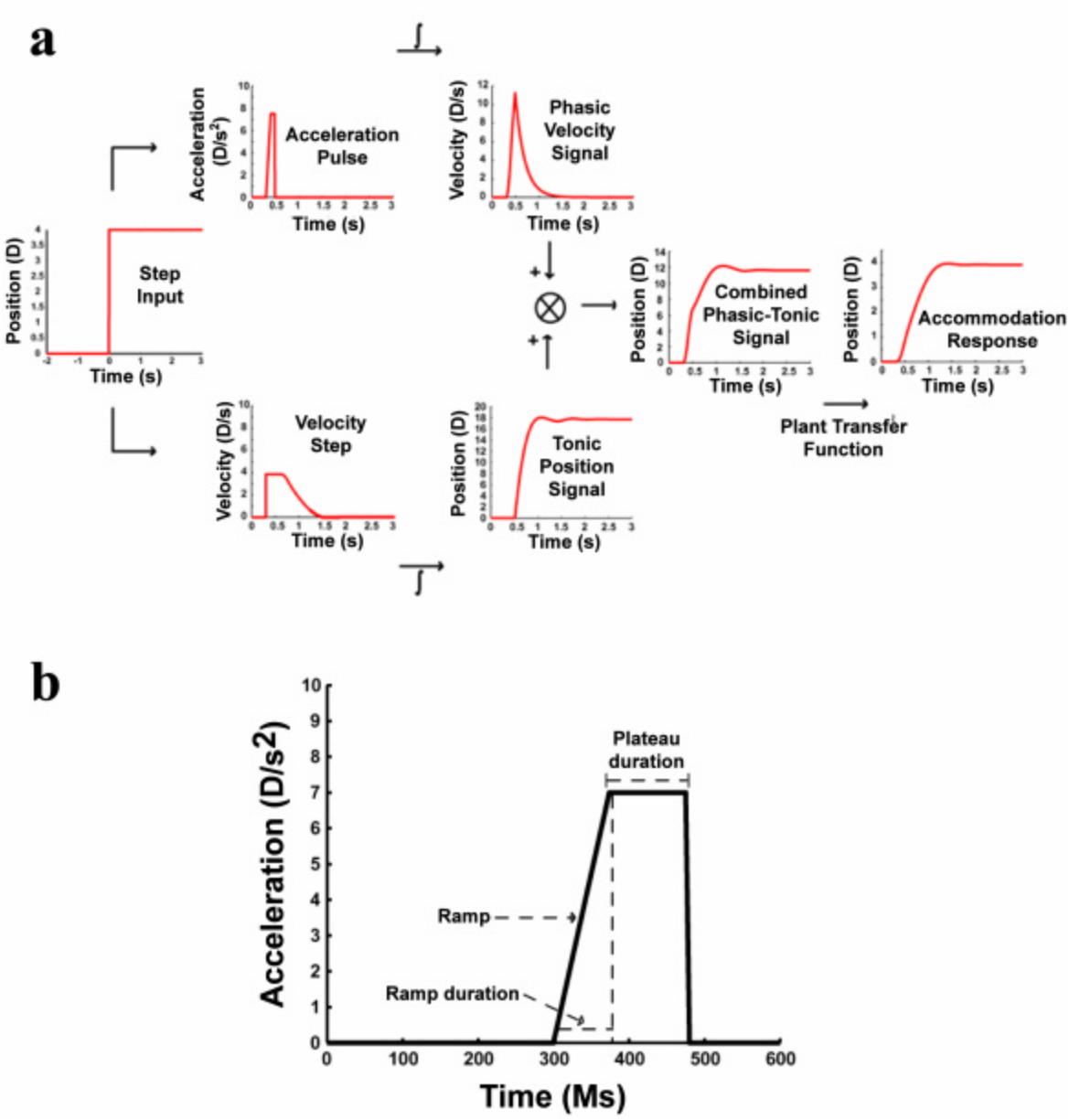

Figure 13. (a). Signal processing flow chart illustrating the independent neural integration of a fixed-height and variable-width acceleration-pulse signal and a variable-height velocity-step signal into phasic-velocity and tonic-position signals respectively. (b). Characteristics of the acceleration-pulse signal. The pulse height controls peak acceleration, the ramp duration controls time-to-peak acceleration and the integral of the pulse controls peak velocity.

The height of the acceleration-pulse is independent of the stimulus amplitude and because the acceleration-pulse is brief, it is not influenced by feedback. The acceleration-pulse signal has a ramped onset, whose height determines peak acceleration. The duration of the abrupt ramped onset of the acceleration-pulse determines the time-to-peak acceleration of the step response that we found to vary systematically with age (Bharadwaj & Schor, 2005a). The ramp is followed by a plateau whose width determines the peak-velocity of the final response (Figure 12b).

These timing factors change with age to preserve peak velocity of the step response of the aging eye (Table III). Neural integration of the fixed-height acceleration-pulse produces the phasic-velocity signal. Increasing the width of the acceleration-pulse increases the amplitude (height) of the phasic-velocity signal with age (Figure 12a) to preserve peak velocity. Neural integration of the velocity-step signal produces the tonic-position signal. The velocity-step height is proportional to the motor error for accommodation, obtained from negative feedback. Increasing the amplitude of both the phasic-velocity signal and tonic-position signal with age by a common scalar adjusts both peak acceleration and the time constant of the step response respectively. These parameters compensate for age-related increases in visco-elastic properties of the capsule-lens complex. The phasic and tonic signals are combined in the EW nucleus to innervate the ciliary muscle.

Age	Ramp duration (ms)	Plateau duration (ms)	? t (ms/D)	Pulse Scalar	Single - step scalar
15	115	10	14	1.0	1.0
25	96	49	25	2.2	1.3
35	76	69	30	2.7	1.5
45	65	90	30	3.1	1.6

Table III. Four age-dependent pulse-step model parameters for neural control and a fifth parameter for the single-step model

(1). The ramp duration of the fixed-height acceleration-pulse determines the time to reach peak acceleration. (2). The plateau duration determines the peak velocity, independent of peak acceleration. The plateau durations are specified for a representative 2D step input. (3). Plateau duration was incremented by a constant duration per diopter ? t ?2D, for every diopter over 1.5 D, to increase velocity with response magnitude. (4) Gain of the phasic-velocity and tonic position signals was increased with age to adjust for age-related changes in biomechanics. (5). Gain of the tonic-position signal for the *single-step* model was scaled to optimize amplitude without producing overshoots.

An assumption of the neural module that has been demonstrated physiologically (Gamlin *et al*., 1994) is that accommodation is linearly related to activity of EW neurons controlling accommodation. Changes in accommodation are linearly related to firing patterns of neurons in the EW nucleus where firing rates have an average sensitivity to accommodation of 3.3 spikes/s/D (Gamlin *et al*., 1994). Interestingly, increases of the dioptric power of the lens are related to the square root of increases in force of the ciliary muscle (Fisher, 1977), suggesting that a nonlinear transformation takes place to produce the linear relationship between firing rate and accommodation. A likely mechanism

proposed by Gamlin *et al.* (1994) for the linear relation between firing rate and accommodation is that a linear increase in firing rate of post-ganglionic ciliary fibers results in a nonlinear force generation by the ciliary muscle that is required to produce the linear increase in accommodation. The non-linear transformation of the firing rate to ciliary muscle force and ciliary muscle force to dioptric power change cancel each other. We have not included these two non-linearities in the model and we go directly from innervation to change in dioptric power.

A simplified block diagram of the combined neural and biomechanics modules is shown in Figure 13. The velocity-step is an error signal that is computed from the difference between the desired accommodative-step response and internal negative feedback from an efference copy signal (Figure 13). This is analogous to an internal feedback model for the vergence system that produces a stable response deceleration from the high velocity produced by the pulse to a final end point of the step response (Zee & Levi, 1989). Our model was designed to illustrate how the independent acceleration-pulse and velocity-step signals and their integrals could be adjusted to compensate for age-related changes in the biomechanics of accommodation.

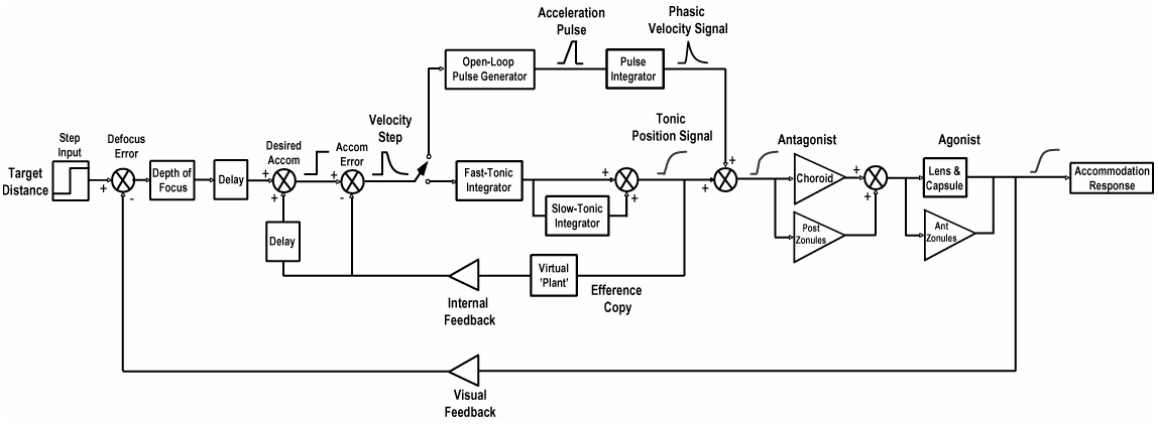

Figure 14. Block diagram illustrates the generation of acceleration-pulse and velocity-step signals, their neural integration to phasic-velocity and tonic-position signals, and transformation by the plant to the accommodative step response. Signal profiles corresponding to Figure 2a are inset into the block diagram.

4. Methods

4.1. Pulse-Step Model

The pulse-step control model of accommodation was developed using MATLAB/SIMULINK®. This model was composed of the following components: acceleration-pulse and velocity-step signals, their integrated phasic-velocity and tonic-position signals and a passive-plant. A simplified block diagram of the combined neural and biomechanics module is shown in Figure 13.

4.2. Velocity input

The accommodative response to a step change in optical vergence is initiated by triggering the fixed-height acceleration-pulse by a velocity threshold criterion. The fixed-height acceleration-pulse is composed of a brief ramped onset followed by a constant height plateau of variable duration that is proportional to the stimulus amplitude (Figure 12b). These acceleration-pulse parameters contribute to the second-order and first-order

dynamics of the accommodative-step response respectively. The height of the ramp determines the peak acceleration of the accommodative response, and the ramp duration determines the time-to-peak acceleration [Appendix I]. The slope and height are fixed for a given age so that when combined with age-related changes in the plant, peak acceleration and time-to-peak acceleration are independent of response amplitude. The fixed height of the acceleration-pulse corresponds to an acceleration signal of 7.5 D/s^2. This value was set arbitrarily and it could be altered by adjusting the gain of the integrated acceleration-pulse signal that produces a phasic-velocity signal (see section 3.3 for a more detailed description).

The duration of the acceleration-pulse plateau determines the peak velocity of the response, independent of peak acceleration. An increase in peak velocity with response magnitude is achieved by increasing the duration of the pulse plateau at a fixed proportion of response amplitude (? t pulse plateau/D increment of accommodation). The acceleration-pulse signal is unaffected by negative feedback since pulse duration (approximately 120 ms) is shorter than the 300 ms latency period for accommodation.

The velocity-step signal begins at the termination of the acceleration-pulse. The amplitude of the velocity-step signal is reduced by internal feedback from efference copy signals of accommodation until a steady state is achieved. The internal feedback takes the plant transfer function into account (virtual plant). The main purpose of the internal feedback is to prevent overshoots of high-velocity responses that would occur with slower acting visual feedback. Table III presents durations of ramp and plateau portions

of the acceleration-pulse signal for a 2 D response for four different age groups and the rate at which the plateau duration was incremented per diopter of accommodation.

4.3. Integration of acceleration-pulse and velocity-step signals.

The acceleration-pulse and velocity-step signals are integrated to phasic-velocity and tonic-position signals respectively. The acceleration-pulse is integrated by a first-order lag element with a time constant of 200 ms. The time constant of the acceleration-pulse integrator was chosen to yield a phasic-velocity signal that had the same width (duration) as the derivative of the accommodation step response (velocity profile). The velocity-step signal is integrated independently by the serial combination of a fast and a slow tonic integrator that were adopted from the accommodation and vergence interaction model proposed by Schor (1992). The accommodative-vergence interaction model describes the increase of the decay-time-constant of the adapted accommodative-step response with prolonged stimulus exposures that can be revealed when the stimulus to accommodation is removed by darkness or a pinhole pupil (open-loop condition). In the current model, the fast tonic integrator influences the time constant and amplitude of the accommodative-step response and the slow tonic integrator maintains the response amplitude for prolonged periods of time. Baseline gains and time constants for fast and slow tonic integrators are presented in Table IV. These parameters were the same for all age groups. The gains of the combined phasic-velocity and tonic-position signals were increased with age (Table III) by a single scalar to compensate for age-related biomechanical changes of the plant. This age-dependent scalar adjusts the peak acceleration, peak velocity, and amplitude of the final response.

4.4. Passive-plant controller in the Laplace domain

The lens complex is modeled as a first-order lag element, and the choroid and zonules are modeled as gain elements that are proportional to their compliance (compliance = 1 / elastic coefficient). Elasticity and viscosity of the combined agonist lens complex and anterior zonules are represented in the Laplace domain with a gain and a time constant respectively (Figure 14). The time constant is proportional to both viscosity and compliance. The time constant for a 15-yr old lens was taken from in vivo measures by Beers & van der Heijde (1996). The time constant for a 41-yr old lens was estimated from an illustration of the time course for relaxation of compressive force applied to the lens in vitro by Glasser & Campbell (1999, see their Figure 12a). Time constant estimates for intermediate ages were interpolated between these two values. Ideally, we would have liked to use isolated crystalline lens in-vitro measures for all the ages. But, since Glasser & Campbell (1999) do not provide an illustration for the 15-yr old, we used the in-vivo measure of Beers & van der Heijde (1996). As will be shown by the simulations, the in vivo measures overestimate the time constant of the lens.

Latency (delay)	300 ms
Pulse height	7.5 D/s^2
Phasic integrator	0.75 / [0.2S + 1]
Tonic integrators	
Fast - tonic	15.0 / [2S + 1]
Slow - tonic	50.0 / [100S + 1]

Table IV. Age-independent neural control parameters

The transfer functions in this table are also applicable to column 2 in Table 3. They are represented in the Laplace notation format K / ?s + 1 where, K = gain of the transfer function and ? = time constant of the transfer function.

Estimates of the elastic coefficients for the lens complex, zonules and choroid were obtained from in vitro measures by Fisher (1969, 1971) and van Alphen & Graebel (1991), as analyzed by Wyatt (1993). The model parameters can be updated as more accurate measures of time constant and visco-elastic coefficients become available. The main purpose of this model is to illustrate how the neural signals for accommodation might be organized to compensate for age-related changes in biomechanics of the accommodation system. The model can also be used to predict the dynamic performance of prosthetic devices such as accommodating intraocular lenses that are inserted into the lens bag (i.e. capsule) to replace the natural lens.

Mechanically, the lens capsule and lens matrix can be modeled as two springs in parallel (van Alphen & Graebel, 1991), however in the Laplacian domain they are modeled as two springs in series (see 'lens capsule gain' and 'lens matrix time constant' blocks in Figure 14). In our model, the spring constants of the lens capsule and matrix were lumped together and modeled as a single gain element by summing their respective elastic coefficients. Appendix II shows the mathematical calculations involved in converting the published values of moduli of elasticity of the lens capsule and matrix into spring constant measures. Normalized lens gains were computed from age-dependent estimates of spring constants from the analysis of Wyatt (1993). The gain of the lens module for a 15-yr old was normalized to unity and the lens gains of other age groups were made proportional to the normalized lens gain of the 15-yr old. For example, for a 15-yr and a 35-yr old, the spring constants of the lens were estimated at 700 dynes/mm and 3000 dynes/mm respectively (Wyatt, 1993). Given the normalized gain of the 15-yr

old lens (1.0), the proportional gain of the 35-yr old lens was 0.23. The gains of other elements in the accommodative plant were also made proportional to the normalized lens gain of the 15-yr old. For example, for a 15-yr old, the elastic coefficient for the lens was estimated at 700 dynes/mm and the choroid at 1500 dynes/mm (Wyatt, 1993). Given the normalized gain of the lens (1.0), the proportional gain of the choroid of the 15-yr old was 0.47. The elastic moduli of the anterior and posterior zonules are fixed across all age groups at 1700 dynes/mm (proportional gain of 0.42) and the elastic modulus of the lens complex and choroid increase with age. The combined gain of the parallel arrangement between the posterior zonule (K_{zp}) and elastic tendons of the posterior ciliary muscle (K_{cb}) (Figure 11b) was set to equal the gain of the posterior zonule (K_{zp}) because no measures have been reported for the elasticity of the tendons that attach the posterior ciliary muscle to the choroid (Tamm *et al*., 1996). Table 3 summarizes the proportional gains and time constants used for the lens complex and the proportional gains used for the zonules and choroid of four different age groups.

Figure 14 is a detailed description of the agonist components of the plant. It illustrates that the amplitude of accommodation depends in part on the ratio of compliance of the lens complex and the anterior zonules. The lumped biomechanics model shown in Figure 14 illustrates the serial arrangement of the lens and anterior zonule. When the ciliary muscle constricts, the diameter of the ciliary ring decreases, causing the combined length of the lens and anterior zonule springs to decrease. The change in ciliary ring diameter is distributed between the anterior zonule and lens in proportion to their compliance.

Wyatt's (1993) analysis indicates that the anterior zonule is stiffer than the lens in younger eyes and the reverse occurs in older eyes (see Table V). Thus as the eye ages, the lens changes less and the anterior zonule length changes more as the ciliary ring constricts during attempts to accommodate (Strenk *et al*., 1999). This age-related trade off between changes in the compliance of the lens and anterior zonule was modeled with a local unity-gain feedback loop in parallel with the forward loop gains of the lens and

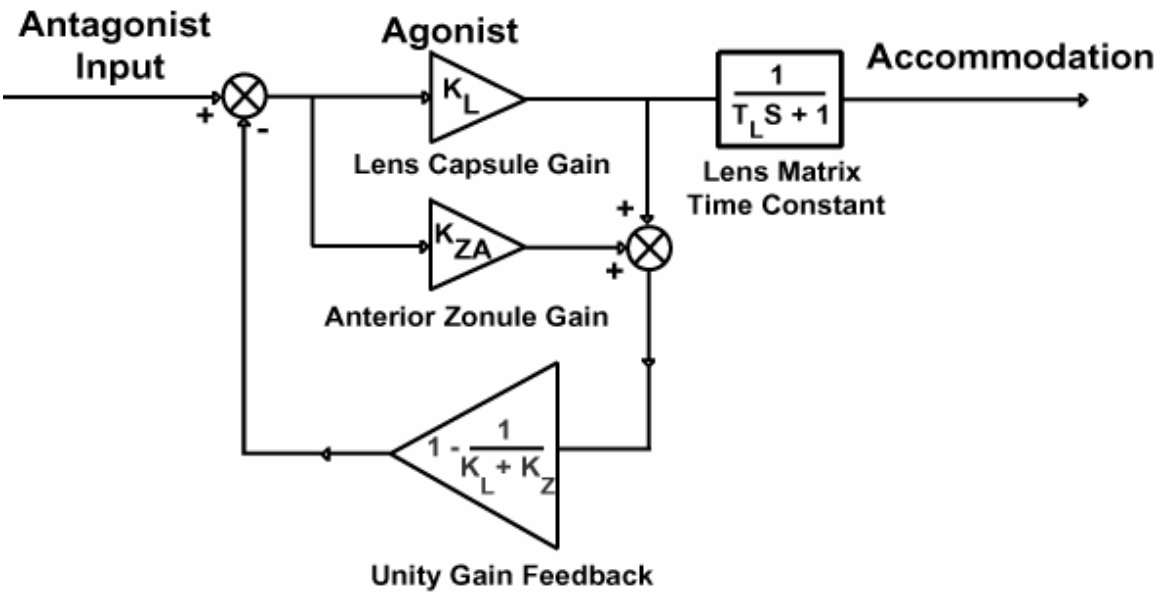

Figure 15. Description of the agonist components of the accommodative plant

The amplitude of accommodation depends in part on the ratio of compliance of the lens complex and the anterior zonules. A trade off between length changes in the lens and anterior zonules spring elements is modeled with a local unity-gain negative feedback loop in parallel with the combined forward loop gains of the lens and anterior zonules spring elements, where the feedback gain equals $1 - 1 / (k_l + k_z)$. This feedback circuit makes the change in ciliary ring diameter equal to the combined change in length of the anterior zonules and lens springs. The circuit is followed by a unity-gain- lag element with an age-appropriate time constant for the lens (see parameters in Table 3).

Age	Lens transfer function	Choroid Gain	Zonule Gain
15	1.0 / [0.154S + 1]	0.47	0.42
25	0.34 / [0.190S + 1]	0.25	0.42
35	0.23 / [0.226S + 1]	0.20	0.42
45	0.18 / [0.262S + 1]	0.15	0.42

Table V.
Age-dependent passive plant parameters

anterior zonule, where the ring diameter equal to the combined change in length of the anterior zonule and lens springs. The circuit is followed by a unity-gain-lag element with an age-appropriate time constant for the lens. Note that the serial arrangement of spring elements in Figure 11b is represented as a parallel arrangement in the Laplace notation illustrated in Figure 14.

4.5. Simulations

Model simulations were performed for four age groups ranging from 15 to 45 years. Simulations of accommodative responses to step changes in defocus were performed for both the pulse-step model and a single-step model to illustrate the improvement in dynamics produced by the acceleration-pulse signal. The single-step model differed from the pulse-step model only by the absence of the acceleration-pulse signal, with all the other model components remaining the same. For the single-step model, the gain of the velocity-step integrator shown in column 6 of Table III was scaled from corresponding values in column 5 of Table III to achieve the same steady-state error or lag of

accommodation as found in the simulations with the pulse-step model. Higher gains for the single-step model than those shown in Table III would have resulted in overshoots of the 4 D response.

As an illustration, we compared simulations with 2 D and 4 D stimuli for the pulse-step and single-step models. We performed a quantitative analysis of first-order and second-order components over the linear range of accommodation. The range of accommodative stimuli was made to lie within the linear 75% of the range of the accommodative stimulus-response function for each age group. This criterion resulted in a stimulus range of 1.5 – 4.5 D for the 15 yr- and 25 yr-old age groups, 3.5 D for the 35 yr-old group and 2.5 D for the 45 yr-old group. However for illustration purposes, we have compared simulations with 2 D and 4 D stimuli for the two models (Figures 15, 16 & 18). Simulations were performed in steps of 0.5 D, each for a period of 4 s. Time constants of the simulated accommodative response were computed as the time taken to reach 63% of the final magnitude. Accommodative responses were differentiated using a 2-point difference algorithm to compute the velocity and acceleration profiles. The peak velocity of accommodation was plotted for both models as a function of the response magnitude (main sequence relationship), and compared with the empirical observations reported for subjects who were 25 to 35 years old (Bharadwaj & Schor, 2005a).

The parameters used in the pulse-step model are grouped into three categories:

Age-dependent parameters for neural control: These include the duration of the ramped-pulse onset, the rate that the duration of the pulse plateau was incremented per

diopter of accommodation, and the scalar that controlled the gain of the combined phasic-velocity and tonic-position signals. Parameters were adjusted for age to match the empirical measures of first-order and second-order components of the accommodative-step responses. These parameters are shown for four age groups in Table III. Column 6 of Table III also lists values for the scalar that controlled the gain of the tonic-position signal for the single-step model needed to achieve the same steady-state error or lag of accommodation as the pulse-step model.

Age-independent parameters for neural control: These include the latency of the response, fixed height of the acceleration-pulse signal, and gains and time constants of the neural integrators of the acceleration-pulse and velocity-step signals. These parameters are represented in Table IV as Laplace transfer functions.

Age-dependent parameters for biomechanical estimates of the plant: These parameters include the gain and time constant of the lens, gain of the choroid and gain of the anterior and posterior zonules. These parameters are represented in Table V as Laplace transfer functions.

Copies of the Matlab script of this model can be obtained from the authors upon request or from our website, http://schorlab.berkeley.edu/. The scripts for the four age categories can be downloaded and run with MATLAB/SIMULINK®. Examples of MATLAB® scripts for pulse-step and single-step responses by 15- and 45-yr olds are also available as supplementary files published online alongside the electronic version of this article in Elsevier Science website. To perform a simulation, save and unzip the file and

run it from you computer. MATLAB® and its SIMULINK® module are needed to run the simulations.

5. Results

Static responses of both the pulse-step and single-step models had similar magnitudes, however there were significant differences in their dynamic responses as described by response time constant, peak velocity and peak acceleration. Figure 15 illustrates position traces of simulated 2D and 4D step responses for the four age groups. Time constants of simulated 2D responses by the pulse-step model increased by approximately 25 ms over a 30-year span from age 15 to 45 years whereas they increases by approximately 150 ms over the same age span for the single-step model. For the 4D responses, the time constants increased over the same age span by 110 ms for the pulse-step model simulations and by 190 ms for the single-step model simulations. The time constant for the lens complex increased by over 100 ms. over the same 30-yr age range (column 2 in Table V). Note that time constants used for the lens complex were shorter than the time constants of the simulated step response, suggesting that precise estimates of lens time constant require in vitro measures. The pulse-step simulations agree well with empirical measures of response duration and time constant of step responses that do not to change appreciably with age (Tucker & Charman, 1979; Heron *et al*., 2001; Mordi & Ciuffreda, 2004).

Figure 16 compares the peak velocity plots for the same simulations. For the 2D response, the peak velocity of the simulated pulse-step model remains constant at all

ages. Peak velocity for the single-step model is lower than for the pulse-step model at all response magnitudes. For all ages, the peak velocity of a 2D response of the single-step model was approximately $1/3^{rd} - 1/4^{th}$ the peak velocity of the pulse-step model response. Velocity increased with response magnitude for both models. Figure 17a plots the simulated main sequence relationship for the two models for each age group. The pulse-step model had a linear increase in the peak velocity with amplitude for smaller responses and a saturation of the peak velocity at larger response amplitudes (dashed lines in Figure 17a). This saturation of the main sequence for accommodation is similar to empirical observations of Kasthurirangan *et al* (2003). The simulated peak velocities saturated at earlier response levels for the older age groups. In contrast, the slope of the main sequence for the single-step model simulations increased linearly across all response magnitudes. Accordingly, a linear regression equation was fit only to the linear portion of the main sequence in the pulse-step model and to the entire main sequence in the single-step model. No age-dependent changes occurred for the slope of the main sequence of the pulse-step model while the slope progressively decreased with age for the single-step model. Figure 17b describes the main-sequence plot for empirical measures of peak velocity for two subjects whose ages were 25 and 35 years (Bharadwaj & Schor, 2005a). For both ages, the coefficients of the linear regression equations of the main-sequence relationships (Figure 17b) were significantly different from zero (Student's T-test; P-value: < 0.001). However, there was no significant difference between the coefficients for the two ages (Student's T-test (Kleinbaum *et al*., 1998); P-value: > 0.7). These data can be described by the same regression equations that describe the simulated main-sequence plots of the pulse-step model shown in Figure 17a. The simulated main-sequence

functions for a 25-yr old (y = 1.33x + 4.08) and a 35-yr old (y = 1.34x + 4.08) were similar to the 25-yr old (y = 0.86x + 5.26) and 35-yr old (y = 1.02x + 4.51) empirical measures. The main-sequence simulations are similar to other empirical measures made on ages ranging from 15-45 yrs (Heron *et al*., 2001; Mordi & Ciuffreda, 2004).

Figure 18 compares acceleration plots for the same simulations. Peak acceleration of the pulse-step model was equal for the 2D and 4D response amplitudes within each age group, and it declined gradually as the age increased over a 30-year period. In contrast, for the single-step model, peak acceleration within each age group increased in proportion to response magnitude. The peak acceleration for the single-step model was always less than the peak acceleration for the pulse-step model. For a 2D response, the peak acceleration for the single-step model was approximately $1/3^{rd}$ – $1/4^{th}$ the peak acceleration of the pulse-step model for all age groups. For larger step sizes (4D), the peak acceleration of the single-step model was approximately 1/2 the peak acceleration of the pulse-step model in the 15-yr old age group and was approximately $1/6^{th}$ the peak acceleration of the pulse-step model for the 45-yr-old age group. Figure 19a plots the simulated peak acceleration for the two models as a function of response size for each age group. The plots representing the pulse-step model for all age groups have slopes of zero. The height of the Y-intercept decreases as age increases. In contrast, the slope of the acceleration plots representing the single-step model decrease markedly as age increases. The single-step model had a proportional increase in the peak acceleration with the response magnitude that was most pronounced for the youngest age group (15-yr old) (y = 15.75x + 1.66). These simulations of peak acceleration for the pulse-step model are

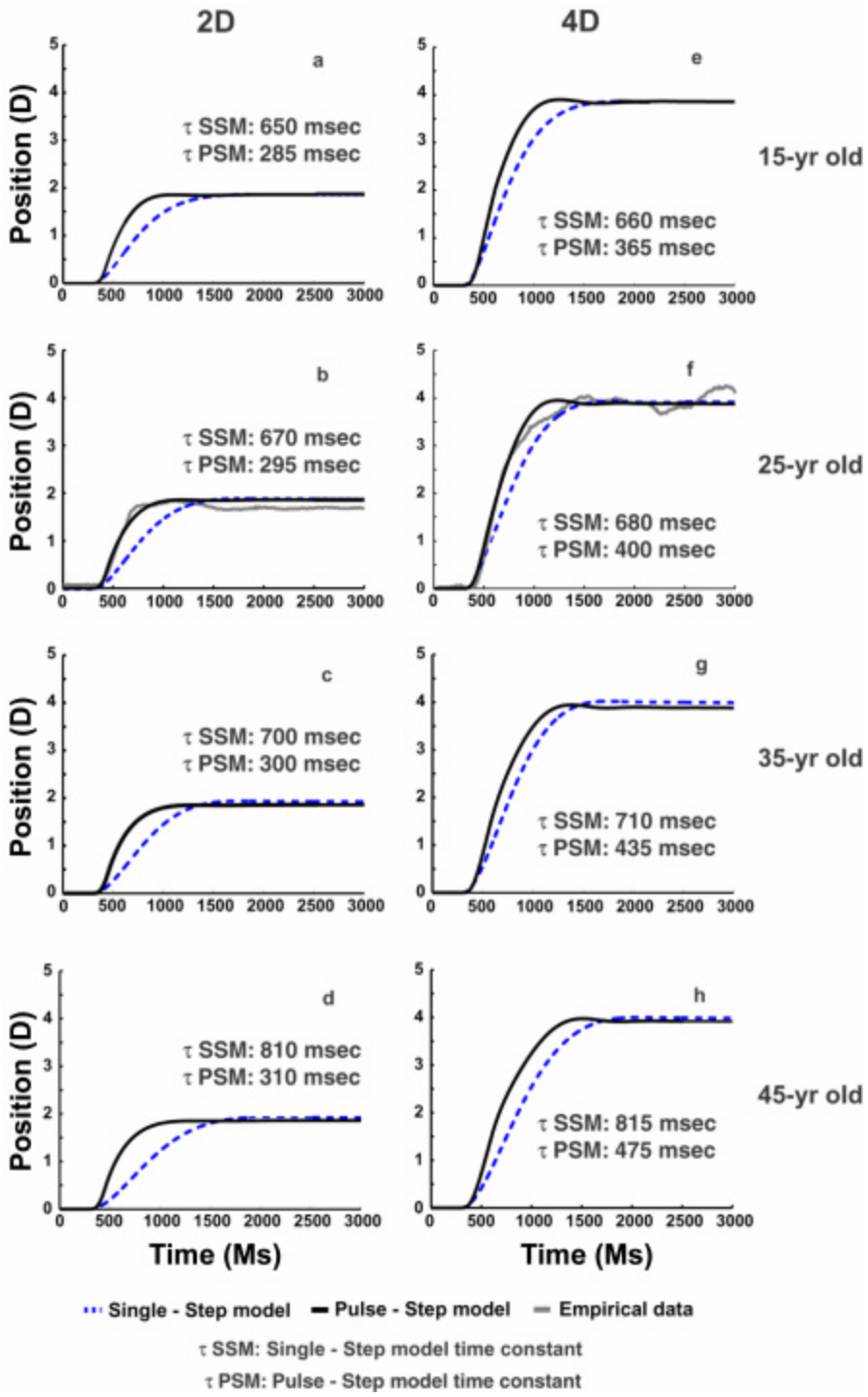

Figure 16. Position traces for simulated 2D and 4D step responses for the four age groups.

The solid curves represent pulse-step model (PSM) simulations and the dashed curves represent single-step model (SSM) simulations. The gray traces in the row for the 25-yr old represent the empirical data superimposed with the simulations.

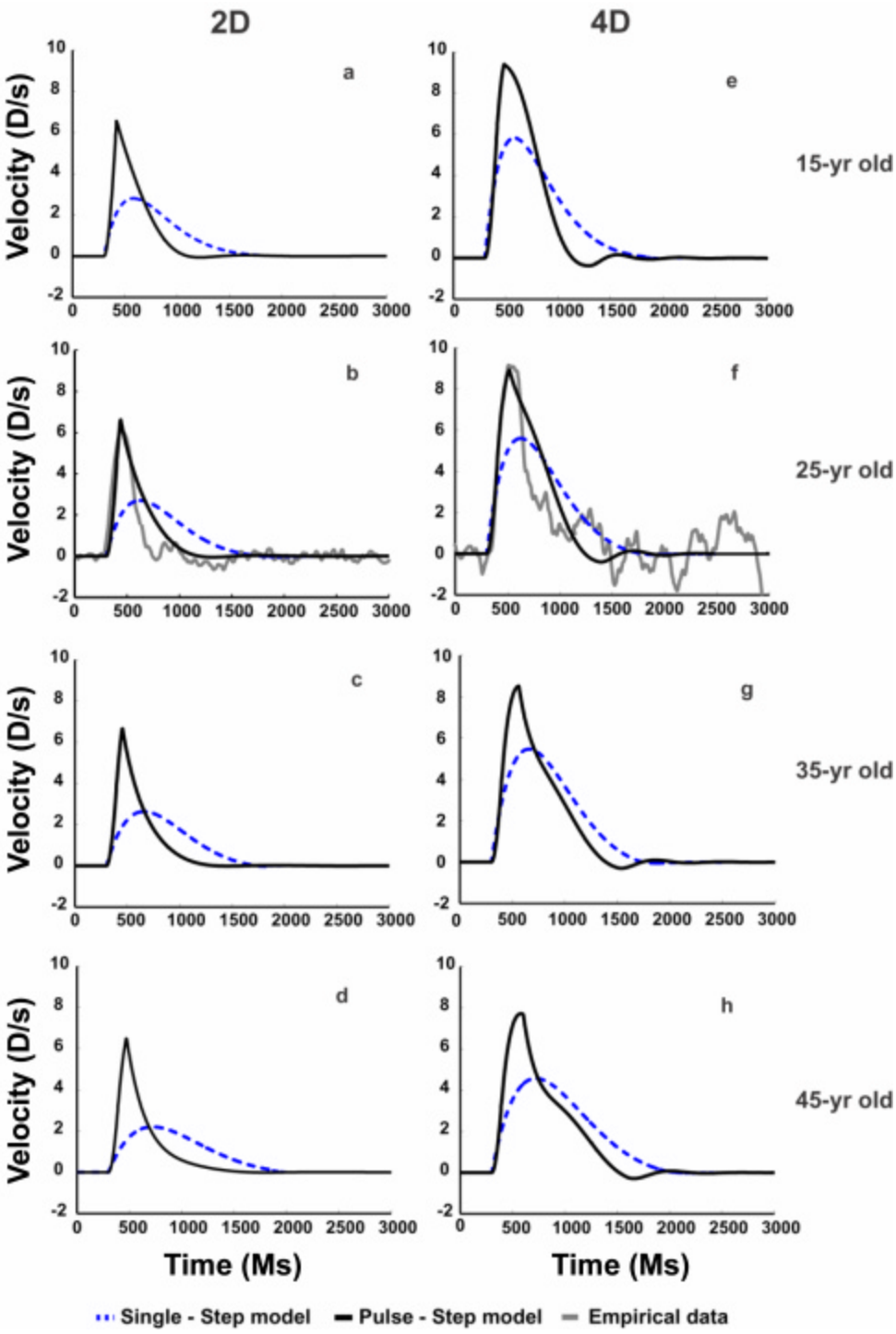

Figure 17. Velocity traces for simulated 2D and 4D step responses shown in figure 16.

The solid curves represent pulse-step model (PSM) simulations and the dashed curves represent single-step model (SSM) simulations. The gray traces in the row for the 25-yr old represent the empirical data superimposed with the simulations.

similar to empirical measures (Bharadwaj & Schor, 2005a) (Figure 19b). For both ages, the slopes of the linear regression equations fit to the empirical data for the peak acceleration as a function of response magnitude (Figure 19b) were not significantly different from zero (Student's T-test; P-value: > 0.7). There was no significant difference between the slopes for the two ages (Student's T-test; P-value: > 0.7) however there was a significant difference between their intercepts (Student's T-test; P-value: < 0.05), illustrating that peak acceleration was reduced with age.

Empirically, acceleration increases gradually during the step response until it reaches a peak (Bharadwaj & Schor, 2005a). The time-to-peak acceleration decreases with age (Bharadwaj & Schor, 2005a), and this is modeled by decreasing the duration of the ramped onset of the acceleration pulse with age. Figure 20a plots simulations of the time-to-peak acceleration for the four age groups as a function of response amplitude. These functions had a zero slope and a Y-intercept that decreased progressively with age to simulate the empirically observed reduction of the time to reach peak acceleration with age (Bharadwaj & Schor, 2005a). The simulated time-to-peak accelerations ranged from 130 ms to 75 ms over a 30-year period and decreased by approximately 15% – 20% per decade of age. These simulations accurately represent the changes in the time-to-peak acceleration observed with age in the empirical measures shown in Figure 20b (Bharadwaj & Schor, 2005a). For both ages, the slopes of the linear regression equations describing time-to-peak acceleration as a function of response magnitude (Figure 20b) were not significantly different from zero (Student's T-test; P-value: > 0.5). There was no significant difference between the slopes or the intercepts for the two ages (Student's T-

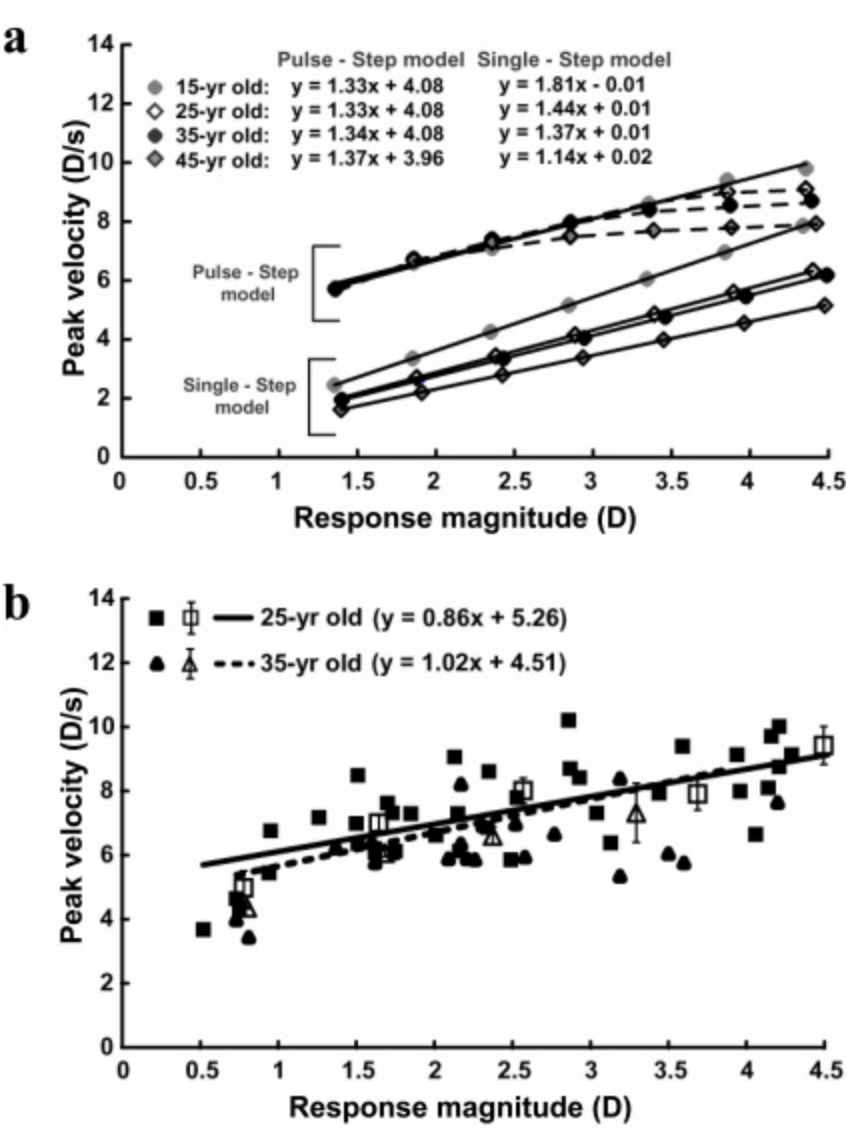

Figure 18. (a). Simulations of peak velocity for the two models are plotted as a function of response magnitude for the four age groups. Linear regression equations were fit only to the linear portion of the main sequence relationship in all age groups. Peak velocity data points at larger response magnitudes were connected using dashed lines for ease of comparison. (b). The main sequence function is plotted for empirical measures of peak velocity for two subjects aged 25 and 35 yrs (Bharadwaj & Schor, 2004). The raw data were fit with regression equations shown by solid and dashed lines. In addition, the main sequence data points were clumped into 1D response bins and the mean and +/- 1 SEM were computed for each of the bins. The open squares and open triangles with error bars show the mean and SEM for the 25-yr old and 35-yr old subject respectively. The coefficients of the linear regression equations were not significantly different from one other. These data can be described by a regression equation whose slope and intercept are similar to the fit of the simulated main-sequence plots in figure 17a.

test; P-value: > 0.5). Simulations of the single-step model, however, had abnormally short durations of time-to-peak acceleration (approximately 17.5 ms – 22.5 ms). The slopes of these functions were close to zero, however they did not show the age-dependent reduction of the time to reach peak acceleration that was found empirically and simulated by the pulse-step model.

6. Discussion

As the eye ages, changes in visco-elastic properties of the accommodation system cause peak acceleration to decline, however peak velocity and time constant of the accommodative-step response remain constant (Heron *et al*., 2001; Mordi & Ciuffreda, 2004; Bharadwaj & Schor, 2005a). Within a give age group, peak velocity increase with response amplitude while peak acceleration is fixed. These observations were simulated by a dynamic model of accommodation that is based on the biomechanics of the accommodation plant (Beers & van der Heijde, 1994) and the neurophysiological correlates of cortical and brainstem circuitry that control the near response (Gamlin & Yoon, 2000).

The accommodative-step response is characterized in the pulse-step model by an open-loop acceleration-pulse component whose height is invariant with response amplitude (Bharadwaj & Schor, 2005a), and closed-loop velocity-step component that increases with response amplitude (Campbell & Westheimer, 1960; Ciuffreda & Kruger, 1988; Kasthurirangan *et al*., 2003). These signals are integrated to form phasic-velocity

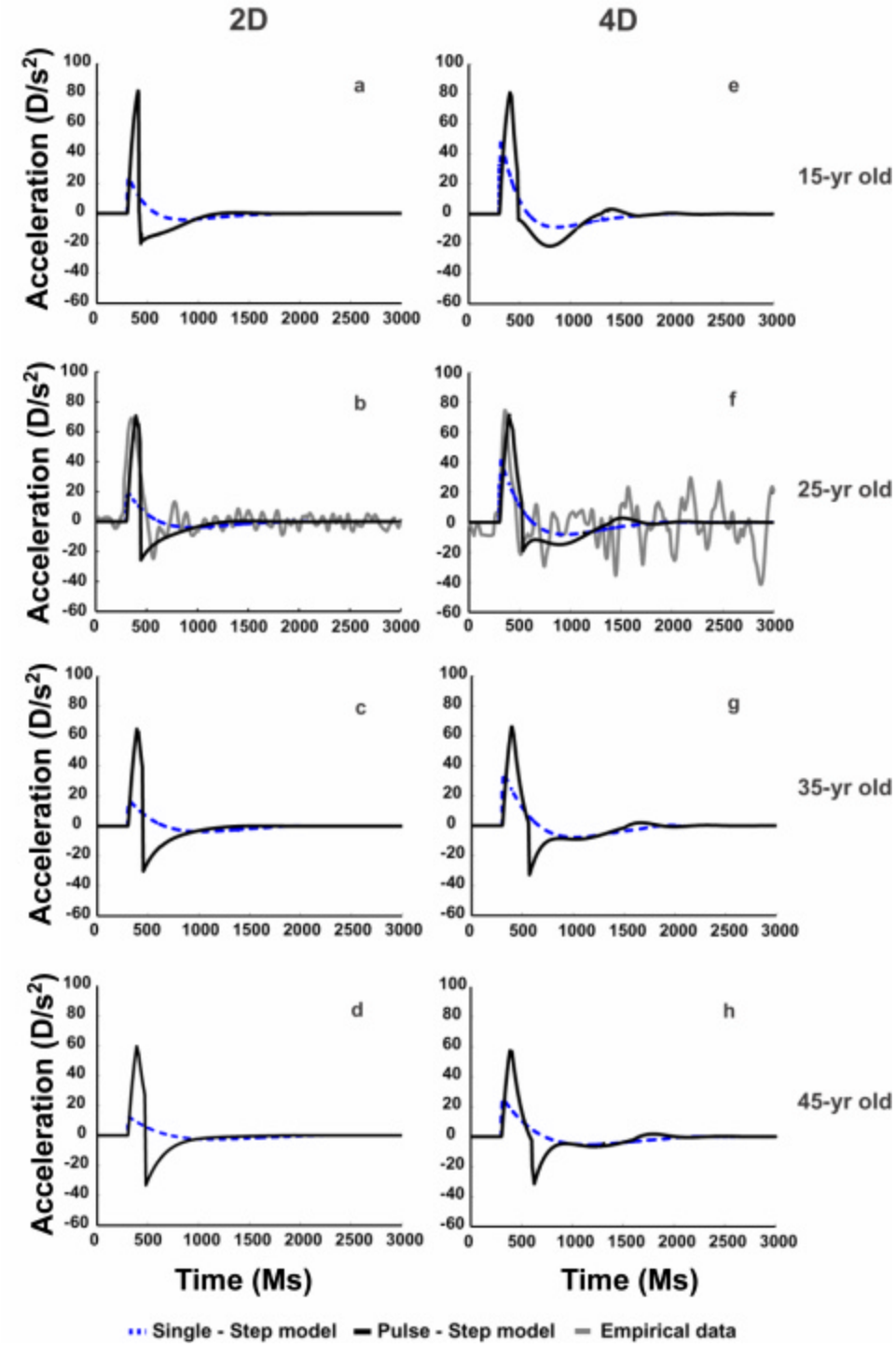

Figure 19. Acceleration traces for simulated 2D and 4D step responses shown in figure 16.

The solid curves represent PSM simulations and the dashed curves represent SSM simulations. The gray traces in the row for the 25-yr old represent the empirical data superimposed with the simulations.

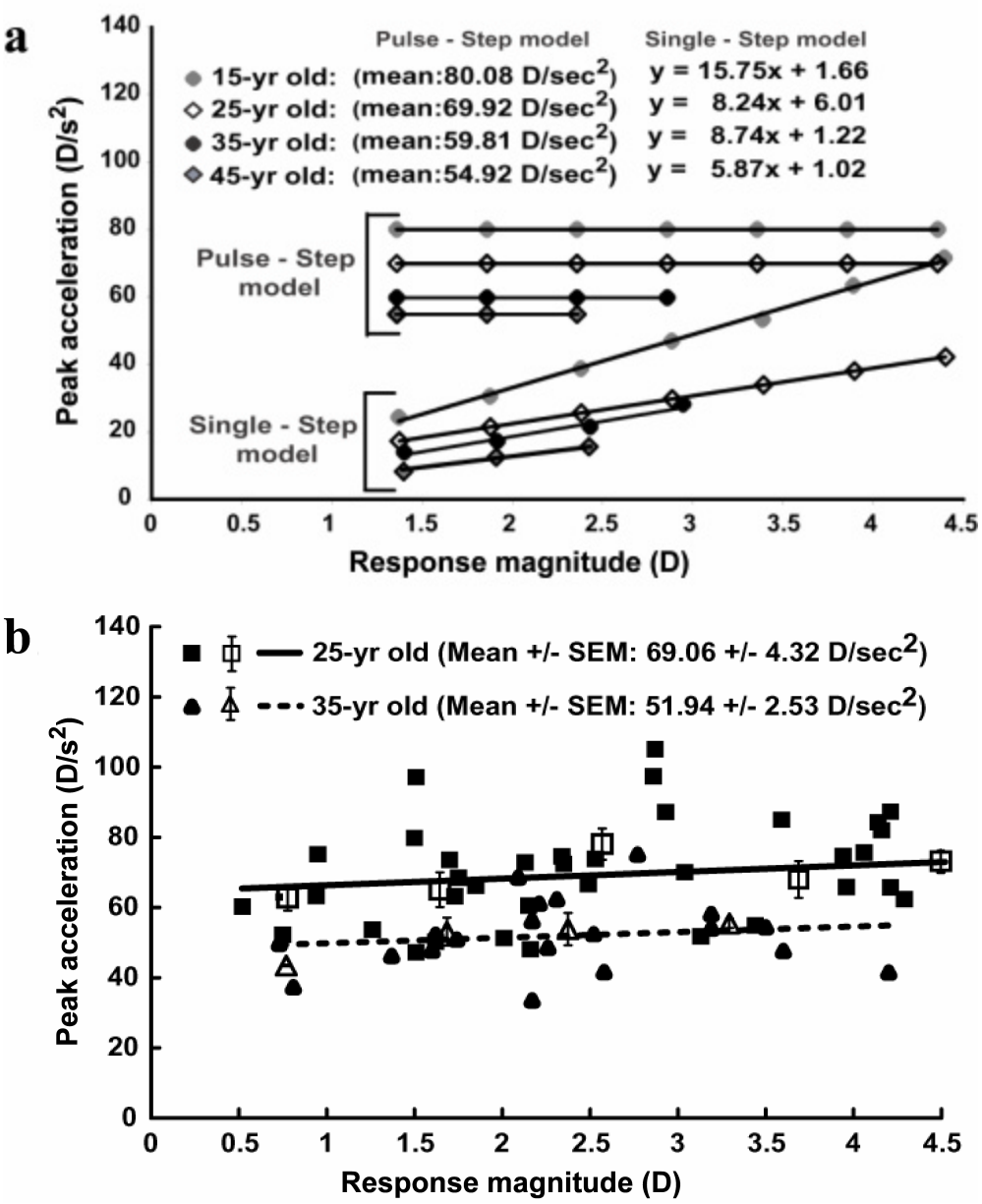

Figure 20. (a). Simulations of peak acceleration for the two models are plotted as a function of response magnitude for each age group. (b). Empirical measures of peak acceleration, plotted as a function of the response magnitude. The raw data were fit with regression equations shown by solid and dashed lines. In addition, the peak acceleration data points were clumped into 1D response bins and the mean and +/- 1 SEM were computed for each of the bins. The open squares and open triangles with error bars show the mean and SEM for the 25-yr old and 35-yr old subject respectively. The slopes of these equations did not differ significantly from one other while their intercepts were significantly different. The empirical measures of peak acceleration are similar to simulations shown in Figure 19a.

and tonic-position signals that are combined in the EW nucleus to control the dynamic and static components respectively of the accommodative-step response. Our dynamic model passes these neural signals through the transfer function of the accommodative plant (Figure 2a). The simulated responses help to understand how the neural control of the first-order and second-order properties of the accommodative-step response is organized and how neural signals might be adjusted to compensate for age-related changes in the biomechanics of the accommodative system.

6.1. Comparison of pulse-step models of motor control

The model was developed to test the plausibility that the accommodation system was guided by acceleration and velocity signals that were integrated to phasic-velocity and tonic-position signals, in a manner similar to how saccades (Robinson, 1975) and vergence (Gamlin & Mays, 1992; Hung *et al.*, 1986) are thought to be controlled. Models of the saccadic system use a velocity-pulse signal that is integrated to a position-step signal, and the pulse and step are combined as burst-tonic cells in motor nuclei located the final common pathway to control initial velocity and final position of the response. In our model, independent acceleration-pulse and velocity-step signals are integrated into independent phasic-velocity and tonic-position signals respectively for independent control of the acceleration, velocity and final position of accommodation. In order to achieve high velocity step responses, both the saccadic and accommodation systems have to overcome a common problem. They both employ a phasic-velocity signal to overcome muscle viscosity for saccades, and lens viscosity for accommodation.

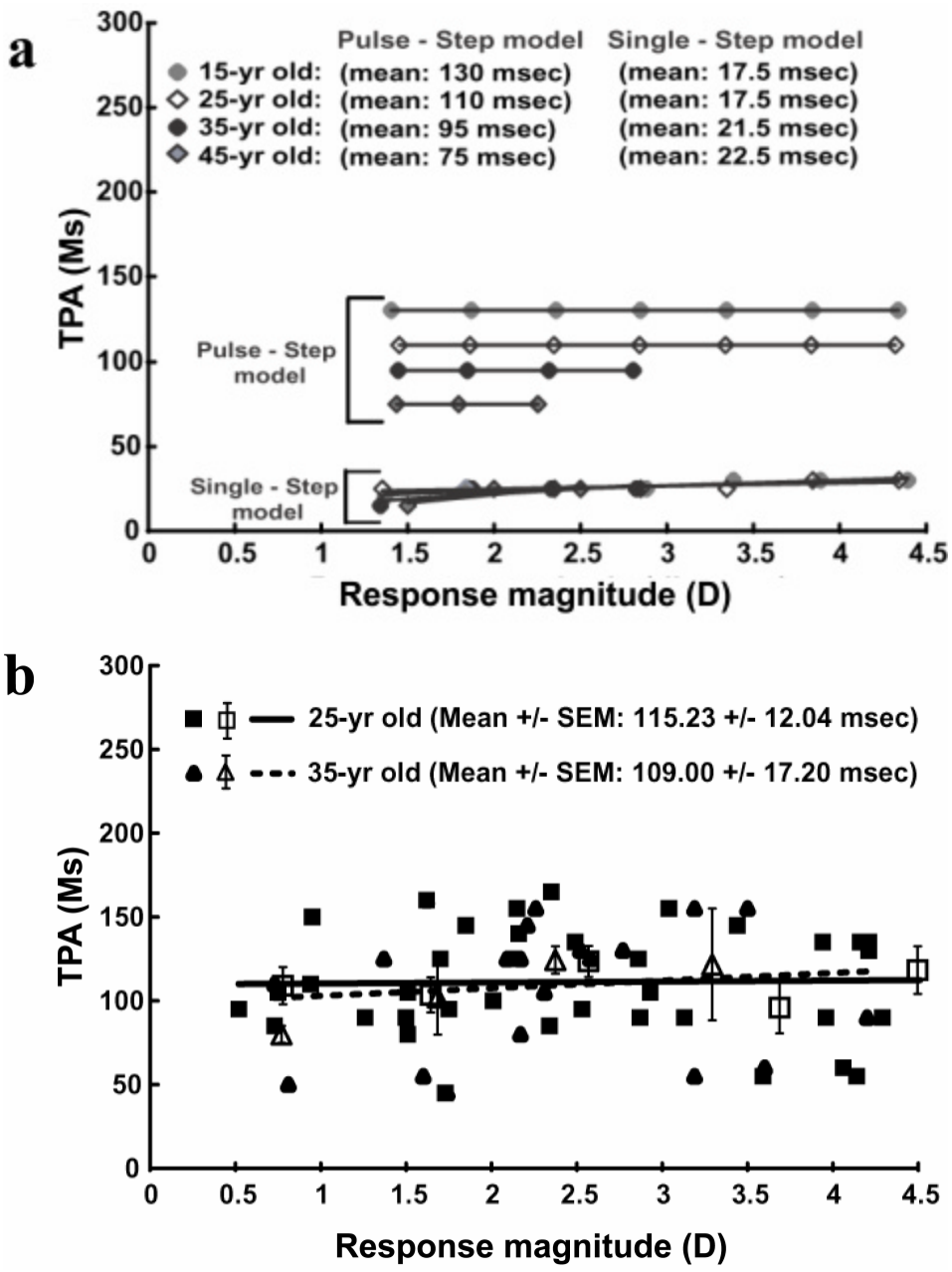

Figure 21. (a). Simulations of the time-to-peak acceleration (TPA) plotted for the four age groups as a function of response magnitude. (b). Empirical measures of TPA plotted as a function of response magnitude for two subjects aged 25 and 35 years. The raw data were fit with regression equations shown by solid and dashed lines. In addition, the TPA data points were clumped into 1D response bins and the mean and +/- 1 SEM were computed for each of the bins. The open squares and open triangles with error bars show the mean and SEM for the 25-yr old and 35-yr old subject respectively. The slopes and intercepts of these equations were not significantly different from one other. The empirical measures of time to peak acceleration are similar to simulations shown in Figure 20a.

The phasic-velocity and tonic-position signals proposed by our pulse-step model resemble activity of phasic and tonic cells in the FEF that are associated with accommodation and convergence (see Fig 1a in Gamlin & Yoon, 2000). The phasic cells of the FEF have the same velocity profile as the phasic-velocity signals of our model, and these resemble the empirical and modeled velocity profile of the accommodative-step response illustrated in Figures 2a and 6f. Phasic and tonic firing patterns during step changes in the near response are also observed in the SOA (Mays *et al*., 1986) and these responses could also correspond to the phasic-velocity and tonic-position signals proposed in our model. The model illustrates that separate phasic-velocity and tonic-position signals that are represented in pre-motor sites such as the SOA could be combined in the EW motor nucleus for accommodation. Indeed, some cells in the EW nuclei appear to have complex onsets composed of abrupt followed by gradual onsets of step firing patterns that resemble the combined phasic-velocity and tonic-position signals modeled in Figure 12a (see figures 7a and 11a in Gamlin *et al*., 1994). Note that the rate of onset for tonic near-response cells is also affected by the relative amplitudes of combined stimuli for accommodation and convergence (Zhang *et al*., 1992).

The independent phasic-velocity and tonic-position signals proposed in the pulse-step model could account for the independent control of acceleration and velocity of accommodation described by Bharadwaj & Schor (2005a). The pulse-step model of the saccadic system does not predict the independence between acceleration and velocity properties that is observed for the accommodative response because the saccade model obtains the step by neural integration of the pulse. However, note that a systematic study

of the first-order and second-order dynamics of human saccadic eye movements by Collewijn *et al* (1988; see Figure 2 in their paper) demonstrated that the time for a saccade to reach peak velocity increased proportionally with the response magnitude while the initial velocity slope (acceleration) remained constant with the response magnitude. These results are consistent with our observations of invariant peak acceleration and increasing peak velocity of accommodation with step response magnitude. The pulse-step model of saccades and our dynamic model of accommodation both predict that phasic-velocity and tonic-position signals are combined in the final common pathway, as modeled here for the EW nucleus of the accommodative system.

6.2. Attributes of the acceleration- pulse signal

In the pulse-step model of accommodation, the acceleration-pulse signal occurs before the velocity-step signal in order to control the acceleration profile of the step response independent of response amplitude. Because the acceleration-pulse is much shorter than the latency period for accommodation (< 300 ms.), it is unaffected by feedback and its response is classified as open loop (Figure 13). The functional significance of the fixed-height acceleration-pulse and corresponding phasic-velocity signal for a given age group is illustrated in figures 15 - 20. Peak acceleration and time to reach peak acceleration remain constant as response magnitude increases. Small response magnitudes are the main beneficiaries of this pulse-enhanced acceleration because for small stimuli, the fixed height of the acceleration-pulse is large compared to the height of the velocity-step. For example, for a 15-yr old, the time constant for a small (2 D) response by the pulse-step model was approximately 1/2 the time constant for the 2D

response of the single-step model, while the time constant of a larger (4 D) response by the pulse-step model was approximately 1/1.5 the time constant for the 4D response by the single-step model (Figure 15). Similarly for a 15-yr old, the peak velocity for a small (2 D) response by the pulse-step model was approximately twice than the peak velocity for a 2 D response of the single-step model, while peak velocity of a larger (4 D) response of the pulse-step model was only 1.12x the peak velocity of the 4 D response by the single-step model (Figure 16). These differences between the small and large responses become more pronounced with age. The enhanced peak velocity that results from including an acceleration-pulse signal illustrates that its integration to a phasic-velocity signal could be used to overcome lens viscosity.

6.3. Non-linear saturation of the 'Main Sequence' function

The empirical 'main sequence' function described by Kasthurirangan *et al*. (2003) saturates above 4 D for individuals in the age range of 20 - 30 years even though the accommodative stimuli are well within the linear range of the accommodative stimulus response function. The saturation of the main sequence function could be modeled in two ways. In both cases, pulse width increases with response amplitude to increase peak velocity. A non-linear model with an upper limit or maximum duration for the acceleration pulse plateau would limit the linear range of the main sequence. This model predicts an increase of peak velocity with response magnitude as width of the acceleration pulse increased, and a saturation of peak velocity when the maximum pulse width was reached. An alternative linear mechanism is suggested by our pulse-step model. It describes the saturation of the main sequence as a consequence of the rise time

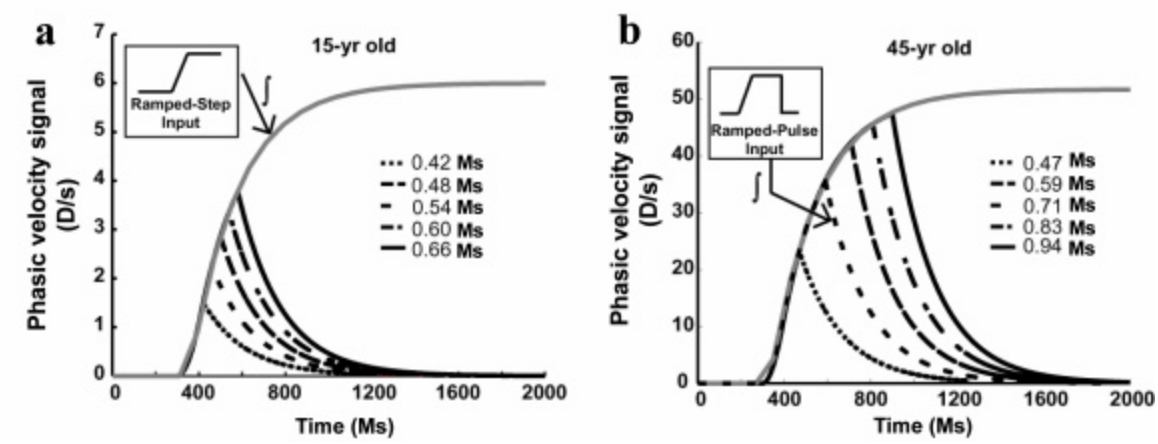

Figure 22. (a & b). Five different phasic-velocity signals were produced for a 15 and 45 yr old by integrating acceleration–pulse signals with plateau durations that produced peak velocities for 2 D, 4 D, 6 D, 8 D & 10 D step responses. The gray curve in each figure represents an envelope function generated by integrating a ramped-step input (*see inset in 21a*). Saturation of the peak velocity occurred when then pulse duration approached the steady state of the envelope function.

to reach steady-state of the phasic integrator that transforms the acceleration pulse to a phasic-velocity signal (Figure 13). The output of this open-loop phasic integrator reaches steady-state value determined by its transfer function and the slope of the ramped-onset of the acceleration-pulse input shown in Figure 21b (see Table IV for phasic integrator Laplace transfer function). The peak velocity obtained by increasing the width of the acceleration-pulse increases as long as the pulse duration is less than the rise time of the phasic integrator (Figure 21a). When pulse duration exceeds the rise time of the phasic integrator, then peak velocity will saturate. This saturation will occur at lower response magnitudes for the older than younger age group because the pulse width is wider for the older group in order maintain the peak velocity (see column 2 & 3 in Table III).

A schematic representation of this linear model is shown in Figure 21a & b for the 15-yr old and 45-yr old. Five different phasic-velocity signals were produced by

integrating acceleration–pulse signals that had plateau durations that produced peak velocities described by the main sequence for 2 D, 4 D, 6 D, 8 D & 10 D step responses. The gray curve represents an envelope function generated by integrating a step with a ramped onset. The phasic-velocity signals peaked in the saturation portion of the envelope function in the 45-yr old age group while the peaks were still under the saturation limit in the 15-yr old age group. One might also consider that the saturation of the main sequence could be caused by the non-linear saturation of biomechanical properties of the plant that limit the peak amplitude of accommodation. However this is unlikely because the saturation of the main sequence occurs at response amplitudes near the center of the linear range of the accommodation stimulus-response function.

6.4. Attributes of the velocity-step signal

The stability of the step response is largely due to the control of the velocity-step signal with internal negative feedback. The velocity-step signal for accommodation begins immediately after the acceleration-pulse is completed in order for peak acceleration to be invariant with response magnitude. Figure 13 illustrates that the velocity-step signal is proportional to the motor error signal for accommodation that is influenced by feedback. Internal feedback is used to estimate position errors between the desired and actual accommodative responses. Desired accommodation is computed from the sum of the retinal error (defocus) and a positive internal feedback loop that is derived from efference copy and that takes into account the plant transfer function with a virtual plant. Estimates of actual accommodation position (efference copy) are subtracted in a negative feedback loop from the desired position signal to produce the velocity-step

signal. This internal source of feedback is analogous to that proposed for vergence eye movements by Zee & Levi (1989). Demonstrations of voluntary step changes of accommodation to targets viewed through a pinhole pupil (McLin & Schor, 1988) or in total darkness (Ciuffreda & Kruger, 1988) illustrate that visual feedback is not necessary to complete a step response, and that desired position is an effective input signal for accommodation. The estimated errors of accommodation (velocity-step signals) are integrated to produce slow-rising tonic-position signals (Figure 12a) that dampen the end of the step response and prevent overshoots and response instability. The latency for visual feedback is too long to provide stable control without overshoots of the step response. Of course, visual feedback is used to guide accommodative pursuit tracking responses to smooth changes in target distance (Khosroyani & Hung, 2002).

6.5. Comparison of the pulse-step model to a dynamic dual-mode model of accommodative smooth tracking

Khosroyani & Hung (2002) have developed a dynamic dual-mode model of accommodative smooth tracking of continuously changing optical vergence stimuli that was originally proposed by Hung & Ciuffreda (1988). Their dual-mode model illustrates how accommodation makes abrupt corrections for position errors that result from low-gain smooth tracking by accommodation of continuous changes in target distance. Our dynamic pulse-step model of accommodation has a different objective. It was developed to describe the first-order and second-order dynamics of the accommodative response to step changes of target distance. The two models share some characteristics, however

because they have different objectives, it is not surprising that they differ in several respects.

Both models initiate abrupt position changes without visual feedback and they complete position changes with feedback. The initial response of the dual-mode model is driven by a desired distance signal that is unaffected by feedback and is nearly equal to the original position error. This fast response is proportional to the magnitude of the input signal such that both acceleration and velocity are predicted to increase with response magnitude. In contrast, the fast component of our pulse-step model is generated by an acceleration-pulse signal that is triggered by a velocity threshold. The acceleration-pulse height is fixed and independent of the amplitude of the step stimulus in order to achieve a constant acceleration that is independent of response amplitude. The width of the acceleration-pulse plateau is increased with response amplitude to increase peak velocity without changing peak acceleration. The dual-mode model completes its response using visual feedback to produce both position and velocity error signals. The fast and slow components of the dual-mode model operate sequentially so that when one is active, the other is disabled. In contrast, our pulse-step model uses internal feedback to control the velocity-step signal in order to produce stability of the final response. The neural integration of acceleration-pulse and velocity-step signals produces phasic-velocity and tonic-position signals that operate in parallel during the mid portion of the step response. Finally the pulse-step model takes into account the biomechanics of the plant (Beers & van der Heijde, 1994) and it is based on neurophysiological correlates of cortical areas

and brainstem pre-motor and motor nuclei known to control accommodation (Gamlin & Yoon, 2000).

6.6. Neural compensation for age-related changes in biomechanics of accommodation

As the eye ages, the visco-elastic properties of the lens complex increase, the elastic coefficient of the choroid increases, and elasticity of the zonular suspensory ligaments remains constant (Wyatt, 1993; Beers & van der Heijde, 1996). An increased elastic coefficient corresponds to a decreased compliance that is modeled as decreased gain. The time constant for the lens is proportional to the ratio of viscosity over elastic coefficient. Thus the time constant is proportional to viscosity and inversely proportional to the elastic coefficient. Viscosity can be estimated from the product of time constant and elastic coefficient. For example, the decrease of the lenticular gain from age 15 to 25 years (from 1.0 to 0.34) corresponds to a proportional increase of the elastic modulus by a factor of 2.94. The change in time constant from 154 ms in a 15-yr old to 190 ms in a 25-yr old corresponds to a proportional increase by a factor of 1.234. The product of these two factors corresponds to a proportional increase in lens viscosity by a factor of 3.63 between ages 15 and 25 yrs, yet peak velocity of step responses appears to be unaffected.

Compared to the single-step model, peak velocity of accommodation is enhanced by the inclusion of the acceleration-pulse signal in the pulse-step model. Without the acceleration-pulse signal, the low peak velocities predicted by the single-step model are not surprising, given the large increase of lens viscosity with age. The pulse-step model maintains the high velocity step response as lens viscosity increases with age by

increasing the plateau width of the acceleration-pulse and the amplitude of combined phasic-velocity and tonic-position signals found in the EW nucleus. The gain could be increased by cerebellar modulation of the near response involving interactions between the precerebellar nucleus reticularis tegmenti ponti (NRTP) (Gamlin & Clarke, 1995), the deep cerebellar nuclei such as the posterior interposed nucleus (Zhang & Gamlin, 1998) and the SOA (Gamlin, 2002).

6.7. Model Applications

The pulse-step model of accommodation could be used to estimate the stability and dynamic performance of prosthetic devices, such as accommodating intraocular lens implants (AIOL) (Haefliger & Parel, 1994; Nishi & Nishi, 1998). The AIOL's are used to replace the presbyopic intraocular lens for the purpose of restoring dynamic accommodation. To use the pulse-step model to predict dynamics of the A-IOL step response, the elastic properties of the lens capsule would be retained, and the visco-elastic properties of the lens cortex and nucleus would be replaced with those of the A-IOL. The lens capsule and lens matrix can be modeled as two springs in parallel and simulated in the Laplacian domain as two springs in series (see 'lens capsule gain' and 'lens matrix time constant' blocks in Figure 4). The capsule would be a pure gain element, and the lens matrix would be a visco-elastic first-order lag element as shown in 'lens matrix time constant' block in Figure 4.

7. Conclusion

The pulse-step model illustrates a neural control strategy that combines phasic-velocity and tonic-position signals in the final common pathway for accommodation in a manner that is similar to the classical neural control model of step changes by the saccadic and vergence systems. The pulse-step model of accommodation provides a heuristic tool that illustrates how several parameters of an acceleration-pulse signal and the gain of combined phasic-velocity and tonic-position signals might be increased with age to maintain the youthful peak velocity of accommodation in the presence of increasing lens viscosity.

Chapter III. Dynamic control of ocular disaccommodation: First and second-order dynamics

1. Abstract

Velocity and acceleration characteristics provide valuable information about dynamic control of accommodation. We investigated velocity and acceleration of disaccommodation from three starting positions. Peak velocity and peak acceleration of disaccommodation increased with the proximity of starting position however for a given starting position they were invariant of response magnitude. These results suggest that all disaccommodation responses are initiated towards a constant primary destination and are switched mid-flight to attain the desired final position. Large discrepancies between the primary destination and desired final position appear to produce overshoots and oscillations of small responses from proximal starting positions.

2. Introduction

Ocular disaccommodation refers to the change in focus of the human eye from a proximal target to a distal target. Two general trends describe the first-order dynamics of disaccommodation step responses from a near starting position to the far point. First, the response time (duration from start to completion of disaccommodation response) and the time constant (time taken for 63% of the disaccommodation response to be completed) increases with the response magnitude (Shirachi *et al*., 1978; Tucker & Charman, 1979; Heron & Winn, 1989; Heron *et al*., 1999 & 2002). Second, the peak velocity of disaccommodation increases with the response magnitude [main sequence relationship (Bahill *et al*., 1975)] (Kasthurirangan *et al.*, 2003; Mordi & Ciuffreda, 2004; *see Yamada & Ukai, 1997; Kasthurirangan & Glasser, 2003 for slightly different results*). Previously, the second-order (acceleration) characteristics of accommodation (far-to-near focusing) (Bharadwaj & Schor, 2005a; Schor & Bharadwaj, 2005) and disparity vergence eye movements (Alvarez *et al*., 1999) have been described, however the second-order dynamics of disaccommodation are unknown. The first- and second-order properties of the accommodation step response provide valuable information about the neural control strategies that initiate the step response (Bharadwaj & Schor, 2005a; Schor & Bharadwaj, 2005). Our primary aim was to investigate the first- and second-order properties of disaccommodation step responses to find behavioral manifestations of a neural control strategy of disaccommodation.

Behavioral studies of the dynamics of disaccommodation are usually performed in conjunction with accommodation (Phillips *et al*., 1972; Shirachi *et al*., 1978; Tucker &

Charman, 1979; Schaeffel *et al*., 1993; Heron *et al.*, 2001; Kasthurirangan *et al*., 2003; Mordi & Ciuffreda, 2004). In most of these experiments, accommodation and disaccommodation step responses were elicited in response to pulse changes in optical defocus (Figure 22a), with the ascending limb of the pulse used to stimulate accommodation from the far point and the descending limb of the pulse used to stimulate disaccommodation to the far point (Tucker & Charman, 1979; Beers & van der Heijde, 1994 & 1996; Yamada & Ukai, 1997; Kasthurirangan *et al.*, 2003). Larger accommodation and disaccommodation stimulus magnitudes were produced by increasing the height of the pulse. Pulse changes in electrical current have also been employed in primates to stimulate the Edinger-Westphal (EW) nucleus in order to elicit accommodation and disaccommodation responses (Crawford *et al*., 1989; Croft *et al*., 1998; Vilupuru & Glasser, 2002; Vilupuru *et al*., 2005). The different amplitude defocus-pulse changes always stimulated accommodation responses from a constant starting position, and disaccommodation responses from different starting positions that ended at the far point (optical infinity) (Figure 22a). Under such experimental conditions, the response time, time constant and peak velocity of disaccommodation increases with the response magnitude (Croft *et al.*, 1998; Vilupuru & Glasser, 2002; Kasthurirangan *et al*.., 2003; Mordi & Ciuffreda, 2004). However, Yamada & Ukai (1997) qualitatively observed that disaccommodation step responses of different magnitudes elicited from a constant starting position traveled initially on a 'common path'. This suggests that the velocities of disaccommodation responses from a constant starting position could be independent of the response magnitude. More recently, Kasthurirangan & Glasser (2003) reported that the peak velocities of disaccommodation step responses were indeed

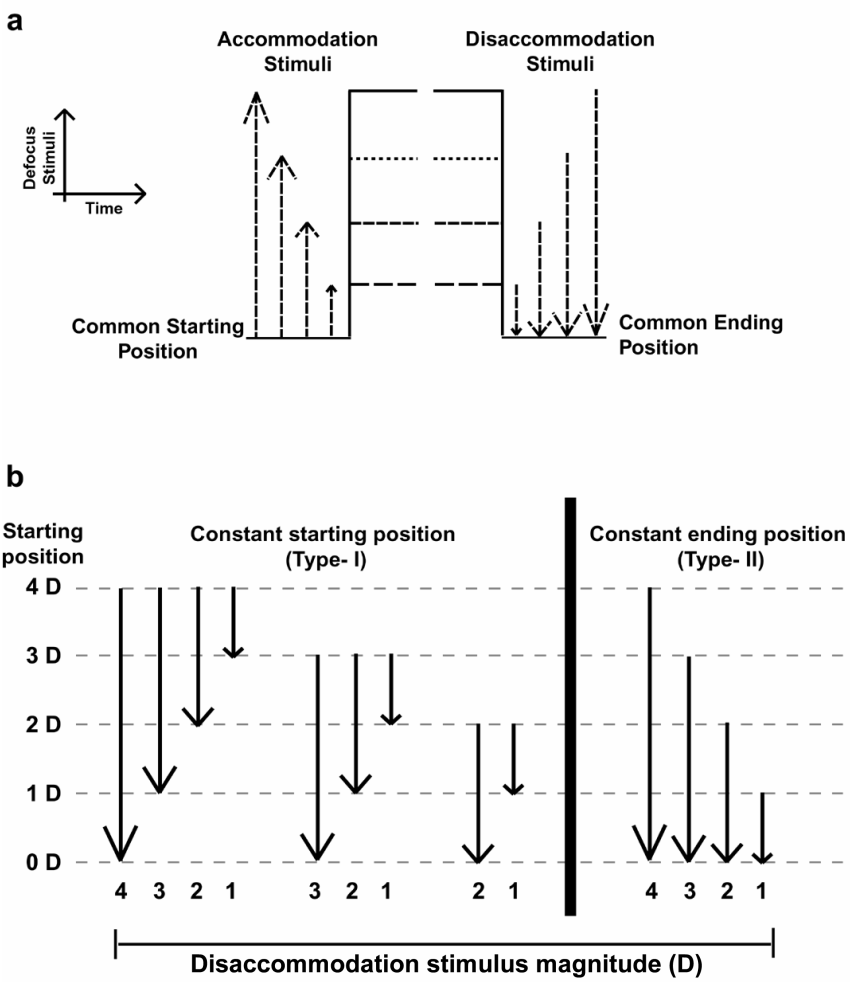

Figure 23. Schematic representation of defocus stimulus paradigm

(a) Defocus stimuli paradigm used in earlier experiments (Tucker & Charman, 1979; Beers & van der Heijde, 1994 & 1996; Kasthurirangan *et al*., 2003). Accommodation and disaccommodation step responses were elicited in response to pulse changes in defocus. The ascending limb of the pulse (upward pointing arrows) stimulated accommodation while the descending limb of the pulse (downward pointing arrows) stimulated disaccommodation. (b) Disaccommodation stimulus paradigm used in this experiment. The 'constant starting position' schema describes the stimulus paradigm used to construct the Type-I main sequence relationship and the 'constant ending position' schema describes the stimulus paradigm used to construct the Type-II main sequence relationship.

independent of response magnitude when they were elicited from a 6 D starting position. However, these experiments did not analyze the second-order dynamics of

disaccommodation. Here, we systematically investigated the first-order dynamic characteristics from three different starting positions (2 D, 3 D and 4 D) and also examined if the second-order dynamics of disaccommodation also exhibited similar starting position dependent characteristics?

We describe the dynamics of disaccommodation using two first-order parameters, peak velocity and time-to-peak velocity (TPV) and two second-order parameters, peak acceleration and time-to-peak acceleration (TPA). These dynamic parameters have been used earlier to characterize the pulse component of a pulse-step innervation model of accommodation (Schor & Bharadwaj, 2005).

3. Methods

3.1. Subjects

Seven subjects (age range: 21 to 32 yrs; mean $\pm$ SD: 25.17 $\pm$ 3.65 yrs) with normal visual and oculomotor functions took part in the experiment. Subject SRB was one of the authors and he was aware of the aims of the experiment while the others were naïve to the aims of the experiment and were inexperienced observers. Four subjects were ametropic (DS: +0.75 D; AB: -1.25 D; SRB: -1.75 D; KS: -3.75 D) and were fully corrected during the experiment. All the subjects took part in the experiment after signing an informed consent form approved by the Committee for Protection of Human Subjects (CPHS), University of California at Berkeley.

3.2. Measurement of dynamics of disaccommodation

A detailed description of the apparatus and the general procedure employed to measure disaccommodation can be found in our earlier paper (Bharadwaj & Schor, 2005a). Briefly, a Generation-V SRI Dynamic Infrared Optometer (Cornsweet & Crane, 1970; Crane & Steele, 1986) was used to stimulate and measure disaccommodative responses. Step changes in optical defocus were generated in a Badal optometer set-up (Badal, 1876) using the 'visual stimulus deflector' of the SRI Optometer (Crane & Steele, 1978b). The visual target was a black and white Maltese cross (Figure 2) centered in a 20? circular aperture of the SRI visual stimulator. The Maltese cross filled the entire field of view of the subject. Disaccommodation responses were measured monocularly (left eye) in each subject using the SRI recording optometer (sampling frequency: 200 Hz). The SRI recording optometer utilizes the Scheiner principle to monitor the conjugate focus of the eye. The left pupil of each subject was dilated using 2.5% PHCL eye drops to improve the signal-to-noise ratio of the instrument. Although 10% PHCL has been known to reduce the speed of disaccommodation step responses, it does so equally at all response magnitudes (Mordi *et al*., 1986). Further, we used a much smaller concentration of PHCL (2.5%) than that was used by Mordi *et al* (1986). Thus, it is very unlikely that the drug would alter the trends in the dynamics of disaccommodation. The subject's refractive correction was placed in the optical path of the left eye at a point conjugate with the eye's entrance pupil. The subject's head was stabilized in the instrument using a bite bar and a forehead rest.

3.3. Calibration trials

Disaccommodative responses were calibrated using the SRI stimulus optometer. A calibration trial consisted of unit-dioptric step changes in optical vergence from 0 D to 4 D in the accommodation direction and 4 D to 0 D in the disaccommodation direction. Each step stimulus lasted for a period of 4 seconds. At least three calibration trials were collected on each subject and the averaged output voltages were fit with a linear regression equation. This linear regression equation was subsequently used to convert the optometer output into units of diopters. The calibration equation obtained from each subject was used on an individual basis to analyze the data from the test trials.

3.4. Test trials

Each experimental session consisted of twenty trials. Every trial contained a single disaccommodative stimulus that lasted for a period of 4 seconds. Three different disaccommodative starting positions (4 D, 3 D, and 2 D) were used such that the disaccommodative demands from each of these starting positions were always within 75% of the subject's maximum amplitude of accommodation. In each session, a single disaccommodative starting position was chosen and it was kept constant throughout the session. Disaccommodative stimulus magnitudes ranged from 0 D to 4 D for the 4 D starting position, 0 D to 3 D for the 3 D starting position and 0 D to 2 D for the 2 D starting position (Figure 22b) and they were presented in a pseudorandomized fashion. Subjects initiated each trial with a button press which was followed by a disaccommodative defocus stimulus that was presented after a randomized delay (0 to 200 ms) to eliminate effects of prediction (Phillips *et al.*., 1972). Frequent breaks were

provided during the experimental session to prevent the disaccommodative system from fatiguing. Lubricating eye drops were administered during the breaks to minimize any corneal irritation caused by refrained blinking during the test trials. At least four sessions were conducted for each subject on separate days and the data for each session were pooled together for statistical analysis.

The data for one of the authors (SRB) was collected on two occasions. First data (first session) were collected during initial pilot experiments while second data (second session) were collected one year later. During this period, the trends in the dynamics of disaccommodation changed significantly. Hence his data were not included in the data analysis of the other subjects and it will be discussed separately as an example of versatility of disaccommodation. In his first session, disaccommodation step responses were measured from two starting positions: 4 D and 6 D while in his second session, the disaccommodation responses were measured from 2 D to 6 D starting positions in 1 D steps. The step stimuli for the 2 D – 4 D starting positions were same as used for other subjects. The step stimuli ranged from 0 D – 5 D for the 5 D starting position and 0 D – 6 D for the 6 D starting position. In both the sessions, the disaccommodative demands from each starting position were always within 75% of the subjects' accommodative amplitude. All the other data recording and data analysis procedures were similar to those employed on other subjects.

3.5. Measurement of dynamics of disaccommodation to combined defocus and size changes (Size + defocus experiment)

Defocus *per se* has been deemed an insufficient cue for estimating both the magnitude and direction (far vs. near) of accommodation (Fincham, 1951; Campbell & Westheimer, 1959), especially when the defocus magnitude is greater than 2D (Fincham, 1951; Troelstra *et al*., 1964; Crane, 1966; Toates, 1972). Retinal image defocus was the primary cue for disaccommodation in our experiment. Thus, the trends in the dynamics of disaccommodation could be due to the non-availability of reliable magnitude-estimation cues. To rule out this possibility, the reliability of the magnitude-estimation cues was increased by coupling retinal image size changes to optical defocus (Kruger & Pola, 1985, 1986, 1987; McLin *et al*., 1988; Bharadwaj & Schor, 2005a). In the current experiment, we measured the dynamics of disaccommodation by coupling size changes in the target with step defocus changes on one subject (DS). For all other subjects, the size remained constant with step changes in defocus.

Size changes in the target (black and white Maltese cross) were generated on a CRT screen using the Visual Stimulus Generator (VSG) graphics board (Cambridge Research Systems Limited). These visual stimuli were electronically coupled with the SRI stimulus optometer to produce size changes in conjunction with defocus changes. The Maltese cross subtended 6° at the entrance pupil of the eye for the three starting positions (2 D, 3 D and 4 D) and was minified at the rate of 1.25°/D. All other data acquisition and data analysis procedures were similar to the first experiment.

4. Data Analysis

The data were analyzed using custom routines in Microsoft Excel® and MATLAB® . Dynamic disaccommodative responses (diopters) to step stimuli were plotted as a function of time. The start of the response was marked by the first sample point where the velocity exceeded 0.5 D/s and continued to do so for the next 100 ms (Bharadwaj & Schor, 2005a). The data were averaged over a 200 ms window prior to the start of the disaccommodation response to compute the starting dioptric vergence. For a given stimulus starting position, the disaccommodation responses exhibited variability in their starting positions. Hence, for all quantitative analyses involving the starting position of disaccommodation, the responses were grouped together if their starting positions were within +/- 0.5 D of the stimulus starting position.

Disaccommodation responses showed overshoots and oscillations before attaining a stable steady-state in four of the seven subjects. Hence, to obtain the end position and to quantify the magnitude of overshoots, an exponentially damped sinusoidal function (Eq. 1) was fit to the portion of the disaccommodation response following the latency period. Examples of position traces fit with exponentially damped sinusoidal functions are shown for responses with and without oscillations in figure 23a.

$$y = k_0 + [(k_1 * e^{-?t}) * (\cos(? t) - ?)] \quad (1)$$

Where, y = disaccommodation response; k_0 = dioptric vergence at the end of disaccommodation response; ? = reciprocal of the decay time constant for the exponential

function; ? = frequency of the sinusoidal function; t = time; ? = phase of the sinusoidal function.

The five independent variables of the equation: k_0, k_1, ?, ? and ? were solved using the non-linear least squares technique (*lsqcurvefit* routine in MATLAB?) until the best fit exponentially damped sinusoidal function was obtained. This function has been commonly used to describe the characteristics of second-order systems (Nise, 2000). However, we only used the variable k_0 to determine the amplitude at the end of the disaccommodation response. The difference between the accommodative states at the start and end of the response determined the disaccommodative response magnitude.

We quantified the magnitude of only the first and most prominent overshoot (primary overshoot) in the position trace before the response attained a steady-state. In responses showing multiple overshoots, the secondary overshoots were not analyzed. The difference between the accommodative states at the primary overshoot position and the end of the response determined the magnitude of the primary overshoot (Figure 23a). To quantify the magnitude of the primary overshoot as a function of response magnitude, the amplitude of primary overshoot for all subjects (except SRB) were plotted as function of the response magnitude separately for each starting position. Separate exponential equations were fit to these plots for each starting position separately. To quantify the frequency of responses exhibiting a primary overshoot, a three-step procedure was employed. First, the responses from all the subjects (except SRB) were grouped into 0.5 D response magnitude bins. The mean response magnitude for each bin was calculated.

Second, the frequency (in %) of disaccommodation responses that exhibited a primary overshoot of >0.10 D was calculated for each response magnitude bin. Third, the frequency (in %) of responses exhibiting the primary overshoot was plotted as a function of the mean response magnitude of each bin. This three-step procedure was performed separately for each starting position. The disaccommodation parameters (k_0 and primary

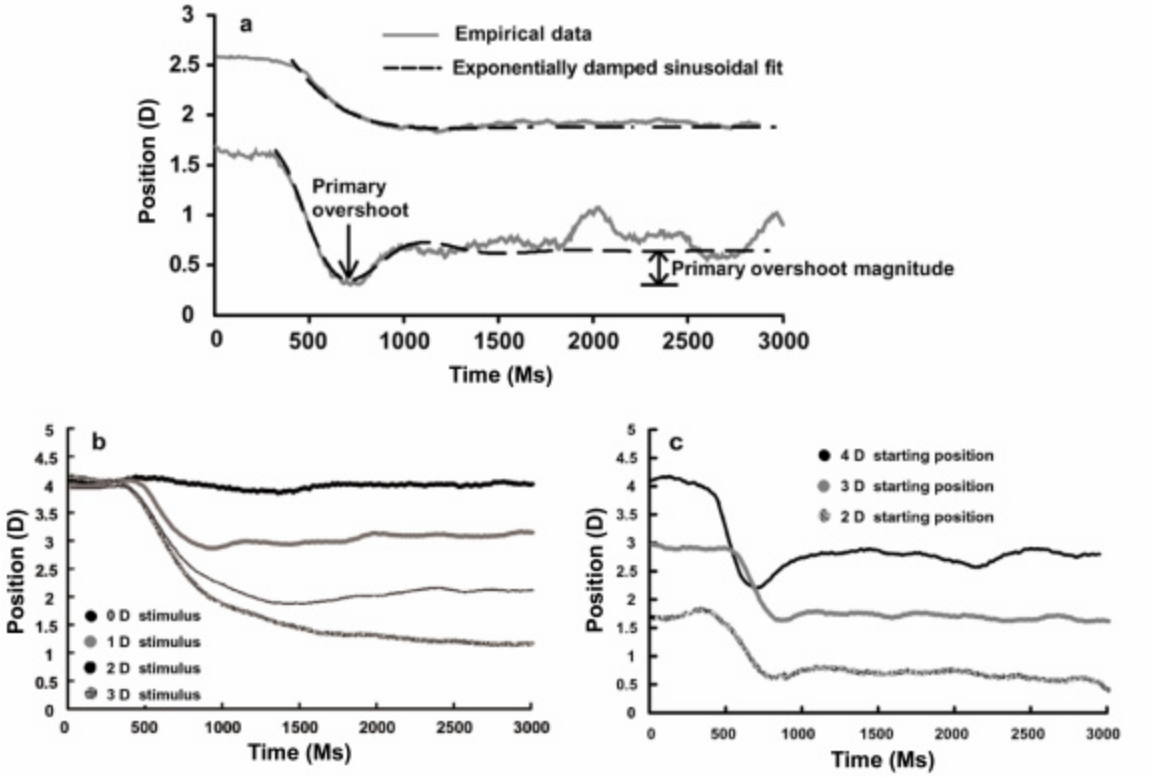

Figure 24. Disaccommodation position traces plotted as a function of time

(a) Two different types of response traces fit with exponentially damped sinusoidal functions shown in Eq. 1. The coefficients of the equation are described in the text. The upper dashed line shows the fit for a response without oscillations $y = 1.42 + [(0.77 * e^{-3.88t}) * (\cos(2.62t) - 0.07)]$ and the lower dashed line shows the fit for a response with oscillations $y = 0.99 + [(0.91 * e^{-3.04t}) * (\cos(7.85t) - 0)]$. The two traces have been displaced along the ordinate for sake of clarity. (b & c) Sample disaccommodation position traces plotted as a function of time. (b) Response traces of approximately 0 D, 1 D, 2 D & 3 D magnitudes from a 4 D starting position. (c) Response traces of approximately 1.5 D magnitude from 4 D, 3 D & 2 D starting positions.

overshoot magnitude) computed by the exponentially damped sinusoidal function were confirmed by visually inspecting the data for each response trace.

Velocity (D/s) profiles were computed by differentiating the response traces using a 2-point-difference algorithm and subsequently smoothing the data using a 100 ms window. The peak velocity of the disaccommodative response was obtained from the highest value of the velocity profile. The main-sequence relationship was plotted in two ways for each subject. First, separate main-sequences were derived for the each starting position by plotting the peak velocity as a function of the response magnitude (Type-I main sequence). Second, a composite main-sequence was derived by plotting the peak velocity as a function of the response magnitude for all defocus stimuli stepped from the three different starting positions to an ending position of 0-D (Type-II main sequence). Thus, the Type-II main sequence was a subset of the Type-I main sequence plot. The time-to-peak velocity (TPV) was computed for each starting position and response magnitude. The TPV was defined as the duration between the start of the response and the time when the peak velocity occurred. To assess the differences in peak velocity and TPV with starting position two different analyses were performed. First, the peak velocities and TPV's for all subjects were lumped together, irrespective of response amplitude, and plotted as a function of starting position and linear regression equations were fit to each data set. Second, the peak velocity and TPV were averaged across different response magnitudes for each starting position and the differences in mean peak velocity and TPV were compared in a histogram for the three starting positions.

Acceleration (D/s^2) profiles were computed by differentiating the velocity traces using a 2-point-difference algorithm and subsequently smoothing the data using a 100 ms window. Only the acceleration lobe was analyzed in the acceleration profiles. The peak acceleration of the disaccommodative response was obtained from the highest value of the acceleration profile. Similar to the peak velocity the time-to-peak acceleration (TPA) was computed for each starting position and response magnitude. The TPA was defined as the duration between the start of the response and the time when the peak acceleration occurred. To assess the differences in peak acceleration and TPA with starting position two different analyses were performed. First, the peak accelerations and TPA's for combined response amplitudes of all subjects were lumped together and plotted as a function of starting position and linear regression equations were fit to each data set. Second, the peak acceleration and TPA were averaged across different response magnitudes for each starting position and the differences in the mean peak acceleration and TPA were compared for the three starting positions.

4.1. Statistical analysis

Statistical analysis was performed on the data of every subject. Separate linear regression equations were fit to the Type-I and Type-II main sequence plot, and to the plots of time-to-peak velocity (TPV) and peak acceleration as a function of response magnitude. The slopes of the linear regression functions were tested for statistically significant difference from zero using a t-statistic. The average peak velocities, TPV's and peak accelerations from the three starting positions were assessed for statistically significant differences using a single-factor ANOVA (factor = starting position) test. The

individual averages were also assessed for statistical significance using the Bonferroni multiple comparisons procedure (Devore & Peck, 1993). The same statistical techniques were used to analyze the data in the defocus + size experiment.

The slopes and intercepts of the main sequence relationship's linear regression equation were compared in the defocus + size experiment and the defocus-only experiment using a T-test measure that compared the slopes and intercepts of two straight lines (Kleinbaum *et al*., 1998). A P-value and an F-value (in the case of single-factor ANOVA) of <0.01 was considered statistically significant in all cases.

5. Results

5.1. Defocus-only experiment

5.1.1. Position characteristics

Figure 23b shows examples of disaccommodation position traces of approximately 0 D, 1 D, 2 D and 3 D responses magnitudes from a 4 D starting position. Figure 23c shows examples of position traces of approximately 2D from 2 D, 3 D and 4 D starting positions. The disaccommodation position traces showed a characteristic latency period (approximately 300 ms) followed by a smooth and steady increase until the steady state was achieved. Response latency was invariant with both response magnitude and starting position (Table VI). The exponentially damped sinusoidal function provided very good fits to the disaccommodation response traces (Figure 23a). The stimulus-response function for each starting position showed a linear increase in the response magnitude as

	Start pos (D)	Latency (ms)
KS	2	348.53 ± 65.99
	3	307.50 ± 44.06
	4	305.17 ± 44.37
ER	2	312.56 ± 47.20
	3	339.31 ± 87.17
	4	426.30 ± 59.25
AB	2	376.46 ± 76.53
	3	323.75 ± 92.31
	4	349.32 ± 64.34
JM	2	397.73 ± 111.8
	3	376.53 ± 113.3
	4	274.87 ± 88.53
MM	2	342.30 ± 73.39
	3	307.86 ± 73.79
	4	303.30 ± 76.64
DS	2	317.88 ± 105.1
	3	394.17 ± 180.8
	4	301.67 ± 124.3
DS¶	2	323.86 ± 80.44
	3	384.24 ± 95.43
	4	323.33 ± 129.2

Table VI. Response latencies for the 2 D, 3 D & 4 D starting positions for the six subjects in the defocus-only experiment and for one representative subject (DS¶) in the defocus + size experiment. The ± errors indicate 1-standard deviation from the mean.

a function of the stimulus magnitude *(not shown)*. None of the responses showed large 'lags' or 'leads' of disaccommodation.

5.1.2. Primary overshoot characteristics

The magnitude of primary overshoot was plotted as a function of response magnitude for each starting position (Figure 24a). Separate exponential equations ($y = k_0 + k_1 * e^{-?x}$) were fit to the data of each starting position. The best fit exponential equation for each starting position (2 D starting position: $y = -0.082 + 6.379 * e^{-3.96x}$; 3 D starting position: $y = -0.048 + 2.097 * e^{-1.99x}$; 4 D starting position: $y = -0.093 + 1.670 * e^{-0.72x}$) showed three characteristic trends. First, for a given starting position, the magnitude of the primary overshoot was larger for the smaller response magnitudes than for the larger

response magnitudes (Figure 24a). Second, the magnitude of the primary overshoots of smaller response magnitudes increased with the proximity of the starting position (Figure 24a). Third, the rate of regression of the magnitude of primary overshoots with response magnitude (?) decreased with the starting position of disaccommodation (Figure 24a).

The frequency of responses exhibiting the primary overshoot was plotted as a function of the average response magnitude for each 0.5 D response magnitude bin (Figure 24b). Separate exponential equations ($y = k_0 + k_1 * e^{-?x}$) were fit to the data of each starting position. The best fit exponential equation for each starting position (2 D starting position: $y = -3.53 + 47.67 * e^{-1.50x}$; 3 D starting position: $y = -1.18 + 157.04 * e^{-1.05x}$; 4 D starting position: $y = -15.57 + 152.51 * e^{-0.57x}$) showed three characteristic trends. First, for a given starting position, the primary overshoots were more frequent in smaller response magnitudes than in larger response magnitudes (Figure 24b). Second, the frequency of responses showing the primary overshoot of the smaller response magnitudes increased with the proximity of the starting position (Figure 24b). Third, the rate of regression of the frequency of response showing primary overshoots with response magnitude (?) decreased with the starting position of disaccommodation (Figure 24b).

5.1.3. Velocity characteristics

Figure 25a & b show the velocity profiles for the position traces shown in figure 23b & c respectively. The velocity profiles showed a linear increase in velocity during the beginning of the response until the peak velocity was reached. This was followed by a gradual deceleration to a steady-state position. In responses showing oscillations prior to

steady-state position, positive lobes in the velocity profiles were noted during the deceleration phase of the response *(not shown)*. Two significantly different trends were noted in the velocity profiles. First, for a constant starting position, the peak velocity of disaccommodation remained invariant of the response magnitude (Figure 25a). Second, the peak velocity of responses those were similar in magnitude (change in position)

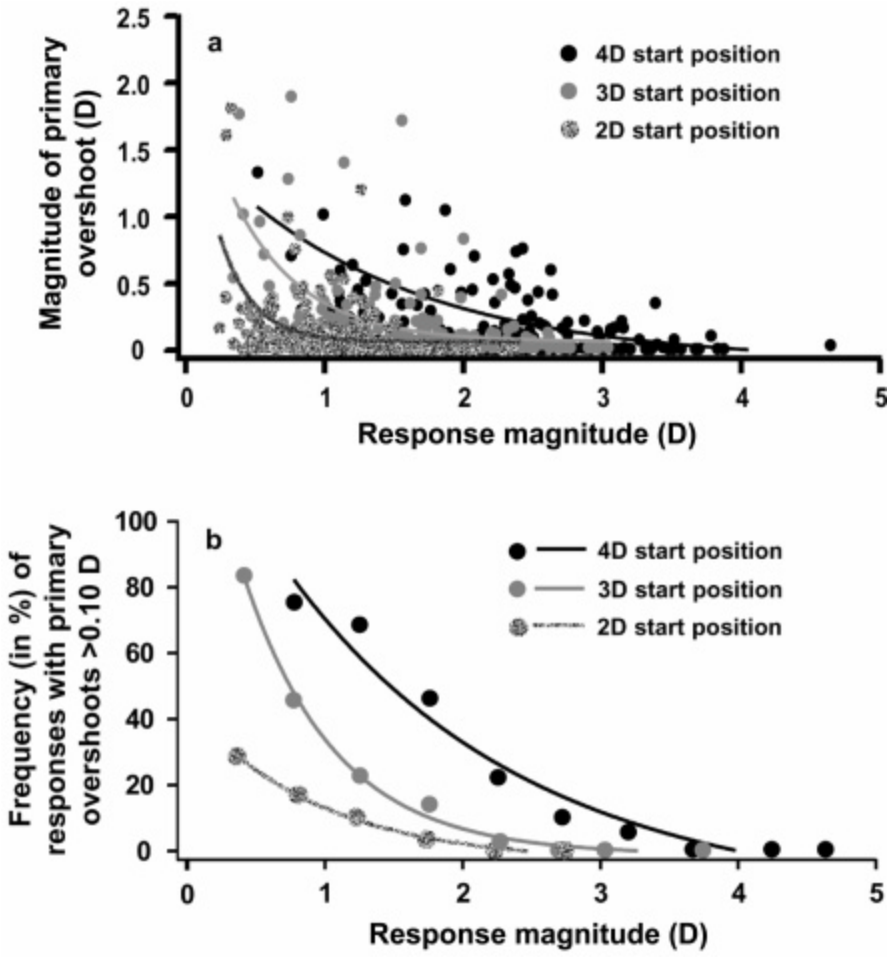

Figure 25. (a) The magnitude of the primary overshoot in the position traces plotted as a function of response magnitude for the 4 D, 3 D & 2 D starting positions. (b) Frequency (in %) of position traces showing a primary overshoot of >0.10 D plotted as a function of the mean response magnitude for each 0.5 D response magnitude bin. For each starting position, the data from all the subjects (except SRB) were pooled together in this plot. The black, gray and mottled circles represent data for the 4 D, 3 D and 2 D starting positions respectively. The black, gray and mottled lines represent the best-fit exponential equations to the data of the 4 D, 3 D and 2 D starting positions respectively.

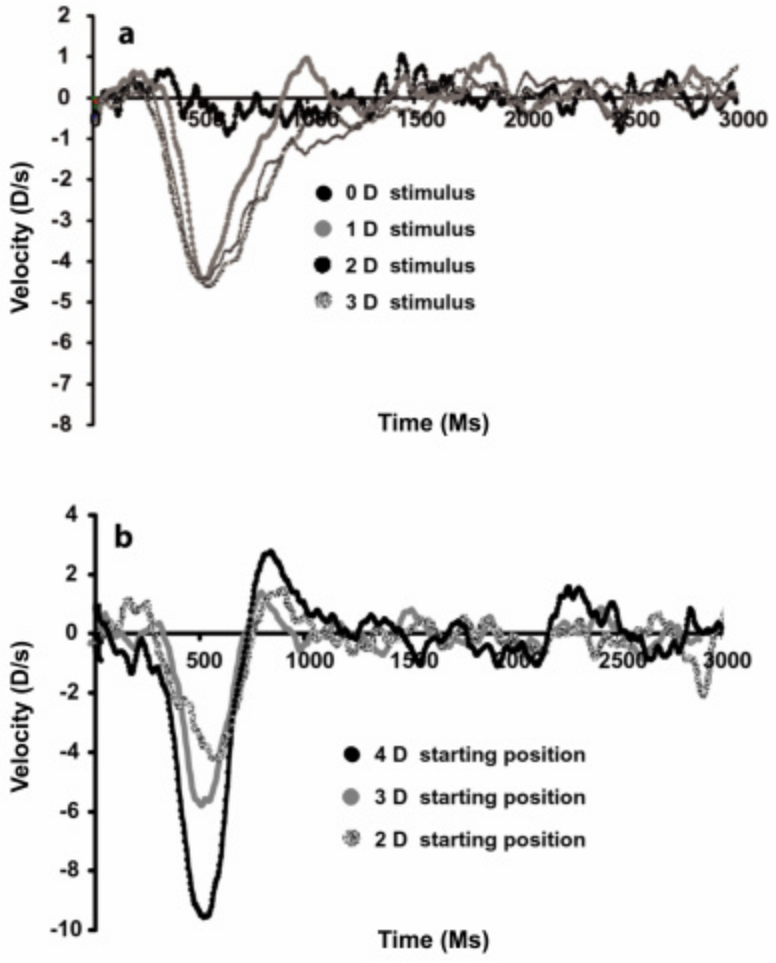

Figure 26. Disaccommodative velocity profiles plotted as a function of time.

(a). Velocity profiles for approximately 0 D, 1 D, 2 D & 3 D magnitude responses from a 4 D starting position. (b). Velocity profiles for approximately 1.5 D magnitude responses from 4 D, 3 D & 2 D starting positions.

These velocity profiles correspond to the position profiles shown in figures 23 b & c.

increased with the proximity of starting position (Figure 25b). Thus a 2 D disaccommodation response starting at 4 D had a higher velocity than a 2 D response starting at 2 D.

For each starting position, the slopes of the linear regression equation fit to the Type-I main sequence showed a small non-zero value that was statistically insignificantly-different from zero (p-value: >0.5) (Figure 26a, b, Table VII) indicating that peak velocity was independent of response magnitude from a common starting point. The y-intercepts of the Type-I main sequence linear regression equation progressively increased with the starting position (Figure 26a, b, Table VII). The Type-II main sequence relationship showed an increase in the peak velocity as a function of response magnitude (Figure 26c, d). The slopes of the linear regression function fit to the Type-II main sequence differed significantly from zero in all subjects (P-value: <0.001) (Figure 26c, d, Table VII).

The linear regression equation fit to the data of peak velocity as a function of starting position for all response magnitudes and subjects ($y = 1.44x + 1.14$), showed a statistically significant increase in peak velocity with starting position (P-value: <0.01) (Figure 27a). The mean peak velocities of all response magnitudes from a common starting position also increased significantly with the proximity of the starting position for all subjects (F-value: <0.01) (Figure 27b). The subjects and conditions in which statistical significance was obtained are denoted with an asterisk symbol. These results indicated that the velocity characteristics of disaccommodation were dependent on the starting position of disaccommodation and not on the disaccommodation response magnitude. Second, for a constant starting position, the peak velocity of disaccommodation remained invariant with the response magnitude and they increased with the proximity of the starting position.

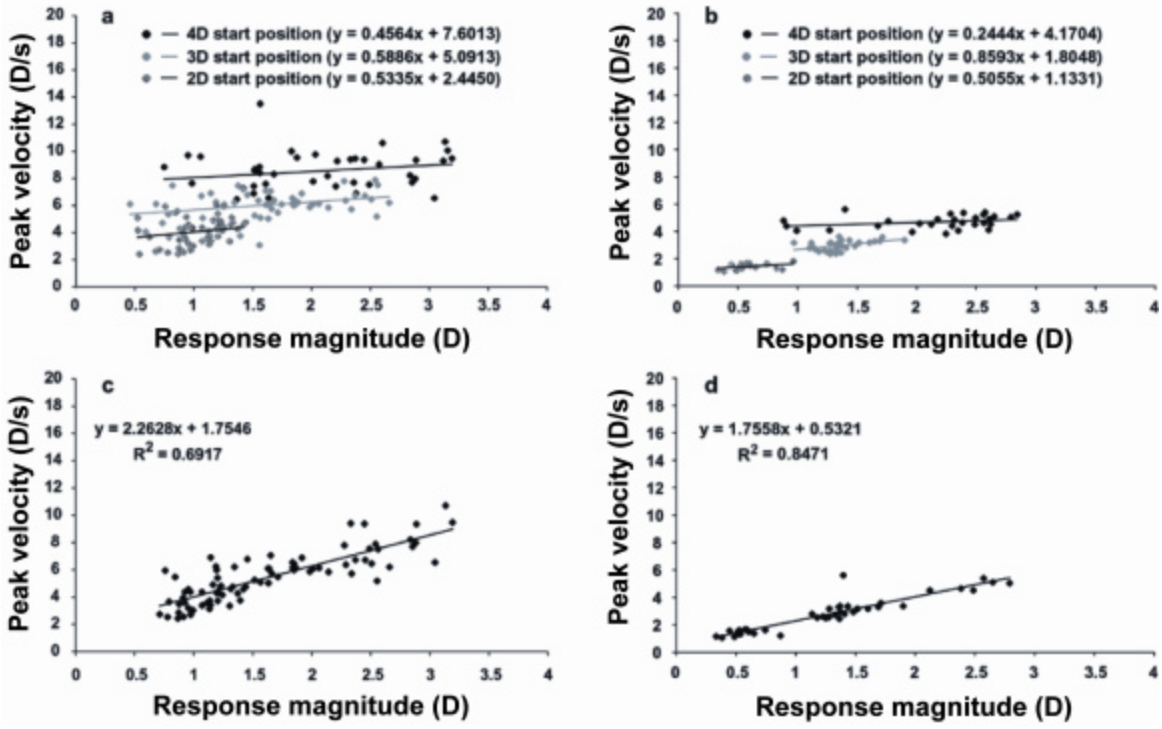

Figure 27. Type-I (a) & (b) and Type-II (c) & (d) main sequence relationships are plotted for two representative subjects (MM & KS). The solid lines in each figure represent the linear regression equation fit to the data points. The slope of the Type-I main sequence is insignificantly different from zero for all three starting positions while the slope of the Type-II main sequence differs significantly from zero.

For a constant starting position, the time-to-peak velocity (TPV) remained constant with the response magnitude for all the subjects (P-value: >0.5). The linear regression equation fit to the lumped data of TPV as a function starting position (y = 12.46x + 168.98) showed a statistically insignificant change in TPV with starting position (P- value: >0.3) (Figure 27c). The mean TPV for all response magnitudes from a common starting position changed significantly between the 2D and 4D stating positions in three of the six subjects (Figure 27d) however the changes were not significant for 2D versus 3D and 3D versus 4D starting positions because of the variable responses (Figure 27d). The subjects

and conditions in which statistical significance was obtained are denoted with an asterisk symbol.

	Start pos (D)	Type – I Main Sequence	Mean peak velocity (D/s)	Mean TPV (ms)	Type – II Main Sequence
KS	2	y = 0.51x + 1.13	1.44 ± 0.22	154.67 ± 58.29	y = 1.75x + 0.53
	3	y = 0.86x + 1.81	2.98 ± 0.36	222.33 ± 94.70	
	4	y = 0.24x + 4.17	4.70 ± 0.70	232.41 ± 58.09	
ER	2	y = 0.23x + 2.63	2.89 ± 0.43	231.60 ± 82.50	y = 0.89x + 1.90
	3	y = 0.36x + 3.39	4.02 ± 0.88	260.24 ± 107.3	
	4	y = 0.11x + 5.18	5.50 ± 0.82	275.83 ± 82.88	
AB	2	y = 0.70x + 2.81	3.81 ± 0.99	197.18 ± 69.29	y = 1.28x + 1.77
	3	y = 0.51x + 3.92	4.90 ± 0.97	231.09 ± 94.26	
	4	y = 0.36x + 4.99	5.84 ± 1.02	228.19 ± 94.57	
JM	2	y = 0.20x + 3.65	3.83 ± 1.09	162.50 ± 80.95	y = 2.31x + 2.15
	3	y = 0.14x + 6.47	6.69 ± 1.68	166.18 ± 96.18	
	4	y = 0.34x + 7.59	8.36 ± 1.39	196.05 ± 70.03	
MM	2	y = 0.54x + 2.45	4.02 ± 0.97	189.20 ± 69.75	y = 2.26x + 1.76
	3	y = 0.59x + 5.09	6.06 ± 0.95	194.91 ± 76.07	
	4	y = 0.46x + 7.60	8.33 ± 1.68	191.42 ± 74.68	
DS	2	y = 0.30x + 5.51	5.72 ± 1.31	155.19 ± 65.03	y = 1.55x + 4.92
	3	y = 0.17x + 7.68	7.90 ± 1.08	201.81 ± 124.2	
	4	y = 0.04x + 9.96	10.05 ± 0.54	224.44 ± 83.31	
DS¶	2	y = 0.54x + 4.02	4.66 ± 0.69	160.86 ± 80.69	-
	3	y = 0.77x + 5.41	6.59 ± 1.14	184.82 ± 85.37	
	4	y = 0.35x + 8.56	9.30 ± 1.12	216.83 ± 79.23	

Table VII. Type – I and Type – II main sequence linear regression equations, mean peak velocity and mean time-to-peak velocity (TPV) for the 2 D, 3 D & 4 D starting positions for the six subjects in the defocus-only experiment and for one representative subject (DS¶) in the defocus + size experiment. The ± errors indicate 1 standard deviation from the mean.

5.1.4. Acceleration characteristics

Figure 28a & b shows the acceleration profiles for the velocity traces shown in Figure 25a & b respectively. They showed a prominent acceleration lobe and a less prominent deceleration lobe. Although more variable than the peak velocity, the peak

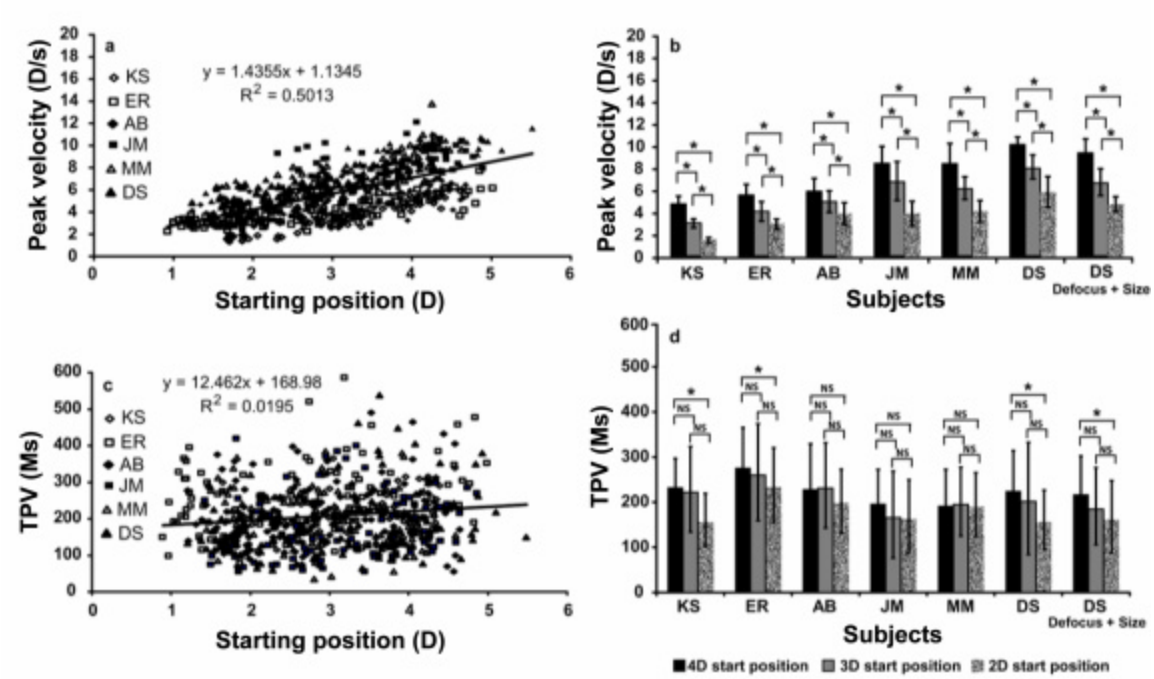

Figure 28. (a) Peak velocity of disaccommodation is plotted as a function of starting position for all subjects (except SRB). The solid line represents the linear regression equation fit to the data. (b) Mean peak velocity for the three starting positions for all the subjects in the defocus-only experiment and for subject DS in the defocus + size experiment. (c) Time-to-peak velocity (TPV) is plotted as a function of starting position for all subjects (except SRB). The solid line represents the linear regression equation fit to the data. (d) Mean TPV is plotted for the three starting positions for all the subjects in the defocus-only experiment and for subject DS in the defocus + size experiment. The error bars in b & d indicate +/- 1 standard deviation and the asterisk (*) symbol indicates statistical significance at a p-value of =< 0.01 and 'NS' indicates statistical insignificance.

acceleration of disaccommodation showed similar trends as the peak velocity of disaccommodation. For a constant starting position, the peak acceleration remained invariant with response magnitude (P-value: >0.5). The linear regression equation fit to the data of peak acceleration as a function starting position for all response magnitudes and subjects (y = 15.413x + 17.822) showed a statistically significant increase in peak acceleration with starting position (P-value: <0.01) (Figure 29a). The averaged peak accelerations of all response magnitudes from a common starting position increased

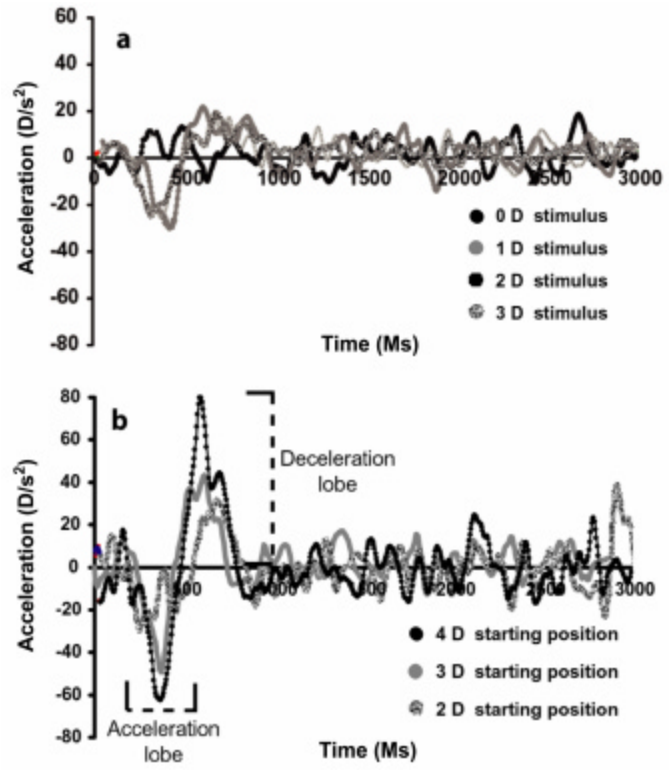

Figure 29. Disaccommodative acceleration profiles plotted as a function of time.

(a). Acceleration profiles are shown for approximately 0 D, 1 D, 2 D & 3 D magnitude responses from a 4 D starting position. (b). Acceleration profiles are shown for approximately 1.5 D magnitude responses from 4 D, 3 D & 2 D starting positions.

These acceleration profiles correspond to the velocity profiles shown in figures 25 a & b.

significantly with the proximity of the starting position in all but a few conditions (F-value: <0.01) (Figure 29b, Table VIII). The subjects and conditions in which statistical significance was obtained are denoted with an asterisk symbol. These results indicated that the peak acceleration characteristics of disaccommodation also depend on the starting position.

For a constant starting position, the time-to-peak acceleration (TPA) remained constant with the response magnitude for all the subjects (P-value: >0.5). The linear regression equation fit to the lumped data of TPA as a function starting position (y = 6.93 x + 79.43) showed a statistically insignificant change in TPA with starting position (P-value: >0.5) (Figure 29c). The mean TPA for all response magnitudes from a common starting position did not change significantly with the starting position, except in subject

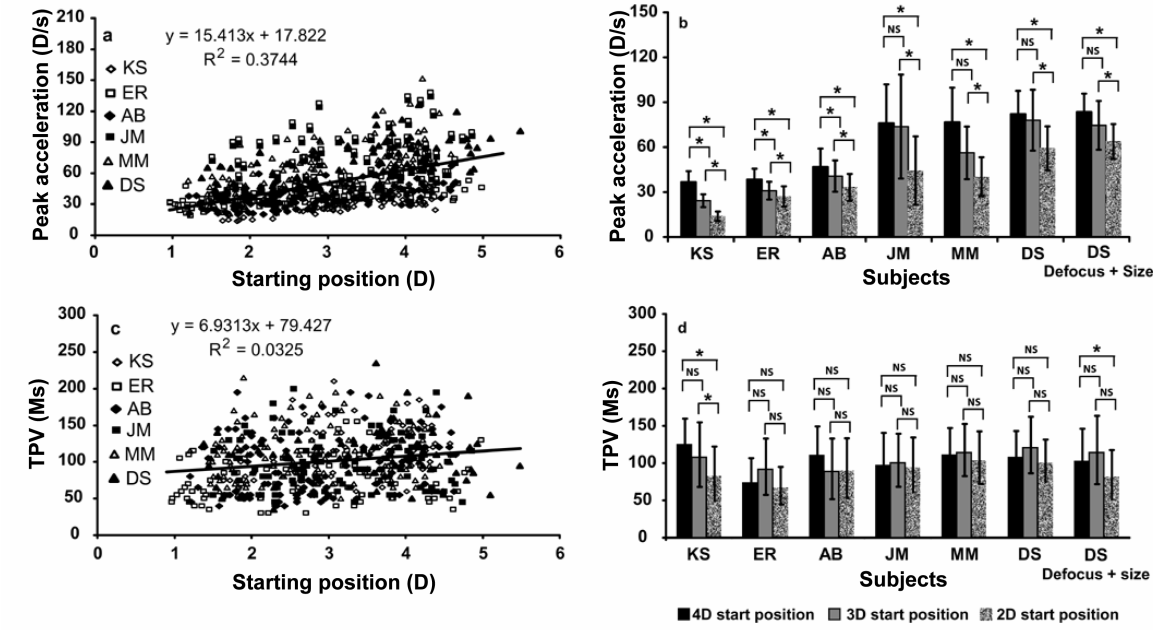

Figure 30. (a) Peak acceleration of disaccommodation is plotted as a function of starting position for all subjects (except SRB). The solid line represents the linear regression equation fit to the data. (b) Mean peak acceleration is plotted for the three starting positions for all the subjects in the defocus-only experiment and for subject DS in the defocus + size experiment. (c) Time-to-peak acceleration (TPA) is plotted as a function of starting position for all subjects (except SRB). The solid line represents the linear regression equation fit to the data. (d) Mean TPA for the three starting positions for all the subjects. The error bars in b & d indicate +/- 1 standard deviation and the asterisk (*) symbol indicates statistical significance at a p-value of =< 0.01 and 'NS' indicates statistical insignificance.

KS (Figure 29d, Table VIII). The subjects and conditions in which statistical significance was obtained are denoted with an asterisk symbol.

5.2. Data of subject SRB

5.2.1. Position characteristics

Characteristic differences were seen in the position, velocity and acceleration profiles between the first and second sessions. The oscillations and overshoots seen in the smaller responses (2 D) of the first session were completely absent in the smaller responses (2 D)

of the second session (Figure 30a, b). The larger response magnitudes did not show any significant oscillations in the two sessions (Figure 30a, b). Exponential functions describing the magnitude of primary overshoot as a function of response magnitude quantitatively confirmed the findings seen in the position traces of the two sessions (Figure 31a, b). Overall, in the first session, the magnitude of primary overshoots was larger for the smaller response magnitudes than for the larger response magnitudes and was more prominent in the 6 D starting position than in the 4 D starting position (Figure 31a). In the second session, the magnitude of primary overshoot did not change significantly with the response magnitude or with the starting position. An analysis of the frequency of responses exhibiting overshoots for each response magnitude bin could not be performed due to insufficient test conditions in the two sessions.

	Start pos (D)	**Mean PA (D/s^2)**	**Mean TPA (ms)**
KS	2	13.68 ± 3.13	82.31 ± 36.55
	3	23.99 ± 4.29	107.85 ± 43.27
	4	36.38 ± 7.38	125.17 ± 31.04
ER	2	26.86 ± 6.76	66.82 ± 24.65
	3	30.72 ± 5.95	91.73 ± 37.76
	4	38.12 ± 7.23	74.00 ± 29.23
AB	2	32.86 ± 9.03	89.72 ± 40.13
	3	40.44 ± 10.44	88.83 ± 40.68
	4	46.46 ± 12.36	110.83 ± 34.96
JM	2	44.10 ± 22.82	94.23 ± 36.71
	3	73.50 ± 34.72	100.43 ± 35.57
	4	75.67 ± 26.03	97.30 ± 39.92
MM	2	40.03 ± 12.99	103.78 ± 35.28
	3	55.96 ± 17.57	114.14 ± 34.98
	4	76.40 ± 23.03	111.25 ± 32.33
DS	2	58.99 ± 14.61	99.77 ± 28.43
	3	77.74 ± 20.32	120.83 ± 37.88
	4	81.80 ± 15.53	108.06 ± 31.54
DS¶	2	63.46 ± 11.67	80.94 ± 33.08
	3	74.30 ± 16.30	114.17 ± 45.82
	4	83.20 ± 12.23	102.86 ± 39.70

Table VIII. Mean peak acceleration (PA) and mean time-to-peak acceleration (TPA) for the 2 D, 3 D & 4 D starting positions for the six subjects in the defocus-only experiment and for one representative subject (DS¶) in the defocus + size experiment. The ± errors indicate 1 standard deviation from the mean.

5.2.2. Velocity characteristics

The velocity profiles shown in figure 30c & d showed a linear increase in velocity with time in both sessions until the peak velocity was reached. The peak velocity remained invariant of the response magnitude for both starting positions in the first session (Figure

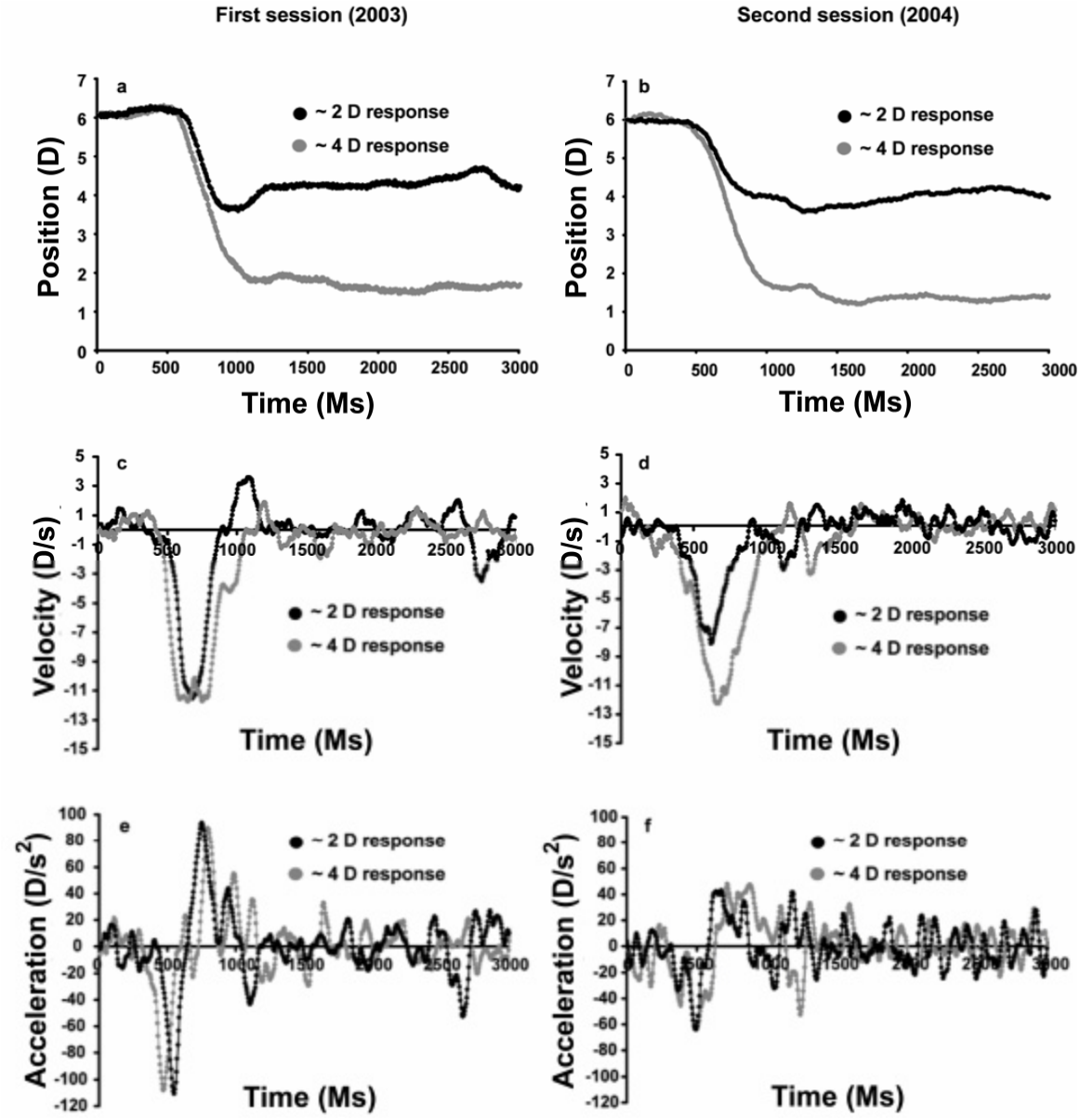

Figure 31. An illustration of disaccommodation position (a, b), velocity (c, d) and acceleration (e, f) profiles for subject SRB. Figures a, c & e show traces for the first session, and figures b, d & f show traces for the second session.

31c) while it increased significantly with response magnitude for each starting position in the second session (Figure 31d). The peak velocity for the smaller response magnitudes was higher in the first session than in the second session while the peak velocity for the larger response magnitudes was similar in both sessions (Figure 30c, d). The peak velocity increased with the proximity of the starting position in both sessions (except 4 D & 5 D starting positions in second session) (Single Factor ANOVA and Bonferroni multiple comparison procedure: F-value: <0.01). The Type-I main sequence relationships shown in figure 31c & d and Table IX quantitatively confirmed the findings seen in the velocity traces. Overall, in both the 4 D and 6 D starting positions, the smaller response magnitudes (e.g. 2 D) had higher peak velocities in the first session than in the second session while the larger response magnitudes (e.g. 4 D) had similar peak velocities in both sessions. The time-to-peak velocity (TPV) was constant with both response magnitude and starting position in the first session (F-test: >0.05, Figure 31e). In the second session, the TPV increased significantly with the response magnitude for the 2 D, 5 D and 6 D starting position (P-value: <0.01), marginally for the 4 D starting position (P-value: <0.05) and insignificantly for the 3 D starting position (P-value: >0.4) (Figure 31f). The TPV did not change significantly with the starting position in the both sessions (F-value: >0.05) (Figure 31e, f). The mean TPV's for both the 4 D and 6 D starting positions were significantly shorter in the first session than in the second session for both the 4 D and 6 D starting positions.

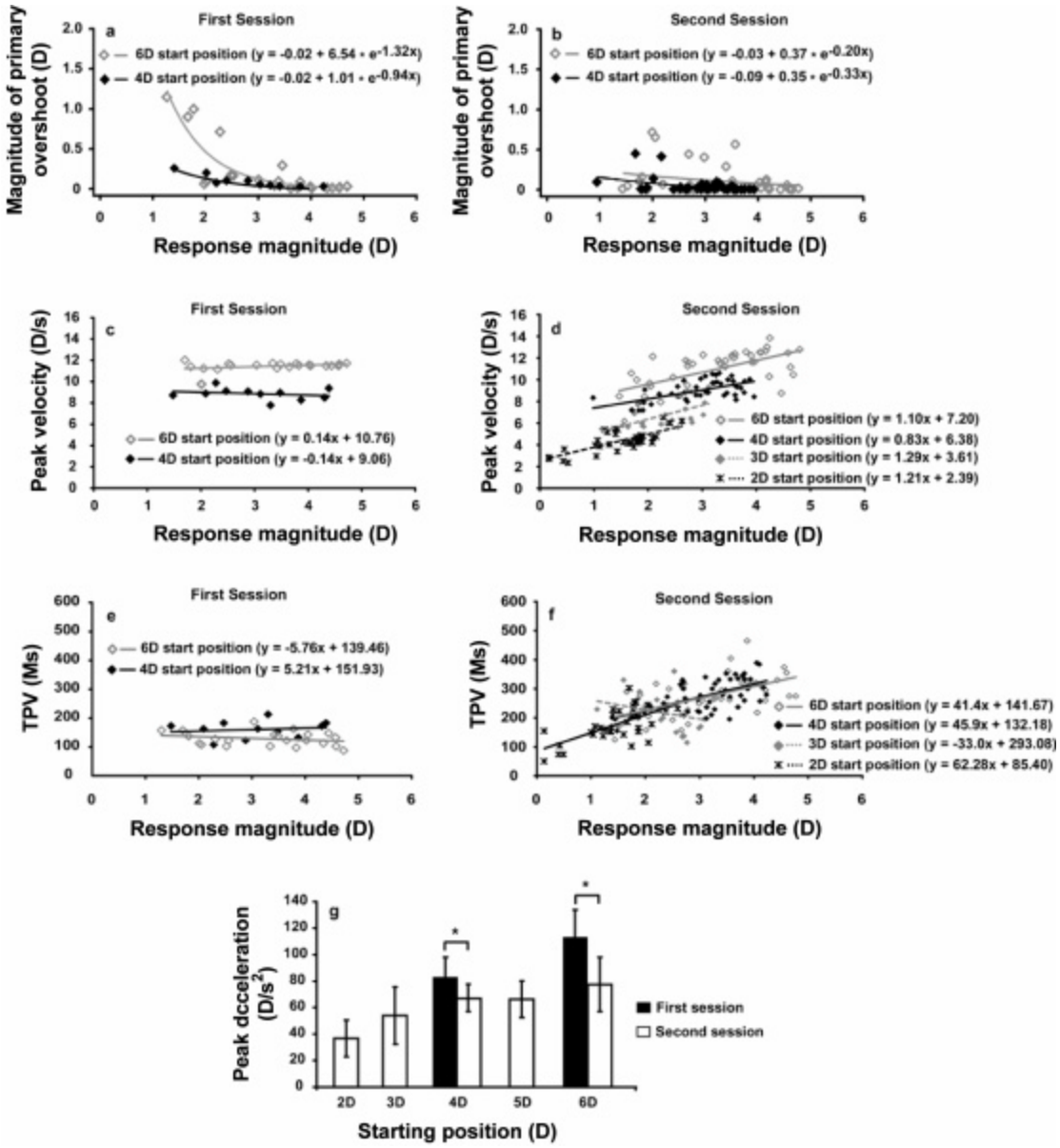

Figure 32. First- and second-order dynamic characteristics of disaccommodation for the first session and second session of subject SRB. The magnitude of the primary overshoot is plotted as a function of response magnitude for the 6D & 4 D starting positions in the first session (a) and second session (b). Type-I main sequence is plotted for the 4 D and 6 D starting positions in the first session (c) and second session (d). In the second session, the main sequence plot of the 5 D starting position has been omitted in the figure for the sake of clarity. TPV is plotted as function of response magnitude for the 4 D and 6 D starting position in the first session (e) and in the second session (f). Peak acceleration (g) for the 4 D and 6 D starting positions is plotted for the first session and 2 D – 6 D starting positions for the second session. The closed histograms represent the first session and the open histograms represent the second session. The error bars indicate +/- 1 standard deviation and the asterisk symbol indicates statistical significance at =< 0.01.

5.2.3. Acceleration characteristics

Similar trends were seen in the peak accelerations for the first session and second session (Figure 30e, f). In both sessions, the peak accelerations remained invariant of the response magnitude for a constant starting position (Figure 30e, f). In the first session the mean peak acceleration was higher for the 6 D starting position than for the 4 D starting position (Figure 31g, Table IX). In the second session, the peak acceleration increased only marginally with the proximity of the starting position, except for the 2 D starting position (F-value: <0.2) (Figure 31g, Table IX). For both the 4D and 6D starting positions, the mean peak accelerations were significantly higher in the first session than in the second session (P-value: <0.01) (Figure 31g) and peak acceleration increased significantly with starting position in the first session, but only marginally in the second session. The time-to-peak accelerations (TPA) remained constant with response magnitude and starting position in both sessions (not shown).

Session	Start pos (D)	Type-I Main sequence	Mean PV (D/s)	Mean TPV (ms)	Mean PA (D/s^2)
First session	4	y = -0.14x + 9.06	8.62 ± 0.56	166.93 ± 31.75	82.72 ± 15.32
	6	y = 0.14x + 10.76	11.10 ± 0.57	123.28 ± 25.22	112.76 ± 21.14
Second session	2	y = 1.21x + 2.39	-	-	36.73 ± 13.84
	3	y = 1.28x + 3.61	-	-	53.95 ± 21.70
	4	y = 0.83x + 6.38	-	-	66.93 ± 15.89
	5	y = 1.52x + 4.78	-	-	66.36 ± 13.88
	6	y = 1.10x + 7.20	-	-	77.44 ± 20.52

Table IX. First session and second session data for subject SRB. Type-I main sequence linear regression equations, mean peak velocity (PV), mean time-peak velocity (TPV) and mean peak acceleration (PA) for 4 D & 6 D starting positions in first session and 2 D, 3 D, 4 D, 5 D & 6 D starting positions in second session. The dashes (-) indicate that the parameter was not constant but increased linearly with response magnitude. The linear regression equations for these parameters could be found in the text and in the respective figures.

5.3. Defocus + size experiment

The position, velocity and acceleration data of subject DS showed similar trends in the defocus + size experiment as in the defocus-only experiment. For a constant starting position, the defocus + size data showed the peak velocity, time-to-peak velocity (TPV) and the peak acceleration of disaccommodation to remain invariant of the response magnitude from a common starting position (P-values: peak velocity: >0.5; TPV: >0.5; peak acceleration: >0.7). For each starting position, the peak velocities, TPV's and peak accelerations were averaged across response magnitude. The peak velocities and peak accelerations increased significantly with the proximity of the starting position (Single-factor ANOVA and Bonferroni multiple comparison procedure, F-value: <0.01) (see right most histograms in Figures 27b & 29b). The TPV and TPA increased significantly between the 2D and 4D the starting positions (see right most histogram in Figure 27d & 29d). No statistically significant differences were found in any of the data obtained from the defocus + size experiment and the defocus-only experiment (Type-I main sequence slope and intercept, P-value: >0.5; TPV as a function of response magnitude, P-value: >0.7; peak acceleration as a function of response magnitude, P-value: >0.8). The linear regression equations for the peak velocity and peak acceleration data and the averaged peak velocities, TPV's and peak accelerations for the three starting positions are given in the bottom row of Table VII. These results indicate that the constant peak velocity, TPV and peak acceleration for a given starting position did not result from reduced cues for changes of target distance.

6. Discussion

The results of the first experiment are summarized by the following four points

1. For a constant starting position, the peak velocity, time-to-peak velocity (TPV), peak acceleration and time-to-peak acceleration (TPA) of disaccommodation remains invariant of the response magnitude.
2. For all disaccommodative stimuli stepped to a common ending position (0 D), the peak velocity and peak acceleration of disaccommodation increased as a function of the response magnitude while the TPV and TPA remained invariant of the response magnitude.
3. For the 2D, 3D and 4D starting positions, the peak velocity and peak acceleration of disaccommodation increase with the proximity of the starting position while the TPV and TPA remain constant with starting position.
4. Smaller magnitude responses from near starting positions are unstable and have overshoots or oscillations.

The data of subject SRB could be summarized in the following five points

1. Position characteristics: In the first session, the smaller magnitude responses showed significant overshoots and oscillations before attaining a stable steady-state. These oscillations were either minimal or completely absent in the smaller magnitude responses in the second session. This demonstrates that overshoots or oscillations can be reduced with practice by lowering both peak acceleration and peak velocity and increasing time-to-peak velocity.

2. Peak velocity characteristics: For a constant starting position, the peak velocity remained invariant with the response magnitude, in the first session, but the peak velocities increased with the response magnitude in the second session. In both the sessions, the peak velocities increased with the proximity of the starting position. The peak velocities for smaller magnitude responses were higher in the first session than in the second session while the peak velocities for larger magnitude responses were similar in both sessions.
3. TPV characteristics: For a constant starting position, the TPV remained invariant with response magnitude, in the first session, but the TPV increased with the response magnitude in the second session. The TPV did not change with starting position in either session. The TPV's for all response magnitudes were shorter in the first session than in the second session.
4. Peak acceleration characteristics: For a constant starting position, the peak acceleration was invariant of response magnitude in both the sessions. The peak acceleration also increased with the proximity of the starting position in the first session but less so in the second session. The mean peak accelerations were higher in the first session than in the second session.
5. TPA characteristics: For a constant starting position, the TPA remained invariant with response magnitude and starting position, in the both sessions. The TPA did not differ in magnitude in the two sessions.

The Type-I and Type-II main sequence trends observed for the six subjects and in the first session for subject SRB (Figure 26a – d) are consistent with previous

observations of the invariance of peak velocity with response magnitude when the starting position of disaccommodation stimuli is constant (Yamada & Ukai, 1997; Kasthurirangan & Glasser, 2003) and an increase in peak velocity with response magnitude when the ending position of disaccommodation stimuli is constant (Vilupuru & Glasser, 2002, Kasthurirangan *et al.*., 2003; Mordi & Ciuffreda, 2004). Our results clearly demonstrate the importance of measuring both the Type-I and Type-II main sequences to understand the dynamics of disaccommodation. The Type-II main sequence alone might lead one to believe that increase in peak velocity of disaccommodation is associated with increased response magnitudes. However, the Type-II main sequence was constructed using a subset of data (data for all stimuli ending at 0-D) from the Type-I main sequence. In the Type-II main sequence, larger response magnitudes corresponded to more proximal starting positions and smaller response magnitudes corresponded to more distal starting positions. This shows that the increase in starting position was responsible for the increase in peak velocity as opposed to an increase in response magnitude. In addition, this study also showed that the trends in peak acceleration were similar to those for peak velocity, demonstrating that both the first- and second-order dynamics of disaccommodation step responses depend on starting position.

Alvarez *et al* (2005) reported that disparity driven divergence step responses also exhibit similar starting position dependent velocity characteristics. The peak velocity of similar magnitude (4?) divergence eye movements increased with the proximity of starting position. Our inspection of their illustrations reveals that the initial slope of the velocity profiles (giving an estimate of the response acceleration) also increased with the

proximity of starting position. The time-to-peak velocity (taken as the time from start of the response to the time when the peak velocity is reached) changed insignificantly with the starting position. These observations are very similar to those obtained for disaccommodation step responses in our experiment and suggest that the starting position dependent characteristics could have a common neural origin. Gamlin and colleagues (Gamlin & Clarke, 1995; Gamlin *et al*., 1996) have identified near-response cells in the primate prearcuate cortex, nucleus reticularis tegmenti pontis (NRTP) and the posterior interposed nucleus (IP) that modulate their firing rates in response to combined changes in disaccommodation and divergence (far-response). The starting position dependent characteristics of the two systems could be a reflection of the firing properties of these neurons. Since the mechanical properties of the disaccommodation plant (crystalline lens, ciliary muscle, choroid and suspensory zonules) are very different from those of the oculomotor plant (lateral rectus and medial rectus muscles), it is unlikely that the starting position dependent characteristics of disaccommodation and divergence are mechanical in origin.

6.1. Dynamic control of disaccommodation and starting position

The peak velocity and peak acceleration remained invariant of the response magnitude for a constant starting position and they increased with the proximity of starting position in all our subjects, including SRB (Figures 27a, b, 29a, b & 31c, d). This suggests that, for a constant starting position, a constant relaxation force is applied by the ciliary muscle and the magnitude of this relaxation force increases with the proximity of the starting position. Further, none of the responses showed large 'lags' or 'leads' of

disaccommodation implying that the responses attained their desired steady-state responses. However, small responses tend to overshoot before reaching the steady-state at the end of the response (Figure 24a & b). These responses are qualitatively similar to those observed for relaxation of accommodation by Shirachi *et al.* (1978), Sun & Stark (1986) and Yamada & Ukai (1997). These observations suggest that all disaccommodation responses, irrespective of the step stimulus magnitude, are initiated towards a constant primary destination and are switched mid-flight to attain their desired final position. Large discrepancies between the primary destination of the initial response and the final desired position of the steady-state appear to produce the overshoots of small responses from proximal starting positions. The initial response appears to determine both the peak velocity and peak acceleration properties of the disaccommodation step response. This interpretation is in accordance with a model proposed by Yamada & Ukai (1997). They suggested that, for a constant starting position, the disaccommodation responses were initiated towards a common initial destination point which they proposed was the resting focus of accommodation (Leibowitz & Owens, 1978), and the distance of the starting position from the resting focus determined the peak velocity of disaccommodation.

6.2. Effect of size and defocus changes on disaccommodation dynamics

Here and in our earlier experiment on the dynamics of accommodation (Bharadwaj & Schor, 2005a), retinal image defocus was used as the primary cue for accommodation and disaccommodation. Retinal image defocus greater than 2D is an ambiguous cue for the direction of focus error (Fincham, 1951; Troelstra *et al*., 1964; Crane, 1966; Toates,

1972). This makes the focus error estimate for disaccommodation to step stimuli greater than 2D unreliable. It is possible that trends in the dynamics of accommodation and disaccommodation could have resulted from the ambiguous nature of the defocus stimulus. In both these experiments, we improved the saliency of the defocus-magnitude estimate by coupling retinal image size changes with optical defocus. No significant differences in the trends of the dynamics of either accommodation or disaccommodation were observed in the defocus + size and defocus-only conditions. This suggests that the trends in the peak velocity and peak acceleration of accommodation and disaccommodation do not arise from the ambiguous nature of retinal image defocus signal. Instead, for disaccommodation, the increase in peak velocity and peak acceleration with starting position and not defocus magnitude could thus be a behavioral strategy employed by the disaccommodation control system.

For accommodation, the increase in peak velocity with response magnitude suggests that subject's could have calibrated the initial open-loop phase of the accommodation response to the magnitude of defocus based on exposure to the stimuli at the beginning of the experiment. Such a recalibration could have also been necessitated by the dilation of the pupils in our experiment. Following geometric optics predictions, in a diffraction-limited eye, the amount of retinal image blur for constant focus-error increases with the size of the pupil. Thus for accommodation, subjects may have had to recalibrate the relationship between blur magnitude and defocus error with the dilated pupil. However, factors such as the Stiles-Crawford effect make the effective pupil size smaller (Stiles & Crawford, 1933; Campbell, 1957; Charman & Whitefoot, 1977), and the increased

aberrations associated with larger pupils (Charman, 1991) reduce the change in contrast associated with defocus (Levi, 1968; Charman & Whitefoot, 1977), thus making a recalibration unnecessary. Finally, Kotulak & Schor (1986) developed a computational model that estimates the stimulus amplitude by taking the first derivatives of two time-varying functions based on steady-state oscillations of the lens: the lens power and retinal-image contrast. The ratio of these two derivatives could yield the focus error magnitude.

6.3. Comparing the dynamics of accommodation and disaccommodation

Earlier, we examined the first-and second-order dynamics of accommodation step responses (Bharadwaj & Schor, 2005a). Here, we sought to compare the dynamic characteristics of accommodation with those obtained for disaccommodation in this experiment. Since the dynamics of accommodation and disaccommodation were obtained from two different groups of age-matched individuals (accommodation: 23 – 35yrs; disaccommodation: 21 – 32yrs), we have compared the trends in their dynamic properties. This comparison revealed both similarities and dissimilarities in the dynamic trends of accommodation and disaccommodation, which suggests differences in their neural control strategies.

Contrasting trends were observed in the velocity characteristics (peak velocity and TPV) of accommodation and disaccommodation responses for a given starting position. The peak velocity of accommodation responses starting at 0D increased linearly with response magnitude ($y = 1.58x + 3.42$) while the peak velocity of disaccommodation

from a fixed starting position remained invariant of response magnitude. Similarly, the TPV of accommodation increased with the response magnitude ($y = 29.53x + 134.08$) while the TPV of disaccommodation changed insignificantly with the response magnitude. Similar trends were observed in the acceleration characteristics (peak acceleration and TPA) of accommodative and disaccommodative responses from a constant starting position. The peak acceleration of both accommodation and disaccommodation remained invariant of the response magnitude. Similarly, the TPA of both accommodation and disaccommodation also remained invariant of the response magnitude. These trends in the dynamics of accommodation and disaccommodation suggest that accommodation step responses have a variable initial response that depends on the response magnitude while disaccommodation step responses have a constant initial response that is independent of the response magnitude from a constant starting position. Further, the initial and final components of the step responses have a common destination for accommodation but they have different destinations for disaccommodation.

The peak velocity of accommodation step responses increased with response magnitude when they were elicited from a constant starting point of 0-D ($y = 1.58x + 3.42$). Similarly, the peak velocity of disaccommodation step responses also increased with response magnitude when they were elicited towards a constant ending point of 0-D (Type-II main sequence: $y = 1.67x + 2.18$) (Figure 26c, d). The coefficients of the regression equation imply that accommodation and disaccommodation step responses of similar magnitudes stepped from and to a common distance (0-D) traveled with similar speeds. The accommodation and disaccommodation main sequence trends obtained in

our experiments were similar to those obtained in earlier studies (Ciuffreda & Kruger, 1988; Schaeffel *et al.*, 1993; Croft *et al.*, 1998; Vilupuru & Glasser, 2002; Kasthurirangan *et al.*, 2003; Mordi & Ciuffreda, 2004).

Our results differ from those of Schaeffel *et al* (1993) and Kasthurirangan *et al.* (2003) in that they observed disaccommodation step responses to have higher peak velocities than accommodation step responses. However, their results cannot be compared directly with ours for atleast two reasons. One, we measured accommodation and disaccommodation step responses on age-matched but different individuals while Schaeffel *et al* (1993) and Kasthurirangan *et al* (2003) measured both accommodation and disaccommodation step responses on the same individuals. The dynamics of these step responses are known to exhibit significant inter-individual variability (Schaeffel *et al.*, 1986; Heron *et al.*, 2001). It is possible that, in our results, the differences in the peak velocities of accommodation and disaccommodation could have been masked by the inter-individual variability and that these differences would become more salient if both accommodation and disaccommodation were tested on the same individual. Second, different methods were employed to collect and analyze the data in these experiments. We used an infrared optometer with a high sampling frequency (200 Hz) to record accommodation and disaccommodation responses and estimated the peak velocity directly from the position traces without assuming any function for the step responses. Schaeffel *et al* (1993) and Kasthurirangan *et al* (2003) used the photorefraction technique with relatively lower sampling frequency (5.23 Hz and 25 Hz respectively) to measure accommodation and disaccommodation step responses. Schaeffel *et al* derived their

velocity profiles using a seven-point sliding regression algorithm (Schaeffel, 2005) while Kasthurirangan *et al* derived the peak velocity by assuming an exponential fit to the position traces. Shirachi *et al* (1978) show that the exponential function is only a first-order approximation of the accommodative step responses and it is best described with higher-order non-linear function. Another limitation with the exponential function is that it predicts the peak velocity of disaccommodation and accommodation to be achieved instantaneously (Suryakumar, 2005), which is physiologically implausible. These approximations could also account for the differences in the results of our experiment and those of Kasthurirangan *et al* (2003).

Do accommodation and disaccommodation step responses use similar strategies to increase their peak velocities? Peak velocities could be increased by either increasing the peak acceleration in proportion to the response magnitude, or by holding fixed peak acceleration for longer durations. For accommodation step responses, the peak acceleration remained invariant of the response magnitude while the time-to-peak velocity increased with response magnitude (Bharadwaj & Schor, 2005a). This suggests that increments in peak velocity of accommodation are achieved by holding fixed peak acceleration for longer durations of time. For disaccommodation step responses, the peak acceleration increased with the starting position while the TPV remained invariant of the starting position. This suggests that increments in peak velocity of disaccommodation are achieved by increasing the peak acceleration in proportion to the response magnitude. Thus, accommodation and disaccommodation step responses use different strategies to increase their peak velocities with response magnitude.

6.4. Data of subject SRB: Influence of training on the dynamics of disaccommodation

The first- and second-order dynamics of subject SRB were on average more sluggish or damped in the second session than in the first session. The sluggishness was more prominent for the 6 D starting position than for the 4 D starting position. The mean peak acceleration was lower in the second session than in the first session (Figure 31g). The smaller magnitude responses had a lower peak velocity in the second session than in the first session while the larger magnitude responses had similar peak velocities in the two sessions (Figure 30c, d & 31c, d). The reduction in peak acceleration and peak velocity of the smaller magnitude responses could be caused by dampening the amplitude of the first and second-order components of the response to avoid unstable oscillations of small responses from near starting positions. The time-to-peak velocity was longer in the second session than in the first session (Figure 31e, f). This suggests that the peak velocities were fully restored for larger magnitude responses, and partially restored for smaller magnitude responses in the second session by accelerating longer at lower peak accelerations.

The changes in the dynamic trends in the second session could be a result of an alteration in the neural control strategy of disaccommodation to one similar to the dynamic control of accommodation, as described by Schor & Bharadwaj (2005). Over the course of this experiment, subject SRB became well trained in the disaccommodation task by taking part in numerous experiments. We speculate that the change in his control strategy is a result of this extensive training. Disaccommodation normally begins with a response toward a common initial destination point as described by Yamada & Ukai

(1977), however after training; disaccommodation by SRB appears to have begun with a response toward the final destination. This is the same control strategy as described for accommodation by Schor & Bharadwaj (2005). Adaptation of static and dynamic properties of human ocular accommodation has been demonstrated earlier. For example, the resting focus of accommodation is adapted following prolonged periods of near work (Schor *et al.*, 1984; Rosenfield *et al.*, 1994) and the abnormally sluggish dynamics of accommodation can be improved with practice (Liu *et al.*, 1979; Bobier & Sivak, 1983). The changes in dynamics of disaccommodation between the first and second sessions by subject SRB provides additional evidence for the adaptable nature of the dynamics of disaccommodation. Further experiments are however warranted to explore these dynamic adaptable properties in greater detail.

7. Conclusion

This study demonstrates and confirms earlier findings (Yamada & Ukai, 1997; Kasthurirangan & Glasser, 2003) that disaccommodation step responses exhibit starting position dependent first- and second-order dynamics. For a constant starting position, the peak velocity and peak acceleration of disaccommodation remained invariant of the response magnitude and they increased with the proximity of the starting position. These observations suggest that all disaccommodation step responses, irrespective of their response magnitude, are initiated towards a constant primary destination and are switched mid-flight to attain their desired final position. Large discrepancies between the primary destination of the initial response and the final desired position of the steady state appear to produce the overshoots and oscillations of small responses from proximal starting

positions. These overshoots or oscillations can be reduced with practice by reducing both peak acceleration and peak velocity and increasing time-to-peak velocity.

Chapter IV. Initial destination of the disaccommodation step response

1. Abstract

Peak velocity and peak acceleration of disaccommodation step responses remain invariant of response magnitude for a constant starting position and they increase linearly with proximity of starting position. This suggests that disaccommodation response is initiated towards an initial (default) destination and is switched mid-flight to attain the desired final destination. The dioptric location of initial destination was estimated from the x-intercept of regression of peak velocity on response starting position. The x-intercept correlated well with subject's cycloplegic refractive state and poorly with their dark focus of accommodation. Altering the dark focus by inducing fatigue in the accommodative system did not alter the x-intercept. These observations suggest that cycloplegic refractive state is a good behavioral correlate of initial destination of disaccommodation step responses.

2. Introduction

Ocular disaccommodation refers to the reduction of the accommodative response from a near target to a far target. The first- and second-order dynamics of disaccommodation step responses exhibit two characteristics that depend on starting position (Bharadwaj & Schor, 2005b; Kasthurirangan & Glasser, 2005). First, for a given starting position, the peak velocity and peak acceleration of disaccommodation remain invariant of the response magnitude (Figure 33a, c, e). Second, both peak velocity and peak acceleration of disaccommodation increase linearly with proximity of the starting position (Figure 33b, d, f). Based on these results we postulated that, for a given starting position, the same relaxation force is applied by the ciliary muscle to initiate all disaccommodation responses towards an initial (default) destination, irrespective of the magnitude of the final response. Initially, the disaccommodation response is under open-loop control (without feedback) and subsequently it is switched mid-flight to closed-loop control to attain the desired final position (Bharadwaj & Schor, 2005b; Schor & Bharadwaj, 2005b). Peak acceleration and peak velocity describe the dynamic properties of the initial open-loop component. The linear increase in peak velocity and peak acceleration with proximity of starting position suggests that the initial open-loop component of all disaccommodation responses could have a common initial destination. The main aim of this paper was to estimate the dioptric location of the initial destination of the disaccommodation step response. A secondary aim was to obtain a behavioral correlate for the initial destination of disaccommodation.

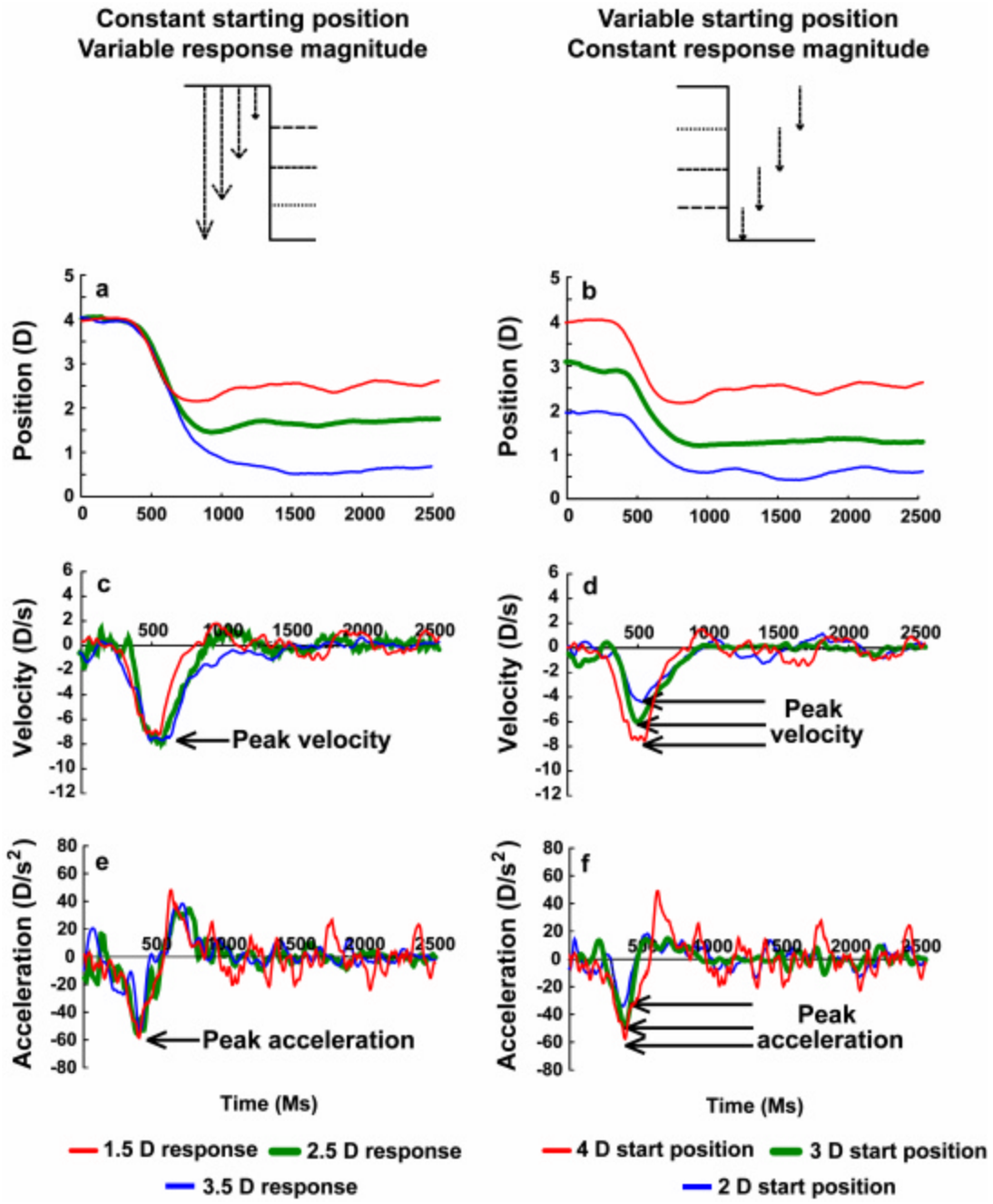

Figure 33. Position (a & b), velocity (c & d) and acceleration (e & f) profiles of disaccommodation plotted as a function of time for one representative subject. Profiles shown in the left-hand column belong to different response magnitudes from a constant starting position (4 D). Profiles shown in the right-hand column belong to similar response magnitudes (1.5 D) from three-different starting positions (4 D, 3 D & 2 D). Disaccommodation position profiles were collected using the SRI-dynamic infrared optometer, in response to step changes in optical defocus. Response profiles were differentiated and smoothed to compute velocity and acceleration profiles. A detailed account of the data collection and data analysis techniques can be found in Bharadwaj & Schor (2005a).

In a study of the role of defocus as an odd-error cue to accommodation, Yamada and Ukai (1997) observed that the initial trajectories of disaccommodation step responses from different starting positions were on the "same path" and were initiated towards a common destination. They estimated the location of the initial destination by fitting exponential functions to the "first half" of the disaccommodation step responses. The location of the initial destination was indicated by the final steady-state position of the exponential function. They observed in two of the three subjects that the initial destination was close to the dark-focus of accommodation (Leibowitz & Owens, 1975, 1978; Rosenfield et al., 1993). However, as discussed in detail later (discussion section); estimates of initial destination were based on the incorrect assumption that an exponential function was a good fit to the initial step response. Hence we found it necessary to re-examine the location of the initial destination of disaccommodation using a different analytical technique.

Here, we estimated the dioptric location of the initial destination from the x-intercept of the regression of peak velocity on starting position of disaccommodation. We assume that the peak velocity of disaccommodation is proportional to the dioptric difference between the starting position and the initial destination of disaccommodation (Yamada & Ukai, 1997; Bharadwaj & Schor, 2005b). This assumption predicts that the peak velocity decreases as the dioptric difference between the starting position and initial destination decreases and that the peak velocity is reduced to 0 D/s when the starting position equals the initial default destination. Thus, the x-intercept of the linear regression of peak velocity on starting position would estimate the dioptric location of the initial

destination. To obtain a behavioral correlate of the estimated initial destination, we measured the correlation between x-intercept and either the dark focus of accommodation or the cycloplegic refractive state*.

3. Methods

A total of eleven subjects took part in the experiment. Ten subjects were naïve to the aims of the experiment and they were inexperienced observers. One of the authors (SRB) was the eleventh subject and he was aware of the aims of the experiment. Data for subject SRB were analyzed separately for reasons discussed below. None of SRB's data has been included with the analyses of other subject's, however they are shown for comparison purposes in Figures 34 & 36 and Table X. The subjects' ages ranged from 21-yrs to 34-yrs. Their refractive errors, as denoted by the spherical equivalent of refraction, ranged from -3.75 D to +0.50 D (Table X). The first- and second-order dynamic characteristics of their disaccommodation step responses were similar to those described in an earlier paper (Bharadwaj & Schor, 2005b). Overall, peak velocity and peak acceleration of all eleven subjects were invariant with response magnitude of disaccommodation from a constant starting position and peak velocity and peak acceleration of disaccommodation increased with the proximity of the starting position.

---

* Cycloplegia is a clinical term that refers to a complete relaxation of accommodation (Pragnen, 1931; Giles, 1965; Michaels, 1985) and it occurs as a result of blocking the parasympathetic innervation (paralysis) to the ciliary muscle (Mitchell, 1960).

The peak velocity of disaccommodation was plotted separately for ten subjects as a function of the starting positions of disaccommodation step responses and best-fit linear regression equations were fit to these plots to calculate the x-intercepts (Figure 34). In ten subjects, the relationship between the peak velocity and response starting position was described by a single linear regression equation. The robustness of the linear regression fit was assessed by computing the +/- 95% confidence intervals (Devore & Peck, 1993a). The x-axis zero-crossings of the confidence intervals provided the range of initial destination estimates permitted by the confidence intervals.

Prior to the measurement of the dark focus, subjects were seated in a dark room for approximately 5 min to allow any residual accommodation to decay (Fisher et al., 1987; Wolf et al., 1987). Following this, subjects were instructed to focus on a dark screen while their accommodation was measured using the Grand Seiko open-field binocular auto-refractor (Hiroshima, Japan) (Whiteside, 1953; Westheimer, 1957; Schor et al., 1986). The dark screen (field of view: 47.48°; mean luminance: 0.52 cd/m^2) was devoid of any accommodative stimuli and hence provide a good viewing condition to measure the open-loop dark-focus of accommodation (Whiteside, 1953; Westheimer, 1957; Schor et al., 1986). Fifteen measurements of the dark-focus were obtained from the left eye of each subject and they were averaged to obtain the mean dark-focus. The right eye was occluded during all the measurements. Subsequently, correlation between the dark-focus and the initial destination, estimated from the x-intercept of the regression analysis using the Pearson's sample correlation coefficient (Devore & Peck, 1993b), was tested.

The cycloplegic refractive states were measured on ten subjects (except subject AB who was not available for the experiment) on a separate day after the dynamic properties of the disaccommodation step responses were determined. Cycloplegia was achieved 20 – 30 minutes following instillation of 2 – 3 drops of 1% Tropicamide (Gettes & Belmont, 1961; Michaels, 1985; Lovasik, 1986). Cycloplegia was verified two ways. First, as a cursory check on the accommodative ability of the subject, a high contrast near-acuity card was slowly and progressively brought closer or moved away from the subject (push-up test; Grosvenor, 1996). The dioptric equivalent of the nearest distance where the subject could not read the smallest line of letters in the card was considered the maximum amplitude of accommodation. Maximum amplitude of accommodation of less than 0.5D was considered as full cycloplegia (Lovasik, 1986). Once an accommodative amplitude of less than 0.5 D was observed using the push-up test, the subjects were aligned in the SRI optometer and were asked to focus on a black and white Maltese cross that was optically defocused (step changes of 1D – 4D) using the SRI stimulating optometer and accommodation was measured using the SRI recording optometer. The absence of any significant accommodation response to these step changes in optical defocus indicated full cycloplegia. Following this, the cycloplegic refractive states were measured fifteen times on each subject using the Grand Seiko open-field binocular auto-refractor (Hiroshima, Japan) and these measurements were averaged to obtain the mean cycloplegic refraction. Only the left eye was cyclopleged while the right eye was occluded during all the measurements.

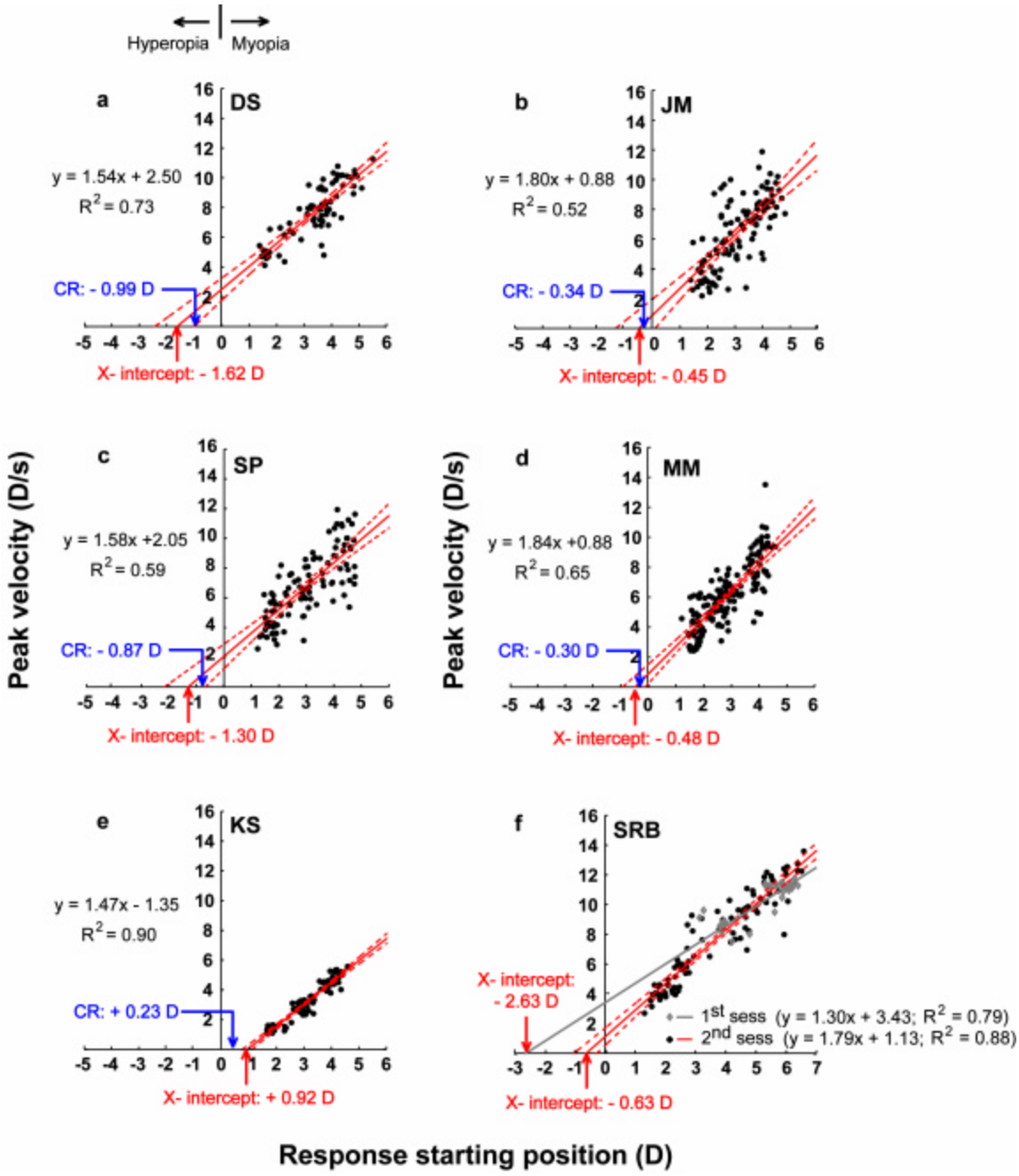
Hyperopia
Myopia
a
DS
y = 1.54x + 2.50
R2 = 0.73
CR: - 0.99 D
X- intercept: - 1.62 D
b
JM
y = 1.80x + 0.88
R2 = 0.52
CR: - 0.34 D
X- intercept: - 0.45 D
c
SP
y = 1.58x +2.05
R2 = 0.59
CR: - 0.87 D
X- intercept: - 1.30 D
d
MM
y = 1.84x +0.88
R2 = 0.65
CR: - 0.30 D
X- intercept: - 0.48 D
e
KS
y = 1.47x - 1.35
R2 = 0.90
CR: + 0.23 D
X- intercept: + 0.92 D
f
SRB
X- intercept: - 2.63 D
1st sess (y = 1.30x + 3.43; R2 = 0.79)
2nd sess (y = 1.79x + 1.13; R2 = 0.88)
X- intercept: - 0.63 D
Peak velocity (D/s)
Peak velocity (D/s)
Response starting position (D)

Figure 34. Peak velocity of disaccommodation plotted as a function of response starting position for five representative subjects (a - e) and for subject SRB (f). The solid red lines in each figure represent the linear regression equation fit to the data and the dashed red lines indicate the +/- 95% confidence intervals. The x-intercept indicates the estimated initial destination of disaccommodation and the zero-crossings of the confidence intervals indicated the range of x-intercepts permitted by the confidence intervals. For subject SRB, two separate linear regression equations were computed, one for the first session (open squares, gray solid and dashed line) and the other for the second session (filled circles, red solid and dashed line). The x-intercept for the first session was more distal than the x-intercept for the second session. In figures a - f, the dioptric location of x-intercept is identified by the red arrowhead and the dioptric location of the cycloplegic refraction (CR) is identified by the blue arrowhead.

Subsequently, the cycloplegic refractive states were correlated with initial destinations as estimated from the x-intercept of the regression analysis using the Pearson's sample correlation coefficient (Devore & Peck, 1993b).

The data presented in this paper have taken into account each subject's distance refractive error that was measured and corrected in the aforementioned measurements. The results are normalized with respect to refractive error so that 0-diopter indicates the accommodative response at which the conjugate focus equaled the subject's far point. As a convention, positive values of cycloplegic refraction and dark foci indicated refractions closer than optical infinity (myopic refractions) and negative values of cycloplegic refraction and dark foci indicated refractions beyond optical infinity (hyperopic refractions).

4. Results

Data from ten of the eleven subjects (except SRB) were analyzed together. Data of subject SRB will be described separately. Peak velocities of disaccommodation for the ten subjects increased significantly with the response starting position (Figure 34a – e) (P-value: <0.001). This relationship was well described by the linear regression equations shown in Figure 34a – e suggesting that a default position could be used to describe the initial destination of disaccommodation. The slopes of the linear regression equations ranged from 0.82 sec^{-1} to 2.04 sec^{-1} and the y-intercepts ranged from -1.35 D/sec to +4.30 D/sec across the ten subjects (Table X). Among the ten subjects, the x-intercepts had negative values (range: -0.45 D to -2.48 D) in nine subjects, implying that the initial destination of disaccommodation was located beyond optical infinity (Figure 34a - d Table X). In the tenth subject (KS), the x-intercept had a positive value (+0.92 D), implying that the initial destination was located closer than optical infinity (Figure 34e, Table X). The range of x-intercepts permitted by +/- 95% confidence intervals is shown in Table X for each subject. This range varied from +/- 0.19 D to +/- 1.22 D across the ten subjects.

Figure 35 shows representative traces of accommodation responses to step changes in optical defocus (1 D – 4 D) prior to- and following complete cycloplegia. The response trace prior to cycloplegia illustrated clear accommodation and disaccommodation step responses whose amplitudes were correlated with the step changes in stimulus defocus (Figure 35). In contrast, the response traces following cycloplegia for accommodation or disaccommodation did not change significantly with stimulus defocus (Figure 35). The post-cycloplegic responses also had a significant shift towards a negative (hyperopic)

Subject	Refractive error (D)	Peak velocity Vs. starting position reg. eq.	Estimated initial destination (D)	Cycloplegic refractive state (D)	Dark focus (D)
KS	- 3.75	y = 1.47x – 1.35	+ 0.915 ± 0.19	+ 0.228 ± 0.08	+ 1.388
ER	+ 0.50	y = 0.82x + 1.74	- 2.129 ± 0.94	- 1.811 ± 0.100	+ 0.250
JM	0.00	y = 1.80 + 0.80	- 0.446 ± 0.72	- 0.343 ± 0.115	+ 0.575
MM	0.00	y = 1.84x + 0.88	- 0.477 ± 0.41	- 0.297 ± 0.267	+ 0.505
DS	+ 0.50	y = 1.54x + 2.50	- 1.620 ± 0.72	- 0.995 ± 0.103	+ 1.043
SP	- 3.25	y = 1.58x + 2.05	-1.299 ± 0.75	- 0.870 ± 0.210	+ 0.785
MT	- 2.50	y = 1.92x + 2.67	-1.240 ± 1.05	- 0.760 ± 0.127	+ 1.315
SL	- 0.37	y = 1.91x + 4.08	- 2.136 ± 0.57	- 0.870 ± 0.130	+ 0.880
KY	- 0.25	y = 1.58x + 1.17	- 0.745 ± 0.80	- 0.87 ± 0.210	+ 0.063
AB	- 2.50	y = 0.89x + 2.16	- 2.418 ± 1.22	-	+ 0.808
SRB I	- 1.50	y = 1.30x + 3.43	- 2.630	-	-
SRB II	- 2.25	y = 1.79x + 1.13	- 0.63 +/- 0.38	- 1.58 ± 0.268	+ 0.113

Table X. Distance refractive errors, linear regression equation of plot of peak velocity as a function of response starting position, initial destination estimated from x-intercept, mean cycloplegic refraction and dark-focus of accommodation for all subjects. The refractive errors in column 1 indicate the spherical equivalent of refraction. The ± errors in column 3 indicate the range of x-intercepts permitted by the +/- 95% confidence intervals. The ± errors in other columns indicate 1-standard deviation from the mean.

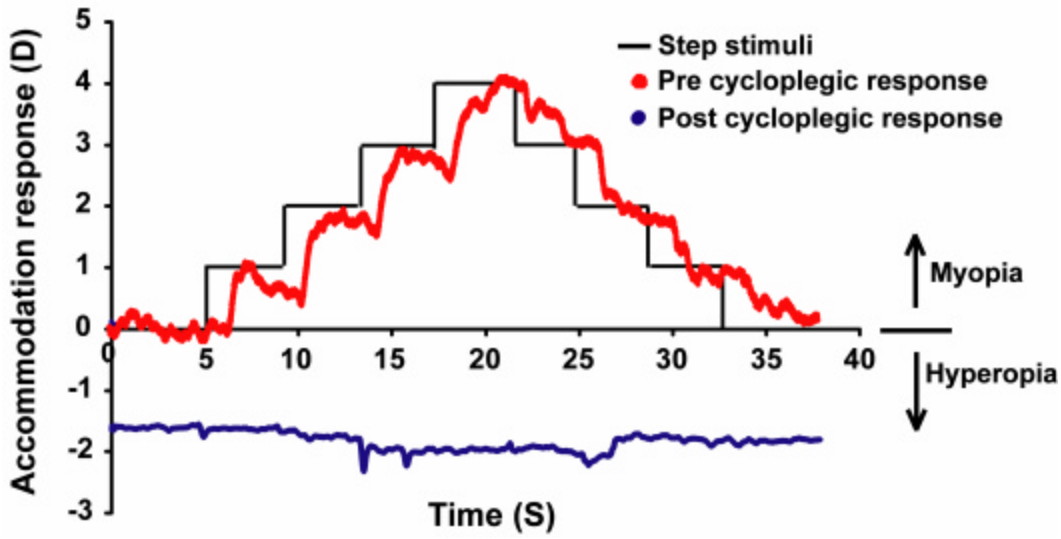

Figure 35. Representative accommodation and disaccommodation responses to step changes in optical defocus (1 D – 4 D in 1 D steps; solid black line) prior to- and following cycloplegia. The response trace prior to cycloplegia (solid red trace) showed clear accommodation and disaccommodation step responses that were correlated with the step changes in stimulus defocus. The response trace following cycloplegia (solid blue trace) showed no significant changes in accommodation and disaccommodation response.

refraction (Figure 35). The mean cycloplegic refractive state was hyperopic (range: -0.297 D to -1.811 D) in nine of the ten subjects (Figure 36a, Table X), showing that the cycloplegic refractive state of accommodation was located beyond optical infinity. For the tenth subject (KS), the mean cycloplegic refractive state was positive (+0.228 D), showing that the cycloplegic refractive state was located closer than optical infinity (Figure 36a, Table X). The mean dark-focus of accommodation (range: +0.11 D to +1.39 D) were positive (myopic refractive state) for all ten subjects (Figure 36a, Table X). This illustrates that the dark-focus of accommodation were located closer than optical infinity in all ten subjects. The cycloplegic refractive state measured in nine subjects (except AB), was well correlated with the estimated initial destination of disaccommodation ($y = 0.54x – 0.13$; r^2: 0.81) (Figure 36b) while the dark-focus of accommodation, measured in

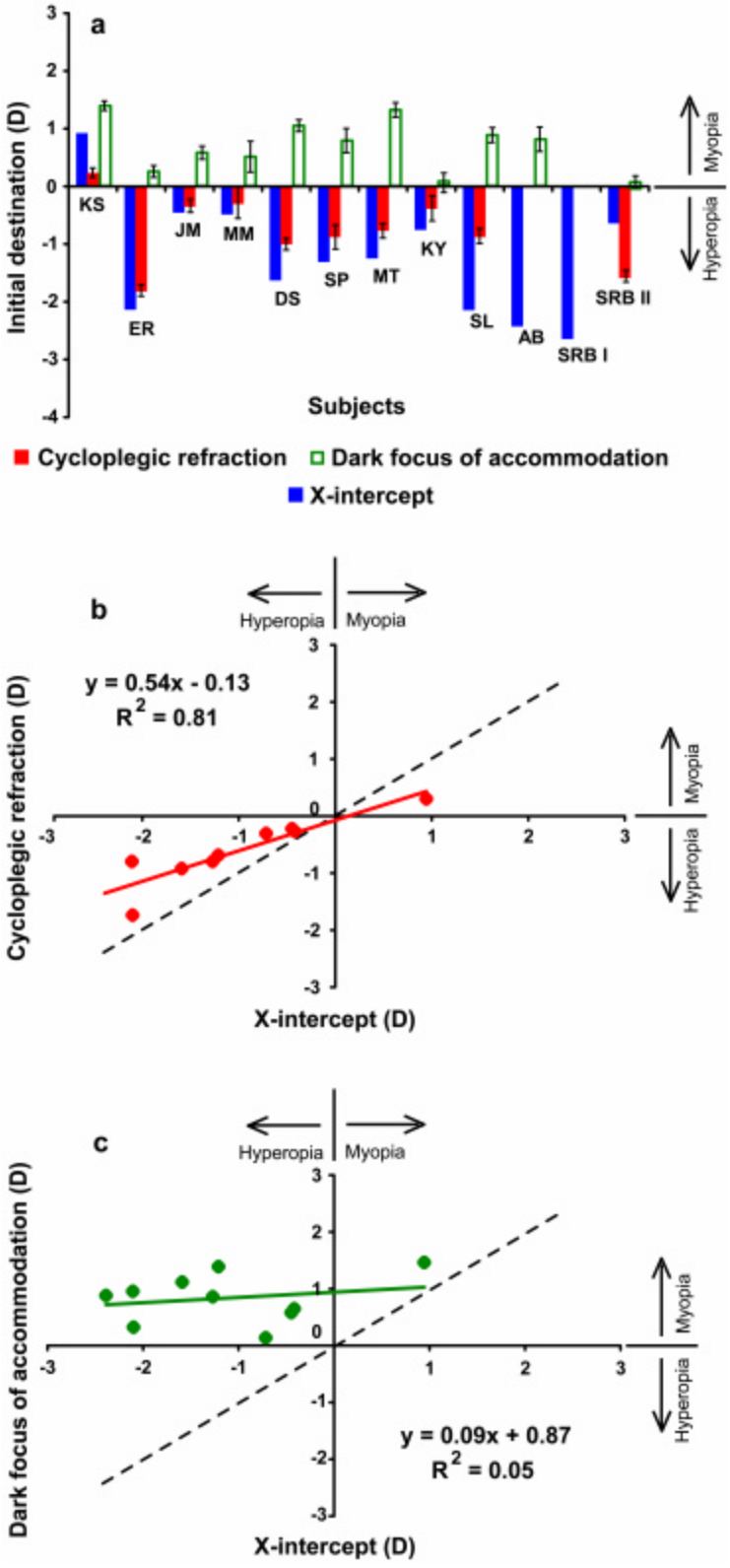

Figure 36. (a) Bar graphs of initial destination of disaccommodation, cycloplegic refractions and dark focus for all subjects. Since the cycloplegic refractions and dark focus measurements for subject SRB were made after the second session, they are shown along with the estimated initial destination from the second session. (b) Cycloplegic refraction is plotted for nine subjects as a function of estimates based on x-intercepts of their initial destination of disaccommodation. (c) Dark-focus of accommodation plotted for ten subjects as a function of the x-intercept estimates of initial destination of disaccommodation. The dashed line in figures b & c is the 1:1 line that indicates perfect correspondence between the parameters in the abscissa and ordinate.

ten subjects, were poorly correlated with the estimated initial default destination of disaccommodation ($y = 0.09x + 0.87$, r^2: 0.05) (Figure 36c).

5. Effects of training on the dynamics of disaccommodation: Methods and results

Disaccommodation step responses for subject SRB were collected on two occasions (first session and second session), separated by a one-year period. Effects of training on the dynamics of disaccommodation were illustrated by different dynamic properties on the two occasions. A detailed account of the changes in his dynamics can be found in Bharadwaj & Schor (2005b). Overall, in the first session, SRB's dynamic disaccommodation responses had the same pattern as for the other subjects: peak velocity increased with starting position, irrespective of response magnitude. In the second session, the pattern was different: peak velocity of his disaccommodation response increased with response magnitude from a common starting position, demonstrating a different control strategy than used by the other subjects or in the first session (Schor & Bharadwaj, 2005b). Linear regressions of peak velocity on response starting position were compared for both sessions. Because peak velocity in the second session increased with response magnitude from a fixed starting position, only those data points that corresponded to responses to the far point were used to fit the regression equation. +/- 95% confidence intervals were computed only for the data of the second session. The x-intercepts of the linear regression equations for both sessions had a negative value implying that the initial destination of disaccommodation was located beyond optical infinity. The x-intercept was located more distally in the first session (-2.63 D) than in the second session (-0.63 D) (Figure 34f, Table X). In retrospect, it would have been ideal to

measure changes in the dark focus of accommodation and the cycloplegic refraction in the first session along with the changes in the dynamic trends of disaccommodation. However, the observed change in the dynamic strategy of disaccommodation in the second session was serendipitous and was not being predicted. Hence the dark-focus and the cycloplegic refractive state are only reported for the second session. The mean dark-focus of accommodation for his second session was +0.113 D. The mean cycloplegic refractive state was -1.578 +/- 0.27 D after his second session.

6. Effect of altering the dark-focus of accommodation on the dynamics of disaccommodation

Yamada & Ukai (1997) proposed that the peak velocity of disaccommodation was determined by the dioptric difference between the response starting position and the dark-focus of accommodation. This proposition was tested by changing the dark focus and its dioptric difference from the starting position. This should result in predictable changes in the peak velocity of responses toward the initial destination of disaccommodation. Shifting the dark-focus in the myopic direction should reduce the dioptric difference between start position and initial destination. This should decrease the peak velocity and peak acceleration of disaccommodation (Figure 37a). Conversely, shifting the dark-focus in the hyperopic direction should, increase the dioptric difference and increase the peak velocity and peak acceleration of disaccommodation (Figure 37a). We tested this prediction by shifting the dark-focus of accommodation in the hyperopic direction and concurrently measuring its influence on the peak velocity and peak acceleration of disaccommodation. Hyperopic shifts in the dark-focus were produced by fatiguing the

accommodative system using repeated optical stimulation of accommodation and disaccommodation step responses (Hasebe et al., 2001).

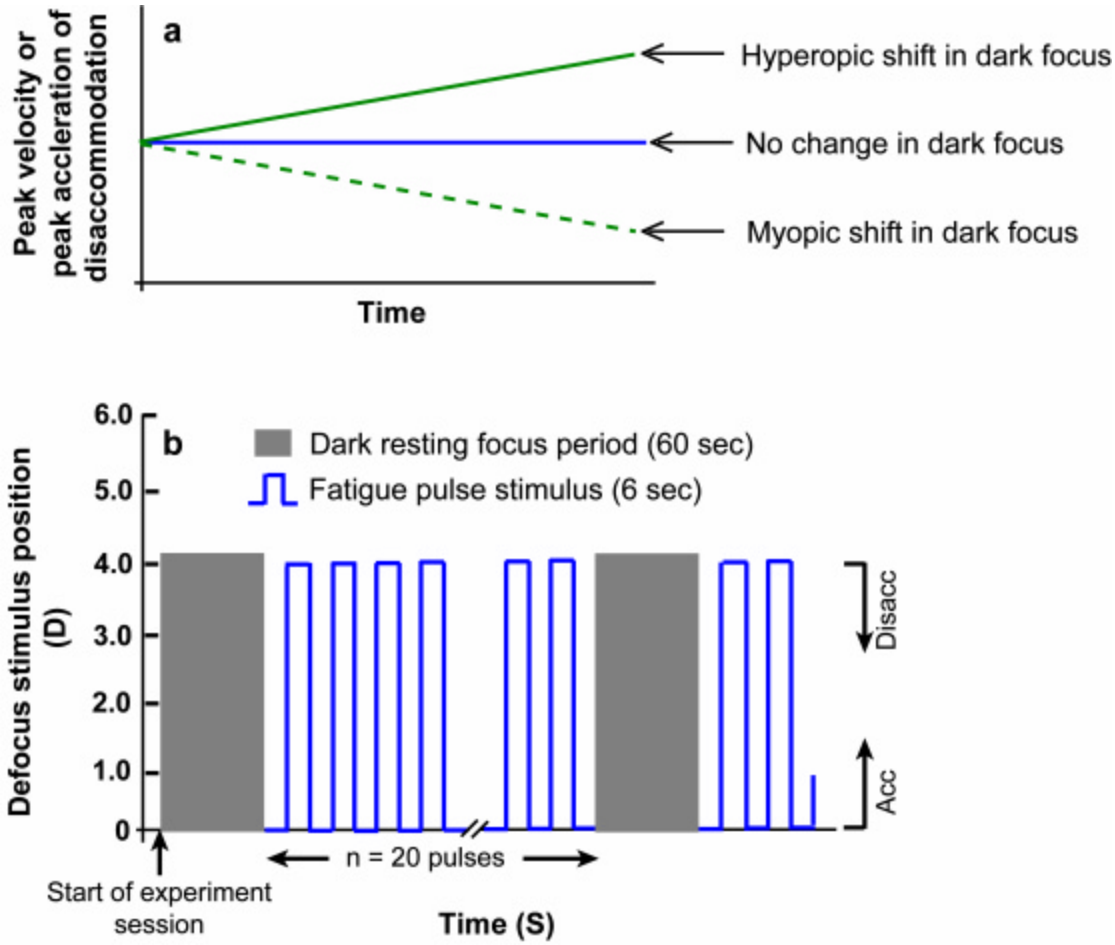

Figure 37. (a) Hypothetical changes of peak velocity or peak acceleration of disaccommodation during changes of dark focus produced by fatigue. The initial destination of disaccommodation is assumed to correspond to the dark-focus of accommodation. Peak velocity or peak acceleration increase with fatigue duration when the dark-focus of accommodation shifts in a hyperopic direction (solid green line). Peak velocity or peak acceleration decrease with fatigue duration when the dark-focus of accommodation shifts in a myopic direction (dashed green line). Peak velocity or peak acceleration would not change with time if the dark-focus did not change or if the dark-focus of accommodation did not correspond to the initial destination of disaccommodation (solid red line). The slopes of the solid and dashed green lines are set to an arbitrary scale. (b). Schematic illustration of the experimental paradigm used to induce fatigue in the accommodation system. The gray rectangles represent periods of complete darkness used to measure the dark-focus of accommodation. The red lines represent pulse changes in optical defocus with the ascending limb of the pulse stimulating accommodation and the descending limb of the pulse stimulating disaccommodation.

A subset of the subjects who took part in the main experiment also took part in this control experiment. Subjects were corrected for their distance refractive error and aligned in the SRI dynamic optometer (Crane & Steele, 1986) after their left eye was dilated with 2.5% Phenylephrine hydrochloride eye drops. Once the calibration routine was completed (Bharadwaj & Schor, 2005a; b), pulse changes in optical defocus were presented repeatedly with the SRI stimulus optometer while the subjects maintained focus a black and white Maltese cross. Ideally, to study if the x-intercept described earlier is influenced by the hyperopic shift of the dark-focus, peak velocity of disaccommodation from multiple starting positions should be assessed. However, considering the cumbersome nature of the experiment, the peak velocity from only two starting positions (4 D and 2 D) were studied. The two disaccommodation stimuli were presented as two different pulse stimulus configurations. In the first configuration, the pulse stimulus had a magnitude of 4 D and duration of 6 secs (Figure 37b). In the second combination, the pulse stimulus had a magnitude of 2 D and duration of 4 secs (not shown). The ascending limb of the pulse (0 – 4 D or 0 – 2 D) stimulated accommodation responses and the descending limb of the pulse (4 – 0 D or 2 – 0 D) stimulated disaccommodation responses (Figure 37b). Both the pulse stimulus configurations had a duty cycle of 0.8, where the duty cycle was defined as the ratio of the sum of all pulse durations during the experimental session to the total duration of the experimental session. This resulted in total durations of 25 min and 17 min for the first and second configurations respectively. Pulse stimuli with a similar duty cycle have been used before to induce fatigue in the accommodation system (Hasebe et al., 2001; Vilupuru et al., 2005). In a given experimental session, only one of the two configurations was presented and the two

configurations were tested on separate days. Dark-focus measurements were obtained for a period of 1 min once before the start of the fatigue session and once after every set of 20 pulse stimuli (Figure 37b). During measurements of the dark-focus of accommodation, the light source illuminating the Maltese cross was turned off to create a completely dark setting. The experimental session was continued for either the entire length (25 min or 17 min) or until the subject could no longer sit comfortably inside the instrument. Accommodation and disaccommodation responses to the pulse stimuli and the dark-focus measurements were recorded (sampling frequency: 200 Hz) with the SRI recording optometer (Cornsweet & Crane, 1970) and were stored for offline analysis. The peak velocity and peak acceleration of accommodation and disaccommodation were obtained from the ascending and descending limbs respectively of the pulse stimulus using the same procedure described by Bharadwaj & Schor (2005b). The peak velocity and peak acceleration data from each set of 20 pulse stimuli were grouped and compared for statistical significance using a single-factor ANOVA test. The mean and +/- 1-standard deviation of peak velocity and peak acceleration of each data group were also computed. Dark-focus recordings usually showed a rapid decay in dioptric power until a steady-state was attained. Dark-focus of accommodation was defined as the dioptric power of the eye during this steady-state period.

Six subjects (ER, SP, MT, KS, DS and SL) took part in the experimental session with the first configuration (4 D amplitude and 6 secs duration) and three subjects (KS, DS and SL) took part in the experimental session with the second configuration (2 D amplitude and 4 secs duration). Figure 38 plots the result of the dark-focus of

accommodation and of the first- and second-order dynamics obtained from the first configuration. Four subjects showed a progressive hyperopic shift in the dark-focus of accommodation as the sessions progressed while the fifth subject (ER) did not show any significant shift in his dark-focus of accommodation (Figure 38a, Table XI). Figure 38b & c illustrate peak velocity of disaccommodation and accommodation respectively plotted as a function of session number. None of the subjects showed a significant change

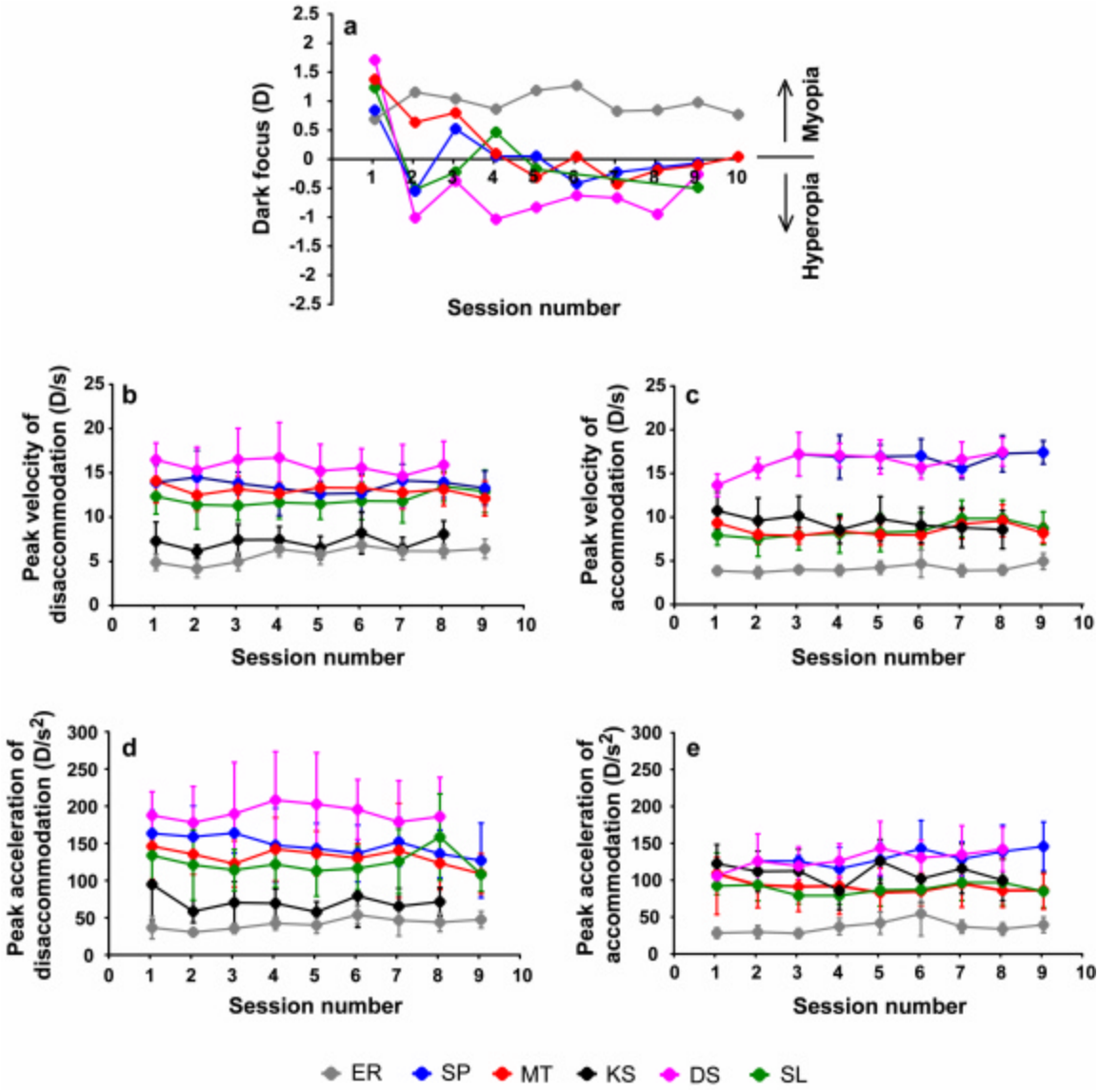

Figure 38. Results of the fatigue experiment wherein the dark-focus of accommodation was shifted in the hyperopic direction inducing 'fatigue' in the system. The peak velocity and peak acceleration of disaccommodation and accommodation were measured concurrently with the dark-focus. (a). Dark-focus of accommodation plotted as a function of session number for the first configuration (4 D pulse amplitude and 6 sec pulse duration).This experiment was run on 6 subjects but reliable dark-focus measurements were obtained only from 5 subjects. Positive values of the ordinate indicate refractions closer than optical infinity and negative values of the ordinate indicate refractions beyond optical infinity. The first data point for each subject represents the dark-focus measurement prior to the start of the 'fatigue' trials and each subsequent data point represents the dark-focus measurement made after the end of each session (comprising of 20 trials each). (b & c). Peak velocity of disaccommodation and accommodation plotted as a function of session number respectively for six subjects obtained with the first configuration stimulus. (d & e). Peak acceleration of disaccommodation and accommodation plotted as a function of session number respectively for six subjects obtained with the first configuration stimulus. In figures b - e, each data point and error bar represents an average and +/- 1-standard deviation of one session (comprising of 20 trials).

in the peak velocity of either disaccommodation (Figure 38b, Table XI) or accommodation (Figure 38c) as the sessions progressed. The single-factor ANOVA test did not show a significant change in peak velocity of either disaccommodation or accommodation with session number (P-value: >0.5). Similar results were obtained in the data of peak acceleration of disaccommodation (Figure 38d, Table XI) and accommodation (Figure 38e). None of the subjects showed any significant change in peak acceleration of either disaccommodation or accommodation with session number (P-value: >0.5). Results of the experimental session with the second configuration (not shown) were qualitatively similar to the results described above. The dark-focus of accommodation showed a hyperopic shift as the sessions progressed. However, this shift in dark-focus was not as sustained or robust as those seen with the first configuration. Neither the peak velocity nor the peak acceleration of disaccommodation and

Subjects	Session type	Session number									
		1	**2**	**3**	**4**	**5**	**6**	**7**	**8**	**9**	**10**
ER	**DF**	0.63	1.10	0.98	0.81	1.13	1.21	0.77	0.77	0.92	0.71
	PV	4.48 ± 0.88	3.78 ± 1.00	4.58 ± 1.00	5.99 ± 0.86	5.43 ± 1.16	6.44 ± 0.74	5.78 ± 1.00	5.75 ± 0.79	6.02 ± 1.09	
	PA	32.05 ± 14.86	26.01 ± 5.10	31.10 ± 6.85	37.93 ± 8.92	35.51 ± 10.87	49.19 ± 12.25	42.02 ± 21.01	39.20 ± 12.24	43.04 ± 11.17	
SP	**DF**	0.79	-0.60	0.46	-0.01	-0.02	-0.48	-0.29	-0.20	-0.13	
	PV	13.56 ± 1.93	14.12 ± 3.01	13.44 ± 1.26	12.88 ± 3.08	12.24 ± 1.42	12.32 ± 2.19	13.75 ± 1.84	13.54 ± 1.75	12.89 ± 1.93	
	PA	158.87 ± 30.9	154.42 ± 41.4	159.29 ± 27.0	142.93 ± 49.8	138.34 ± 34.1	131.91 ± 38.2	147.39 ± 32.9	131.38 ± 32.1	122.49 ± 50.2	
MT	**DF**	1.31	0.58	0.74	0.04	0.37	-0.01	-0.48	-0.25	-0.16	-0.02
	PV	13.70 ± 2.48	12.10 ± 1.78	12.77 ± 1.41	12.29 ± 1.22	12.94 ± 1.38	12.91 ± 1.38	12.41 ± 1.87	12.74 ± 1.85	11.72 ± 1.96	
	PA	141.52 ± 44.5	130.89 ± 27.3	118.03 ± 30.9	137.59 ± 42.6	132.00 ± 29.8	125.64 ± 19.3	135.86 ± 63.4	118.80 ± 35.3	104.62 ± 26.8	
KS	**DF**	-	-	-	-	-	-	-	-	-	-
	PV	6.90 ± 2.15	5.76 ± 0.71	7.05 ± 1.73	7.07 ± 1.47	6.15 ± 1.30	7.83 ± 2.39	6.05 ± 1.27	7.69 ± 1.50		
	PA	90.35 ± 48.57	53.92 ± 15.15	65.77 ± 28.14	64.85 ± 19.25	53.16 ± 13.87	74.83 ± 24.21	60.83 ± 24.21	66.82 ± 19.09		
DS	**DF**	1.52	-1.20	-0.56	-1.12	-1.02	-0.81	-0.85	-1.14	-0.45	
	PV	16.10 ± 1.90	14.92 ± 2.61	16.11 ± 3.54	16.34 ± 4.00	14.85 ± 2.99	15.18 ± 2.17	14.26 ± 3.54	15.52 ± 2.66		
	PA	183.05 ± 31.9	173.42 ± 48.6	185.26 ± 69.1	203.61 ± 53.2	198.17 ± 69.3	191.01 ± 40.2	174.35 ± 55.5	181.38 ± 52.8		
SL	**DF**	0.88	-0.87	-0.57	0.11	-0.52	-	-	-	-0.84	
	PV	11.96 ± 1.99	11.01 ± 2.75	10.90 ± 1.68	11.27 ± 1.85	11.13 ± 1.76	11.44 ± 2.10	11.40 ± 2.44	13.08 ± 1.68	12.52 ± 2.40	
	PA	129.14 ± 35.5	116.46 ± 47.3	109.61 ± 27.7	117.36 ± 30.5	108.59 ± 34.2	111.94 ± 29.4	121.16 ± 43.4	154.03 ± 58.1	103.78 ± 22.8	

Table XI. Dark focus of accommodation (DF), mean peak velocity of disaccommodation (PV) and mean peak acceleration of disaccommodation (PA) measured on six subjects for sessions 1 – 10 during the fatigue experiment. The first measurement of the dark focus was made prior to the start of the fatigue sessions. Dark focus is denoted in diopters, peak velocity is denoted in diopters/s and peak acceleration is denoted in diopters/s^2. Positive values of dark focus indicate myopic refractions while negative values of dark focus indicates hyperopic refractions. The $\pm$ errors in the PV and PA rows of each subject indicate 1-standard deviation from the mean.

accommodation changed significantly with session number (p-value: >0.5) in the three subjects. As expected (Bharadwaj & Schor, 2005a; b), the peak velocity and peak acceleration of both accommodation and disaccommodation were smaller in the second configuration than in the first configuration. For example, for subject DS, the peak velocity and peak acceleration of disaccommodation in the first configuration was 15.41 $\pm$ 0.73 D/s and 186.28 $\pm$ 10.73 D/s^2 respectively (Figure 38b & c). For the same subject, the peak velocity and peak acceleration of disaccommodation in the second configuration was 5.92 $\pm$ 0.86 D/s and 60.97 $\pm$ 10.58 D/s^2 respectively. Similarly, for subject DS, the peak velocity and peak acceleration of accommodation in the first configuration was 15.90 $\pm$ 1.25 D/s and 123.93 $\pm$ 12.31 D/s^2 respectively (Figure 38d & e). For the same subject, the peak velocity and peak acceleration of disaccommodation in the second configuration was 10.41 $\pm$ 1.00 D/s and 110.00 $\pm$ 9.49 D/s^2 respectively.

7. Discussion

The results of this experiment are summarized by the following four points

1. The plots of peak velocity as a function of response starting position have negative x-intercepts in nine subjects and a positive x-intercept in the tenth subject (KS). The

linear regression fit to these data suggests that the estimated initial destination of disaccommodation is to a position located beyond optical infinity in nine subjects and it is located at a finite distance in front of optical infinity in the tenth subject.

2. Among the nine subjects for whom cycloplegic refractive state was measured, the estimated initial destination correlated well with the cycloplegic refractive state and poorly with their dark-focus of accommodation.
3. For subject SRB, the estimated initial destination of disaccommodation was located beyond optical infinity in both sessions. The initial destination was located more distally in the first session and its location moved more proximally in the second session demonstrating a change in the control strategy for dynamic disaccommodation.
4. The peak velocity and peak acceleration of disaccommodation did not change in a subset of six subjects despite a progressive hyperopic shift in their dark-focus of accommodation. This finding is contrary to the prediction that, if the dark-focus of accommodation is the initial destination of disaccommodation, then a hyperopic shift in the dark-focus should result in an increase in the peak velocity and peak acceleration of disaccommodation.

7.1. Dioptric location of the initial (default) destination of disaccommodation and its behavioral correlate

The first- and second-order dynamic properties of disaccommodation from a constant starting position remain invariant of the response magnitude, and they increase linearly with the proximity of the starting position of disaccommodation (Bharadwaj &

Schor, 2005a). These observations suggest that the disaccommodation responses are initiated towards a constant initial destination and they are switched mid-flight to attain their desired final destination (Yamada & Ukai, 1997; Bharadwaj & Schor, 2005b; Schor & Bharadwaj, 2005b). In our experiment, the estimated initial destination of disaccommodation was located beyond optical infinity in nine of the ten subjects. Hyperopic refractions ranging from 0.5 D – 1.5 D are often observed in humans (Giles, 1965; Michaels, 1985) and in primates (Westheimer & Blair, 1972; Gamlin et al., 1994) following complete cycloplegia. Since our estimates of the initial destination of disaccommodation (range: -0.45 D to -2.58 D) were in the range of hyperopia produced by complete cycloplegia, we conjectured that the subject's cycloplegic refractive state of accommodation was a possible behavioral correlate of the initial destination of disaccommodation.

Yamada & Ukai (1997) however found that the initial destination of disaccommodation of their subjects to corresponded with the dark-focus of accommodation. We explored these two possibilities by measuring the cycloplegic refractive states and the dark-focus of accommodation and correlating these measurements with the initial destination of disaccommodation that was estimated from the x-intercept of the linear regression of peak velocity and starting position. Across subjects, the x-intercept correlated well with the cycloplegic refractive states (r^2: 0.81) (Figure 36b) and poorly with the dark-focus of accommodation (r^2: 0.05) (Figure 36c). This illustrates that the cycloplegic refractive state is a better behavioral correlate of the initial destination of disaccommodation than is the dark-focus of accommodation. The

differences in the results of our experiment and those of Yamada & Ukai could be due to inter-individual variability (Schaeffel et al., 1993) or it could be due to the methodological differences discussed in the next section.

The cycloplegic refractive state reduces innervation of the ciliary muscle to zero. Good behavioral correlation between the initial destination and the cycloplegic refractive state suggests that disaccommodation step responses from a starting position are initiated towards the cycloplegic refraction state by a reduction of innervation of the ciliary muscle toward zero. However, the linear regression equation ($y = 0.54x - 0.13$) of a plot of cycloplegic refraction as a function of the x-intercept had a non-unity slope (solid line in Figure 36b), thus raising a possibility that the reduction in ciliary muscle innervation during initiation of the step response is not coincident with the neural correlate of the cycloplegic refraction. While there is no simple behavioral test that would argue for or against this possibility, the non-unity slope could be a result of incomplete cycloplegia. The cycloplegic refractions of all our subjects (except KS) were less hyperopic than the x-intercept (Figure 36a, Table X), presumably due to weak cycloplegic effect of 1% Tropicamide. This suggests that the non-unity slope in figure 36b could be due to an incomplete relaxation of the ciliary muscle following cycloplegia. Another factor is that the cycloplegic refractions for all our subjects (except SL) lie within the range of x-intercepts permitted by their +/- 95% confidence intervals (Figure 34, Table X). This suggests that estimates of initial destination and cycloplegic refraction are within the range of experimental variability and that the non-unity slope in figure 36b could be affected by variability in measures of peak velocity and response starting positions.

7.2. Exponential-fit analysis of initial destination

Yamada & Ukai (1997) estimated the initial destination of disaccommodation by fitting exponential functions of the form f(t) = a + b * (exp (- t / ?) to the 'first half' of the disaccommodation response. The coefficient 'a' of the exponential equation indicated the initial destination of disaccommodation when time (t) becomes large. The dioptric value of coefficient 'a' was positive in all their subjects and it corresponded well with the dark-focus of accommodation measured in these subjects. To examine if the assumption that an exponential-fit to the 'first half' of the response predicted initial destination, we repeated Yamada & Ukai's analysis on the disaccommodation responses of two of our subjects (Figure 39a – d). The location of the initial destination was determined for different response magnitudes (Figure 39a) and for different starting positions (Figure 39b). We measured the initial destination, estimated from coefficient 'a' of the exponential fit, for five different response-window widths, corresponding to 100 ms, 300 ms, 500 ms & 700 ms following the response-latency period (Figure 39a, b). Three significant trends were observed in this analysis. First, the estimated initial destination for all response magnitudes and starting positions shifted systematically towards optical infinity as the analyzed response-window width increased (Figure 39c, d). Second, for a given response-window width, the estimated initial destination also shifted systematically towards optical infinity as the response magnitude increased (Figure 39c), except for the 100 ms window where a minimal shift occurred. Third, for a given width of the response-window, the estimated initial default destination shifted towards optical infinity as starting position decreased (Figure 39d). The distal shift in the initial destination of disaccommodation as width of response-window increased raises the possibility that the

response-window width chosen by Yamada & Ukai was too narrow to apply the exponential analysis fit, and this caused the initial destinations to correspond with their subjects' dark-focus of accommodation. Had a wider width response-window been chosen for the analysis, the initial destination probably would have been more distal than the dark-focus of accommodation. Furthermore, the second and third trends observed in our exponential fit analysis were qualitatively very similar those obtained by Yamada & Ukai (1997) illustrating that when this analysis is based on the first half of the response, it produces results that are neither stable across different response magnitudes nor across different starting positions.

Alternatively, we can estimate the dioptric location of the initial destination of disaccommodation using our analytical technique to calculate the x-intercept of linear regression of peak velocity on response starting position from the raw data provided by Yamada & Ukai (Ukai, 2005). We performed our regression analysis on the data of only one subject whose raw data is presented in their paper (see their Figure 3). Our analysis estimated the initial destination of this subject to be located at 1.15 +/- 0.87 D proximal to optical infinity (Figure 40), which is close to his mean dark-focus of accommodation (1.20 D). The authors however did not report their subject's cycloplegic refractive states. Even so, this result is contrary to the results obtained in our experiment. Although no conclusions can be derived from the data of one subject, the result does indicate that the initial destination of disaccommodation could lie close to the dark-focus of accommodation in some subjects and that significant inter-individual variability

(Schaeffel et al., 1993) could account partially for the difference in the results of the two experiments.

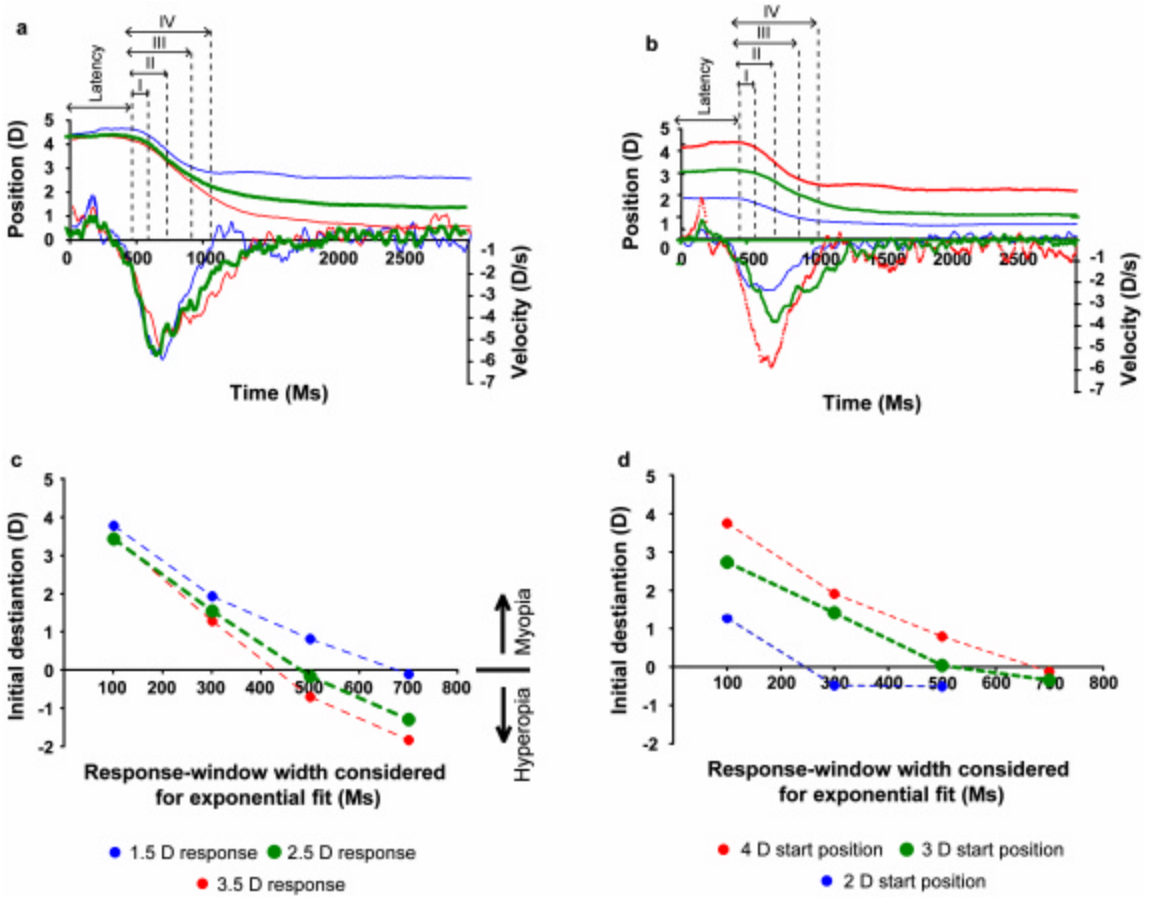

Figure 39. The initial destination of disaccommodation estimated by fitting exponential functions to responses of different magnitudes from the same starting position (a) and to responses of similar magnitudes from three-different starting positions (b). Five different response-window widths (I: 100 ms, II: 300 ms, III: 500 ms & IV: 700 ms following the response-latency period) were considered for the exponential curve fitting (dashed-vertical lines in a & b). Estimated initial destination of disaccommodation plotted as a function of response-window width for different magnitude responses from the same starting position (c) and for responses of similar magnitudes from three-different starting positions (d).

7.3. Influence of shifting the dark-focus of accommodation on the dynamics of disaccommodation

If the dioptric difference between the dark-focus of accommodation and the starting position of disaccommodation determines the peak velocity of disaccommodation, then the experimentally altered dioptric location of the dark-focus should produce predictable changes in the dynamics of disaccommodation. Reducing the dioptric difference (by shifting the dark-focus in the myopic direction) should decrease the peak velocity of disaccommodation (Figure 37a) and increasing the dioptric difference between starting

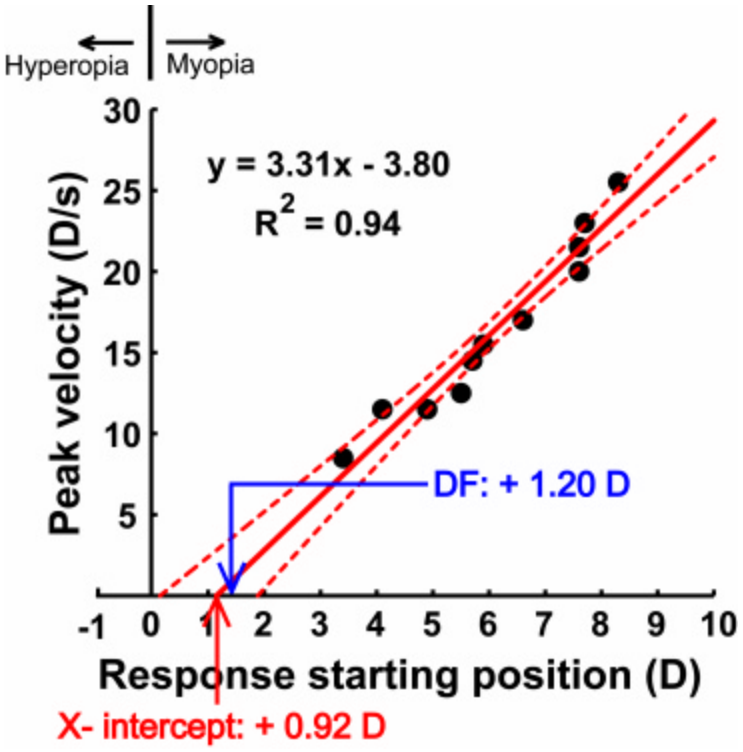

Figure 40. Initial destination of disaccommodation estimated from a plot of peak velocity as a function of response starting position for one subject who took part in Yamada & Ukai's experiment. Raw data of peak velocity and response starting position were obtained from figure 3 in their paper. A best fit-linear regression equation is fit to this data (solid line) along with the +/- 95% confidence intervals (dashed lines). The dioptric location of x-intercept is identified by the red arrowhead and the dioptric location of the dark-focus (DF) is identified by the blue arrowhead.

position and dark focus, by shifting the dark-focus in the hyperopic direction, should increase the peak velocity of disaccommodation (Figure 37a). Our fatigue experiment revealed that a significant hyperopic shift in the dark focus (Figure 38a), induced by fatiguing the accommodation system (Hasebe et al., 2001), had no influence on the peak velocity and peak acceleration of disaccommodation (Figure 38b & d). No significant change in the peak velocity and peak acceleration of disaccommodation from both the 4 D and 2 D starting positions were seen with the hyperopic shift of dark-focus. These results indicate that the x-intercept (obtained from the linear regression of peak velocity as a function of starting position) did not change with the hyperopic shift of the dark-focus and that the dark-focus of accommodation is not the initial destination of disaccommodation. Our findings corroborate the results of Vilupuru et al (2005) for the 5 D and 6 D starting positions of disaccommodation. It is possible that neuro-muscular fatigue in the accommodative system and/or a generalized reduction in performance associated with visual fatigue (Owens & Wolf-Kelly, 1987; Takeda et al., 1988; Hasebe et al., 2001; Vilupuru et al., 2005) could have masked the enhancement of peak velocity and peak acceleration of disaccommodation that was associated with the hyperopic shift in dark-focus. The dynamics of accommodation step responses do not follow an 'initial-destination' strategy (Schor & Bharadwaj, 2005b) and hence are unlikely to be affected by changes in the location of the dark-focus. Indeed, neither the peak velocity (Figure 38c) nor the peak acceleration (Figure 38e) showed any significant reduction in magnitude with fatigue. Overall, our results suggest minimal influence of accommodative and visual fatigue on the dynamics of accommodation and disaccommodation.

We used accommodative fatigue as a technique to alter the dark focus of accommodation. This technique was chosen over more conventional ways of altering the dark focus, such as by using pharmacological agents (Gilmartin, 2000) or by sustained nearwork (Rosenfield et al., 1994), for the following reasons. Pharmacological agents such as timolol maleate or isoprenaline sulphate change the dark focus by intervening with the peripheral autonomic innervation at the level of the ciliary muscle (Gilmartin, 2000). It would thus be contextually inappropriate to employ this technique to assess the relationship between the dark focus and the neural control disaccommodation dynamics.

The myopic shift in the dark focus following sustained nearwork (Rosenfield et al., 1994) could be influenced by both parasympathetic and sympathetic innervations. For example, a sustained nearwork prolongs the duration of disaccommodation step-responses in myopes who show diminished sympathetic inhibition (Ciuffreda & Wallis, 1998; Culhane & Winn, 1999; Culhane et al., 1999; Winn et al., 2002) but it does not influence the response duration in emmetropes (Ciuffreda & Wallis, 1998; Culhane & Winn, 1999). However, a lack of precise understanding of the interactions between sympathetic and parasympathetic activity that causes the dark focus to shift myopically following sustained nearwork, precludes one from using this technique to study the relationship between dark focus and the neural control strategies of disaccommodation. When compared to pharmacological intervention and sustained nearwork, the use of accommodative fatigue to hyperopically shift the dark focus seems relatively straightforward. Unlike sustained nearwork, accommodative fatigue does not show any refractive-error dependent behavior (Hasebe et al., 2001). Further, repeatedly exercising

accommodation and disaccommodation step responses prevents the slow build-up of sympathetic activity (Culhane et al., 1999; Gilmartin, 2000) and is therefore unlikely to interact with the parasympathetic activity in determining the dark focus.

7.4. Variance of estimates of initial destination

In our experiment, the initial destination of disaccommodation was inferred from the x-intercept of the linear regression of peak velocity on response starting position. It is possible that the variability in the measures of response starting position and peak velocity could have influenced the linear regression equation fit, and reduced the accuracy of our estimate of initial destination from the x-intercept. However, the linear regression equations provided good fits (correlation coefficient range: 0.52 – 0.95) to the data of peak velocity as a function of starting position and the range of initial destinations determined by +/- 95% confidence intervals of the linear regression equation fit were still within the vicinity of the cycloplegic refractive state. Hence, it is unlikely that our estimates of the initial default destination of disaccommodation were influenced significantly by the variability in the measures of response starting position and peak velocity.

Similar to the increase in peak velocity of disaccommodation with the proximity of starting position, the peak acceleration of disaccommodation also increased with the proximity of the starting position (Bharadwaj & Schor, 2005b). Thus, the x-intercept of the regression of peak acceleration of disaccommodation on starting position would have also estimated the initial destination of disaccommodation. However, the relationship of

peak acceleration with starting position was more variable than the relationship of peak velocity with starting position. R^2 for peak velocity as a function of starting position was 0.57; while r^2 for peak acceleration as a function of starting position was 0.37 (Bharadwaj & Schor, 2005b). Hence, we derived the dioptric location of the initial destination from the plots of peak velocity as a function of starting position.

7.5. The influence of training on the initial destination of disaccommodation

Disaccommodation step responses were collected on subject SRB on two occasions. Data from the first session were collected during initial pilot experiments and data for the second session were collected after a period of 1-year. The trends in his dynamics of disaccommodation changed significantly over the 1-year period of data collection. A detailed account of the changes in his dynamics can be found in Bharadwaj & Schor (2005b). Overall, the first- and second-order dynamics of his disaccommodation responses were more sluggish or damped in the second session than in the first session. For a given starting position, the peak acceleration of all responses and the peak velocity of smaller responses were lower in the second session than in the first session (Bharadwaj & Schor, 2005b).

We speculate that the reduction in peak acceleration and peak velocity for smaller responses could have resulted in part from a shift in the initial destination of disaccommodation to a more proximal location in the second session. The initial destination of disaccommodation was located more distally in first session (-2.63 D) than in the second session (-0.63 D) (Figure 34f). The disaccommodation responses in the first

session were initiated toward the more distal initial destination and hence traveled with higher peak acceleration and peak velocity. In the second session, the disaccommodation responses were initiated towards a more proximal initial destination and hence traveled with lower peak acceleration and peak velocity than the first session. The proximal shift in the initial destination of subject SRB could have been associated with a proximal shift in his cycloplegic refractive state. However, since the cycloplegic refraction was measured only after his second session, we can only speculate that, like the initial destination, the cycloplegic refractive state may also have shifted from a more distal location in the first session to a more proximal location in the second session. Further experiments that can produce a reliable change in the control strategy for dynamic disaccommodation are required to examine this question in a more systematic fashion.

8. Conclusion

For a constant starting position, the peak velocity and peak acceleration of the disaccommodation step response remains invariant of the response magnitude. The peak velocity and peak acceleration increase linearly with the proximity of starting position. These observations suggest that disaccommodation step responses are initiated towards a constant or default initial destination (Bharadwaj & Schor, 2005b). This study further demonstrates that the initial destination of disaccommodation is located beyond optical infinity, close to the cycloplegic refractive state of accommodation. The dioptric difference between the starting position and the cycloplegic refractive state determines the peak velocity and peak acceleration of disaccommodation step response.

Chapter V. The pulse-step model of disaccommodation dynamics: comparing the dynamic control strategies of accommodation and disaccommodation

1. Abstract

Dynamic properties and control strategies of step responses by accommodation and disaccommodation differ from one another. Peak velocity of accommodation increases with response magnitude while peak velocity and peak acceleration of disaccommodation increase with starting position. These dynamic properties can be modeled as control strategies that use independent acceleration-pulse and velocity-step components that are integrated respectively into phasic-velocity signals that control movement and tonic-position signals that control magnitude. Accommodation is initiated toward its final destination by an acceleration-pulse whose width increases with response magnitude to increase peak velocity. Disaccommodation is initiated toward a default destination (the far point) by an acceleration-pulse whose height increases with dioptric distance of the starting position to increase peak velocity and peak acceleration. Both responses are completed and maintained by tonic-position signals whose amplitudes are proportional to the final destination. Mismatched amplitudes of phasic-velocity and tonic-position signals in disaccommodation produce unstable step responses.

2. Introduction

Accommodation adjusts the optical power of the eye by applying forces to the lens capsule and matrix with an active agonist (ciliary muscle) and a passive antagonist (choroid tissue). During accommodation, innervation to the ciliary muscle is increased from some initial level to increase the refractive power of the lens. During disaccommodation, innervation to the ciliary muscle is lowered to reduce the refractive power of the lens, and the roles of the ciliary muscle and choroid are reversed: the former becomes the antagonist and the latter becomes the agonist.

We are interested in the dynamic behavior and the corresponding neural control strategies used by accommodation to compensate the age-related changes in the visco-elastic properties of the lens and to achieve fast step responses. Dynamic neural control strategies are reflected by empirical measurements of accommodation and disaccommodation step responses and they can be summarized using dynamic systems-engineering lumped models (Koshroyani & Hung, 2002; Schor & Bharadwaj, 2005). Behavioral observations show that accommodation and disaccommodation have different dynamic characteristics, indicating that different neural control strategies are used to increase and decrease innervation of the ciliary muscle in order to optimize the accuracy and speed of dynamic step changes of accommodation and disaccommodation (Bharadwaj & Schor, 2005a; 2005b). In this paper we briefly describe the dynamic characteristics of accommodation and disaccommodation step responses and we present a model of their dynamic properties and response strategies. The disaccommodation model has the same pulse-step structure as used of our dynamic model of accommodation

(Schor & Bharadwaj, 2005). Both models control velocity by adjusting dynamic properties (i.e. height and width of the acceleration pulse). Strategies describe how velocity is increased, either with response magnitude for accommodation or with response starting position for disaccommodation.

2.1. Behavioral characteristics of accommodation and disaccommodation

Accommodation and disaccommodation responses to step changes in optical defocus have different dynamic properties and control strategies. First, during accommodation from a constant far position to various near positions (Figure 39a), peak velocity increases with response magnitude (Bharadwaj & Schor, 2005a; Ciuffreda & Kruger, 1988; Kasthurirangan *et al*., 2003; Mordi & Ciuffreda, 2004) but peak acceleration is invariant of response magnitude (Bharadwaj & Schor, 2005a). In contrast, during disaccommodation from a constant near position to various far positions (Figure 39a), both peak velocity and peak acceleration remain invariant of response magnitude (Bharadwaj & Schor, 2005b). The position, velocity and acceleration profiles shown in figure 39b – g clearly show this difference. Figure 39b & c compares accommodation and disaccommodation position traces of three different magnitudes (1.5 D, 2.5 D & 3.5 D) from a constant starting position (1 D & 4 D respectively). These position traces show that disaccommodation has a shorter time constant than accommodation and it exhibits overshoots only for small disaccommodation response magnitudes (e.g. 1.5 D) whereas larger disaccommodation response magnitudes and all of the illustrated accommodation response magnitudes are more stable. The corresponding velocity traces illustrate that the

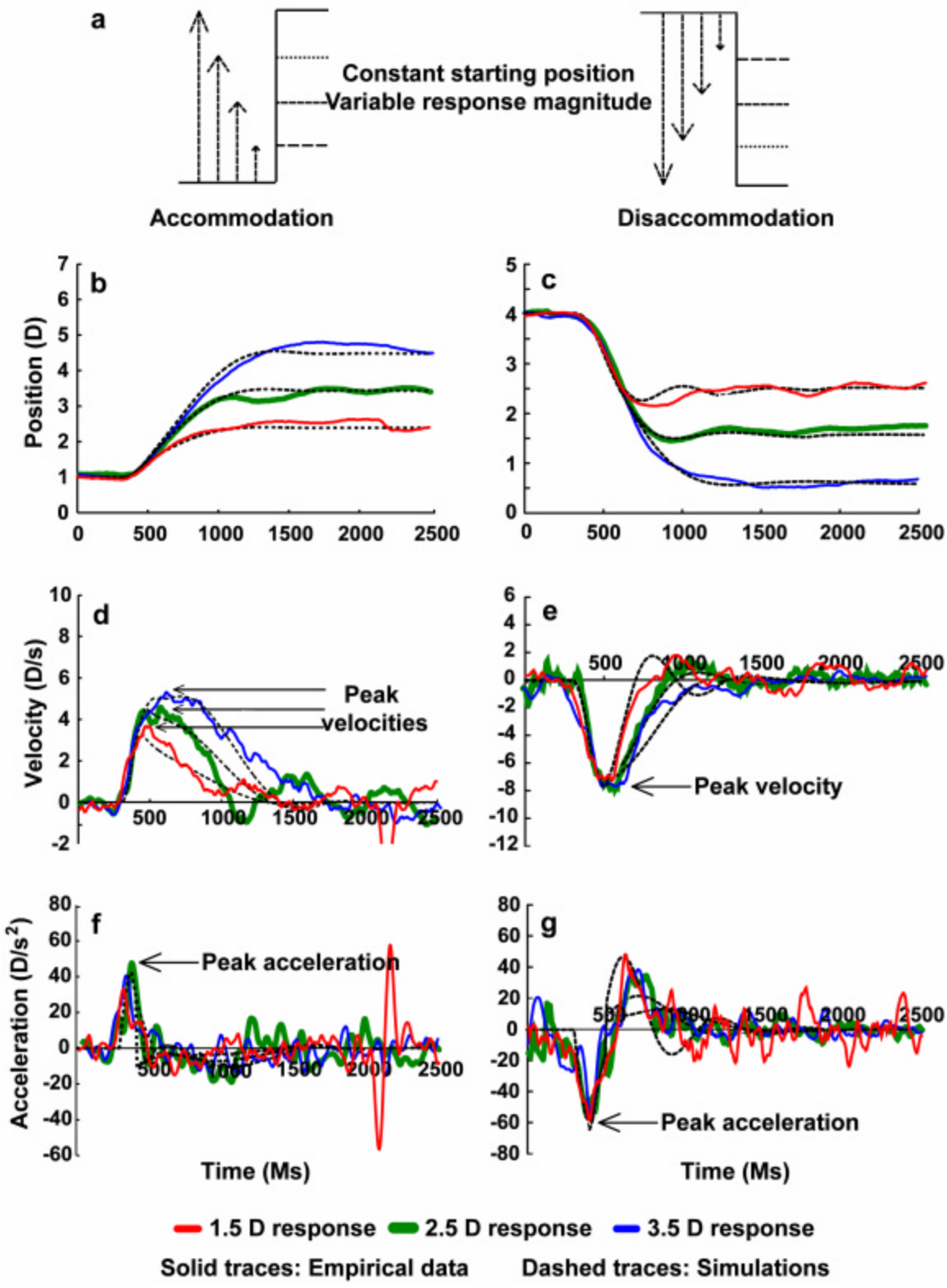
a
Constant starting position
Variable response magnitude
Accommodation
Disaccommodation
b
Position (D)
c
d
Velocity (D/s)
Peak velocities
e
Peak velocity
f
Acceleration (D/s²)
Peak acceleration
g
Peak acceleration
Time (Ms)
Time (Ms)
1.5 D response
2.5 D response
3.5 D response
Solid traces: Empirical data
Dashed traces: Simulations

Figure 41. Position, velocity and acceleration characteristics of accommodation (b, d & f) and disaccommodation (c, e & g) step responses of different magnitudes from a constant starting position. Solid lines represent empirical measures and dashed lines are model simulations. (a) Schematic stimulus sequence for accommodation and disaccommodation. Arrow heads indicate three defocus stimulus magnitudes (1.5 D, 2.5 D, and 3.5 D) for accommodation and disaccommodation from fixed starting positions (1D for accommodation and 4D for disaccommodation). (b & c) Accommodation and disaccommodation position traces (1.5 D, 2.5 D & 3.5 D response magnitudes) are plotted as a function of time from 1 D and 4 D starting position respectively. (d & e) Velocity profiles are plotted as a function of time for the position traces shown in b & c. Velocity traces were obtained by differentiating the position traces using a 2-point difference algorithm and followed by smoothing the traces using a 100-ms smoothing window. The highest point in the velocity traces was denoted as the peak velocity of the response. (f & g) Acceleration profiles plotted as a function of time for the position traces shown in b & c. Acceleration traces were obtained by differentiating the velocity traces using a 2-point difference algorithm and followed by smoothing the traces using a 100-ms smoothing window. The highest point in the acceleration traces was denoted as the peak acceleration of the response. In figures b – g, the solid colored lines represent empirical data collected by Bharadwaj & Schor (2005a, b) and the thin dotted lines indicate pulse-step model simulations.

peak velocity of accommodation increases systematically with response magnitude (Figure 39d) and the peak velocity of disaccommodation from a fixed starting position remains invariant of response magnitude (Figure 39e). Similarly, the corresponding acceleration traces illustrate that the peak acceleration of neither accommodation (Figure 39f) nor disaccommodation (Figure 39g) changes with response magnitude.

Second, the first- and second-order dynamic properties of accommodation do not vary with the starting position of accommodation (*see however*, Kasthurirangan & Glasser, 2005 for slightly different results). In contrast, both the first- and second-order dynamic properties of disaccommodation increase with the dioptric distance of the starting position of disaccommodation (Bharadwaj & Schor, 2005b; Kasthurirangan &

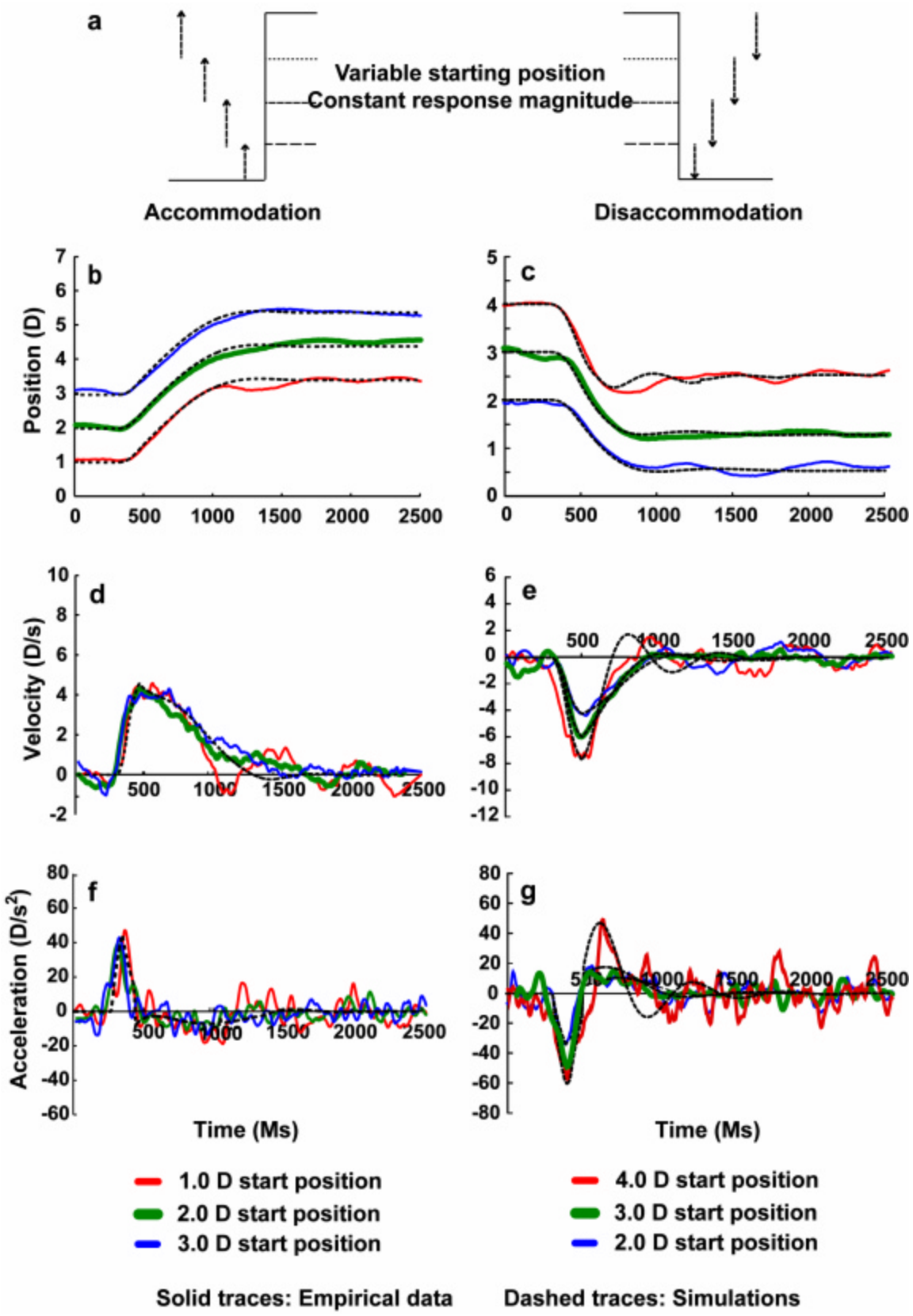
a
Variable starting position
Constant response magnitude
Accommodation
Disaccommodation
b
c
Position (D)
d
e
Velocity (D/s)
f
g
Acceleration (D/s²)
Time (Ms)
Time (Ms)
1.0 D start position
2.0 D start position
3.0 D start position
4.0 D start position
3.0 D start position
2.0 D start position
Solid traces: Empirical data
Dashed traces: Simulations

Figure 42. Position, velocity and acceleration characteristics of accommodation (b, d & f) and disaccommodation (c, e & g) step responses of approximately 1.5 D magnitude from three-different starting positions (accommodation: 1 D, 2 D & 3 D; disaccommodation: 4 D, 3 D & 2 D). Solid lines represent empirical measures and dashed lines are model simulations. a) Schematic stimulus sequence for accommodation and disaccommodation. Arrow heads indicate a fixed amplitude (1.5D) stimulus for accommodation and disaccommodation from four different starting positions (1 D, 2 D, 3 D and 4 D). b & c) Accommodation and disaccommodation position traces plotted as a function of time. d & e) Velocity profiles are plotted as a function of time for the position traces shown in b & c. Velocity traces were obtained by differentiating the position traces using a 2-point difference algorithm and followed by smoothing the traces using a 100-ms smoothing window. The highest point in the velocity traces was denoted as the peak velocity of the response. f & g) Acceleration profiles are plotted as a function of time for the position traces shown in b & c. Acceleration traces were obtained by differentiating the velocity traces using a 2-point difference algorithm and followed by smoothing the traces using a 100-ms smoothing window. The highest point in the acceleration traces was denoted as the peak acceleration of the response. In figures b – g, the solid colored lines represent empirical data collected by Bharadwaj & Schor (2005 b) and the thin dotted lines indicate pulse-step model simulations.

Glasser, 2005; Yamada & Ukai, 1997). This starting-position-dependent strategy can be illustrated with stimuli of fixed magnitude from different starting positions (Figure 40a). Figure 40b – g shows examples of the position, velocity and acceleration traces for a 1.5 D stimulus defocus from three different starting positions (accommodation: 0 D, 1 D & 2 D; disaccommodation: 4 D, 3 D & 2 D). The position traces show that disaccommodation has a shorter time constant than accommodation for all starting positions, and that overshoots of disaccommodation occur only for responses from a 4 D starting position while these instabilities do not occur from more distal starting positions or for any of the illustrated accommodation starting positions (Figure 40b & c). The corresponding velocity and acceleration traces illustrate that the peak velocity and peak acceleration of accommodation remains invariant with starting position (Figure 40d & f) but the peak

velocity and peak acceleration of disaccommodation systematically increase with the dioptric distance of the starting position (Figure 40e & g).

In summary, in the control strategy for accommodation, the first-order dynamic properties are determined by the response magnitude while the second-order dynamic properties are independent of both response magnitude and starting position. Accommodation responses of any magnitude and from any starting position do not show overshoots. In the control strategy for disaccommodation, both the first- and second-order dynamic properties are determined by the starting position of disaccommodation. Disaccommodation responses of smaller magnitude and from more proximal starting positions have overshoots while disaccommodation responses of larger magnitude and from distal starting positions do not show overshoots.

The linear dependence of peak velocity and peak acceleration of disaccommodation on starting position and their independence from response magnitude suggest that disaccommodation step responses of any magnitude and from any starting position are initiated toward a default and remote initial destination (Bharadwaj & Schor, 2005b; Yamada & Ukai, 1997). These initial responses are switched mid-flight to attain their desired final destinations. The initial (default) destination has been estimated from the x-intercept of linear regression equation of peak velocity as a function of response starting position (Bharadwaj & Schor, 2005c). The x-intercept has a negative value that corresponds well with the cycloplegic refractive state of the eye (Bharadwaj & Schor,

2005c). This observation is representative of the disaccommodation response resulting from near-zero innervation to the ciliary muscle (Bharadwaj & Schor, 2005c).

2.2. Pulse-step dynamic model of accommodation

The pulse-step model for the dynamic control of the step response by accommodation has been described in detail in an earlier publication (Schor & Bharadwaj, 2005). Hence, only a brief description will be presented here. In the pulse-step model schema for accommodation, step changes in defocus stimuli generate independent acceleration-pulse and velocity-step signals, which are integrated to produce phasic-velocity and tonic-position signals respectively. The phasic-velocity and tonic-position signals are summed and transformed by the accommodative plant to produce the final accommodation response (Figure 41a). The initial movement or change in accommodation is controlled by the open-loop phasic-velocity signal while the final position of accommodation is maintained under closed-loop conditions by the tonic-position signal. Three important characteristics of the acceleration-pulse signal control the dynamic properties of accommodation. The height of the pulse determines the peak acceleration, the width of the pulse determines the phasic-velocity signal and its time-to-peak velocity, and finally the integral of the pulse determines the peak velocity. Either increasing the height or the width of the pulse can increase the phasic-velocity signal. In the control strategy for dynamic accommodation, the peak acceleration remains invariant with response magnitude while the time-to-peak velocity and the peak velocity increase with response magnitude (Bharadwaj & Schor, 2005a). Based on these observations, the increase in peak velocity of accommodation with response magnitude

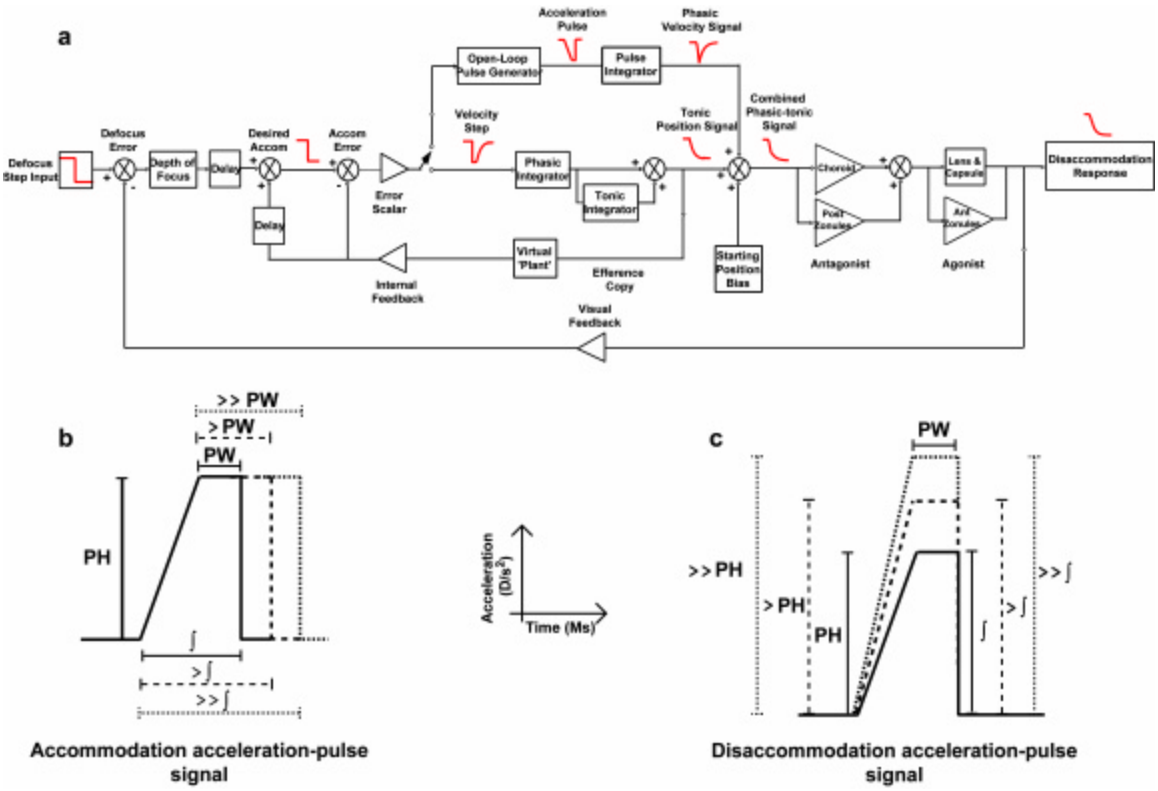

Figure 43. Block diagram (a) and characteristics of the acceleration-pulse signal in the pulse-step model of accommodation (b) and disaccommodation (c). a) Block diagram illustrating the generation of acceleration-pulse and velocity-step signals, their neural integration to phasic-velocity and tonic-position signals respectively, and the final transformation of the signals by the plant into a disaccommodation step response. Insets in figure a show signal profiles at each stage of the models. The block diagram for the pulse-step model of accommodation is identical to the block diagram of the disaccommodation model shown in figure 41a. b) Schematic representation of acceleration-pulse parameters in accommodation and how the pulse width (PW) is increased to increase the integral of the pulse. The pulse height (PH) remains constant in accommodation. c) Schematic representation acceleration-pulse parameters in disaccommodation and how the pulse height (PH) is increased to increase the integral of the pulse. The pulse width (PW) remains constant in disaccommodation.

was modeled by increasing the width of a constant-height acceleration-pulse (Figure 41b). The velocity-step signal was under feedback control. Its height equaled the defocus error signal and it increased proportionally with the response magnitude. Internal feedback was used to achieve response stability (Schor & Bharadwaj, 2005).

Several studies have assumed that the disaccommodative step response is controlled by a step relaxation of the tonic-position signal from an initial state to a level proportional to the response magnitude (Beers & van der Heijde, 1996; Crawford *et al.*, 1989; Croft *et al.*, 1998; Vilupuru & Glasser, 2002). However, the first- and second-order dynamic properties described above suggests that like accommodation, disaccommodation could also be controlled by independent acceleration-pulse and velocity-step components that reduce innervation to the ciliary muscle. Our dynamic model of disaccommodation takes these aspects into consideration.

3. Model structure

Our goal was to model the dynamic control of disaccommodation with the same pulse-step structure as used in our model of dynamic accommodation (Schor & Bharadwaj, 2005). This common structural organization facilitates the comparison of the neural control strategies of accommodation and disaccommodation with as few parameters as possible. The model was constructed using MATLAB/SIMULINK® and it incorporated the neural processes and the biomechanical plant of a 25-yr old individual. Copies of the Matlab scripts can be obtained from the authors upon request or from our website, http://schorlab.berkeley.edu/. The scripts for three different starting positions and response magnitudes of disaccommodation can be downloaded and run with MATLAB/SIMULINK®.

Since the structural organization of the models for dynamic accommodation and disaccommodation is identical, only the simplified block diagram of the

disaccommodation model is shown (Figure 41a). The simplified block diagram of the accommodation model can be found in Schor & Bharadwaj, 2005. Disaccommodation has the same plant and neural components as does the pulse-step model for accommodation (Schor & Bharadwaj, 2005). Both dynamic models are based on empirical measures of the first- and second-order dynamic properties of the accommodation step responses (Bharadwaj & Schor, 2005a, b), and on the reported measures of visco-elastic properties of the lens and extra-lenticular accommodation apparatus (Glasser & Campbell, 1999; Wyatt, 1993). However the control strategies of these two models differ in how the open-loop acceleration-pulse and the closed-loop velocity-step control peak velocity, peak acceleration and response magnitude either with response magnitude (e.g. accommodation) or with starting positions (e.g. disaccommodation). The basic structural organization of the disaccommodation model is discussed below. The systems-engineering parameters used in both the accommodation and disaccommodation models are listed in Table XII.

3.1. Acceleration-pulse and Phasic-velocity signals

Similar to accommodation, the dynamic properties of disaccommodation are modeled by an acceleration-pulse signal. However unlike accommodation, the acceleration pulse for disaccommodation has a constant-width and a height that increases linearly with the dioptric distance of the starting position (Eq. 1) (compare Figure 41b & c). In both models, the pulse is integrated to produce a phasic-velocity signal. The phasic signal for disaccommodation increases with the height of the pulse instead of its width (Figure 41c). The variable height of the acceleration-pulse is suggested by increases in

	Accommodation	Disaccommodation
Latency (delay)	300 ms	300 ms
Pulse characteristics		
Pulse height	12.5 D/s^2	variable
Pulse width	variable	180 ms
Phasic integrator	0.75 / [0.2S + 1]	0.80 / [0.2S + 1]
Tonic integrators		
Fast-tonic	15.0 / [2.0S + 1]	10.0 / [1.33S + 1]
Slow-tonic	50.0 / [100S + 1]	50.0 / [100S + 1]
Choroid gain	0.25	0.25
Zonule gain	0.42	0.4
Lens transfer function	0.34 / [0.19S + 1]	0.34 / [0.19S + 1]

Table XII. Neural control and accommodative plant parameters used in the pulse-step model of accommodation and disaccommodation. The transfer functions in this table are represented in the Laplace notation format K / ?S + 1 where, K = gain of the transfer function and ? = time constant of the transfer function. The parameters shown in this table are for a 25-yr old subject.

both peak acceleration and peak velocity of disaccommodation with starting position (Bharadwaj & Schor, 2005b). The constant width of the acceleration-pulse is suggested by the invariance of the duration of acceleration (200 ms) and time-to-peak acceleration (100 ms) [Appendix I] from different starting positions (Bharadwaj & Schor, 2005b). For responses from a constant starting position, the acceleration-pulse signal for a full-

disaccommodation (responses from the starting position to the far point) and partial-disaccommodation (responses from the starting position to a destination proximal to the far point) have the same heights. Accordingly, the height of the integrated phasic-velocity signal is also invariant with response magnitude from the same starting position. Together, the acceleration pulse and phasic-velocity signals initiate disaccommodation responses toward an initial destination that corresponds to near-zero innervation of the ciliary muscle (Bharadwaj & Schor., 2005c). The model incorporates this initial destination in the x-intercept of the linear regression equation used to scale the height of the acceleration-pulse with starting position (-0.43 D in Eq. 2). Values for the heights of the acceleration-pulse and phasic-velocity signal are shown in Table XII for different starting positions.

$$P_{accel} = 1.4\ SP_{diop} + 0.6 \qquad (1)$$

Where, P_{accel} = height of the acceleration-pulse (D/s^2) and SP_{diop} = starting position of disaccommodation (D). X-intercept = -0.43 D.

3.2. Velocity-step and Tonic-position signals

The steady-state magnitude of the disaccommodation step response at the final destination is determined by the velocity-step signal, which is integrated to produce a tonic-position signal. The stability of the disaccommodation step responses results from the control of the height and width of the velocity-step signal with internal negative feedback. Unlike accommodation, where the initial height of the velocity-step increases with response magnitude, in the disaccommodation model, the initial height of the velocity-step increases with the dioptric distance of the starting position (Eq. 2),

irrespective of response magnitude. The velocity step is derived from an error signal equal to the dioptric difference between the input (desired final position) and the output (efference correlate of the current state of accommodation). This focus error is scaled by the ratio of full to partial disaccommodation in order to produce an initial step height equal to the initial motor error for a full-disaccommodation response to the far point. This error is reduced by negative feedback which shortens the width of the velocity step so that it is proportional to the difference between the starting position and final destination of the partial-disaccommodation response. Thus, 2 D of disaccommodation from a 4 D starting position has a narrower step width than a full 4 D disaccommodation to the far point, even though the height of the initial step is the same for both response magnitudes. The rate that the velocity-step amplitude is reduced by negative feedback is proportional

Starting position (D)	**Acceleration-Pulse height (D/s^2)**	**Acceleration-Pulse width (Ms)**	**Velocity-Step height (D/s)**	**Phasic velocity (D/s)**	**Tonic Position (D)**
1 D	2.00	200	0.60	3.25	4.50
2 D	3.40	200	1.20	5.65	9.00
3 D	4.80	200	1.80	8.00	13.50
4 D	6.25	200	2.40	10.25	18.00

Table XIII. Model parameters for full-disaccommodation and starting position. Values in a single row illustrate the phasic-velocity and tonic-position signal heights when the initial and final destinations of disaccommodation are equal (i.e. full-disaccommodation). Pulse and step heights increase linearly with starting position.

to the error normalization scalar. Note that this scalar has a value of 1.0 in the dynamic model for accommodation (Schor & Bharadwaj, 2005).

$$S_{vel} = SP_{diop} \quad (2)$$

Where, S_{vel} = height of the velocity-step (D/s) and SP_{diop} = starting position of disaccommodation (D).

The velocity-step is integrated to produce the tonic-position signal whose magnitude is proportional to the dioptric distance to the final destination.

3.3. Internal feedback

Internal feedback is used to estimate position errors between the desired and actual disaccommodative responses (Figure 41a). Desired disaccommodation is computed from the sum of the retinal error (defocus) and a positive internal feedback-loop that is derived from efference copy that takes into account the plant transfer function with a virtual plant. In effect, estimates of actual disaccommodation position (efference copy) are subtracted in a negative feedback loop from the desired position signal to produce the error signal, which is scaled to produce the velocity-step. This internal source of feedback is analogous to that proposed for vergence eye movements by Zee & Levi (1989). Negative feedback produces a velocity-step signal whose initial height is proportional to starting position and whose width is proportional to the magnitude of the disaccommodation response. The velocity-step is integrated to a tonic-position signal whose height is proportional to the response magnitude.

3.4. Refractive errors

Retinal defocus error provides sensory information to produce a motor plan that guides the step response with internal feedback. Retinal error equals the difference between the dioptric distance of the conjugate focus of the eye and the stimulus target. Refractive errors (not shown) would be represented by a response bias at the system output**,** in the feed-forward loop prior to visual feedback. In the unaccommodated eye, this response bias would increase the retinal error in hyperopia (negative bias), and it would decrease the retinal error in myopia (positive bias). Any changes in blur sensitivity associated with refractive error would be represented by the size of the depth of focus and to the size of supra-threshold errors which influence the amplitude of the response (e.g. lag of accommodation) but not its dynamics**,** as described by the main sequence function, when controlled by internal feedback.

3.5. Signal processing flow charts

Figures 42 & 43 display several signal processing flow charts that illustrate how acceleration-pulse and velocity-step signals are integrated to phasic-velocity and tonic-position signals respectively. These signals are combined with a starting position bias and they are transformed by the plant into accommodation and disaccommodation step responses. The acceleration-pulse height for accommodation is independent of both starting position and response magnitude (Figure 42a, b, & c) while the velocity-step height increases only with response magnitude and not with starting position (Figure 42a, b, & c). In contrast, the acceleration-pulse and velocity-step heights for disaccommodation both depend on starting position and are independent of response

magnitude (Figure 43a, b, & c). Figure 43a & b illustrate that the 1.5 D and 4 D disaccommodation pulse and step components from the 4 D starting position have the same heights, and they are larger than the pulse and step heights for a 1.5 D disaccommodation responses from the 1.5 D starting position (Figure 43c). Model simulations of position, velocity and acceleration for accommodation and disaccommodation (dashed lines) are also compared to empirical measures (solid lines) in Figures 39 & 40.

Overshoots that are a characteristic of partial-disaccommodation responses result from combinations of large changes in phasic-velocity signals and smaller changes in tonic-position signals. During full-disaccommodation to the far point, the initial and final destinations are the same and the change in the phasic signal is approximately half the change in height of the tonic signal (Figure 43b). For partial-disaccommodation from the same starting position, the phasic signal remains unchanged, but the change in height of the tonic signal is decreased in proportion to the smaller response magnitude. As demonstrated by figure 5a, when the change in partial-disaccommodation (1.5 D) was less than 50 % of the amplitude of a full disaccommodation response from the starting position (4 D), the amplitude of the phasic-velocity signal was greater than the change of the tonic-position signal, and this mismatch caused overshoots at the final destination. The same 1.5 D amplitude response for a full-disaccommodation response to the far point from 1.5D is stable (Figure 43c) because the height variation of the phasic signal does not exceed that of the tonic signal. Empirical measures demonstrate such overshoots of small partial-disaccommodation responses from proximal starting positions (Figure 39c & 40c).

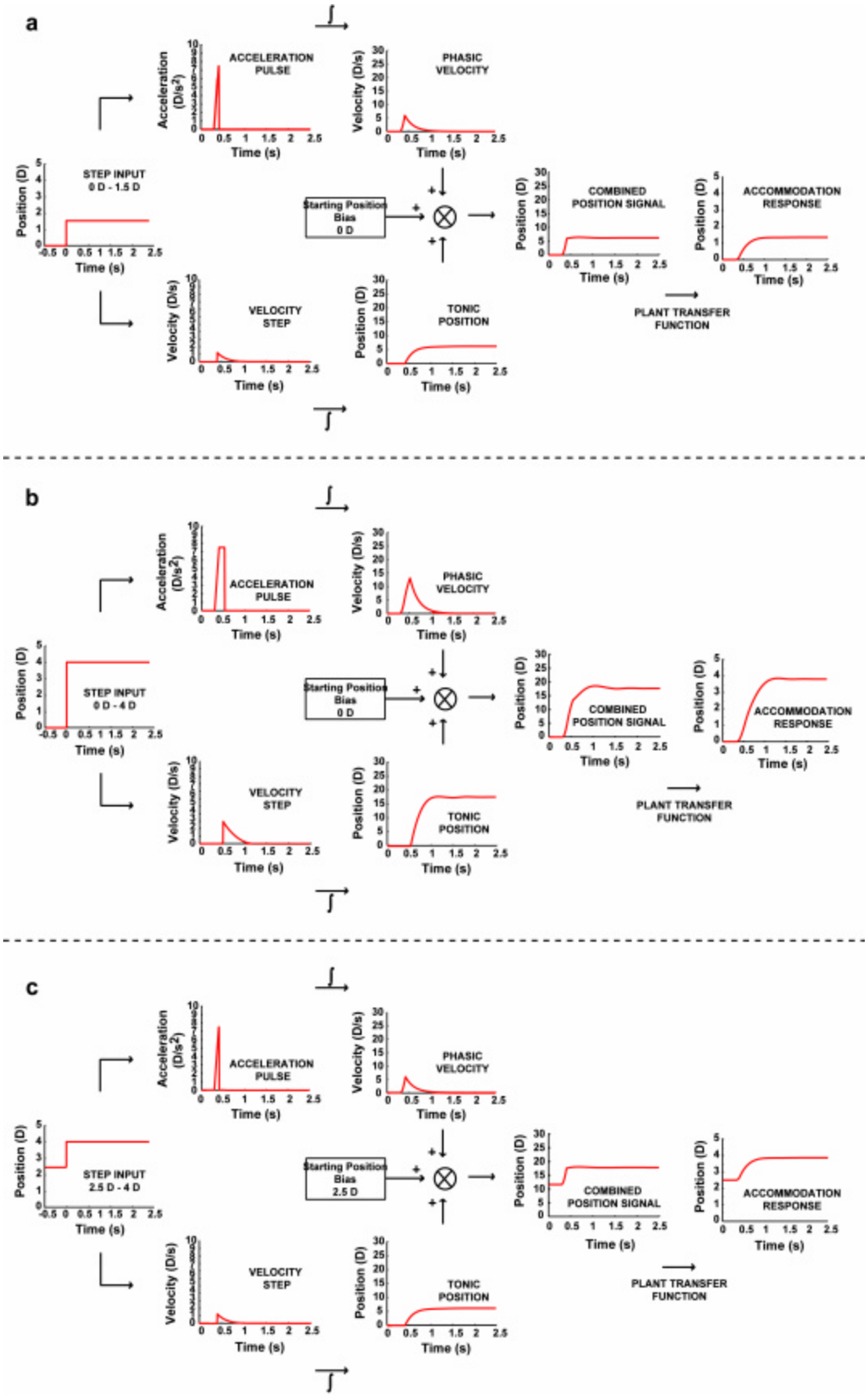
a
ACCELERATION PULSE
PHASIC VELOCITY
STEP INPUT
0 D - 1.5 D
Starting Position Bias
0 D
COMBINED POSITION SIGNAL
ACCOMMODATION RESPONSE
VELOCITY STEP
TONIC POSITION
PLANT TRANSFER FUNCTION
b
ACCELERATION PULSE
PHASIC VELOCITY
STEP INPUT
0 D - 4 D
Starting Position Bias
0 D
COMBINED POSITION SIGNAL
ACCOMMODATION RESPONSE
VELOCITY STEP
TONIC POSITION
PLANT TRANSFER FUNCTION
c
ACCELERATION PULSE
PHASIC VELOCITY
STEP INPUT
2.5 D - 4 D
Starting Position Bias
2.5 D
COMBINED POSITION SIGNAL
ACCOMMODATION RESPONSE
VELOCITY STEP
TONIC POSITION
PLANT TRANSFER FUNCTION
Time (s)

Figure 44. Signal processing flow charts for accommodation illustrating the neural integration of independent acceleration-pulse and velocity-step signals into phasic-velocity and tonic-position signals respectively that are transformed by the plant into accommodation and disaccommodation step responses. Signal-processing for 1.5 D and 4 D accommodation step stimuli from 0 D starting position (a & b) and for a 1.5 D step stimulus from 2.5 D starting position (c). The pulse height remains the same with response magnitude (compare a & b) and starting position (compare a & c) while the pulse width increases only with response magnitude (compare a & b). Increases in the height of the phasic-velocity signal are thus achieved by increasing the width of the pulse. The size of the velocity-step signal increases with response magnitude (compare a & b) but not with starting position (compare a & c).

4. Simulation results

Simulations are compared to empirical measures of dynamic properties of accommodation that were obtained from four subjects for four-different starting positions (0 D, 1 D, 2 D & 3 D) while the empirical measures of dynamic properties of disaccommodation were obtained from six subjects for three-different starting positions (4 D, 3 D & 2 D). Data of one representative subject is shown in this paper (Figures 39, 40, 44, 45 & 46).

4.1. Disaccommodation position traces and stability of partial-disaccommodation

Simulations of accommodation and disaccommodation position traces from a fixed starting position and from different starting positions are shown by the dashed lines in Figures 39b, c and 40b, c. The simulations agree well with the empirical data (solid lines) and they also show overshoots of small partial-disaccommodation responses from proximal starting positions (Figure 39b, 40b). No overshoots are seen in larger magnitude disaccommodation responses, disaccommodation responses from distal starting positions or in any of the accommodation responses. The relationship between the magnitude of

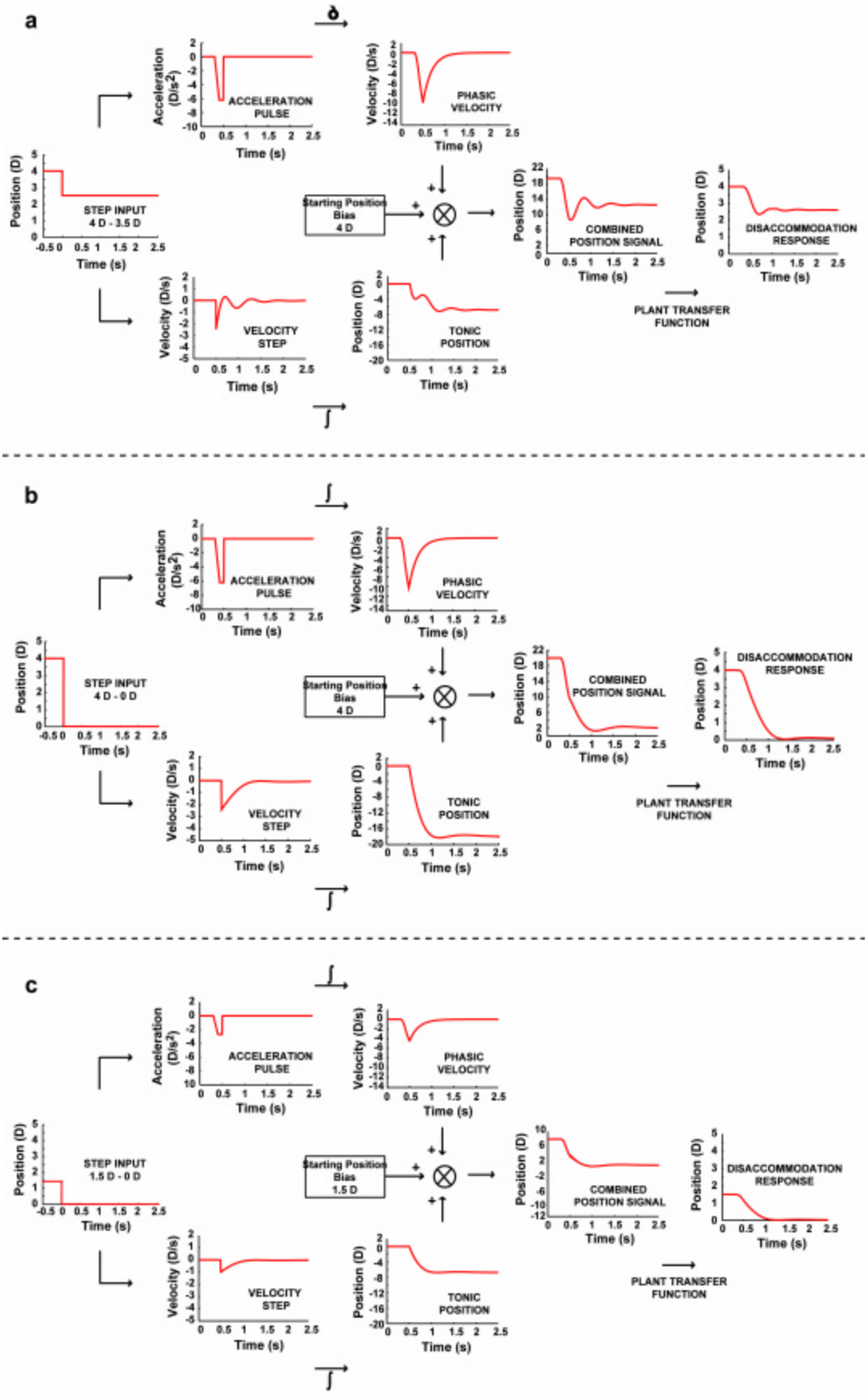
a
δ
Acceleration (D/s²)
ACCELERATION PULSE
Time (s)
Velocity (D/s)
PHASIC VELOCITY
Time (s)
Position (D)
STEP INPUT
4 D - 3.5 D
Time (s)
Starting Position Bias
4 D
Position (D)
COMBINED POSITION SIGNAL
Time (s)
Position (D)
DISACCOMMODATION RESPONSE
Time (s)
PLANT TRANSFER FUNCTION
Velocity (D/s)
VELOCITY STEP
Time (s)
Position (D)
TONIC POSITION
Time (s)
∫
b
∫
Acceleration (D/s²)
ACCELERATION PULSE
Time (s)
Velocity (D/s)
PHASIC VELOCITY
Time (s)
Position (D)
STEP INPUT
4 D - 0 D
Time (s)
Starting Position Bias
4 D
Position (D)
COMBINED POSITION SIGNAL
Time (s)
Position (D)
DISACCOMMODATION RESPONSE
Time (s)
PLANT TRANSFER FUNCTION
Velocity (D/s)
VELOCITY STEP
Time (s)
Position (D)
TONIC POSITION
Time (s)
∫
c
∫
Acceleration (D/s²)
ACCELERATION PULSE
Time (s)
Velocity (D/s)
PHASIC VELOCITY
Time (s)
Position (D)
STEP INPUT
1.5 D - 0 D
Time (s)
Starting Position Bias
1.5 D
Position (D)
COMBINED POSITION SIGNAL
Time (s)
Position (D)
DISACCOMMODATION RESPONSE
Time (s)
PLANT TRANSFER FUNCTION
Velocity (D/s)
VELOCITY STEP
Time (s)
Position (D)
TONIC POSITION
Time (s)
∫

Figure 45. Signal-processing for 1.5 D and 4 D disaccommodation step stimuli from 4 D starting position (a & b) and for a 1.5 D step stimulus from 1.5 D starting position (c). The pulse height remains constant with response magnitude (compare a & b) while it increases with the starting position of disaccommodation (compare a & c). Increases in the height of the phasic-velocity signal are thus achieved by increasing the height of the pulse. The width of the velocity-step signal increases with response magnitude but the height remains constant (compare a & b). The height of the velocity step signal increases with starting position of disaccommodation (compare a & c).

primary overshoot (the first and most prominent overshoot in a disaccommodation response) and magnitude of disaccommodation response is shown for empirical and simulated data in figure 44a & b respectively. These plots show data for a range of response magnitudes (0.5D - 4D) and for a range of starting positions (2 D, 3 D & 4 D). The simulations agree both qualitatively and quantitatively with the empirical data collected by Bharadwaj & Schor (2005b) and show that the magnitude of the primary overshoot increases as step size decreases below 2D and it also increases with the dioptric distance of the starting position (Figure 44a, b).

4.2. The main-sequence relationships

Simulations of velocity profiles of step responses by accommodation and disaccommodation from a fixed starting position and from different starting positions are shown in Figures 39d, e and 40d, e. Figure 45a, b show the main sequence relationships of peak velocity for empirical and simulated data for three different starting positions (plots of peak velocity or peak acceleration as a function of response magnitude). The models described in Figure 41 predict that the main sequence relationship of peak velocity will differ for accommodation and disaccommodation. As shown in figure 45a, the peak velocity of accommodation increases with response magnitude. The simulated

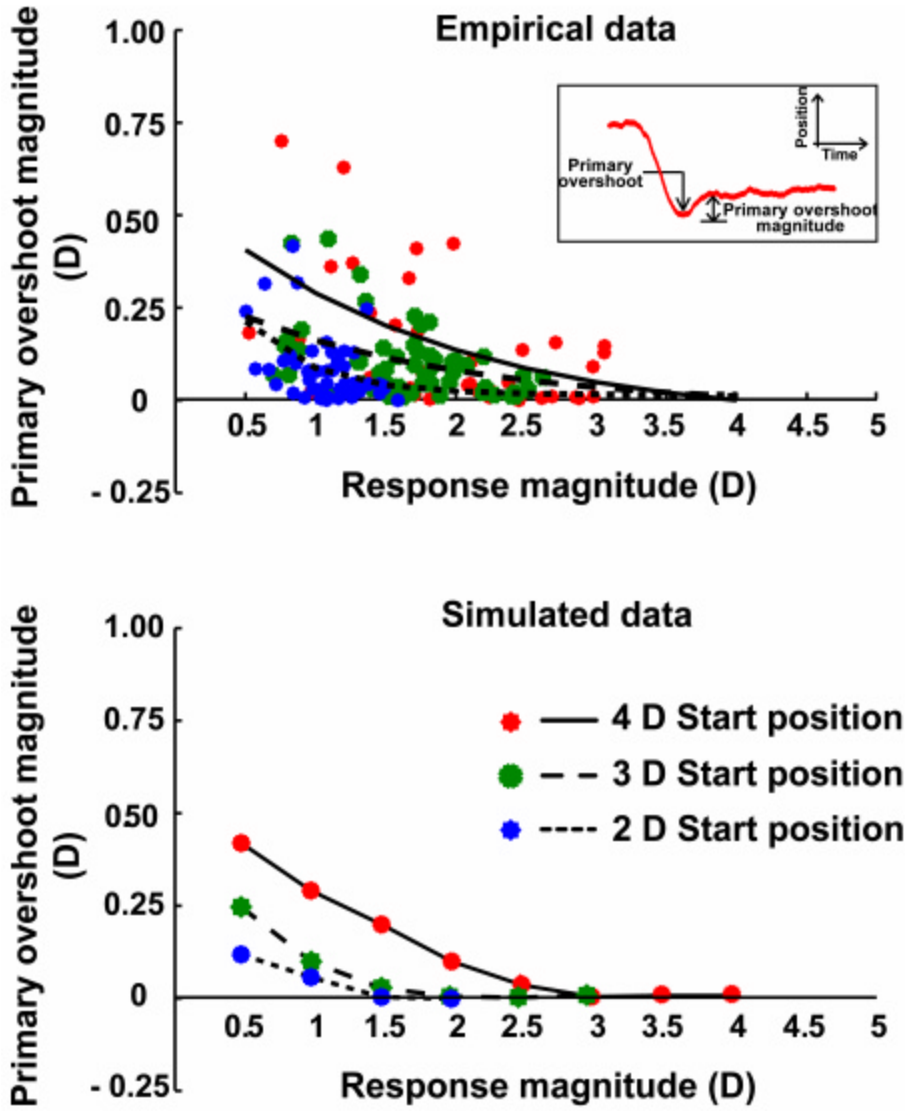

Figure 46. Magnitude of primary overshoot plotted as a function of response magnitude for empirical (a) and simulated (b) disaccommodation responses. The primary overshoot is indicated in the inset for a sample disaccommodation response. In both empirical data and simulations, the magnitude of primary overshoot increased with a reduction in the response magnitude and was most prominent for responses less than 2.0 D and for more proximal starting positions. The solid, dashed and dotted line in figure a shows the best-fit exponential function fit to the empirical data for 4 D, 3 D and 2 D starting positions respectively (Bharadwaj & Schor, 2005b). In figure b, these lines are used only to connect the individual data points.

main sequence saturates at larger response magnitudes as shown empirically by Kasthurirangan *et al* (2003). The peak velocity of accommodation is independent of

starting position (Figure 45c). Figure 45b shows the empirical and simulated peak velocity of disaccommodation to remain invariant of response magnitude for the three starting positions. The mean peak velocities for each of the three simulated starting positions are given in Table XIII. The peak velocity increases with the dioptric distance of the starting position of disaccommodation ($y = 1.37x + 0.85$) and the linear regression equation agrees well with empirical measures (Figure 45d). For both accommodation and disaccommodation, the simulated main sequence agrees well with the empirical data.

Simulations of acceleration profiles of accommodation and disaccommodation from a fixed starting position and from different starting positions are shown in Figures 39f, g and 40f, g. The main sequence data for peak acceleration is shown in figure 46a & b. The peak acceleration for accommodation is invariant with both response magnitude (Figure 46a) and starting position (Figure 46c). The simulated data are similar to the empirical data obtained by Bharadwaj & Schor (2005a). The peak acceleration for disaccommodation remains invariant with response magnitude (Figure 46b) and increases with dioptric distance of the starting position ($y = 8.63x + 18.6$) (Figure 46d). The mean peak accelerations for each of the three simulated starting positions are given in Table XIII.

4.3. Changes in dynamic properties of disaccommodation with practice

The dynamic properties of disaccommodation can be modified with practice. The coauthor (SRB) measured his disaccommodation responses for over one-year. A detailed account of his dynamic properties and how they changed with practice can be found in

Bharadwaj & Schor (2005b). Hence, only a succinct description will be provided here. When the study began (First session), the dynamic properties of his disaccommodation responses were the same as reported for other subjects (Figure 40 b-g). Smaller magnitudes of disaccommodation from proximal starting positions showed overshoots (compare blue and red traces in Figure 47a). Both peak velocity and peak acceleration of

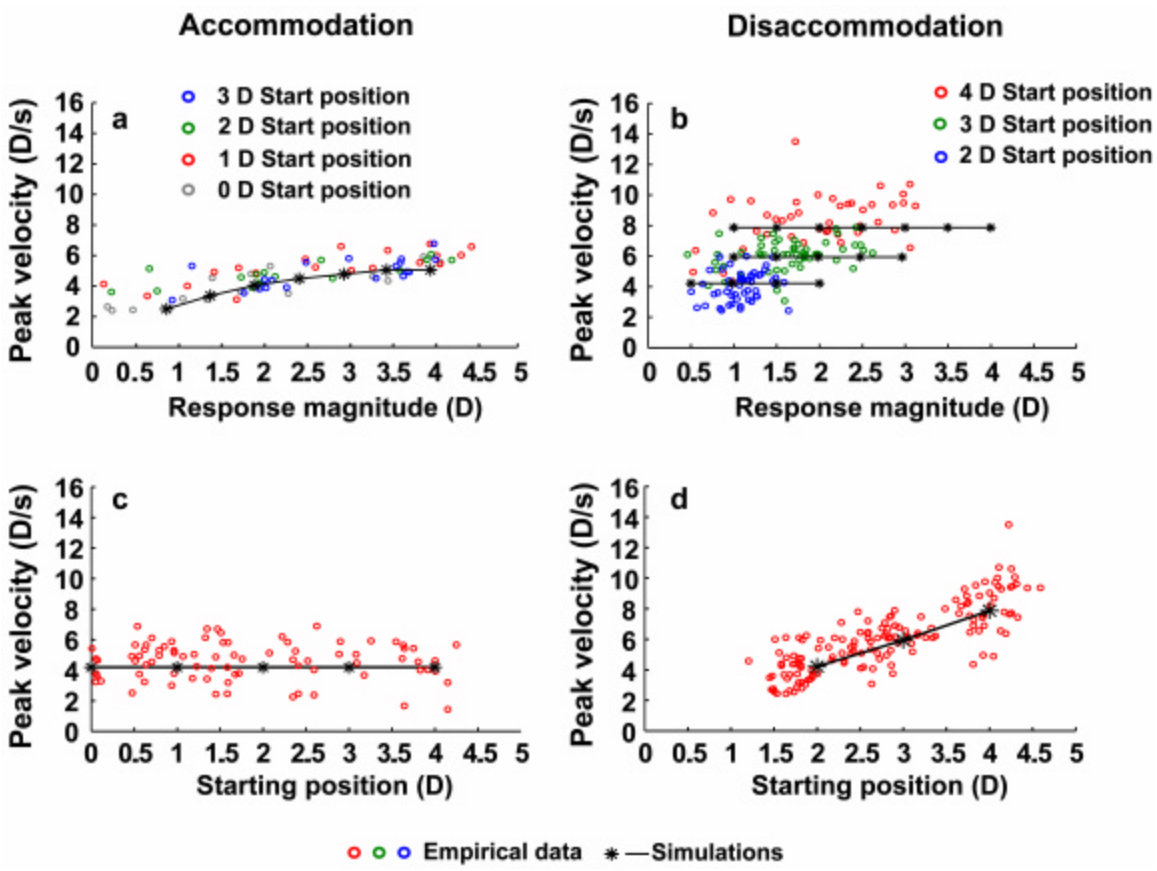

Figure 47. Peak velocity characteristics of accommodation and disaccommodation step responses. a & b) Peak velocity main sequence relationships for accommodation and disaccommodation for different starting positions (accommodation: 0 D, 1 D, 2 D & 3 D; disaccommodation: 2 D, 3 D & 4 D). The peak velocity of accommodation increases with response magnitude while the peak velocity of disaccommodation remains invariant of the response magnitude. c & d). Peak velocity of accommodation and disaccommodation are plotted as a function of starting position. The peak velocity of accommodation does not change with starting position, while the peak velocity of disaccommodation increases systematically with starting position. The colored circles represent the empirical data and black stars and solid lines represent the model simulations.

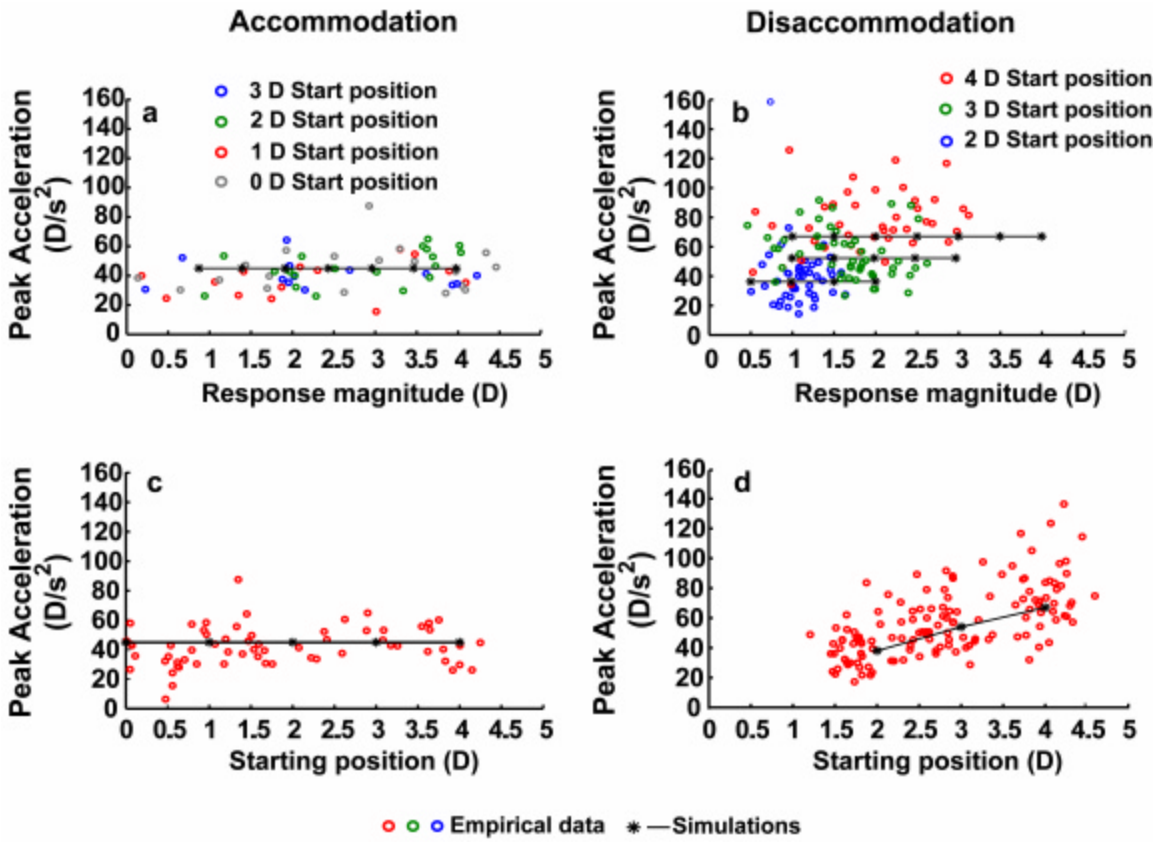

Figure 48. Peak acceleration characteristics of accommodation and disaccommodation step responses. a & b) Peak acceleration main sequence relationships for accommodation and disaccommodation for different starting positions (accommodation: 0 D, 1 D, 2 D & 3 D; disaccommodation: 2 D, 3 D & 4 D). The peak acceleration of both accommodation and disaccommodation remain invariant of the response magnitude. c & d). Peak acceleration of accommodation and disaccommodation plotted as a function of starting position. The peak acceleration of accommodation does not change with starting position, while the peak acceleration of disaccommodation increases systematically with starting position. The colored circles represent the empirical data and black stars and solid lines represent the model simulations.

disaccommodation were independent of response magnitude and they increased with dioptric distance of the starting position (Figure 47b, c). Time-to-peak velocity was invariant with response magnitude and starting position (Figure not shown). However after one year of experience (Second session), these trends changed. Overall, the first-

Starting position (D)	Pk Acceleration (D/s^2)	TPA (Ms)	Pk Velocity (D/s)	TPV (Ms)
1 D	20	100	2.48	200
2 D	35	100	4.20	200
3 D	50	100	6.00	200
4 D	65	100	7.65	200

Table XIV. First- and second-order dynamic characteristics of simulated disaccommodation responses. Values in a single row illustrate heights of the phasic-velocity and tonic-position signals when the initial and final destinations of disaccommodation are equal (i.e. full-disaccommodation). Pk Accel = Peak acceleration (D/s^2); TPV = Time-to-peak acceleration (Ms); Pk Vel = Peak velocity (D/s); TPV = Time-to-peak velocity (Ms).

and second-order dynamic properties of disaccommodation were more sluggish or damped in the second session than in the first session (compare figures 47b & e for velocity and figures 47c & f for acceleration). The sluggishness of his dynamic properties in the second session produced more stable partial-disaccommodation responses without overshoots (compare green and blue traces in figures 47a & d).

In the second session, the peak velocity not only increased with the starting position of disaccommodation (compare green and blue traces in figure 47e) but it also increased with response magnitude from a given starting position (compare blue and red traces in figure 47e). Increases in peak velocity with response magnitude and starting position were associated with an increase in time-to-peak velocity (Figure not shown). Overall,

the control strategy in the second session for dynamic disaccommodation was similar to the control strategy of dynamic accommodation. This indicates that two different control strategies were used for disaccommodation in the two sessions. The starting-position dependent control strategy for peak velocity was used to simulate dynamic disaccommodation in the first session while the response-magnitude dependent control strategy that is typical for determining peak velocity of accommodation was used to simulate dynamic disaccommodation in the second session. The difference in the models of control strategy for disaccommodation in the two sessions was that acceleration-pulse height was increased with dioptric distance of the starting position in the first session, and acceleration-pulse width was increased with response magnitude from a given starting position in the second session. The velocity step equaled the unscaled error signal in the second session. The latter model for the second session was identical to the model for accommodation proposed by Schor & Bharadwaj (2005). As seen in figures 47a – f, the simulation agreed well with the empirical data.

5. Discussion

5.1. Pulse-Step model overview

The first- and second-order dynamic properties of disaccommodation indicate that the step responses are composed of two separate response destinations: an initial destination that correlates well with the cycloplegic refractive state and a final destination (Bharadwaj & Schor, 2005b; Bharadwaj *et al*., 2005). The disaccommodation responses are initiated by a combined pulse-step reduction of innervation of the ciliary muscle toward zero. The open-loop acceleration-pulse signal controls the dynamic properties of

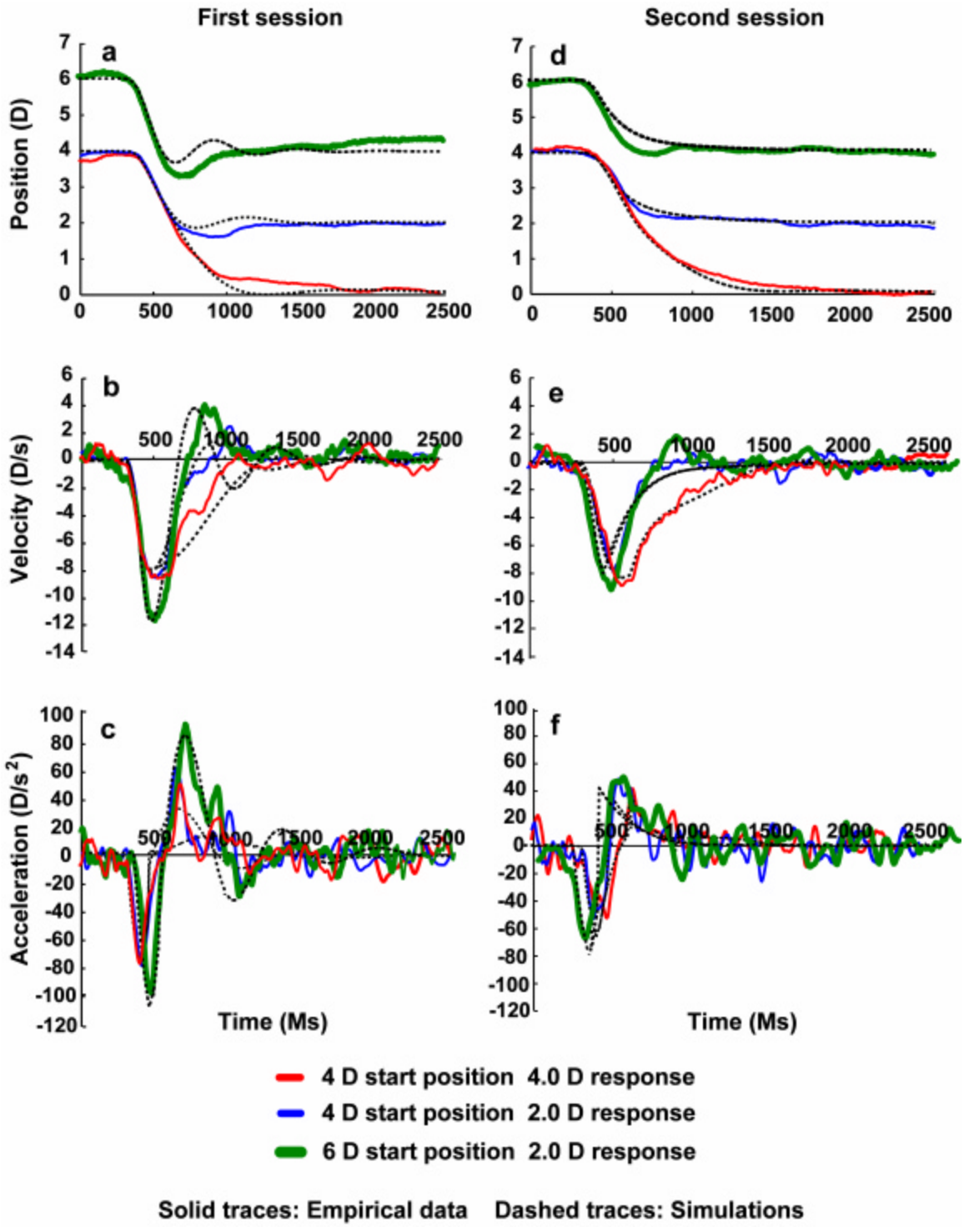
First session
Second session
a
d
b
e
c
f
Position (D)
Velocity (D/s)
Acceleration (D/s²)
Time (Ms)
Time (Ms)
4 D start position 4.0 D response
4 D start position 2.0 D response
6 D start position 2.0 D response
Solid traces: Empirical data
Dashed traces: Simulations

Figure 49. Position, velocity and acceleration traces of disaccommodation for subject SRB. Solid lines represent empirical measures and dashed lines are model simulations. The left-hand and the right-hand panel show data from the first session and the second session respectively. a & d) Position traces plotted as a function of time. In the first session (a), instabilities were seen in the smaller response magnitudes for both starting positions (green & blue traces). These instabilities were reduced in the second session (compare green & blue traces in a & d). b & e) Velocity traces plotted as a function of time. In the first session (b), the peak velocity remained invariant of response magnitude (compare blue & red traces) and it increased with starting position (compare green & blue traces). In the second session (e), the peak velocity increased with both response magnitude (compare blue & red traces) and starting position (compare green & blue traces). The peak velocities were reduced in magnitude in the second session when compared to the first session (compare green traces in b & e). c & f) Acceleration traces are plotted as a function of time. In the first session (c), the peak acceleration remained invariant of response magnitude (compare blue & red traces) and it increased with starting position (compare green & blue traces). The second session (f) showed similar peak acceleration characteristics. The peak accelerations were reduced in magnitude in the second session when compared to the first session (compare green traces in c & f).

the step response and it is followed by the closed-loop velocity-step innervation that serves two purposes. First, together with the acceleration-pulse, the velocity-step initiates the response toward the initial destination and second, with visual feedback the velocity-step innervation guides the response to its desired final destination. Like the acceleration-pulse, the initial amplitude of the velocity-step is the same for all responses from a given starting position. The height of both the acceleration-pulse and velocity-step signals increase with the dioptric distance of the starting position for disaccommodation.

5.2. Single-step model of disaccommodation

Model simulations indicate that the disaccommodation responses are not initiated toward the initial destination by a single step-reduction of innervation of the ciliary muscle. As an alternative to the pulse-step model of disaccommodation described so far,

we simulated a single-step model of the disaccommodation step response by setting the gain of the pulse component of the pulse-step model to zero with all the other model components remaining the same. Similar to the pulse-step model, the negative-feedback error of the single step was scaled by the ratio of full to partial disaccommodation in order to produce an initial step height that was equal to the initial motor error for a full-disaccommodation response to the far point. The scalar produced a feed-forward gain that was inversely proportional to the amplitude of the step change to the final destination.

The simulations (not shown) produced dynamic trends that were not observed in the empirical data. The simulated peak velocity remained invariant of the response magnitude for a given starting position, however the simulated peak acceleration and time-to-peak velocity (TPV) varied with response magnitude. The peak acceleration was higher for smaller responses than for larger responses (e.g. 4 D response from a 4 D starting position: 65 D/s^2; 2 D response from a 4 D starting position: 80 D/s^2). The TPV was shorter for smaller responses and longer for larger responses (e.g. 4 D response from a 4 D starting position: 275 ms; 2 D response from a 4 D starting position: 200 ms). Finally, the time-to-peak acceleration in the simulated single-step disaccommodation responses (TPA) was abnormally short (10 ms). These differences from the empirical responses suggest that disaccommodation responses are not produced by a simple step change in innervation and instead it is more likely that they are produced by a combined pulse and step innervation as described above by the pulse-step model.

5.3. Neural control strategies for accommodation and disaccommodation

Differences in the first- and second-order dynamic properties of accommodation and disaccommodation indicate that they utilize different neural control strategies (Bharadwaj & Schor, 2005a; b). Both systems utilize acceleration-pulse and velocity-step signals to control dynamic properties and the magnitude of responses. Accommodation and disaccommodation utilize different characteristics of the acceleration-pulse signal to control the peak velocity and peak acceleration of the step responses. The first- and second-order dynamic properties of accommodation are produced by varying the width of a fixed-height pulse with response magnitude. In contrast, the first- and second-order dynamic properties of disaccommodation are produced by varying the height of a fixed-width pulse with the dioptric distance of the starting position. Acceleration-pulse parameters for accommodation are invariant with starting position and only depend on response magnitude whereas for disaccommodation, they are invariant with response magnitude and depend only on starting position.

The different dynamic characteristics exhibited by accommodation and disaccommodation step responses illustrate that these two motor systems do not operate with machine-like properties but rather they utilize different dynamic control strategies to optimize the accuracy and/or speed of the step response. Adjusting the acceleration-pulse width for accommodation in proportion to response magnitude, independent of starting position, produces stable but slow responses. Adjusting the acceleration-pulse height for disaccommodation in proportion to the dioptric distance of the starting position, independent of the response magnitude, produces rapid responses that are unstable for small disaccommodation responses from a near starting position. Why do

accommodation and disaccommodation optimize different dynamic features of their step responses (stability versus speed respectively)? Perhaps accommodation and disaccommodation are responding to different tasks or goals that they normally encounter in natural viewing conditions. During accommodation to a specific near object that attracts our attention, if we wish to inspect the object, accuracy of accommodation is more important than speed, whereas during disaccommodation, we usually explore distal space to quickly scan for obstacles or novel events, and if we wish to detect novel objects, speed of disaccommodation is more important than accuracy. The different control strategies employed by accommodation and disaccommodation step responses could be influenced by the instruction set provided to the human subjects during the course of data collection. For example, an instruction to disaccommodate accurately rather than rapidly could have resulted in similar control strategies of accommodation and disaccommodation. However, the same instruction set ("to focus on one of the black and white wedges of the Maltese cross and maintain accurate clarity of this wedge throughout the experiment") was provided to the subjects during data collection of both accommodation and disaccommodation step responses. Hence, even if the instruction set could influence the control strategy of the step response, it would have done so equally to both accommodation and disaccommodation step responses.

5.4. Stability of partial-disaccommodation responses

The acceleration-pulse is open loop and its amplitude determines the first- and second-order dynamic properties of the disaccommodation step response. The velocity-step is closed-loop and negative feedback guides the response to completion and

maintains it in a steady state. In full-disaccommodation (responses from a given starting position to the far point), the final destination equals the far point and the heights of the acceleration-pulse, the velocity-step and their integrated phasic-velocity and tonic-position signals are all proportional to the starting position. During partial-disaccommodation (responses from a given starting position to a position proximal to the far point), the initial heights of the acceleration-pulse, velocity-step and phasic-velocity signals are the same as a full-disaccommodation response to the far point. However, the height of the tonic-position signal is reduced, and it is proportional to the magnitude of the disaccommodation response from the starting position to the dioptric distance of the final destination. When the dioptric value of the final destination is greater than 50 % of the dioptric value of the starting position, the combination of a large change in the phasic-velocity signal and a smaller change in the tonic-position signal produces overshoots in the step response when control switches from the open-loop acceleration-pulse to the closed-loop velocity-step.

5.5. Plasticity of dynamic control of disaccommodation

Changes in the dynamic properties of disaccommodation by subject SRB reduced the overshoots of the partial disaccommodation response in the second session (Bharadwaj & Schor, 2005b). In effect, SRB's control strategy for disaccommodation changed to the control strategy for accommodation where peak acceleration was invariant with response magnitude and starting position while peak velocity increased with response magnitude. These dynamic properties were modeled by increasing pulse width rather than pulse height to control peak velocity. This is a clear demonstration of plasticity of the neural

control of disaccommodation. The advantage of the typical disaccommodation control strategy over the accommodation control strategy is that varying pulse height rather than pulse width results in higher peak acceleration and peak velocity that reduce the response time for near-to-far responses. But the disadvantage of the typical disaccommodation control strategy is that it produces overshoots for small partial-disaccommodation responses from proximal starting positions. Perhaps with many repeated trials in our apparatus, SRB became motivated to disaccommodate accurately, rather than quickly, and accordingly his control strategy was modified, albeit subconsciously.

The accommodation step response also exhibits some plasticity. Kasthurirangan & Glasser (2005) reported a similar starting-position dependence strategy of peak velocity for both accommodation and disaccommodation. In their study, the peak velocity of accommodation step responses increased with dioptric distance of the starting position such that a 1.5 D response from a 4.5 D starting position had a higher peak velocity than a 1.5 D response from the far point. Although we found the peak velocity for a constant magnitude of disaccommodation (1.5 D) to increase with dioptric distance of the starting position (Figure 2e), the same subjects did not show any change in peak velocity of accommodation with starting position (Figure 2d). Comparison of our results with those of Kasthurirangan & Glasser (2005) indicates that highly practiced subjects in either their study or ours can learn to control the peak velocity of accommodation using the strategies of varying acceleration-pulse height or pulse width. Indeed, they found that the peak velocity for small accommodation responses to a 6 D ending position varied by 50 % (13.5 D/s to 9 D/s) depending on the order of stimulus presentation and they interpret this

variation as a training effect. We have modeled the starting-position dependence strategy of peak velocity of accommodation with a model similar to the disaccommodation model. In the starting-position strategy model for accommodation, the pulse height is proportional to the dioptric value of starting position and the initial step height is proportional to the ending position.

5.6. Similarities in the dynamic properties of divergence and disaccommodation

Differences in the dynamic properties of accommodation and disaccommodation are mirrored by the vergence system (Alvarez *et al*., 2005). Peak velocity of convergence increases with response magnitude, independent of starting position, while peak velocity of divergence increases with binocular parallax of the starting position, independent of response magnitude (Alvarez *et al*., 2005). Our inspection of their data reveals three characteristics of the divergence step responses that are similar to disaccommodation step responses. First, the initial slope of the velocity profiles (giving an estimate of the response acceleration) also increased with proximity of the starting position. Divergence may use a similar control strategy as disaccommodation by controlling pulse height with proximity of starting position. Second, as with disaccommodation, the time-to-peak velocity of divergence (measured from the start of the response) changed insignificantly with starting position. Third, there are overshoots and oscillations in partial-divergence step responses from proximal starting positions. These observations suggest that starting position dependent characteristics of disaccommodation and divergence could have a common neural origin. Since the biomechanical plants of these two motor systems are separate and distinct, the similar dynamic properties are probably not a consequence of

the physical plant, but rather they result from a neural control strategy that is matched in the two systems to promote coordinated cross-coupled accommodation and vergence responses (Morgan, 1968; Schor & Kotulak, 1986; Schor, 1992).

5.7. Neural substrates for disaccommodation

Shared neural control of convergence and accommodation has been observed in a number of areas of the primate brain including the prearcuate cortex and frontal eye fields (Gamlin & Yoon, 2000), the posterior interposed nucleus (IP) of the cerebellum (Gamlin *et al*., 1996; Zhang & Gamlin, 1998), the nucleus reticularis tegmenti pontis (NRTP) (Gamlin & Clarke, 1995; Gamlin, 2002) and in the near response cells of the supra-oculomotor area (Judge & Cumming, 1986; Mays *et al*., 1986; Mays & Gamlin, 1995; Zhang *et al*., 1992). All of these areas have both phasic and tonic cells that control the dynamic properties and position of the near responses of accommodation and convergence. Specifically, the NRTP and the IP nucleus have neurons whose activities increase either in a transient fashion (phasic cells) or in a sustained fashion (tonic cells) with the amplitude of the far-response (Gamlin *et al*., 1996; Gamlin & Clarke, 1995; Zhang & Gamlin, 1998). It is possible that the phasic and tonic activity of the NRTP and IP neurons aid disaccommodation step responses by providing inhibitory input to the ciliary muscle via the midbrain near-response cells and the Edinger-Westphal (EW) nucleus (Gamlin, 2002; Zhang & Gamlin, 1998).

6. Conclusion

The first- and second-order dynamic properties and control strategies of accommodation and disaccommodation are different (Bharadwaj & Schor, 2005a; b). The pulse-step model demonstrates how acceleration-pulse and velocity-step signals might be used to form phasic-velocity and tonic-position signals that determine the dynamic properties and magnitudes respectively of step responses by accommodation and disaccommodation. A typical control strategy of accommodation is to adjust the width of a constant height acceleration-pulse signal to control peak velocity in proportion to response magnitude while acceleration is invariant. A typical control strategy for disaccommodation is to adjust the height of the constant-width acceleration-pulse and velocity-step to be proportional to the dioptric value of starting position to control both peak acceleration and peak velocity, independent of response magnitude. The linear dependence of dynamic properties of disaccommodation on the dioptric value of starting position suggests that disaccommodation responses of any magnitude from a fixed starting position are initiated toward a common initial destination (cycloplegic refractive state) by a phasic-velocity signal whose height is proportional to the dioptric value of the starting position (Bharadwaj *et al*., 2005). Responses are completed and maintained at a final destination by an independent tonic-position signal whose height is proportional to the response magnitude to reach the final destination. Partial-disaccommodation responses can have overshoots when the height change of the phasic velocity signal is larger than that of the tonic-position signal. However it is possible to adapt the motor control strategy of disaccommodation to be more like that of accommodation to improve the stability of small partial disaccommodation responses.

Chapter VI: Applying the pulse-step model of accommodation to predict dynamic performance of accommodating intraocular lenses

1. Abstract

We have developed a dynamic model of accommodation that simulates stability and dynamic performance of accommodating intraocular lens (A-IOL) implants when they are controlled by the negative feedback of the accommodation system. A-IOL performance was assessed by substituting the visco-elastic properties of a natural lens matrix with those of an A-IOL. Using Matlab and Simulink, the model simulates first- and second-order dynamic changes in accommodation that result from interactions between the accommodative neural controller of an older eye and a prosthetic lens material with biomechanical properties of a younger lens implanted in the older lens capsule. The model predicts first- and second-order dynamic properties of the accommodative step response based on age-dependent biomechanical properties of the accommodative plant and neural control signals that independently control the dynamic and static characteristics of the response with phasic and tonic signals respectively. Simulations illustrate the influence of decreased visco-elastic coefficients of the A-IOL on dynamic accommodation and how adaptation of phasic and tonic signals can restore normal response dynamics. Reducing viscosity and stiffness of the A-IOL to equal the parameters of a younger lens increased the static amplitude of accommodation but with marked dynamic overshoots and oscillations. However, the dynamic response was stabilized by decreasing the amplitudes of phasic and tonic neural control signals. The

model is a tool that simulates dynamic properties of A-IOL materials that have visco-elastic properties of a young lens and adjustments of neural control properties of the older eye that restore stable dynamics. Simulations indicate that neural control must be recalibrated to avoid unstable dynamic accommodation with the A-IOL.

2. Introduction

Presbyopia, the progressive reduction of the amplitude of accommodation, is an inevitable age-related process. Although the cause of presbyopia is considered multi-factorial (Glasser & Kaufman, 2003), the changes in the biomechanical properties of crystalline lens have been shown to play a dominant role (Wyatt, 1993; Glasser & Kaufman, 2003). Age-related changes in the biomechanics of the crystalline lens include changes in the modulus of elasticity of the lens capsule (Fisher, 1971; van Alphen & Graebel, 1991; Krag et al., 1997) and an increase in the viscosity and stiffness of the lens matrix (Glasser & Campbell, 1999; Heys et al., 2004; Weeber et al., 2005). We have developed a pulse-step model of accommodation that predicts the static and dynamic behavior of accommodation by taking into account these age-related biomechanical changes and neural control signals of accommodation (Schor & Bharadwaj, 2005a; b). Position, velocity and acceleration characteristics of accommodation step responses obtained from our pulse-step model simulations closely match those observed under experimental situations (Bharadwaj & Schor, 2005a; b; Kasthurirangan et al., 2003). The overall aim of this paper is to apply the pulse-step dynamic model to predict the static and dynamic performance of accommodation after the implantation of prosthetic accommodating-intraocular lenses (A-IOL's).

2.1. A-IOL designs

The predominant role of age-related changes in elasticity of the lens matrix in presbyopia has led to attempts to replace the natural lens with a prosthetic one inserted in the lens capsule as a potential means of restoring accommodation. These prosthetic

lenses, known as 'accommodating intraocular lenses (A-IOL's),' are inserted into the lens bag which transduces forces applied by the ciliary muscle to change position or shape of the A-IOL. The ciliary muscle is still active in absolute presbyopia (Strenk et al., 1999; 2000). The design of A-IOL's is an up-and-coming technology (see reviews by Doane, 2004; Charman, 2005; Dick, 2005). A-IOL designs currently under development can be grouped broadly into two categories; injectable-deformable polymer gels, and preformed lenses that translate forward during accommodation to increase the effective power of the eye (optical-shift principal). The deformable A-IOL technology involves replacing the lens matrix with a silicone polymer material (Kessler, 1964; 1966; Agarwal et al., 1967a; b; Parel et al., 1986; Haefliger et al., 1987; Haefliger & Parel, 1992; Hettlich et al., 1994; Sakka et al., 1996; Nishi & Nishi, 1998; Nishi et al., 1998) whose refractive index matches approximately the effective refractive index of the natural lens (Haefliger & Parel, 1994; Koopmans et al., 2003; 2004). Accommodation is achieved by shaping the curvature of the silicone polymer with the lens capsule in response to ciliary muscle contraction. Both single-optic and dual-optic preformed-translating A-IOL's have been developed. The single-optic A-IOL technology involves replacing the lens matrix with a monofocal IOL whose 'optic' portion translates within the lens capsule anteriorly during accommodation to increase its effective power (Cumming et al., 2001; Langenbucher et al., 2003; Kuchle et al., 2004). Anterior translation of the single-optic IOL is thought to occur in response to changes in vitreous pressure exerted on the posterior lens capsule due to ciliary muscle constriction (Coleman, 1986; Coleman & Fish, 2001). The dual-optic A-IOL technology involves replacing the lens matrix with an IOL that is designed with two monofocal optical elements held together by flexible springs (Hara et al., 1990;

1992; McLeod et al., 2003). The anterior lens has a high positive power and the posterior lens either has a positive power, similar to the design of a Keplerian telescope (Hara et al., 1990; 1992) or has a negative power, similar to the design of a Galilean telescope (McLeod et al., 2003). Accommodation is achieved by forward translation of the anterior lens in response to changes in lens capsular tension produced by ciliary muscle constriction (Hara et al., 1990; 1992; McLeod et al., 2003).

The success of the A-IOL depends on many factors including biocompatibility (Agarwal et al., 1967a; b), surgical ease to implant (de Groot et al., 2001; Kessler, 1966; Parel et al., 1986; Hara et al., 1990; Hettlich et al., 1994; Nishi & Nishi, 1998), optical qualities (Agarwal et al., 1967a; b; de Groot et al., 2001; Ho et al., 2001; Koopmans et al., 2003), and restoring a functional range of accommodation (Haefliger & Parel, 1994; Sakka et al., 1994; Nishi et al., 1998; Cumming et al., 2001; Langenbucher et al., 2003; Kuchle et al., 2004). Another performance factor that we address in this paper is the dynamic stability of the A-IOL (Haefliger et al., 1987).

Most A-IOL experiments have assessed the ability of their lenses to restore static accommodation by using techniques that stimulate accommodation responses under open-loop conditions. Under open-loop conditions, the static and dynamic behavior of accommodation responses is independent of the negative feedback provided by retinal image defocus. Open-loop techniques used in measuring the accommodative ability of A-IOL's include, stimulating the ciliary muscle pharmacologically with pilocarpine and measuring the change in refraction before and after pharmacological stimulation

(Haefliger & Parel, 1994; Sakka et al., 1994; Nishi & Nishi, 1998; Nishi et al., 1998; Langenbucher et al., 2003) or quantifying accommodative responses by noting the difference in refraction before and after pharmacological cycloplegia (Agarwal et al., 1967a; Kuchle et al., 2004) or by mechanically stretching the lens capsular bag filled with the polymer under *in vitro* conditions (Koopmans et al., 2003). However, under 'natural' viewing conditions, human accommodation works as a closed-loop system, wherein the static and dynamic behavior of accommodation step responses are dependent on the negative feedback provided by retinal image defocus and efference copy signals of ciliary contraction. Hence, the evaluation of static and dynamic accommodation following implantation of A-IOL's should also be conducted under 'natural' closed-loop viewing conditions. Under such conditions, the static and dynamics characteristics of the step response are determined by both the neural control parameters and the visco-elastic properties of the accommodative plant. Negative feedback from retinal image defocus or an efference copy signal is used to guide changes in force applied by the ciliary muscle to alter crystalline lens curvature (Fincham, 1937; Toates, 1972; Krishnan & Stark, 1975; Schor, 1992; Schor & Bharadwaj, 2005a; b). A mismatch between neural control signals and the visco-elastic properties of the lens could lead to either unstable and oscillatory responses (an 'under-damped' response) or sluggish responses (an 'over-damped' response) (Nise, 2000).

2.2. Biomechanical properties of A-IOL.

The neural controller of accommodation step responses can be described as a second-order system (Bharadwaj & Schor, 2005a; b; Schor & Bharadwaj, 2005a; b) that

controls an over-damped second-order accommodative plant composed of the crystalline lens, ciliary muscle, choroid and the suspensory zonules (Weber et al., 1989). If biomechanics of the A-IOL are not matched to the supportive tissues of the accommodative plant and the neural controller, then either unstable or sluggish responses could result. For example, the dual-optic A-IOL's are designed to work as pure spring elements with minimal viscosity (Hara et al., 1990; 1992; McLeod et al., 2003). A significant reduction of the effective lens viscosity could create a highly under-damped control system resulting in unstable and oscillatory accommodation responses (Nise, 2000). Deformable A-IOL's are designed such that the elastic modulus of the silicone polymer is matched with that of the 25-year-old human lens matrix (Haefliger & Parel, 1994; Koopmans et al., 2003; 2004). The viscosity of the silicone polymer materials is usually determined based on their ease of injection into the lens capsule and their ability to maintain shape following refilling (Parel et al., 1986; Hettlich et al., 1994; de Groot et al., 2001). In this paper, we compared the elasticity and viscosity of one deformable silicone polymer (Koopmans et al., 2003; 2004; Koopmans, 2005) to that of the human lens (Krag et al., 1997; Weeber et al., 2005). As will be shown in a later section, the elasticity of the silicone polymer compared well with that of the human lens while the viscosity of the silicone polymer was lower than that of the human lens. Under closed-loop conditions, the significant reduction of the effective lens viscosity created a highly under-damped control system resulting in an unstable and oscillatory accommodative step response. Alternatively, filling the capsular bag with a silicone polymer, which has a higher viscosity than the human lens, could create an over-damped control system resulting in sluggish step responses.

2.3. Neural adaptation to A-IOL

The differences between the biomechanical properties of the injectable A-IOL and the natural lens could be compensated for by adaptation of the accommodative control system (Haefliger & Parel, 1994; Charman, 2005). Adjustment of neural control parameters that determine dynamic properties and response magnitudes of the polymer gel could achieve optimal dynamic and static performance of the A-IOL. The purpose of this report is two fold: first, to use a dynamic model of accommodation (Schor & Bharadwaj, 2005a; b) to predict, with computer simulations, the static and dynamic performance of A-IOL implants in a 45-year-old eye. The model can be applied to any A-IOL whose power can be adjusted continuously with constriction of the ciliary muscle, such as a deformable silicone polymer A-IOL's or a dual-optic A-IOL's. The second purpose is to show, using model simulations, how the performance of an A-IOL, whose visco-elastic properties differ from those of the human lens, could be optimized by adapting the neural parameters controlling dynamic accommodation.

This paper provides the background for the model and information about how to transform biomechanical properties of the A-IOL to the lumped model in order to perform simulations of accommodation step responses (see Appendix **I** & III). The model provides insights into the organization and plasticity of neural control of accommodation based on observed changes of first- and second-order dynamic properties of accommodation and disaccommodation during the progression of presbyopia. The model was constructed using Matlab® and its control system-engineering application module, Simulink®. Two versions of the model are available on our website,

http://schorlab.berkeley.edu. The first one is a user friendly web-based version to gain experience with the model simulations of A-IOL performance dynamics and the second one is a more advanced version created in Matlab Simulink®. The advanced version is available for download on our website, http://schorlab.berkeley.edu. To perform a simulation, the downloaded files have to be saved, uncompressed and run from the computer. Both Matlab® and Simulink® module are necessary to run the advanced version simulations.

3. Pulse-Step model: Background and description

A pulse-step model of accommodation has been developed by Schor & Bharadwaj (2005a; b) to describe the dynamic characteristics of the step response and how it changes with age. The pulse-step model predicts the dynamic properties of step responses for different age groups based on: 1) behavioral measures of first- and second-order dynamic properties of step responses (Bharadwaj & Schor, 2005a; b), 2) reported measures of visco-elastic properties of the lens and extra-lenticular structures of the plant (Wyatt, 1993; Glasser & Campbell, 1999; Heys et al., 2004; Weeber et al., 2005) and 3), reported single-unit recordings of neural control signals for the near response (reviewed by Gamlin, 2002). Detailed descriptions of the pulse-step models of accommodation and disaccommodation can be found in our earlier publications (Schor & Bharadwaj, 2005a; b).

3.1. Neural plasticity of the control of dynamic accommodation.

There are age-related increases in the visco-elastic properties of the lens matrix (Fisher, 1971; van Alphen & Graebel, 1991; Glasser & Campbell, 1999; Heys et al., 2004; Weeber et al., 2005) and in the elastic coefficients of the lens capsule and choroid (Fisher, 1969; van Alphen & Graebel, 1991; Wyatt, 1993; Krag et al., 1997). Despite these age-related biomechanical changes, the peak velocity of accommodation for modest step changes in optical vergence is unaffected by age (Heron et al., 2001; 2002; Mordi & Ciuffreda, 2004; Schor & Bharadwaj, 2005a), suggesting that neural control signals are calibrated in response to age-related changes of the accommodation plant. Inferences about neural control can be made from static and dynamic characteristics of the accommodation step response. During accommodation from a constant far position to various near positions, the peak velocity increases with response magnitude (Ciuffreda & Kruger, 1988; Kasthurirangan et al., 2003; Mordi & Ciuffreda, 2004; Bharadwaj & Schor, 2005a) but the peak acceleration remains invariant of response magnitude (Bharadwaj & Schor, 2005a). As the eye ages, both maximum response magnitude (the near-point of accommodation) (Duane, 1912; Hamasaki et al., 1956; Hofstetter, 1965) and the peak acceleration decline (Bharadwaj & Schor, 2005a; Schor & Bharadwaj, 2005a), however peak velocity is not reduced (Heron et al., 2001; 2002; Mordi & Ciuffreda, 2004; Bharadwaj & Schor, 2005a). These observations suggest independent control of position, velocity and acceleration characteristics of the step response and that the maintenance of peak velocity with age could be due to the continuous calibration of the neural control signal of accommodation (Schor & Bharadwaj, 2005a).

3.2. Pulse-step dynamic model of accommodation: the neural control parameters

Our behavioral measures of accommodative peak acceleration, peak velocity and their timing (Bharadwaj & Schor, 2005a; b) suggest that the viscosity of the crystalline lens is overcome by an acceleration-pulse signal and its stiffness is overcome with a velocity-step signal. The acceleration-pulse and velocity-step signals are integrated into a phasic-velocity signal that controls dynamics and a tonic-position signal that controls response amplitude respectively. These phasic and tonic signals have physiological analogs in near response neurons (Gamlin, 2002). The sum of phasic and tonic signals passes through the transfer function of the accommodative plant to produce the final accommodation response (Figure 50 a, b).

The initial change in accommodation is controlled by the open-loop phasic-velocity signal while the final position of accommodation is maintained under closed-loop conditions by the tonic-position signal. The main variables that control dynamic properties are the height, width and the integral of an acceleration-pulse signal (Figure 50 c, d). The height of the pulse determines the peak acceleration; the width of the pulse determines peak velocity when it is integrated to a phasic-velocity signal. Either increasing the height or the width of the pulse can increase the integral of the acceleration-pulse signal (Figure 50 c, d). Pulse width is adjusted independently of pulse height to have independent control of velocity and acceleration respectively. The invariance of peak velocity with age suggests that the pulse width and its integrated phasic-velocity signal are increased to compensate for age-related increases of lens viscosity. Table XV summarizes the acceleration-pulse signal parameters and the transfer

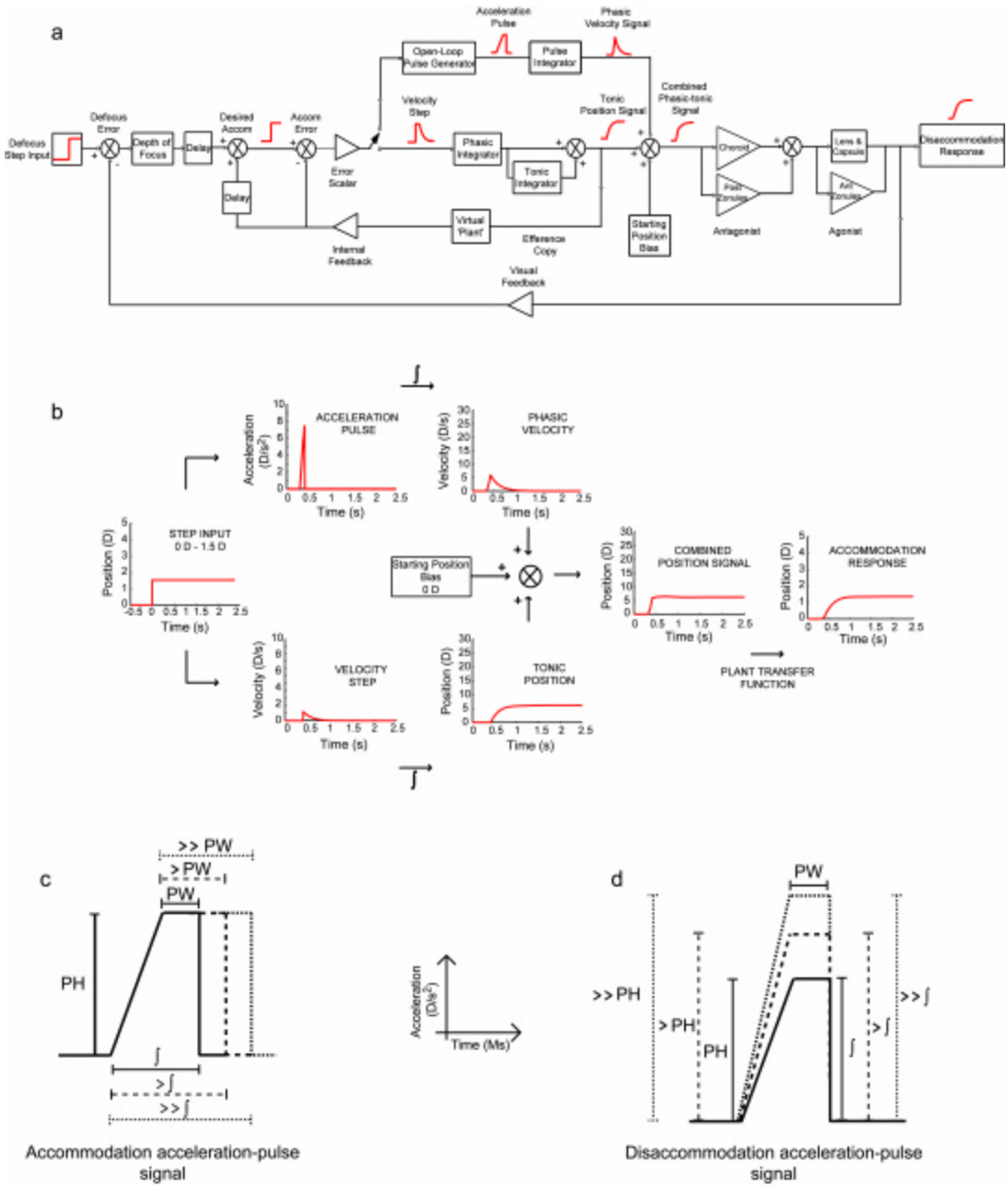

Figure 50. a) Block diagram and b) signal processing flow charts of the pulse-step model of accommodation illustrating the generation of acceleration-pulse and velocity-step signals, their neural integration to phasic-velocity and tonic-position signals respectively, and the final transformation of the signals by the plant into an accommodation step response. Insets in figure a show signal profiles at each stage of the models. c) Schematic representation of acceleration-pulse parameters in accommodation and how the pulse width (PW) is increased to increase the integral of the pulse. The pulse height (PH) remains constant in accommodation. d) Schematic representation acceleration-pulse parameters in disaccommodation and how the pulse height (PH) is increased to increase the integral of the pulse. The pulse width (PW) remains constant in disaccommodation.

Age (yrs)	Pulse height (D/s^2)	Plateau duration (ms)	? t (ms/D)	Phasic integrator	Fast-tonic integrator	Slow-tonic integrator
15	7.5	10	14	2.7 / [0.2S + 1]	28.0 / [2S + 1]	50.0 / [100S + 1]
25	7.5	30	25	2.7 / [0.2S + 1]	28.05 / [2S + 1]	50.0 / [100S + 1]
35	7.5	50	30	2.7 / [0.2S + 1]	28.0 / [2S + 1]	50.0 / [100S + 1]
45	7.5	75	30	2.7 / [0.2S + 1]	28.0 / [2S + 1]	50.0 / [100S + 1]

Table XV. The neural control parameters used in the pulse-step dynamic model of accommodation for the four age-groups. The transfer functions shown in this table are represented in the Laplace notation format K / ?S + 1 where, K = gain of the transfer function and ? = time constant of the transfer function.

functions for the phasic and tonic integrators that produce optimal accommodation responses for the four different age groups ranging from 15 to 45 years.

3.3. Pulse-step dynamic model of accommodation: biomechanical parameters of the plant

Measures of age-related elastic coefficients of the lens matrix and capsule (Figure 51a) were incorporated into our lumped model by transforming them to spring constants (Table XVI; Figure 51b). Appendix II shows the calculations involved in converting the published values of moduli of elasticity of the lens capsule and matrix (Figure 51a) into spring constant measures (Table XVI; Figure 51b) that are used in our lumped model. Figure 51b and Table XVI illustrate that spring constant of the capsule (Krag et al., 1997), changes little with age while the spring constant of the lens matrix progressively increases with age (Weeber et al., 2005). At 25-yrs of age, the spring constant of the lens

capsule and the matrix differ approximately by a factor of 10 while at 65-yrs of age, they differ approximately by a factor of 20 (Figure 51b; Table XVI). Mechanically, the lens capsule and lens matrix can be modeled as two springs in parallel (van Alphen & Graebel, 1991). The effective stiffness of the combined lens matrix and capsule is thus the sum of spring constants for the lens and capsule. Figure 51b and Table XVI illustrate that most of the increased stiffness of the lens complex with age results from age-related changes in the lens matrix, and not the capsule. Figure 51c shows that the sum of these elastic coefficients closely approximates the combined spring constants of the lens capsule and matrix and the zonules as determined by Wyatt (1988; 1993). In the Laplacian domain, two springs in parallel could be modeled as two springs in series (see 'lens capsule gain' and 'lens matrix time constant' blocks in Figure 50a). In our model, the spring constants of the lens capsule and matrix were lumped together as a single gain element by summing their respective elastic coefficients. Normalized lens gains were computed from age-dependent estimates of spring constants from the data of Weeber et al (2005) (Figure 51d). The gain of the lens module for a 15-yr old was normalized to unity and the lens gains of other age groups were made proportional to the normalized lens gain of the 15-yr old (Figure 51d). For example, for a 15-yr and a 35-yr old, the spring constants of the lens were estimated at 313 dynes/mm and 1345 dynes/mm respectively (Weeber et al., 2005). Given the normalized gain of the 15-yr old lens (1.0), the proportional gain of the 35-yr old lens was 0.23. The normalized lens gains obtained from Weeber et al (2005) and Wyatt (1993) closely matches each other (Figure 51d).

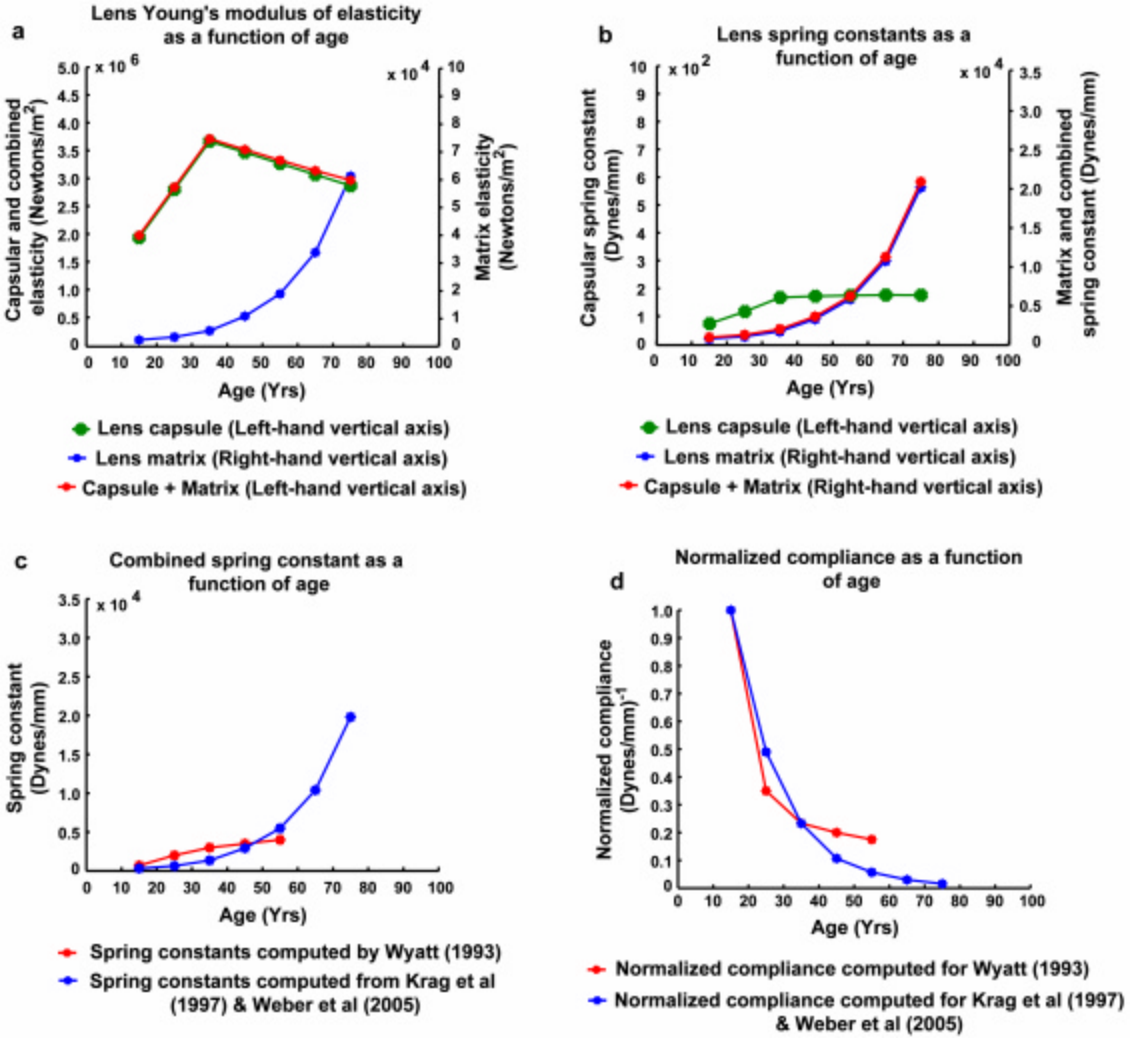

Figure 51. a) Young's moduli of elasticity for the lens capsule (green curve), lens matrix (blue curve) and combined capsule and matrix (red curve) plotted as a function of age. Young's modulus of the lens capsule was obtained from Krag et al (1997). The Young's modulus of lens matrix was calculated from shear compliance data of Weeber et al (2005) using Eq. 9 -11 in Appendix I. The combined Young's modulus of the lens capsule and matrix were computed using Eq. 6 -8 in Appendix I. b) Spring constants (stiffness) of the lens capsule (green trace), lens matrix (blue curve) and combined capsule and matrix (red curve) plotted as a function of age. The Young's moduli of elasticity were converted into spring constants using the Eq. 1 – 8 in Appendix I. c) Combined spring constants (stiffness) of the lens capsule and matrix plotted as a function of age. The red curve shows data computed by Wyatt (1993) and the blur curve shows data computed using Appendix I of this paper. d) Normalized compliance (1 / stiffness) of the combined lens capsule and matrix plotted as a function of age. The red curve shows data computed by Wyatt (1993) and the blur curve shows data computed using Appendix I of this paper. The method employed to obtain normalized compliance values is described in the text.

In the Laplacian domain, the lens matrix was modeled as a first-order visco-elastic lag element as shown in 'lens matrix time constant' block in Figure 50a. The damping coefficient of the lens matrix and the equivalent time constant of the lens complex were computed from the dynamic mechanical analyses of Weeber et al (2005). Appendix III shows the calculations involved in computing the time constants and damping coefficients from the analysis of Weeber et al (2005). Figure 52a and Table XVI shows that the time constant of the lens matrix computed using Weeber et al's technique decreases with age. However, due to an exaggerated increase in the spring constant of the lens matrix, the resultant damping coefficient also increases with age, but at a lower rate than the spring constant (Figure 52b). These estimates of lens complex time constant were used in the model simulations. Table XVII summarizes the proportional gains and time constants used for the transfer function of the lens complex for the four different age groups.

The gains of other elements in the accommodative plant were also made proportional to the normalized lens gain of the 15-yr old. For example, for a 15-yr old, the elastic coefficient for the lens was estimated at 313 dynes/mm and the choroid at 1500 dynes/mm (Weeber et al, 2005; Wyatt, 1993) (Table XVI). Given the normalized gain of the lens (1.0), the proportional gain of the choroid of the 15-yr old was 0.21 (Table XVII). The spring constant of the choroid increased with age. The spring constant of the anterior and posterior zonules was fixed across all age groups at 1700 dynes/mm (proportional gain of 0.19) (Beers & van der Heijde, 1996) (Table XVII).

Age (yrs)	K_C (d/mm)	K_M (d/mm)	K_{Com} (d/mm)	T_M (s)	D_{Coeff} (d.s/mm)	T_{Com} (s)	K_{Ch} (d/mm)	K_Z (d/mm)
15	73	240	313	0.386	92.6	0.296	1500	1700
25	117	522	639	0.316	165	0.258	2800	1700
35	176	1178	1354	0.260	306	0.226	3800	1700
45	172	2756	2928	0.215	592.5	0.202	4100	1700
Sim A-IOL I	172	522	694	0.291	165	0.238	4100	1700
Sim A-IOL II	172	522	694	0.910	592.5	0.854	4100	1700
Sim A-IOL III	172	232	404	0.057	23.2	0.057	4100	1700

Table XVI. The biomechanical parameters of the various structures in the accommodative plant for the four age-groups and for the three A-IOL's used in our simulations. K_C and K_M represent the stiffness of the lens capsule and lens matrix respectively. The stiffness estimates of the capsule and matrix were obtained by converting their respective Young's moduli of elasticities into stiffness metrics using the equations described in Appendix II. K_{Com} represents the stiffness of the lens complex (lens capsule plus lens matrix) obtained by the sum of age-matched K_C and K_M (Eq. 6 – 8 in Appendix II). T_M represents the time constant of the lens matrix obtained by converting the second cole-cole relaxation process into time constants (Eq. 1 in Appendix III). D_{Coeff} represents the damping coefficient of the lens matrix obtained from the product of age-matched T_M and K_M (Eq. 3 in Appendix III). T_{Com} represents the time constant of the lens complex (lens capsule plus lens matrix) obtained by dividing D_{Coeff} by K_{Com} (Eq. 2 in Appendix III). K_{Ch} and K_Z represent the stiffness of the choroid and the zonules respectively. For A-IOL III, K_M was obtained by converting Young's modulus of elasticity into stiffness using Appendix II and D_{Coeff} was obtained by converting viscosity into damping coefficients using Eq. 5 in Appendix III.

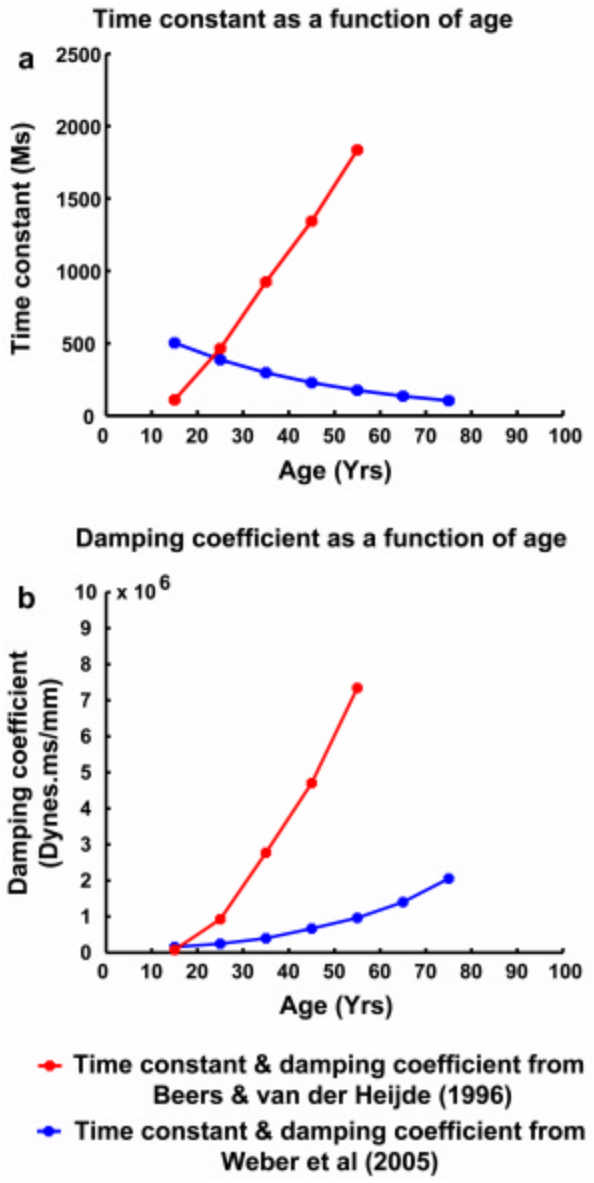

Figure 52. a) Time constant and b) damping coefficient of the lens complex (capsule plus matrix) plotted as a function of age. The red curve shows data computed by Beers & van der Heijde (1996) and the blue curve shows data computed using the method described in Appendix III.

3.4. Model simulations

Our dynamic model of accommodation was used to illustrate how the duration and amplitude of an acceleration-pulse signal could be altered to compensate for increased visco-elastic properties of the lens and maintain youthful velocity in the incipient stages of presbyopia (Schor & Bharadwaj, 2005a). Detailed model simulations and comparison with empirical data can be found in our earlier publications (Schor & Bharadwaj, 2005a; b). Figure 53 a-c shows the position, velocity and acceleration traces of accommodation

Age (yrs)	Model lens gain	Model lens stiffness	Model lens transfer function	Model choroid gain	Model zonule gain
15	1.00	1.00	1.00 / [0.296S + 1]	0.21	0.184
25	0.49	2.04	0.49 / [0.258S + 1]	0.11	0.184
35	0.24	4.30	0.23 / [0.226S + 1]	0.08	0.184
45	0.11	9.35	0.11 / [0.202S + 1]	0.067	0.184
Sim A-IOL I	0.45	2.22	0.45 / [0.238S + 1]	0.067	0.184
Sim A-IOL II	0.45	2.22	0.45 / [0.254S + 1]	0.067	0.184
Sim A-IOL III	0.78	1.29	0.78 / [0.057S + 1]	0.067	0.184

Table XVII. Pulse-step model parameters of the accommodative plant for the four age-groups and for the three A-IOL's used in our simulations. Model lens gain represents normalized compliance (compliance = 1 / stiffness) values obtained using the method described in the text (Figure 2c). Model lens stiffness is the reciprocal of the model lens gain. Model lens transfer function represents the gain and the time constant of the lens complex (capsule and matrix) in Laplace notation. The transfer functions is of the form K / ?S + 1 where, K = gain of the transfer function and ? = time constant of the transfer function. Model choroid gain and model zonule gain represent the gains of the choroid and zonule respectively after they are normalized to the gain of the 15-yr old lens complex. The method of normalization is described in detail in the text.

for a 25- and a 45-yr old lens (red and blue traces respectively). The stiffness and damping coefficient of the lens used for these simulations were obtained using the

methods described later. The neural control parameters were optimized to produce step responses whose static and dynamic characteristics matched closely with empirical responses (Bharadwaj & Schor, 2005a). These simulations are presented here only for the purpose of comparison with the A-IOL simulations. Detailed model simulations and comparison with empirical data can be found in our earlier publications (Schor & Bharadwaj, 2005a; b). In this paper, the pulse parameters for each age group are unchanged, and we adjust the amplitude of phasic and tonic signals of a 45 year-old eye to illustrate its neural adaptation (i.e. calibration) to an A-IOL whose biomechanical properties match those of a younger eye.

3.5. A-IOL applications

The pulse-step model of dynamic accommodation can be used to predict the stability and dynamic performance of A-IOL's when the elastic coefficient as well as either the time constant or viscosity (damping coefficient) of the lens implant is known. This model only applies to A-IOL devices whose optical power can be regulated by a negative feedback control system driven by the ciliary muscle. In order to simulate the performance of an A-IOL, the elastic properties of the natural lens capsule are retained, and the visco-elastic properties of the lens matrix are replaced with those of the A-IOL. The gain (compliance = 1 / spring constant) and time constant (damping coefficient /spring constant) of the model of a 45-year-old lens are substituted with the gain and time constant of the A-IOL using Equations 1 & 2 below. Since a number of parameters of the accommodative plant change with age (Table XVI), the simulations should be applied to the model corresponding to the age of the recipient to predict the performance the A-IOL.

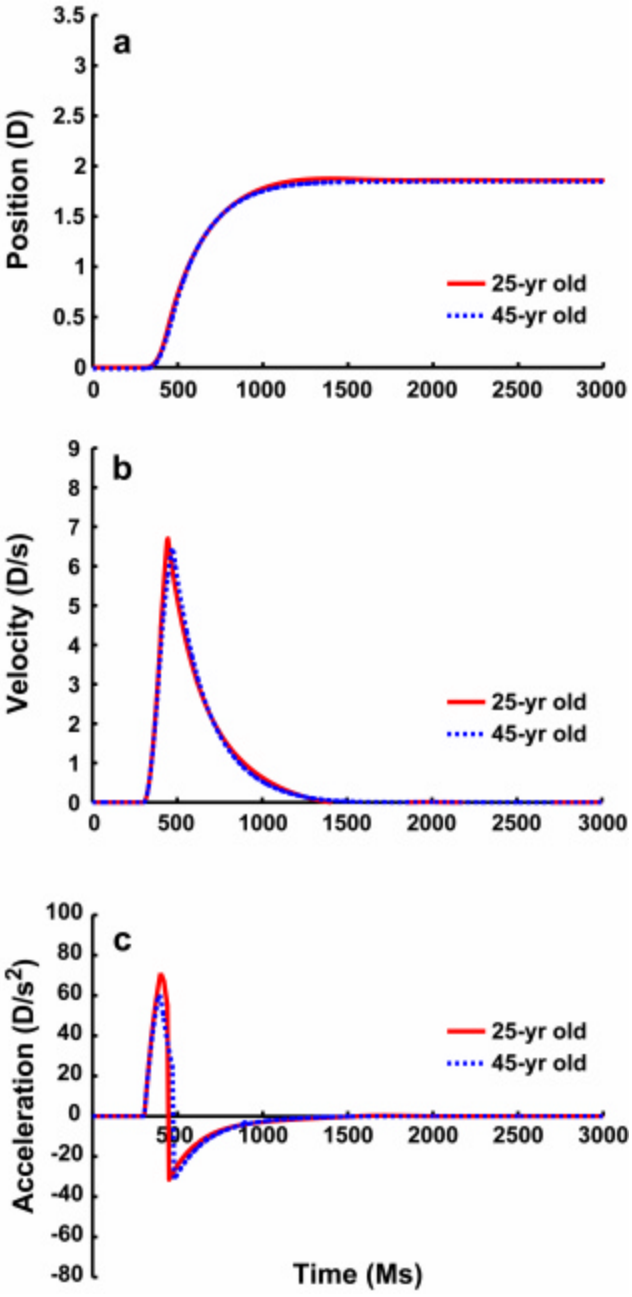

Figure 53. Simulated position (a), velocity (b) and acceleration (c) traces of accommodation plotted as a function of time for a 2 D step stimulus in a 25-yr old (red traces) and a 45-yr old (blue traces) eye. The biomechanical parameters used in this simulation were obtained from the methods described in Appendices I & II. The neural control parameters used in this simulation were optimized to closely match the empirical data described by Bharadwaj & Schor (2005a). Detailed model simulations and comparison with empirical data can also be found in Schor & Bharadwaj (2005a; b).

$$\text{Gain} = 1/ (K_C + K_{A\text{-}IOL}) \quad (1)$$

$$T_L = D_{A\text{-}IOL} / K_{A\text{-}IOL} \quad (2)$$

where, Gain= compliance of the lens-matrix complex; K_C = spring constant of the capsule (dynes/mm); $K_{A\text{-}IOL}$ = spring constant of the A-IOL (dynes/mm); T_L = time constant (sec); $D_{A\text{-}IOL}$ = damping coefficient of the A-IOL (dynes.sec/mm).

As noted above, the elasticity of the lens complex equals the sum of the spring constants of the lens capsule and matrix. Appendix II presents equations to convert measures of elastic coefficient to spring constants for our lumped model. The spring constants of a silicone-polymer gel or of the springs in a translating A-IOL contribute to the mechanical compliance of the combined lens and capsule. Figure 51b illustrates that when the stiffness of the lens matrix of a 45-yr old eye is reduced by 50%, by substituting the natural lens with a more compliant prosthetic lens, the combined lens capsule plus matrix stiffness is approximately reduced to that of a 35-yr-old lens. This lens would now have an accommodative amplitude of 6D (Hofstetter, 1965), assuming that the effective refractive index of the prosthetic lens is similar to that of the 35-yr old natural lens. A smaller reduction of the spring constant of the prosthetic lens would produce smaller amplitude of accommodation. At least 5D of accommodation is needed for functional near vision at a standard working distance of 40 cm (Ho et al., 2001).

4. Pulse-Step model: Simulations

We performed three different simulations that describe the performance of A-IOL's after they are injected into the capsular bag. The simulations also described how adaptation of the phasic-velocity and tonic-position signals of the model can restore normal response dynamics. The first simulation describes the results of reducing both the

stiffness and damping coefficient of a 45-yr old lens matrix to that of a 25-yr old lens matrix while retaining the capsule stiffness of a 45 yr-old eye (Simulated A-IOL I). The second simulation describes the results of reducing only the stiffness of the 45-yr old lens matrix to that of a 25-yr old lens matrix while retaining the matrix damping coefficient and the capsule spring constant of the 45-year-old eye (Simulated A-IOL II). The third simulation describes how replacing the lens matrix with a cured injectable polymer gel (Koopmans et al., 2003; 2004; Koopmans, 2005) while leaving the lens capsule intact influences the dynamics of accommodation (Simulated A-IOL III).

2 D step response of accommodation for a 45-yr old eye was used as a representative candidate in all simulations. Performance of the simulated responses was evaluated in terms of their response magnitude, peak velocity, peak acceleration and stability (presence or absence of overshoots and oscillations). These performance indices were qualitatively compared with that of the age-matched (45-yr old) optimized response shown in figure 53a – c. Input parameters for all simulations include lens capsule and matrix stiffness, lens time constant or damping coefficient as computed from the time constant and the proportional scalars for the phasic and tonic signals. The stiffness and time constant of the lens were represented in the Laplacian domain as the gain and time constant of the transfer function. The numerical calculations involved in computing the lens transfer function for a simulated A-IOL is described below. Simulated A-IOL I has been used as an example. The lens transfer function for all model simulations are shown in Table XVII. The phasic and tonic scalars used in the model simulations are shown in Table XVIII.

Lens capsule stiffness of 45-yr old (K_C) = 172 dynes/mm

Lens matrix stiffness of 25-yr old (K_M) = 522 dynes/mm

Combined lens stiffness (K_{Com}) = $K_C + K_M$

K_{Com} = 172 + 522 = 694 dynes/mm (Column 4 in Table II) (3)

Lens transfer function gain (Compliance) = $1/K_{Com}$

Normalized lens gain transfer function = K_{Com} of 15-yr old / K_{Com} of 45-yr old)

Normalized Gain ($1/K_{Com}$) = 313 / 694 = 0.45 (Column 2 in Table III) (4)

Lens matrix time constant of 25-yr old (T_M) = 0.316 sec

Lens matrix damping coefficient (D_{Coeff}) = $T_M * K_M$

D_{Coeff} = 0.316 * 522 = 164.95 dynes.sec/mm (Column 6 in Table II) (5)

Lens matrix + capsule time constant (T_{Com}) = D_{Coeff} / K_{Com}

Using Eq. 3 & 5; **T_{Com} = 164.95 / 694 = 0.238 sec** (Column 7 in Table II) (6)

In the Laplacian domain, the lens transfer function is **0.45 / [0.238S + 1]** (Column 4 in Table III).

4.1. Simulated A-IOL I

In this simulation, both the stiffness and damping coefficient of a 45-yr old lens matrix was replaced with that of a 25-yr old lens matrix while retaining the capsule stiffness of a 45 yr-old eye. Figure 54a – c illustrates the dynamic performance of this A-IOL by plotting the position, velocity and acceleration traces as a function of time. The red and blue traces show simulations before and after adaptation of the phasic and tonic signals respectively. Reducing the stiffness and damping coefficient to that of 25-yr old lens matrix resulted in a highly under-damped control system. The un-adapted response

traces showed large instabilities and oscillations (Figure 54a). For the time period of the simulation (4 sec), the response did not attain a steady-state position (Figure 54d). The peak velocity (21.23 D/s) and peak acceleration (185.73 D/s^2) of the un-adapted response were abnormally high (Figure 54b, c) when compared to the age-matched optimized response shown in figure 4b & c (blue trace). The peak velocity and peak acceleration of the age-matched response was 6.47 D/s and 58.22 D/s^2 respectively.

Age		Phasic-velocity scalar	Tonic-position scalar
15		1.00	1.00
25		2.00	3.00
35		4.00	7.30
45		7.50	18.00
Simulated A-IOL I	Before adaptation	7.50	18.00
	After adaptation	2.10	4.25
Simulated A-IOL II	Before adaptation	7.50	18.00
	After adaptation	6.00	4.25
Simulated A-IOL III	Before adaptation	7.50	18.00
	After adaptation	0.45	2.50

Table XVIII. The phasic-velocity and tonic-position scalars used in the pulse-step model simulations for the four age-groups and for the three A-IOL's. For the A-IOL's, the values of the phasic-velocity and tonic-position scalars are given prior to and following optimization of the response dynamics. Mathematically, the changes in the scalar values that are necessary to optimize the response dynamics represent 'adaptation' of the accommodative neural control system.

The dynamic performance of this A-IOL could be optimized and restored to within-physiological limits by reducing both the phasic-velocity and tonic-position signals by 72 % and 76% respectively (Table XVIII). Following 'adaptation', the position traces showed no instabilities or oscillations before reaching the steady-state position (Figure 54a). The response showed a characteristic 'lag' of accommodation of approximately 0.14 D. This compared well with the accommodative 'lag' shown by the age-matched optimized response (0.15 D). The peak velocity (6.72 D/s) and peak acceleration (60.75 D/s^2) of the adapted response also compared well with the age-matched optimized response shown in figure 53b & c (blue trace).

4.2. Simulated A-IOL II

In this simulation, only the stiffness of a 45-yr old lens matrix was replaced with that of a 25-yr old lens matrix while retaining the matrix damping coefficient and capsule spring constant of the 45-year-old eye. Figure 54d – f illustrates the dynamic performance of this lens by plotting the position, velocity and acceleration traces as a function of time. The red and blue traces show simulations before and after adaptation of the phasic and tonic signals respectively. Reducing the stiffness of the lens to that of a 25-yr old, resulted in an under-damped control system. The 'un-adapted' position traces showed instabilities and oscillations before attaining a steady-state position (Figure 54d). The steady-state position showed a smaller 'lag' of accommodation (0.06 D) when compared to that of the age-matched optimized response (0.14 D) (Figure 54d). The peak velocity (7.97 D/s) and peak acceleration (73.95 D/s^2) of the 'un-adapted' response were higher than those of the age-matched optimized responses (peak velocity: 6.47 D/s; peak

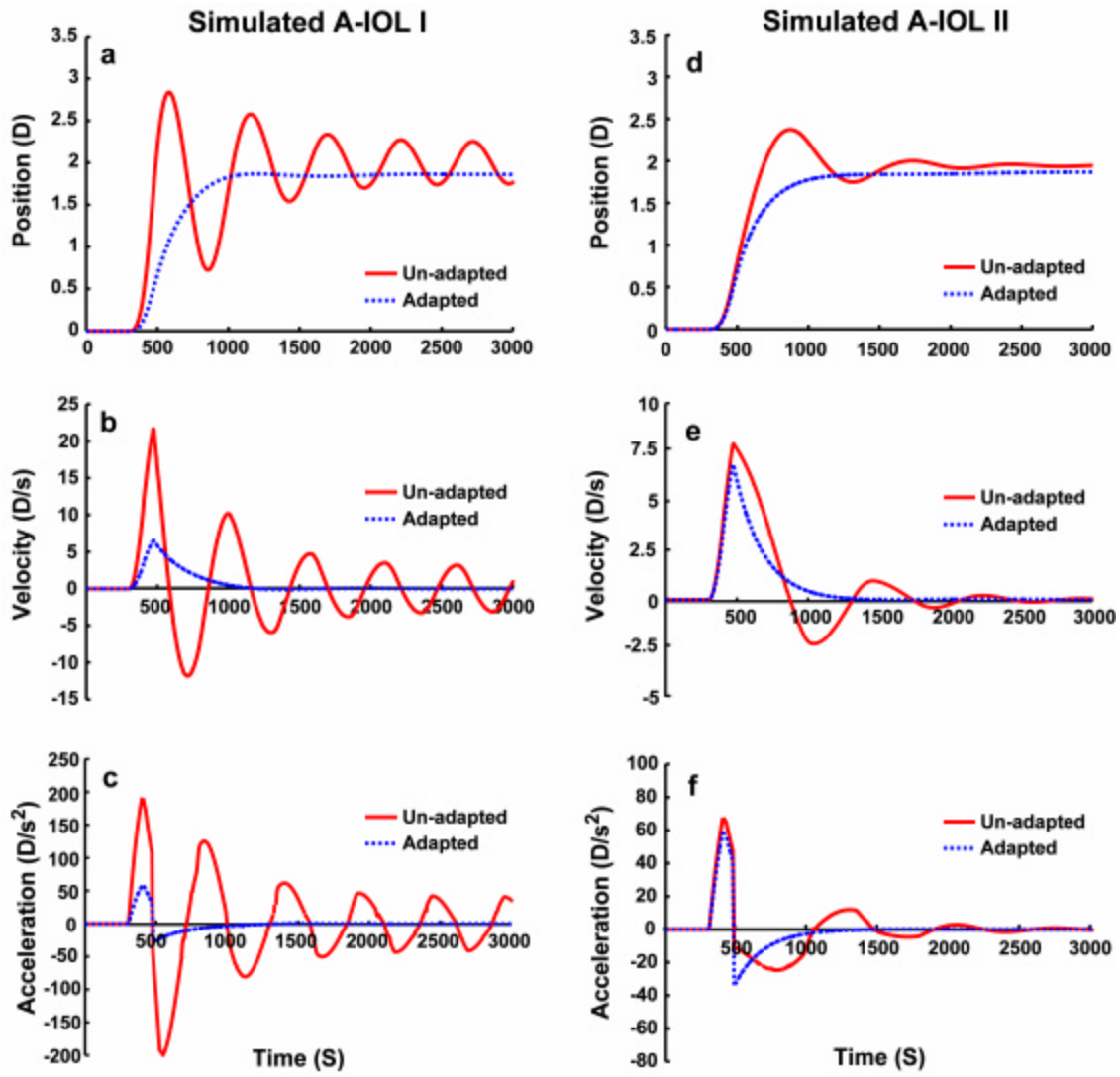

Figure 54. Simulations of position (a & d), velocity (b & e) and acceleration (c & f) plotted as a function of time for a 2 D step stimulus in a 45-yr old eye. The left-hand panel shows simulations for A-IOL I and the right-hand panel shows simulations for A-IOL II. The red traces show simulations prior to optimization of the neural control parameters (un-adapted) and the blue traces show simulations following optimization of the neural control parameters (adapted). In the A-IOL I simulation, both the stiffness and the damping coefficient of the 45-yr old lens matrix was replaced with that of a 25-yr old lens matrix. In the A-IOL II simulation, only the stiffness of the 45-yr old lens matrix was replaced with that of a 25-yr old lens matrix while the damping coefficient was left unaltered. The under-damped control system that results from implanting either of the A-IOL's could be optimized to restore 'normal' response dynamics by reducing the gains of the phasic-velocity and tonic-position signals.

acceleration: 58.22 D/s^2). Overall, the dynamic performance of the 'un-adapted' A-IOL II was qualitatively similar to that of the 'un-adapted' A-IOL I (Compare Figure 54a – c with Figure 54d – f). However, as shown clearly in Figure 54, the effect of reducing only the stiffness of the lens matrix on the dynamics of accommodation was far less exaggerated than the effect of reducing both the stiffness and the damping coefficient of the lens matrix.

The dynamic performance of A-IOL II could be optimized and restored to within-physiological limits by reducing both the phasic-velocity and tonic-position signals by 20% and 76% respectively (Table XVIII). Following 'adaptation', the position traces showed no instabilities or oscillations before reaching the steady-state position (Figure 54d). The accommodative 'lag' (0.14 D) was similar to that seen in the age-matched optimized response (0.15 D). The peak velocity (6.91 D/s) and peak acceleration (56.85 D/s^2) of the adapted response also compared well with the age-matched optimized response shown in figure 53b & c (blue trace).

4.3. Simulated A-IOL III

A-IOL III represents a 'cured' silicone polymer material that has been employed previously as a deformable A-IOL under in-vitro conditions (Koopmans et al., 2003, 2004). The Young's modulus of elasticity of the A-IOL was 800 N/m^2 (Koopmans et al., 2003; 2004) while the viscosity of the silicone polymer after complete polymerization was 80 N.s/m^2 (Koopmans, 2005). Using the equations in Appendix II, the stiffness of the lens matrix was calculated to be 232 dynes/mm (Column 3 in Table XVI) and that of

entire lens complex (capsule and matrix) was calculated to be 404 dynes/mm (Column 4 in Table XVI). Similarly, using the equations in Appendix II, the time constant and damping coefficient of the lens were calculated to be 0.10 sec and 23.2 dynes.sec/mm respectively (Columns 5 & 6 in Table XVI). The overall stiffness of the silicone-polymer filled lens (404 dynes/mm) was smaller than that of a 45-yr old lens (2928 dynes/mm) by approximately a factor of 7.25 (Table XVI). However, the damping coefficient of the silicone polymer filled lens (23.2 dynes.sec/mm) was smaller than that of a 45-yr old lens (592.5 dynes.sec/mm) by approximately a factor of 25.5 (Table XVI).

The reduced stiffness and damping coefficient of the silicone-polymer lens created a highly under-damped control system. As shown in figure 55a-c, the un-adapted accommodation responses showed huge overshoots and oscillations before attaining a steady-state position. The accommodative 'lag' was only slightly larger (0.17 D) than the age-matched optimized lens (0.15 D) (Figure 55a). However, the peak velocity (94.6 D/s) and peak acceleration (>800 D/s^2) of the 'un-adapted' responses were extremely high when compared to the age-matched optimized response (Figure 55b, c). The dynamic performance of A-IOL III could be optimized and restored to within-physiological limits by reducing both the phasic-velocity and tonic-position signals by 94% and 86% respectively (Table XVIII). Following 'adaptation', the position traces showed no instabilities or oscillations before reaching the steady-state position (Figure 55d). The accommodative 'lag' (0.14 D) was similar to that seen in the age-matched optimized response (0.15 D). The peak velocity (6.87 D/s) and peak acceleration (63.25 D/s^2) of the

adapted response also compared well the age-matched optimized response shown in figure 53b & c (blue trace).

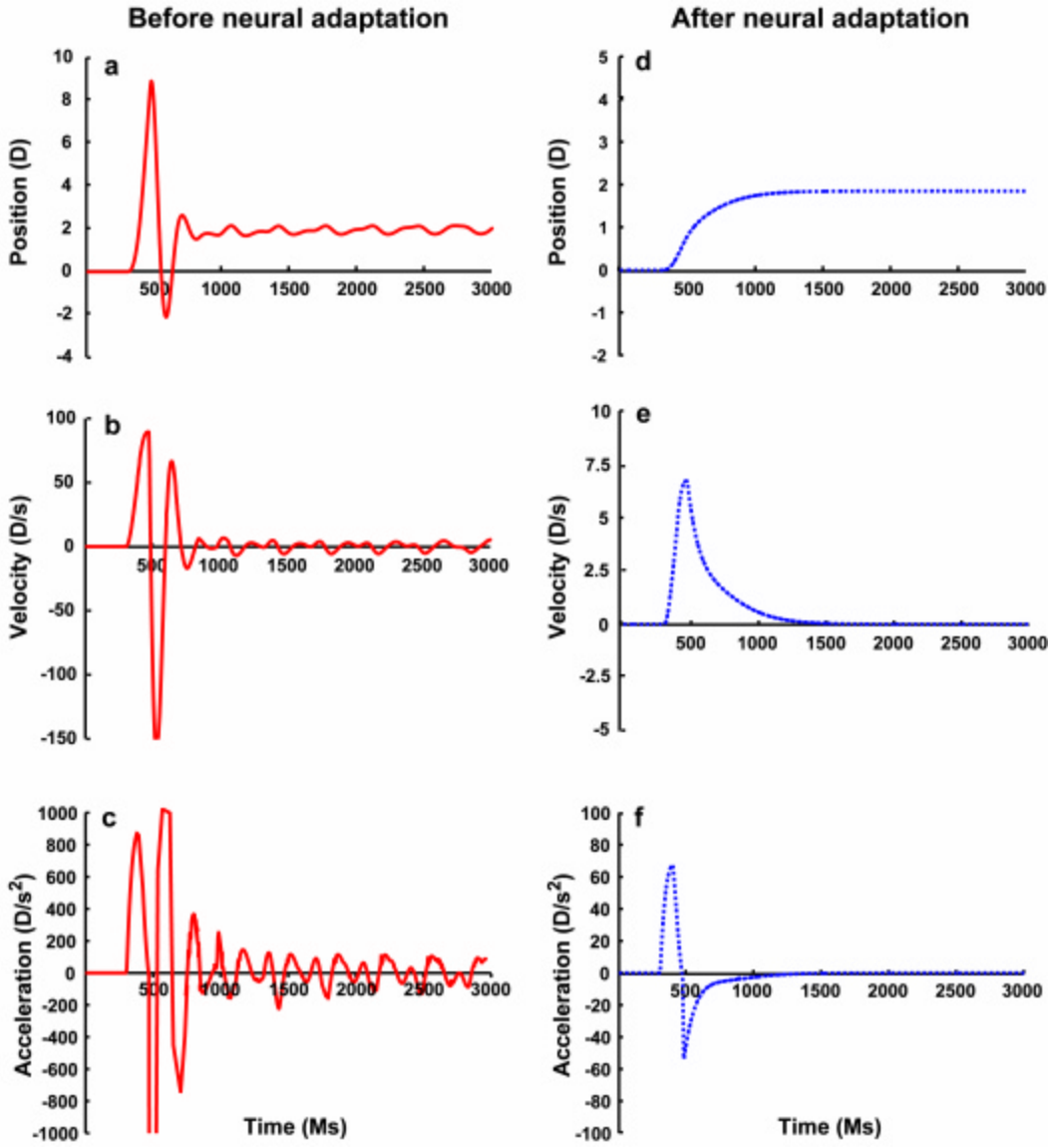

Figure 55. Simulations of position (a & d), velocity (b & e) and acceleration (c & f) plotted as a function of time for a 2 D step stimulus in a 45-yr old eye. The left-hand panel (red traces) shows simulations for A-IOL III prior to optimization of the neural control parameters and the right-hand panel (blue traces) shows simulations for the same A-IOL following optimization of the neural control parameters (adapted). A-IOL III represents a silicone polymer material that has been used previously as a deformable A-IOL under *in-vitro* conditions (Koopmans et al., 2003; 2004). The under-damped control system that results from implanting the A-IOL III could be optimized to restore 'normal' response dynamics by reducing the gains of the phasic-velocity and tonic-position signals.

5. Discussion

5.1. Motivation for the study: rationale for assessing the performance of A-IOL's under closed-loop conditions

The main aim of this paper was to apply the pulse-step dynamic model of accommodation to predict the static and dynamic performance of A-IOL's when they are implanted in a closed-loop control system of a presbyopic eye. The dynamics of accommodation cannot be fully predicted from biomechanical parameters of the lenticular and extra-lenticular components of the accommodative plant. Our experimental work (Bharadwaj & Schor, 2005a; b) and models (Schor & Bharadwaj, 2005 a; b) have demonstrated that the neural control system largely determines the first and second order dynamics of the accommodative step response. The neural system is calibrated to achieve optimal dynamic performance from the lens as it ages during the progression of presbyopia. Under 'natural' viewing conditions, human accommodation behaves as a closed-loop control system (Fincham, 1937; Toates, 1972; Krishnan & Stark, 1975; Schor, 1992; Schor & Bharadwaj, 2005a; b), wherein the optimal performance of accommodation is critically dependent on the match between the characteristics of neural controller of accommodation and biomechanics of accommodative plant. A mismatch between the two could lead to either unstable and oscillatory responses (an 'under-damped' response) or sluggish responses (an 'over-damped' response) (Nise, 2000). However, most of the experiments on A-IOL's have used open-loop techniques to study the performance of A-IOL's (e.g. pharmacological stimulation using pilocarpine and cycloplegic drugs: Agarwal et al., 1967a; Haefliger & Parel, 1994; Sakka et al., 1994; Nishi & Nishi, 1998; Nishi et al., 1998; Langenbucher et al., 2003; Kuchle et al., 2004;

and mechanically stretching under *in vitro* conditions: Koopmans et al., 2003; 2004). While these open-loop techniques do provide good quantitative estimates of the amplitude of accommodation that is restored after implantation of A-IOL's, the techniques do not predict the dynamic performance of A-IOL's when implanted in a living eye. A similar argument would apply to measuring accommodation responses in animals using electrical stimulation of the Edinger-Westphal (EW) nucleus (Crawford et al., 1989; Croft et al., 1998; Vilupuru & Glasser, 2002). Accommodation responses driven by electrical step signals do not tailor neural signals to independently control the first and second order dynamic components of accommodation, nor do they modulate neural activity in response to negative feedback. They are effectively 'open-loop' in nature. A feasible first step towards addressing this issue would be to model the dynamic behavior of A-IOL responses under closed-loop conditions. A good comparison of the pulse-step model simulations (Figure 4) with empirical data (Schor & Bharadwaj, 2005a; b) suggests that the pulse-step model could also be used as a tool to assess the performance of any A-IOL material when implanted in a closed-loop control system. It is not the intent of the simulations presented in this paper to arrive at any conclusions about a specific A-IOL material. Instead, these simulations are intended to illustrate the importance of assessing the performance of A-IOL's under closed-loop conditions. The model simulations can be used to suggest the biomechanical properties of the A-IOL material that produce the least instability without any neural recalibration. The simulations also provide a proof of concept, that dynamic performance of accommodation could be optimized by recalibration of phasic and tonic neural signals.

5.2. Mismatches in the accommodative control system

Studies of dynamic accommodation with aging indicate that the neural control system is capable of adapting the phasic and tonic control of accommodation to compensate for age-related visco-elastic properties of the lens (Heron et al., 2001; 2002; Bharadwaj & Schor, 2005a; b). Age-dependent neural adaptation was modeled by increasing the amplitude of the phasic-velocity and tonic-position control signals. Adapting the phasic gain compensates for viscosity (phasic gain increases with viscosity), and adapting the tonic gain compensates for stiffness (tonic gain increases with stiffness). A-IOL's attempt to restore the accommodative ability in presbyopes by replacing the matrix of the natural lens with a prosthetic material whose biomechanical properties mimic a 'younger' (20 – 25-yr old) lens (Haefliger et al., 1987; Koopmans et al., 2003). Since the 'adapted' neural signals of the 'older' eye would be too large to control the biomechanical properties of the 'younger' A-IOL, it is predictable that the accommodation responses would show characteristics of an under-damped control system. Our simulations (Figure 5 & 6) confirm this prediction by showing that replacing the stiffness and/or damping coefficient of a 45-yr old lens matrix with that of a 25-yr old lens leads to under-damped responses. Under-damping in the control system was evident in all three simulations from the oscillations and instabilities of the accommodative response (Figure 5a & d, 6a) and from the abnormally high peak velocities and peak accelerations (Figure 5c – f, 6b & c). The magnitude of under-damped instabilities were larger when both the stiffness and the damping coefficient (A-IOL I and A-IOL III) were reduced (compare figures 4a & 5a, 6a). The instabilities were smaller when only the stiffness of the lens matrix was reduced (A-IOL II) (compare figures 4a & 5d). This

suggests that the damping coefficient [and thus the viscosity (Appendix II)] of lens matrix plays a more dominant role than its stiffness in optimizing the response dynamics. Indeed, comparison of the silicone polymer material used in our third simulation (A-IOL III) with that of an age-matched (45-yr old) lens revealed that the overall (lens capsule and matrix) stiffness of the A-IOL (404 dynes/mm) was smaller than the 45-yr old lens (2928 dynes/mm) by approximately a factor of 7.25 (Table II) while the damping coefficient of the A-IOL (23.2 dynes.sec/mm) was smaller than the 45-yr old lens (592.5 dynes.sec/mm) by approximately a factor of 25.5 (Table II). Lowering the stiffness of the silicone polymer helps restore the amplitude of accommodation while lowering the viscosity tends to increase in the instabilities and oscillations in the response. Overall, these simulations illustrate that most optimal behavior of accommodation should be expected from a silicone polymer whose stiffness is reduced to restore accommodative amplitude but whose viscosity is retained to minimize under-damped instabilities.

5.3. Adaptation of the accommodative control system

Our simulations also indicate that the under-damped oscillations and instabilities in the control system could be minimized by changing the gains of the phasic-velocity and tonic-position signals. For example, in the first simulation (A-IOL I), the phasic-velocity and tonic-position signals were reduced by 72% and 76% respectively in order to restore the response dynamics within physiological limits (Figure 5a-c). Thus, it is possible for an A-IOL that has the biomechanical properties of a young lens to function effectively in an older eye if the accommodative neural controller can adapt to match the dynamics of the younger lens. As noted earlier, the accommodative system can adapt its neural control

and compensate to some degree for age-related increases in visco-elastic properties of the lens to achieve youthful velocities at (Schor & Bharadwaj, 2005a). The same adaptive process in an older eye could compensate for mismatches between the biomechanical properties of the A-IOL and the senescent lens it has replaced. The two adaptations would however be in opposite directions. In order to compensate for an increase in the age-related visco-elastic properties of the lens, the accommodative controller would have to increase its phasic and tonic gains. Conversely, in order to compensate for the decreased visco-elastic properties of the A-IOL, the accommodative controller would have to decrease in phasic and tonic gains. Overall, our simulations illustrate that increasing the range or amplitude of accommodation by replacing an old lens with a more compliant A-IOL that will not, by itself, restore effective dynamic accommodation without recalibrating the neural control of accommodation.

The magnitude of adaptation required to restore optimal responses would depend on the magnitude of mismatch in the system after implantation of the A-IOL. For example, for A-IOL I, the phasic-velocity and tonic-position signals had to be reduced by 72% and 76% respectively. For A-IOL II, the phasic-velocity and tonic-position signals had to be reduced by 20% and 76% respectively and for A-IOL III, these signals had to be reduced by 94% and 86% respectively. At the current juncture, however, it is difficult to predict if the reduction in gains of the phasic and tonic neural signals is physiologically possible or not. This is due to lack of quantitative information on the adaptive capabilities of the accommodative system. We are currently investigating the range of plasticity of the

adaptation process in older eyes that might be available for calibrating dynamic accommodation step responses to A-IOL's.

5.4. The concept of 'Myodiopter' applied to A-IOL's

Restoring accommodation in presbyopia ultimately amounts to increasing the dioptric change in focal length of the eye produced by changes in force applied by the ciliary body on the lens capsule. The ratio of the optical power change in diopters per unit change of force has been referred to as the myodiopter (diopter/dynes) (Hoeve & Flieringa, 1924; Alpern, 1962). It is analogous to effective compliance of the lens that determines the amplitude of power changes of the eye. In absolute presbyopia, the myodiopter is zero. Even though the ciliary muscle is capable of applying force to the lens capsule (Strenk et al., 1999; 2000), no change in effective lens power occurs. Mechanically, this is because the combined compliance of the lens capsule and matrix are reduced to a level that cannot respond to forces applied by the ciliary muscle. Optically, this could also be because of a reduction in the effective refractive index of the lens with age (Pierscionek, 1990; Ooi & Grosvenor, 1995) which diminishes the change in lens power with changes in lens curvature during attempts to accommodate.

The myodiopter of the A-IOL could be increased to restore accommodation either by mechanical or by optical means. Mechanically, the increase in the myodiopter could be achieved by adjusting the elasticity of the lens material. The elastic coefficient of the silicone-polymer gel or the stiffness of hinges in a single or dual-optic A-IOL contributes to the mechanical compliance of the combined lens and capsule which in turn influences

the magnitude of the myodiopter. Since the effective stiffness of the lens complex is the sum of stiffness of lens matrix and capsule (Appendix II), the range of myodiopter that can be increased by increasing the mechanical compliance of the lens matrix is likely to be constrained by the stiffness of the lens capsule. However, as shown by Krag et al (1997), the stiffness of the lens capsule increases only upto 35-yrs of age beyond which it shows a declining trend (Figure 2b). Furthermore, the stiffness of the lens capsule is on an average 7x (range from 15 – 45 yrs: 3x – 16x respectively) lower than the stiffness of the lens matrix. Hence, the constraint posed by the lens capsule on the increment in the range of myodiopter is likely to be very minimal. Optically, an increase in the myodiopter could be achieved by adjusting the refractive index of a silicone-polymer gel or by adjusting the effective power of the single or dual-optic lenses. Less curvature change is needed to increment optical power as effective refractive index increases. Since this is beyond the scope of our article, the readers are referred to the article by Ho et al (2001) for a detailed description of this concept. The increase in myodiopter produced by mechanical and optical means would supplement each other. It thus likely that highly effective A-IOL designs will be those that increase the myodiopter sufficiently by both mechanical and optical means to restore a functionally-usable range of accommodation

From the pulse-step modeling perspective, the changes in myodiopter produced either mechanically or optically will be described as gain changes in the lens transfer function. Gain is equivalent to effective compliance of the lens complex in units of the myodiopter (diopter/dynes). For example, if the spring constant of the lens matrix of a 45-yr old were reduced by half while retaining the spring constant of the 45-yr old lens

capsule, the combined compliance and gain of the lens complex would be increased by 33%. Similarly, if the refractive index of the lens were doubled, the gain of the lens complex would also be doubled. Irrespective of whether the myodiopter is increased by mechanical or optical means, our pulse-step model could be used to assess the dynamic performance of A-IOL's when these lenses are implanted in a closed-loop control system.

6. Conclusion

The pulse-step model of accommodation was employed to assess the dynamic performance of A-IOL's after they are implanted in a closed-loop control system. Implanting an A-IOL was mimicked in our simulations by replacing the stiffness and damping coefficient of an 'older' lens matrix with that of a 'younger' lens matrix. This experimental manipulation resulted in instabilities and oscillations of the accommodation response. As a proof of concept, stable dynamic performance of A-IOL's was achieved by reducing the gains of the phasic-velocity and tonic-position scalars. This suggests that an optimal performance of A-IOL's requires that the neural control signals be adapted to differences between the visco-elastic properties of the prosthetic lens and the natural lens that it has replaced.

Dissertation Summary

1. Rationale for the thesis

The main aims of the experiments described in this thesis were two fold: first, to gain insight into the neural control of the accommodation and disaccommodation step response and to study the age-related changes in the neural control strategies of these step responses. The second aim was to develop a model of accommodation and disaccommodation dynamics that would faithfully describe the neural control strategies

Under 'natural' viewing conditions, the human focusing mechanism behaves as a closed-loop control system (Fincham, 1937; Toates, 1972; Krishnan & Stark, 1975; Schor, 1992), whose optimal performance depends on the calibration of the neural control parameters to match the biomechanics of the accommodative plant. While there is a consolidated knowledge of the biomechanics of accommodative plant and how it changes with age (reviewed by Glasser & Kaufman, 2003), our understanding of the neural control of the focusing mechanism is still very limited. Neurophysiological experiments have shown a number of areas in the cortex and mid-brain that are involved in the control of accommodation (reviewed by Gamlin, 2002). However, the functional roles of neural signals generated in these areas are still speculative. Furthermore, there was a paucity of experiments and analyses that would interpret behavioral data in light of the neurophysiological and biomechanical observations that are documented in literature. The studies described in this thesis were mainly designed to fulfill this lacuna by systematically studying the behavioral changes in the first-order and second-order

characteristics of accommodation and disaccommodation as a function of response magnitude, starting position and aging.

Overall, the experiments described in this thesis make two major contributions: first, they enhance our understanding of the neural control of focusing mechanism by describing the dynamics in terms of different neural control strategies of accommodation and disaccommodation. Second, they mathematically formalize the dynamics and neural control strategies using the pulse-step dynamic model of accommodation and disaccommodation. In the future, this model could be employed to make predictions about the neural control of focusing mechanism and to assess the dynamic performance of accommodation and disaccommodation under different physiological and experimental situations.

2. What are the behavioral consequences of biomechanical properties of the plant and how do they reflect distinctive neural control strategies?

Response strategies are indicated by distinctive differences in the first- and second-order dynamics of accommodation and disaccommodation were noted in our experiments (figure 41, 42). The peak velocity of accommodation showed an increase with response magnitude (figure 4, 41) while the peak acceleration was invariant with response magnitude (figure 7, 41). Neither the peak velocity nor the peak acceleration changed with starting position of accommodation (figure 42). On the other hand, for a constant starting position, the peak velocity and peak acceleration of disaccommodation did not change with response magnitude (figure 27a, b, 33a) while both of them increased with

the starting position of disaccommodation (figure 27c, d, 33b, 34). The peak velocity of accommodation saturated at larger response magnitudes (Kasthurirangan et al., 2003) while the peak velocity of disaccommodation does not show any saturation (Bharadwaj & Schor, 2005b). Accommodation responses were on an average slower, but more stable than disaccommodation responses of the same magnitude (figure 38b – e).

The dynamic characteristics of accommodation and disaccommodation are a consequence of both biomechanical properties and the anatomical structural arrangement of the lenticular and extra-lenticular components of the accommodative plant (Weber et al., 1989; Beers & van der Heijde, 1994; Glasser & Kaufman, 2003) and the different neural control strategies. Accommodation has been deemed an 'active' process wherein the static and dynamic characteristics of accommodation are actively modulated by the neural innervation to the ciliary muscle (Weber et al., 1989; Beers & van der Heijde, 1994). Disaccommodation has been deemed a 'passive' process wherein the dynamic characteristics of disaccommodation are mainly determined by the visco-elastic nature of the crystalline lens and choroid (Weber et al., 1989; Beers & van der Heijde, 1994; Glasser & Kaufman, 2003). This is mainly based on the observation that the rate of relaxation of ciliary muscle is much faster than the rate at which the choroid to flatten the lens (Weber et al., 1989). For both accommodation and disaccommodation, the visco-elasticity of the crystalline lens has been suggested as the major rate-limiting factor (Glasser & Kaufman, 2003). However, two empirical observations suggest that the plant biomechanics might not be the sole determinants of the dynamics of the focusing mechanism. First, if the accommodative plant were the major determinants of dynamics,

then as long as the optical-defocus demands are within the linear-operating-range of the plant, the dynamics of both accommodation and disaccommodation should be qualitatively similar. Empirical observation of saturation of peak velocity of only accommodation (but not that of disaccommodation) at larger response magnitudes (Kasthurirangan et al., 2003; Bharadwaj & Schor, 2005b) does not support this notion. This suggests that the biomechanics of the plant are not solely responsible for determining the dynamics of accommodation and disaccommodation. Second, as discussed in chapter V, convergence and divergence eye movements also show similar dynamic characteristics as accommodation and disaccommodation respectively (Alvarez et al., 2005). The dynamics of convergence eye movements are response-magnitude dependent while the dynamics of divergence eye movements are starting-position dependent (Alvarez et al., 2005). Since the biomechanical plant of the vergence system and the accommodation system are widely disparate, it is very unlikely that the differences in dynamic characteristics of the two systems (focusing and vergence) are determined by their respective plants.

The differences in dynamics of accommodation and disaccommodation could also reflect separate neural control strategies that tend to optimize either the accuracy or the speed of the response. Slower dynamics but greater stability of accommodation reflect a neural strategy that optimizes the accuracy of the response. Conversely, faster dynamics but greater instability of disaccommodation reflect a neural control strategy that optimizes the speed of the response. While at the current juncture it is not possible to pin-point the reason for the differences in the neural control strategies, the aforementioned

differences in the dynamics suggest that accommodation and disaccommodation step responses do not respond with machine-like properties, but are driven by different control strategies that optimize different response characteristics.

3. The pulse-step dynamic model of accommodation and disaccommodation

As mentioned earlier, one of the main contributions of this thesis is the development of the pulse-step dynamic model of accommodation and disaccommodation. The pulse-step model represents a significant effort towards developing a comprehensive understanding of how the different patterns of neural innervation control the biomechanical plant to produce static and dynamic properties of the accommodation and disaccommodation step responses. The *neural* and the *biomechanical modules* of the pulse-step model are based on previously documented neurophysiological (Gamlin, 2002) and biomechanical (Glasser & Kaufman, 2003) observations respectively. The model illustrates the neural control signals that could produce the observed static and dynamic response components based on the known age-related biomechanical properties of the plant. The dynamics of accommodation and disaccommodation responses are controlled by the open-loop acceleration-pulse and phasic-velocity signals while the final static position is maintained under closed-loop conditions by the velocity-step and tonic-position signals.

The models of accommodation and disaccommodation could be used for two purposes, one to formalize the assumptions underlying the analysis and interpretation of data from various experiments and second, to make predictions for future experiments.

The pulse-step model has been successfully used for both these purposes. It has been used to mathematically formalize the neural control strategies of accommodation and disaccommodation for different age groups, as described above. For example, two parameters of the acceleration-pulse have been used to describe how the peak velocity and peak acceleration of accommodation and disaccommodation change with response magnitude and starting position (Figure 43) The height of the acceleration-pulse determines the peak acceleration and the integral of the acceleration-pulse determines the peak velocity (Figure 43). Increase in the peak velocity of accommodation with response magnitude is achieved by increasing the width of the constant-height acceleration-pulse signal (Figure 43). Increase in both the peak velocity and peak acceleration of disaccommodation with starting position is achieved by increasing the height of the constant-width acceleration-pulse signal (Figure 43). As will be discussed in the next section, the pulse-step model also makes predictions about the adaptable nature of the accommodative control system that paves way for future experiments. Overall, the model is a useful tool for assessing the dynamic performance of accommodation and disaccommodation under various physiological and experimental situations.

4. The adaptable nature of the accommodative control system

The dissertation also highlights the adaptive nature of the accommodation and the fact that it does not operate with rigid machine like control. Three observations presented in the thesis address the adaptable nature of the accommodative control system. First, the peak velocity of accommodation did not change with aging (Figure 18) suggesting that the age-related increase in visco-elasticity of the lens (Figure 51, 52) is compensated for

by adapting the neural controller of accommodation. Second, model simulations of implanting an A-IOL (whose visco-elasticity corresponds to that of a younger lens) in an 'older eye' shows that, unless the phasic-velocity and tonic-position signals of the 'older' eye are reduced to match the biomechanics of the 'younger' lens, large instabilities and oscillations of the accommodation response will result (Figure 53, 54, 55). The reduction in gain of the phasic and tonic signals represents another form of adaptation of the neural controller of accommodation. Third, the extensive training underwent by subject SRB (the author of this thesis) during the course of these experiments resulted in changes in his disaccommodation dynamics (Figure 31, 32) (Bharadwaj & Schor, 2005b). Specifically, the training reduced the speed of smaller disaccommodation responses which minimized the overshoots and instabilities in these responses (Figure 31, 32). These observations of adaptive behavior show great promise for the application of accommodating-intra-ocular lenses as prosthetic devices to reverse the loss of accommodation that normally occurs with age.

References

Agarwal, L. P., Narasimhan, E. C., & Mohan, M. (1967a). Experimental lens refilling. *Oriental Archives of Ophthalmology*, 5, 205 – 212.

Agarwal, L. P., Narasimhan, E. C., & Mohan, M. (1967b). Experimental lens refilling - II (In Monkeys). *Oriental Archives of Ophthalmology*, 5, 278 – 280.

Alpern, M., & Ellen, P. (1956). A quantitative analysis of the horizontal movements of the eyes in the experiment of Johannes Mueller. II. Effect of variation in target separation. *American Journal of Ophthalmology*, 42, 296 - 303.

Alpern, M. (1962). Accommodation. In: H. Davson *Muscular Mechanisms, 2nd Edition* (pp. 191 – 229). London: United Kingdom.

Alvarez, T. L., Semmlow, J. L., Yuan, W., & Munoz, P. (1999). Dynamic details of disparity convergence eye movements. *Annals of Biomedical Engineering*, 27, 380 – 390.

Alvarez, T. L., Semmlow, J. L., & Pedrono, C. (2005). Divergence eye movements are dependent on initial stimulus position. *Vision Research*, 45, 1847 – 1855.

Badal, M. (1876). Optometre metrique international: pour la measure simultanee de la refraction et de l'acuite visuelle meme chez les le illettres. *Annales D'Oculistique (Paris)*, 75, 101 – 117.

Bahill, T. A., Clark, M. R., & Stark, L. (1975). The main sequence, a tool for studying human eye movements. *Mathematical Biosciences*, 24, 191 – 204.

Beers, A. P. A., & van der Heijde, G. L., (1994). *In vivo* determination of the biomechanical properties of the component elements of the accommodation mechanism. *Vision Research*, 34, 2897 – 2905.

Beers, A. P. A., & van der Heijde, G. L., (1996). Age-related changes in the accommodation mechanism. *Optometry & Vision Science*, 73, 235 – 242.

Bharadwaj, S. R., & Schor, C. M. (2005a). Acceleration characteristics of human ocular accommodation. *Vision Research*, 45, 17 - 28.

Bharadwaj, S. R., & Schor, C. M. (2005b). Dynamic control of ocular disaccommodation: First and second-order dynamics. *Vision Research*. In Press.

Bharadwaj, S. R., & Schor, C. M. (2005c). Initial destination of the disaccommodation step response. *Vision Research*. In Press.

Biggs, R. D., Alpern, M., & Bennett, D. R (1959). The effect of sympathomimetic drugs upon the amplitude of accommodation. *American Journal of Ophthalmology*, 48, 169 – 172.

Bobier, W. R. & Sivak, J. G. (1983). Orthoptic treatment of subjects showing slow accommodative responses. *American Journal of Optometry & Physiological Optics*, 60, 678 – 687.

Burd, H. J., Wilde, G. S., & Judge, S. J. (2005). Can reliable values of Young's modulus be deduced from Fisher's (1971) spinning lens measurements? *Vision Research.* In Press.

Campbell, F. W. (1957). The depth of field of the human eye, *Optica Acta*, 4, 157 – 164.

Campbell, F. W., Westheimer, G. (1959). Factors influencing accommodation responses of the human eye. *Journal of Optical Society of America*, 49, 568 – 571.

Campbell, F. W., Westheimer, G. (1960). Dynamics of accommodation responses of the human eye. *Journal of Physiology (London)*, 151, 285 – 295.

Charman, W. N., & Whitefoot, H. (1977). Pupil diameter and the depth-of-field of the human eye as measured by laser speckle. *Optica Acta*, 24, 1211 – 1216.

Charman, W. N. (1991). Optics of the human eye. In: W. N. Charman. *Visual Optics and Instrumentation, Vol. 1, Vision & Visual Dysfunction* (pp. 1 – 20). Boca Raton: CRC Press.

Charman, W. N. (2005). Restoring accommodation: a dream or an approaching reality? *Ophthalmic & Physiological Optics*, 25, 1 – 6.

Ciuffreda, K. J., & Kruger, P. B. (1988). Dynamics of human voluntary accommodation. *American Journal of Optometry & Physiological Optics*, 65, 365 – 370.

Ciuffreda, K. J., & Wallis, D. M. (1998). Myopes show increased susceptibility to nearwork aftereffects. *Investigative Ophthalmology & Visual Science*, 39, 1797 – 1803.

Coleman, D. J. (1986). On the hydraulic suspension theory of accommodation. *Transactions of the American Ophthalmology Society*, 84, 846 – 868.

Coleman, D. J., & Fish, S. K. (2001). Presbyopia, accommodation and the mature catenary. *Ophthalmology*, 108, 1544 – 1551.

Collewijn, H., Erkelens, C. J., & Steinman, R. M. (1988). Binocular co-ordination of human horizontal saccadic eye movements. *Journal of Physiology*, 404, 157 – 182.

Cornsweet, T. N., & Crane, H. D. (1970). Servo-controlled infrared optometer. *Journal of Optical Society of America*, 60, 548 – 554.

Crane, H. D. (1966). A Theoretical Analysis of the Visual Accommodation System in Humans. *Stanford Research Institute*, Proj. 5454.

Crane, H. D., & Steele, C. M. (1978a). Accurate three-dimensional eyetracker. *Applied Optics*, 17, 691 – 705.

Crane, H. D., & Clark, M. R. (1978b). Three-dimensional visual stimulus deflector. *Applied Optics*, 17, 706 – 714.

Crawford, K., Terasawa, E., & Kaufman, P. L. (1989). Reproducible stimulation of ciliary muscle contraction in the cynomolgus monkey via a permanent indwelling midbrain electrode. *Brain Research*, 503, 265 – 272.

Croft, M. A., Kaufman, P. L., Crawford, K. S., Neider, M. W., Glasser, A., & Bito, L. Z. (1998). Accommodation dynamics in aging rhesus monkeys. *American Journal of Physiology*, 275, R1885 – R1987.

Culhane, H. M., & Winn, B. (1999). Dynamic accommodation and myopia. *Investigative Ophthalmology & Visual Science*, 40, 1968 – 1974.

Culhane, H. M., Winn, B., & Gilmartin, B. (1999). Human dynamic closed-loop accommodation augmented by sympathetic inhibition. *Investigative Ophthalmology & Visual Science*, 40, 1137 – 1143.

Cumming, B. G., & Judge, S. J. (1986). Disparity-induced and blur-induced convergence eye movement and accommodation in the monkey. *Journal of Neurophysiology*, 55, 896 - 914.

Cumming, J. S., Slade, S. G., Chayet, A., & AT - Study Group. (2001). Clinical evaluation of the model AT-45 silicone accommodating intraocular lens. *Ophthalmology*, 108, 2005 – 2010.

de Groot, J. H., van Beijma, F. J., Haitjema, H. J., Dilligham, K. A., Hodd, K. A., Koopmans, S. A., & Norrby, S. (2001). Injectable intraocular lens materials based upon hydrogels. *Biomacromolecules*, 2, 628 – 634.

Devore, J., & Peck, R. (1993a). The analysis of variance. In: J. Devore & R. Peck. *Statistics - The Exploration and Analysis of Data, 2nd Edition* (pp. 731 – 802). Belmont: Wadsworth.

Devore, J., & Peck, R. (1993b). Summarizing bivariate data. In: J. Devore & R. Peck. *Statistics - The Exploration and Analysis of Data, 2nd Edition* (pp. 731 – 802). Belmont: Wadsworth.

Dick, H. B. (2005). Accommodative intraocular lenses: current status. *Current Opinion in Ophthalmology*, 16, 8 – 26.

Doane, J. F. (2004). Accommodating intraocular lenses. *Current Opinion in Ophthalmology*, 15, 16 – 21.

Duane, A. (1912). Normal values of the accommodation at all ages. *Journal of the American Medical Association*, 59, 1010 – 1013.

Ejiri, M., Thompson, H. E., & O'Neill, W. D. (1969). Dynamic visco-elastic properties of the lens. *Vision Research*, 9, 233 – 244.

Fincham, E. F. (1937). The mechanism of accommodation. *British Journal of Ophthalmology Monograph*, VIII, 1.

Fincham, E. F. (1951). The accommodation reflex and its stimulus. *British Journal of Ophthalmology*, 35, 381 – 393.

Fisher, R. F. (1969a). Elastic constants of the human lens capsule. *Journal of Physiology*, London, 201, 1 – 19.

Fisher, R. F. (1969b). The significance of the shape of the lens and capsular energy changes in accommodation. *Journal of Physiology*, London, 201, 21 – 47.

Fisher, R. F. (1971). The elastic constants of the human lens. *Journal of Physiology,* London, 212, 147 – 180.

Fisher, R. F. (1977). The force of contraction of the human ciliary muscle during accommodation. *Journal of Physiology*, London, 270: 51 – 74.

Fisher, S. K., Ciuffreda, K. J., Levine, S., & Wolf-Kelly, K. S. (1987). Tonic adaptation in symptomatic and asymptomatic subjects. *American Journal of Optometry & Physiological Optics*, 64, 333 – 343.

Fukushima, K., Kaneko, C. R. S., & Fuchs, A. (1992). The neuronal substrate of integration in the oculomotor system. *Progress in Neurobiology,* 39, 609 – 639.

Gamlin, P. D. R., & Mays, L. E. (1992). Dynamic properties of medial rectus motoneurons during vergence eye movements. *Journal of Neurophysiology*, 67, 64 – 74.

Gamlin, P. D. R., Zhang, Y., Clendaniel, R. A., & Mays, L. E. (1994). Behavior of identified Edinger-Westphal neurons during ocular accommodation. *Journal of Neurophysiology,* 72, 2368 – 2382.

Gamlin, P. D. R., & Clarke, R. J. (1995). Single-unit activity in the primate nucleus reticularis tegmenti pontis related to vergence and ocular accommodation. *Journal of Neurophysiology,* 73, 2115 – 2119.

Gamlin, P. D. R., Yoon, K., & Zhang, H (1996). The role of cerebro-ponto-cerebellar pathways in the control of vergence eye movements. *Eye*, 10, 167 – 171.

Gamlin, P. D. R., & Yoon, K. (2000). An area for vergence eye movement in primate frontal cortex. *Nature*, 407, 1003 – 1007.

Gamlin, P. D. R. (2002). Neural mechanisms for the control of vergence eye movements. *Annals of the New York Academy of Sciences*, 956, 264 – 272.

Gettes, B. C., & Belmont, O. (1961). Tropicamide, comparative cycloplegic effects. *Archives of Ophthalmology,* 66, 336 – 340.

Giles, G. H. (1965). The use of drugs in ophthalmic optical practice. In: G. H. Giles. *The principles and practice of refraction and its allied subjects* (pp. 467 – 479). Philadelphia: Chilton Company.

Gilmartin, B. (2000). Pharmacology of accommodative adaptation. In: O. Franzen, H. Richter, & L. Stark. *Accommodation and vergence mechanisms in the visual system* (pp. 141 – 150). Switzerland: Birkhauser Verlag Basel.

Glasser, A., & Campbell, M. A. (1999). Biometric, optical and physical changes in the isolated human crystalline lens with age in relation to presbyopia. *Vision Research*, 39, 1991 – 2015.

Glasser, A., & Kaufman, P. L. (2003) Accommodation and Presbyopia. In P. L. Kaufman & A. Alm. *Adler's physiology of the eye 10th edition* (pp. 197 - 237). St. Louis: Mosby.

Grosvenor, T. (1996). The binocular vision examination. In. T. Grosvenor. *Primary care optometry. Anomalies of refraction and binocular vision 3rd Edition* (pp. 309 – 333). Boston: Butterworth-Heinemann.

Gullstrand, A. (1924). Appendices by A. Gullstrand: Mechanism of accommodation. In: J. P. C. Southall. *Helmholtz's treatise on Physiological Optics Translated from the Third German Edition, Volumes 1 & II* (pp. 382 – 415). New York: Dover Publications.

Haefliger, E., Parel, J. M., Fantes, F., Norton, E. W. D., Anderson, D. R., Forster, R. K., Hernandez, E., & Feuer, W. J. (1987). Accommodation of an endocapsular silicone lens (Phako-Ersatz) in the nonhuman primate. *Ophthalmology*. 94, 471 – 477.

Haefliger, E., & Parel, J. M. (1994). Accommodation of an endocapsular silicone lens (Phaco-Ersatz) in the aging rhesus monkey. *Journal of Cataract & Refractive Surgery*. 10, 550 – 555.

Hamasaki, D., Ong, J., & Marg, E. (1956). The amplitude of accommodation in presbyopia. *American Journal of Optometry & Archives of American Academy of Optometry*, 33, 3 – 14.

Han, Y., Seideman, M., & Lennerstrand, G. (1995). Dynamics of accommodative vergence movements controlled by the dominant and non-dominant eye. *Acta Ophthalmologica Scandinavia*, 75, 319 - 324.

Hara, T., Hara, T., Yasuda, A., & Yamada, Y. (1990). Accommodative intraocular lens with spring action Part I. Design and placement in an excised animal eye. *Ophthalmic Surgery*, 21, 128 – 133.

Hara, T., Hara, T., Yasuda, A., Mizumoto, Y., & Yamada, Y. (1992). Accommodative intraocular lens with spring action -- Part 2. Fixation in the living rabbit. *Ophthalmic Surgery*, 23, 632 – 635.

Hasebe, S., Graf, E. W., & Schor, C. M. (2001). Fatigue reduces tonic accommodation. *Ophthalmic & Physiological Optics*, 21, 151 – 160.

Helmholtz, H. (1866). Mechanism of accommodation. In: J. P. C. Southall. *Helmholtz's treatise on Physiological Optics Translated from the Third German Edition, Volumes 1 & II* (pp. 143 – 172). New York: Dover Publications.

Heron, G., & Winn, B. (1989). Binocular accommodation reaction and response times for normal observers. *Ophthalmic & Physiological Optics*, 9, 176 – 183.

Heron, G., Charman, W. N., & Gray, L. S. (1999). Accommodation responses and ageing. *Investigative Ophthalmology & Visual Science*, 40, 2872 – 2883.

Heron, G., Charman, W. N., & Schor, C. (2001a). Dynamics of the accommodation response to abrupt changes in target vergence as a function of age. *Vision Research*, 41, 507 – 519.

Heron, G., Charman, W. N., & Schor. C. M. (2001b). Age changes in the interactions between the accommodation and vergence systems. *Optometry & Vision Science*, 78, 754 - 762.

Heron, G, Charman, W. N., & Gray, L. S. (2002). Accommodation dynamics as a function of age. *Ophthalmic & Physiological Optics*, 22, 389 – 396.

Hettlich, H. J., Lucke, K., Asiyo-Vogel, M., Schulte, M., & Vogel, A. (1994). Lens refilling and endocapsular polymerization of an injectable intraocular lens: in vitro and in vivo study of potential risks and benefits. *Journal of Cataract & Refractive Surgery*. 20, 115 – 123.

Heys, K. R., Cram, S. L., Truscott, R. J. W. (2004) Massive increase in the stiffness of the human lens nucleus with age: the basis for presbyopia? *Molecular Vision*, 10, 956-963.

Ho, A., Erickson, P., Manns, F., Pham, T., & Parel, J. -M. (2001). Theoretical analysis of accommodation amplitude and ametropia correction by varying refractive index in phaco-ersatz. *Optometry & Vision Science*, 78, 405 – 410.

Hofstetter, H. W. (1965). A longitudinal study of amplitude changes in presbyopia. *American Journal of Optometry & Archives of American Academy of Optometry*, 42, 3 – 8.

Hung, G.K., Semmlow, J. L. & Ciuffreda K. J. (1986) A dual-mode model of the vergence eye movement system. *IEEE Transactions on Bio-Medical Engineering, BME*-33, 1021-1028

Hung, G. K., & Ciuffreda, K. J. (1988). Dual-model behavior in the human accommodation system. *Ophthalmic & Physiological Optics*, 8, 327 – 332.

Judge, S. J., & Cumming, B. G. (1986). Neurons in the monkey midbrain with activity related to vergence eye movement and accommodation. *Journal of Neurophysiology*, 5, 915 – 929.

Jurgens, R., Becker, W., & Kornhuber, H. H. (1981). Natural and drug-induced variations of velocity and duration of saccadic eye movements: Evidence for a control of the neural pulse generator by local feedback. *Biological Cybernetics*, 39, 87 – 96

Kasthurirangan, S., Vilupuru, A. S., & Glasser, A. (2003). Amplitude dependent accommodative dynamics in humans. *Vision Research*, 43, 2945 – 56.

Kasthurirangan, S., & Glasser, A. (2005). Influence of amplitude and starting point on accommodative dynamics in humans. *Investigative Ophthalmology & Visu*al *Science, 46, 3463 – 3472*.

Kessler, J. (1964). Experiments in refilling the lens. *Archives of Ophthalmology*, 71, 412 – 417.

Kessler, J. (1966). Refilling the rabbit lens: further experiments. *Archives of Ophthalmology*, 76, 596 – 598.

Khosroyani, M., & Hung, G. K. (2002). A dual-mode dynamic model of the human accommodation system. *Bulletin of Mathematical Biology*, 64, 285 – 299.

Kleinbaum, D. G., Kupper, L. L., Muller, K. E., & Nizam, A. (1998). Dummy variables in regression. In: D. G. Kleinbaum, L. L. Kupper, K. E. Muller, & A. Nizam. *Applied*

Regression Analysis & Multivariable Methods, 3rd Edition (pp. 317 – 360). Pacific Grove: Duxbury Press.

Koopmans, S. A., Terwee, T., Barkhof, J., Haitjema, H. J., & Kooijman, A. C. (2003). Polymer refilling of presbyopic human lenses In Vitro restores the ability to undergo accommodative changes. *Investigative Ophthalmology & Visual Sci*ence, 44, 250 – 254.

Koopmans, S. A., Terwee, T., Haitjema, H. J., Deuring H., van Aarle, S., & Kooijman, A. C. (2004). Relation between injected volume and optical parameters in refilled isolated porcine lenses. *Ophthalmic & Physiological Optics*. 24, 572 – 579.

Koopmans, S. A. (2005). Personal communication.

Kotulak, J. C., & Schor, C. M. (1986). A computational model of the error detector of human visual accommodation. *Biological Cybernetics*, 54, 189 – 194.

Krag, S., Olsen, T., & Andreassen, T. T. (1997). Biomechanical characteristics of the human anterior lens capsule in relation to age. *Investigative Ophthalmology & Visual Science*. 38, 357-63.

Krishnan, V. V., & Stark, L. (1975). Integral control in accommodation. *Computer Programs in Biomedicine*, 4, 237 – 245.

Krishnan, V. V., Shirachi, D., & Stark, L. (1977). Dynamic measures of vergence accommodation. *American Journal of Optometry & Physiological Optics*, 54, 470 - 473.

Kruger, P. B., & Pola, J. (1985). Changing target size is a stimulus for accommodation. *Journal of Optical Society of America*, 2, 1832 – 1835.

Kruger, P. B., & Pola, J. (1986). Stimuli for accommodation: blur, chromatic aberration and size. *Vision Research*, 26, 957 – 971.

Kruger, P. B., & Pola, J. (1987). Dioptric and non-dioptric stimuli for accommodation: target size alone and with blur and chromatic aberration. *Vision Research*, 27, 555 – 567.

Kuchle, M., Seitz, B., Langenbucher, A., Gusek-Schneider, G., Martus, P., & Nguyen, N. (2004). Comparison of 6-month results of implantation of the 1CU accommodative intraocular lens with conventional intraocular lens. *Ophthalmology*, 111, 318 – 324.

Langenbucher, A., Huber, S., Nguyen, N. X., Seitz, B., Gusek-Schneider, G. C., & Kuchle, M. (2003). Measurement of accommodation after implantation of an accommodating posterior chamber intraocular lens. *Journal of Cataract & Refractive Surgery*. 27, 677 – 685.

Leibowitz, H. W., & Owens, D. A. (1975). Anomalous myopias and the intermediate dark focus of accommodation. *Science*, 189, 646 – 648.

Leibowitz, H. W., & Owens, D. A. (1978). New evidence for the intermediate position of relaxed accommodation. *Documenta Ophthalmologica*, 46, 133 – 147.

Levi, L. (1968). Lenses and curved mirrors. In: L. Levi. *Applied Optics. A Guide to Optical System Design, Vol. 1* (pp. 393 – 506). New York: John Wiley & Sons.

Lisberger, S. G., & Westbrook, L. E. (1985). Properties of visual inputs that initiate horizontal smooth pursuit eye movements in monkeys. *The Journal of Neuroscience*, 5, 1662 – 1673.

Liu, J. S., Lee, M., Jang, J., Ciuffreda, K. J., Wong, J. H., Grisham, D., & Stark, L. (1979). Objective assessment of accommodation orthoptics. I. Dynamic insufficiency. *American Journal of Optometry & Physiological Optics,* 56, 285 – 294.

Lovasik, J. V. (1986). Pharmacokinetics of topically applied cyclopentolate HCl and tropicamide. *American Journal of Optometry and Physiological Optics*, 63, 787 – 803.

Mays, L. E. (1983). Neurophysiological correlates of vergence eye movements. In: C. M. Schor, & K. J. Ciuffreda. *Vergence Eye Movements: Basic & Clinical Aspects* (pp. 649 - 670). Boston: Butterworths.

Mays, L. E., Porter, J. D., Gamlin, P. D. R., & Tello, C. A. (1986). Neural control of vergence eye movements: Neurons encoding vergence velocity. *Journal of Neurophysiology,* 56, 1007 – 1021.

Mays, L. E., & Gamlin, P. D. R. (1995). Neuronal circuitry controlling the near response. *Current Opinions in Neurobiology,* 5, 763 - 768.

McLeod, S. D., Portney, V., & Ting, A. (2003). A dual optic accommodating foldable intraocular lens. *British Journal of Ophthalmology*, 87, 1083 – 1085.

McLin, L. N. Jr., Schor, C. M., & Kruger, P. B. (1988). Changing size (looming) as a stimulus to accommodation and vergence. *Vision Research*, 28, 883 – 898.

Michaels, D. D. (1985). Drugs in refraction. In: D. D. Michaels. Visual Optics and Refraction. *3rd Edition (pp. 277 – 297) St. Louis: The C. V. Mosby Company.*

Mitchell, D. W. A. (1960). The use of drugs in refraction. 2nd edition (pp. 54) London: Hereford Times.

Mordi, J. A., Lyle, W. M., & Mousa, G. Y. (1986a). Effect of phenylephrine on accommodation. *American Journal of Optometry & Physiological Optics,* 63, 294 – 297.

Mordi, J. A., Tucker, J., & Charman, W. N. (1986b). Effects of 0.1% cyclopentolate or 10% phenylephrine on pupil diameter and accommodation. *Ophthalmic & Physiological Optics*, 6, 221 – 227.

Mordi, J. A., & Ciuffreda, K. J. (2004). Dynamic aspects of accommodation: age and presbyopia. *Vision Research*, 44, 591 – 601.

Morgan, M. W. (1944). Clinical measurements of accommodation and convergence. *American Journal of Optometry & Archives of the American Academy of Optometry,* 21, 301 – 321.

Morgan, M. W. (1968). Accommodation and vergence. *American Journal of Optometry & Archives of American Academy of Optometry*, 7, 417 – 454.

Nise, N. (2000). Time response. In: N. Nise. *Control Systems Engineering, 3rd Edition* (pp. 174 – 249). New York: John Wiley & Sons.

Nishi, O., & Nishi, K. (1998). Accommodation amplitude after lens refilling with injectable silicone by sealing the capsule with a plug in primates. *Archives of Ophthalmology*, 116, 1358 – 1361.

Nishi, O., Nishi, K., Mano, C., Ichihara, M., & Honda, T. (1998). Lens refilling with injectable silicone in rabbit eyes. *Journal of Cataract & Refractive Surgery*. 24, 975 – 982.

Ogata, K. (2002). *Modern Control Engineering*. Upper Saddle River: Prentice Hall.

Ogle, K. N., & Schwartz, J. T. (1959). Depth of focus of the human eye. *Journal of Optical Society of America*, 49, 273 – 280.

Ooi, C. S., & Grosvenor, T. (1995). Mechanisms of emmetropization in the aging eye. *Optometry & Vision Science*, 72, 60 – 66.

Owens, D. A., & Wolf-Kelly, K. (1987). Near-work, visual fatigue and variations of oculomotor tonus. *Investigative Ophthalmology & Visual Science*, 28, 743 – 749.

Parel, J. -M., Gelender, H., Trefers, W. F., & Norton, E. W. D. (1986). Phaco-Ersatz: cataract surgery designed to preserve accommodation. Graefe's *Archive of Clinical & Experimental Ophthalmology*. 224, 165 – 173.

Phillips, S., Shirachi, D., & Stark, L. (1972). Analysis of accommodative response times using histogram information. *American Journal of Optometry & Archives of American Academy of Optometry*, 49, 389 – 401.

Pierscionek, B. (1990). Presbyopia – effect of refractive index. *Clinical & Experimental Optometry*, 73, 23 – 30.

Pragnen, A. D. (1931). What constitutes satisfactory cycloplegia? *American Journal of Ophthalmology*, 14, 665 – 671.

Robinson, D. A. (1964). The mechanics of human saccadic eye movements. *Journal of Physiology*, 175, 245 – 264.

Robinson, D. A. (1973). Models of the saccadic eye movement control system. *Kybernetik*, 31, 71 – 83.

Robinson, D. A. (1975). Oculomotor control signals. In: G. Lennerstrand, & P. Bach-y-Rita. *Basic Mechanisms of Ocular Motility and their Clinical Implication* (pp. 337 – 374). Oxford: Pergamon Press.

Rosenfield, M., Ciuffreda, K. J., Hung, G. K., & Gilmartin, B. (1993). Tonic accommodation: a review. I. Basic aspects. *Ophthalmic & Physiological Optics*, 13, 266 – 284.

Rosenfield, M., Ciuffreda, K. J., Hung, G. K., & Gilmartin, B. (1994). Tonic accommodation: a review. II. Accommodative adaptation and clinical aspects. *Ophthalmic & Physiological Optics*, 14, 265 – 277.

Sakka, Y., Hara, T., Yamada, Y., Hara, T., & Hayashi, F. (1996). Accommodation in primate eyes after implantation of refilled endocapsular balloon. *American Journal of Ophthalmology*. 121, 210 – 212.

Schaeffel, F., Wilhelm, H., & Zrenner, E. (1993). Inter-individual variability in the dynamics of natural accommodation in humans: relation to age and refractive error. *Journal of Physiology (London)*, 461, 301 – 320.

Schaeffel, F. (2005). Personal communication.

Schnider, C. M., Ciuffreda, K. J., Cooper, J., & Kruger, P. B. (1984). Accommodation dynamics in divergence excess exotropia. *Investigative Ophthalmology & Visual Science*, 25, 414 – 418.

Schor, C. M., Johnson, C. & Post, R. (1984). Adaptation of tonic accommodation. *Ophthalmic & Physiological Optics*, 4, 133 - 137.

Schor, C. M., & Kotulak, J. C. (1986). Dynamic interactions between accommodation and convergence are velocity sensitive. *Vision Research*, 26, 927 – 942.

Schor, C. M., Kotulak, J., & Tsuetaki, T. (1986). Adaptation of tonic accommodation reduces accommodative lag and is reduced in darkness. *Investigative Ophthalmology & Visual Science*, 27, 820 – 827.

Schor, C. M. (1992). A dynamic model of cross-coupling between accommodation and convergence: simulations of step and frequency responses. *Optometry & Vision Science*, 69, 258 – 269.

Schor, C. M., Lott, L. A., Pope, D., & Graham, A. D. (1999). Saccades reduce latency and increase velocity of ocular accommodation. *Vision Research*, 39, 3769 – 3795.

Schor, C. M., & Bharadwaj, S. R. (2005a). A pulse-step model of accommodation dynamics in the ageing eye. *Vision Research*, 45, 1237 – 1254.

Schor, C. M., & Bharadwaj, S. R. (2005b). Pulse-step models of control strategies for dynamic ocular accommodation and disaccommodation. *Vision Research*, In Press.

Semmlow, J. S., Hung, G. K., Horng, J. L., & Ciuffreda, K. J. (1993). The initial control of disparity vergence eye movements. *Ophthalmic & Physiological Optics*, 13, 48 - 55.

Semmlow, J. S., Hung, G. K., Horng, J. L., & Ciuffreda, K. J. (1994). Disparity vergence eye movements exhibit preprogrammed motor control. *Vision Research*, 34, 1335 - 1343.

Shirachi, D., Liu, J., Lee, M., Jang, J., Wong, J., Stark, L. (1978). Accommodation dynamics I. Range Nonlinearity. *American Journal of Optometry & Physiological Optics*, 55, 631 – 641.

Stark, L. (1987). Presbyopia in light of accommodation. In: L. Stark, & G. Obrecht. *Presbyopia: Recent Research & Reviews From The Third International Symposium* (pp. 264 – 274). New York: Professional Press Books.

Stiles, W. S., & Crawford, B. H. (1933). The luminous efficiency of rays entering the eye pupil at different points. *Proceedings of the Royal Society of London*, 112, 428 – 450.

Strenk, S. A., Semmlow, J. L., Strenk, L. M., Munoz, P., Gronlund-Jacob, J., & DeMarco, J. K. (1999). Age-related changes in human ciliary muscle and lens: a

magnetic resonance imaging study. *Investigative Ophthalmology & Visual Sci*ence, 40, 1162 – 1169.

Strenk, S. A., Strenk, L. M., & Semmlow, J. L. (2000). High resolution MRI study of circumlental space in the aging eye. *Journal of Refractive Surgery*, 16, S659 – S660.

Sun, F., & Stark, L. (1986). Dynamics of accommodation: measurements for clinical application. *Experimental Neurology*, 91, 71 – 79.

Suryakumar, R., & Bobier, W. R. (2004). Gain and movement time of convergence-accommodation in pre-school children. *Optometry & Vision Science*, 81, 835 – 843.

Suryakumar, R. (2005). Study of the dynamic interactions between vergence and accommodation. Waterloo, Canada: University of Waterloo. Doctoral Thesis.

Takeda, T., Ostberg, O., Fukui, Y., Iida, T. (1988). Dynamic accommodation measurements for objective assessment of eye-strain and visual fatigue. *Journal of Human Ergology*, 17, 21 – 35.

Tamm, E. R., & Lutjen-Drecoll, E. (1996) Ciliary body. *Microscopy Research and Technique*, 33, 390-439

Toates, F. M. (1972). Accommodation function of the human eye. *Physiological Reviews*, 52, 828 – 863.

Troelstra, A., Zuber, B. L., Miller, D., & Stark, L. (1964). Accommodative tracking: A trial-and-error function. *Vision Research*, 4, 585 – 594.

Tucker, J., & Charman, W. N. (1975). The depth-of-focus of the human eye for Snellen letters. *American Journal of Optometry & Physiological Optics*, 52, 3 – 21.

Tucker, J., & Charman, W. N. (1979). Reaction and response times for accommodation. *American Journal of Optometry & Physiological Optics,* 56, 490 – 503.

Ukai, K. (2005). Personal communication.

van Alphen, G. W. H. M., & Graebel, W. P. (1991). Elasticity of tissues involved in accommodation. *Vision Research,* 31, 1417 – 1438.

van der Hoeve, J., & Flieringa, H. J. (1923). Determination of the power of the accommodation muscle. *Proceedings of the Koninklijke Akademie van Wetenschappen te Amsterdam*, 26, 763 – 770.

Vilupuru, A. S., & Glasser, A. (2002). Dynamic accommodation in rhesus monkeys. *Vision Research*, 42, 125 – 141.

Vilupuru, A. S., Kasthurirangan, S., & Glasser, A. (2005). Dynamics of accommodative fatigue in rhesus monkeys and humans. *Vision Research*, 45, 181 – 191.

Warwick, R. (1954). The ocular parasympathetic nerve supply and its mesencephalic sources. *Journal of Anatomy*, 88, 71 – 93.

Weale, R. A. (1963). New light on old eyes. *Nature,* 8, 944 - 946.

Weale, R. A. (1982). Growth. In: R. A. Weale. *A Biography of the Eye: Development Growth Age* (pp. 94 – 121). London: H. K. Lewis & Co. Ltd.

Weber, J., Tuinenburg, A. E., & van der Heijde, G. L. (1989). Effect of timolol on the amplitude and dynamics of accommodation. *Documenta Ophthalmologica*, 72, 341 – 347.

Weeber, H. A., Eckert, G., Soergel, F., Meyer, C.H., Pechhold, W., & van der Heijde, R. G. L. (2005). Dynamic mechanical properties of human lens. *Experimental Eye Research*, 80, 425 – 434.

Westheimer, G. (1957). Accommodation measurements in empty visual fields. *Journal of Optical Society of America*, 47, 714 – 718.

Westheimer, G., & Blair, S. M. (1973). Accommodation of the eye during sleep and anesthesia. *Vision Research*, 13, 1035 – 1040.

Whiteside, T. C. D. (1953). Accommodation of the human eye in a bright and empty visual field. *Journal of Physiology*, 118, 65 – 66.

Winn, B., Culhane, H. M., Gilmartin, B., & Strang, N. C. (2002). Effect of ß-adrenoceptor antagonists on autonomic control of ciliary smooth muscle. *Ophthalmic & Physiological Optics*, 22, 359 – 365.

Wolf, K. S., Ciuffreda, K. J., & Jacobs, S. E. (1987). Time course and decay of effects of near work on tonic accommodation and tonic vergence. *Ophthalmic & Physiological Optics*, 7, 131 – 135.

Wyatt, H. J. (1988). Some aspects of mechanics of accommodation. *Vision Research*, 28, 75 - 86.

Wyatt, H. J. (1993). Application of a simple mechanical model of accommodation to the aging eye. *Vision Research*, 33, 731 – 738.

Yamada, T., & Ukai, K. (1997). Amount of defocus is not used as an error signal in the control system of accommodation dynamics. *Ophthalmic & Physiological Optics*, 17, 55 – 60.

Zee, D. S., & Levi, L. (1989). Neurological aspects of vergence eye movements. *Review of Neurology (Paris)*, 145, 613 – 20.

Zhang, H. Y., & Gamlin, P. D. R. (1998). Neurons in the posterior interposed nucleus of the cerebellum related to vergence and accommodation. I. Steady-state characteristics. *Journal of Neurophysiology*, 79, 1255 – 1269.

Zhang, Y., Mays, L. E., & Gamlin, P. D. R. (1992). Characteristics of near-response cells projecting to the oculomotor nucleus. *Journal of Neurophysiology*, 76, 944 – 960.

Appendices

Appendix I: Ramped onset of acceleration-pulse innervation

The acceleration-pulse for both accommodation and disaccommodation models has a ramped onset whose width determines the time-to-peak acceleration (Figures 12b; 41b; c). Trapezoidal and triangular shaped pulses with ramped onsets have also been proposed for the pulse component of the saccadic control system (Robinson, 1973; Jurgens et al., 1981). Empirical measures of accommodation and disaccommodation indicate that the time-to-peak acceleration is approximately constant (100 ms), and is invariant with response amplitude and starting position (Bharadwaj & Schor, 2005a). A pulse plateau follows the ramped onset. The combined width of the ramped onset and pulse plateau for the disaccommodation models is set by empirical measures of time to reach peak velocity after the response begins. Time-to-peak velocity for disaccommodation (200 ms) is invariant with starting position and response magnitude, (Bharadwaj & Schor, 2005b) and this parameter was used to indicate when the open-loop acceleration-pulse ended and the closed-loop velocity step started.

Appendix II: Conversion of moduli of elasticity of the lens capsule and matrix into their spring constants

The elastic properties of the lens capsule and matrix are usually represented in terms of their modulus of elasticity. The modulus of elasticity describes the change in length of an extended surface when a force is applied per unit area of that surface. However, for a lumped model of the accommodative system, one is more likely to describe the mechanical properties of the tissues using its spring constant (van Alphen & Graebel, 1991). The spring constant describes the change in length of a spring that will result from a small change in force, after accounting for the area of the surface. The following conversion regimen was employed to obtain spring constant measurements from published values of moduli of elasticity.

F = Force applied on a elastic body (Newtons)

L = Baseline length of the elastic body (Meter)

A = Cross-sectional area (CSA) of the elastic body ($Meter^2$)

?L = Change in length of the elastic body as a result of the force (Meters)

K = Spring constant (Newtons / Meter)

E = Young's modulus of elasticity (Newtons / $Meter^2$)

Stress = Force applied per unit area (Newtons / $Meter^2$)

Strain = Change in length from the baseline length (Unit less quantity)

Conversion factor: 1 Newtons / Meter = 100 Dynes / Millimeter

$$F = K * \Delta L \text{ (Hooke's Law)} \quad (1)$$

Young's modulus of elasticity = Stress / Strain

$$E = (F / A) / (\Delta L / L) \quad (2)$$

Rearranging Eq. 5; $F = (E * \Delta L * A) / L$ (3)

Comparing Eq's 4 & 6; $K * \Delta L = (E * \Delta L * A) / L$

$$K \text{ (Newtons / m)} = (A / L) * E \quad (4)$$

Applying conversion factor to Eq. 7; $\mathbf{K \text{ (Dynes / mm)} = 100 * (A / L) * E}$ (5)

Mechanically, the lens capsule and lens matrix can be modeled as two springs in parallel (van Alphen & Graebel, 1991). In our model, the modulus of elasticities of the lens capsule and matrix were converted into spring constant measures using Eq. 8 and were lumped together and modeled as a single gain element by summing their respective spring constants (Eq. 11).

Lens capsule spring constant; $K_C = 100 * (A_C / L_C) * E_C$ (6)

Lens matrix spring constant; $K_M = 100 * (A_M / L_M) * E_M$ (7)

Combined spring constant; $\mathbf{K_{Com} = K_C + K_M}$ (8)

The CSA, length and Young's modulus of elasticity (stress on the lens capsule at 30% strain) of the lens capsule were obtained from Krag *et al* (1997)*. The CSA and the equatorial diameter of the entire lens (lens capsule + lens matrix) were obtained by averaging the *in-vitro* measurements of van Alphen & Graebel (1991) and the MRI measurements of Strenk et al (1999, 2000). The CSA of the entire lens was subtracted

from the CSA of the lens capsule (Krag *et al*., 1997) to obtain the CSA of the lens matrix. The Young's modulus of elasticity of lens matrix was obtained from in-vitro measurements of lens matrix shear-compliance performed by Weeber et al (2005)*. Shear-compliance measures were converted into Young's modulus of elasticity measures using the following regimen.

E_S = Shear modulus of elasticity (Newtons / Meter^2)

C_S = Shear compliance (Newtons / Meter^2)$^{-1}$

Compliance (Newtons / Meter^2)$^{-1}$ = 1 / Elastic modulus (Newtons / Meter^2)

P = Poisson's ratio

$$E_S = 1 / C_S \quad (9)$$

$$E = E_S / 2\,(1 + P) \quad (10)$$

Assuming a Poisson's ratio of 0.5, Eq. 13 reduces to; $\mathbf{E = E_S / 3}$ (11)

---

* The Young's modulus of elasticity of the lens capsule obtained by Krag et al (1997) and that of the lens matrix obtained by Weeber et al (2005) were used in our model instead of the more conventionally used values of Fisher (1969; 1971) for two reasons. First, the Young's moduli of elasticity obtained by Fisher (1969; 1971) were mathematically computed from the change in geometry of the lens during his lens-spinning experiments. The assumptions in the mathematical procedures employed by Fisher (1971) have been shown to produce systematic errors in the measures of the Young's modulus of the lens matrix (Burd et al., 2005). Second, even if these errors were to be discounted, Fisher's measures of the Young's moduli of the lens capsule and matrix represent the stress on the lens at the 'yield' strain level. As noted by Krag et al (1997), stresses and strains of this magnitude are rarely encountered by the lens during 'normal' accommodation and hence may not represent the physiological Young's modulus of elasticity of the lens.

Figure 51a shows the individual spring constants of the lens capsule and lens matrix and the combined spring constant of lens capsule and matrix computed for ages 15 – 75 yrs using the equations shown above. For comparison purposes, the moduli of elasticity of the lens capsule, matrix and the combination of capsule and matrix are shown in figure 51b. Figure 51c shows that the spring constants obtained using the method described above compares well with the spring constants of the lens complex (lens capsule, matrix and zonules) obtained by Wyatt (1993). Figure 51a & b shows that at any age the modulus of elasticity is much higher for the lens capsule than for the lens matrix. However the lens capsule also has a much smaller area when compared to the lens matrix (Krag et al., 1997; van Alphen & Graebel, 1991; Strenk *et al*., 1999; 2000). When area and length are taken into account by the spring constant, the capsule stiffness varies little with age. Since the spring constant of the capsule is invariant with age, when the lens matrix is replaced by a prosthetic lens that has a lower stiffness, equivalent to that of a younger lens, the overall stiffness of the lens and prosthetic matrix complex will be equivalent to that of the younger lens.

In our dynamic model of accommodation, the combined spring constants of the lens capsule and matrix (Eq. 11) were described as gain elements by normalizing the compliance of the lens of a given age with that of the 15-yr old lens. The methods employed to obtain normalized gains is described in detail in section 2.3. Figure 51d shows that the normalized compliances obtained using the method described above also compares well with the normalized compliance data obtained by Wyatt (1993).

Appendix III: Conversion of time constant of lens matrix into its damping coefficient

Quantitative estimates of human lens viscosity were obtained from by Weeber et al (2005) by performing an *in-vitro* dynamic mechanical analysis on the lens matrix. They mathematically described the visco-elastic properties of the matrix using three cole-cole relaxation terms and one viscous flow term. Quantitatively, the time constants obtained from frequency of the second cole-cole relaxation process compared well with behavioral estimates of time constants of accommodation step responses (Beers & van der Heijde, 1996). The following conversion regimen was employed to obtain lens-damping coefficients from the measures of time constant of the lens matrix (Weeber et al., 2005) and from measures of spring constant of lens capsule and matrix (Appendix II).

T_C = Time constant of lens matrix (Seconds)

F_2 = Frequency of the second cole-cole relaxation process (Hertz)

K_C = Spring constant of the lens matrix (Dynes / Millimeter)

K_M = Spring constant of the lens capsule (Dynes / Millimeter)

K_{Com} = Combined spring constant of the lens matrix and capsule (Dynes / Millimeter)

D_{Coeff} = Damping coefficient of the lens matrix (Dynes. Second / Millimeter)

Computing constants from second cole-cole relaxation process (Weeber et al (2005); Figure 7a in their paper);

$$T_C = 1 / (2 * pi * 10^{-F2}) \quad (1)$$

Time constant = Damping coefficient / Spring constant (2)

Rearranging Eq. 2 Damping coefficient = Time constant * Spring constant

$$\mathbf{D_{Coeff}\ (Dynes.\ s / mm) = T_C\ (s) * K_{Com}\ (Dynes / mm)} \quad (3)$$

In our pulse-step model, the damping coefficient of the lens matrix was obtained for ages 15 – 75 yrs using Eq. 3. Time constants of the lens were obtained using the equations shown above. Combined spring constants of the lens capsule and matrix were obtained using the equations described in Appendix II. Figure 52a plots the change in time constant as a function of age for the lens matrix (Weeber et al., 2005) and for the entire accommodative system (accommodative plant plus accommodative neural controller) (Beers & van der Heijde, 1996). The time constant of the lens matrix decreases with age while the time constant of the entire system increases with age. While the reason for the difference in trends of the two data sets is unclear (Weeber et al., 2005), it is intuitively obvious that the time constant of the lens matrix is more representative of the crystalline lens than the time constant of the entire accommodative system. Hence, the pulse-step model simulations were performed with these updated estimates of lens matrix time constant. Figure 52b plots the damping coefficients obtained from our analysis of Weeber et al's (2005) data with the damping coefficients obtained by Beers & van der Heijde (1996) as a function of age. Both the data sets show an increase in damping coefficient with age. The exaggerated increase in damping coefficient seen in Beers & van der Heijde's data is due to the exaggerated increase in time constant with age shown in figure 52a (Eq.3).

An alternative way to compute the damping coefficient of the lens matrix is using the viscosity of the lens matrix. Since this conversion regimen is analogous to the conversion of Young's modulus of elasticity into spring constants, only the final steps in the conversion are shown below.

D_{Coeff} = Damping coefficient of the lens matrix (Dynes. Second / Millimeter)

V = Viscosity of the lens matrix (Newtons. Second / $Meter^2$)

A = Cross-sectional area (CSA) of the elastic body ($Meter^2$)

L = Baseline length of the elastic body (Meter)

Conversion factor: 1 Newtons. Sec / Meter = 100 Dynes. Sec / Millimeter

$$D_{Coeff}\ (Newtons / m) = (A / L) * V \quad (4)$$

Applying conversion factor to Eq. 4; $\mathbf{D_{Coeff}\ (Dynes / mm) = 100 * (A / L) * V}$ (5)

Eq. 5 was used to calculate the damping coefficients of the A-IOL III from the measures of its viscosity provided by Koopmans (2005).